INVESTIGATING THE FUNCTIONALITY OF *PAPAVER S*-DETERMINANTS IN HIGHLY DIVERGED HETEROLOGOUS SYSTEMS

by

CARLOS ALBERTO FLORES ORTIZ

A thesis submitted to
The University of Birmingham
For the degree of
DOCTOR OF PHILOSOPHY

School of Biosciences
University of Birmingham
September 2015

ABSTRACT

Self-incompatibility (SI) is an important genetic mechanism that angiosperms utilize to reject “self” pollen. In *Papaver rhoeas* (poppy) SI is controlled in an allele-specific manner by a single locus with multiple haplotypes; each haplotype encodes male (PrpS) and female (PrsS) *S*-determinants. PrsS-PrpS interaction triggers SI, stimulating cation channel activity and increases in cytosolic free Ca^{2+} ($[Ca^{2+}]_i$), triggering a signalling network involving actin cytoskeleton alterations and programmed cell death (PCD). PrpS was recently functionally transferred into self-compatible, highly diverged *Arabidopsis thaliana*. Transgenic *Arabidopsis* pollen expressing PrpS-GFP was shown to undergo a “*Papaver*-SI-like response”, involving actin and PCD when challenged by recombinant PrsS.

Here we investigated function of PrpS in several other heterologous model systems, including *Arabidopsis* mesophyll protoplasts, yeast, barley and mammalian HeLa cells. Although more work is needed on some of these systems, data were obtained suggesting that PrpS is functional in mammalian HeLa cells. A key finding was that HeLa cells expressing PrpS, when exposed to cognate PrsS, exhibited transient increases in $[Ca^{2+}]_i$ and inward cation currents; actin reorganization and decrease in cell adherence. These data suggest that: PrsS-PrpS interaction can recruit endogenous components in HeLa cells to achieve a biological response.

Acknowledgement

I would like to thank my supervisor Prof. Noni Franklin-Tong, for her support and guidance during the last four years. I would also like to thank Prof. Chris Franklin and Dr Eugenio Sanchez Moran for their constant encouragement and help.

I must also thank Dr Wendy Harwood, Dr Steve Publicover, Dr Neil Hotchin, and Dr Rhein Parri and all the people in their groups for helping me to develop my project. Also a massive thanks to all the current and past members of “Team Poppy”: Tamanna, Deb, Zongchen, Javi, Andrew and Katie. A huge thank to all the colleagues, staff, and friends on the second floor.

I would like to thank my funding agency “Becas Chile” from “Conicyt” for the fellowship to study at the University of Birmingham.

Lastly, I would like to especially express my gratitude to my family in Chile and my “new” family in London. In particular I would like to mention my partner Marcella for her constant and daily support, mil gracias!

TABLE OF CONTENTS

LIST OF FIGURES AND TABLES

CHAPTER 1: Introduction

CHAPTER 2: Materials and Methods

ABBREVIATIONS

$[Ca^{2+}]_i$	Intracellular calcium levels
488-phalloidin	Alexa Fluor® 488 phalloidin
ABP	Actin-biding proteins
ADF	Actin-depolymerizing factor
ATP	Adenosine Triphosphate
CAP	Cyclase-associated protein
Caspase	Cysteinyl aspartate-specific protease
CFU	Colony-forming Unit
CHA	Chemical hybridising agents
CHO	Chinese hamster ovary cells
CMS	Cytoplasmic male sterility
COS	Fibroblast-like cell line derived from monkey kidney tissue
DMEM	Dulbecco's Modified Eagle's medium
EGFP	enhanced GFP
ER	Endoplasmic retucilum
F-actin	Filamentous actin (actin MFs)
F-actin	Filamentous actin
FBS	Fetal Bovine Serum
FDA	Fluorescein diacetate
FITC	Fluorescein isothionynate
GA	Golgi apparatus
GAPDH	Glyceraldehyde 3-phosphate dehydrogenase
GFP	Green Fluorescence Protein
GSI	Gametophytic SI
HeLa	Henrietta Lack epithelial human cell line
hpt	Hygromycin phosphotransferase
kb	kilobases
MAS	Marker-assisted selection
MS	Murashige and Skoog
MWCO	Molecular weight cut-off
MYA	Million years ago
NO	Nitric Oxide
ON	Overnight
PAGE	Polyacrylamide gel electrophoresis
PBS	Phosphate-buffered saline
PCD	Programmed cell death
PCR	Polymerase chain reaction
PEP	Polyethylene glycol
PFA	Parafolmaldeyde
PrpS	Papaver rhoeas pollen S-determinant

PrsS	Papaver rhoeas stigma S-determinant
ROS	Reactive oxigen species
RT-PCR	Reverse Transcription PCR
SDW	Sterilised Distilled Water
sem	Standard Error of the Mean
SI	Self-incompatibility
SLG	S-locus glycoproteins
SRK	S-locus receptor kinase
SSI	Sporophytic SI
TBS	Tris buffered saline
TBST	TBS + 0.1% Tween 20
TEMED	N,N,N',N',-Tetramethylenediamine
TGN	Trans-golgi network
UT	Untreated

CHAPTER 1

INTRODUCTION

1.1 Mechanism of cell-cell communication: conserved signalling networks

Communication between cells is essential for both multicellular and unicellular organisms in order to organise and respond efficiently to external stimuli. Most of the communication strategies have two phases: 1) sensing, usually by a protein (receptor) that recognises the extracellular signal (ligand), and 2) transmission of the signal, which triggers several downstream events leading to alterations in the cellular physiology. The components associated with the transmission of a signal, are part of the signalling network (Figure 1.1) (Alberts *et al*., 2008).

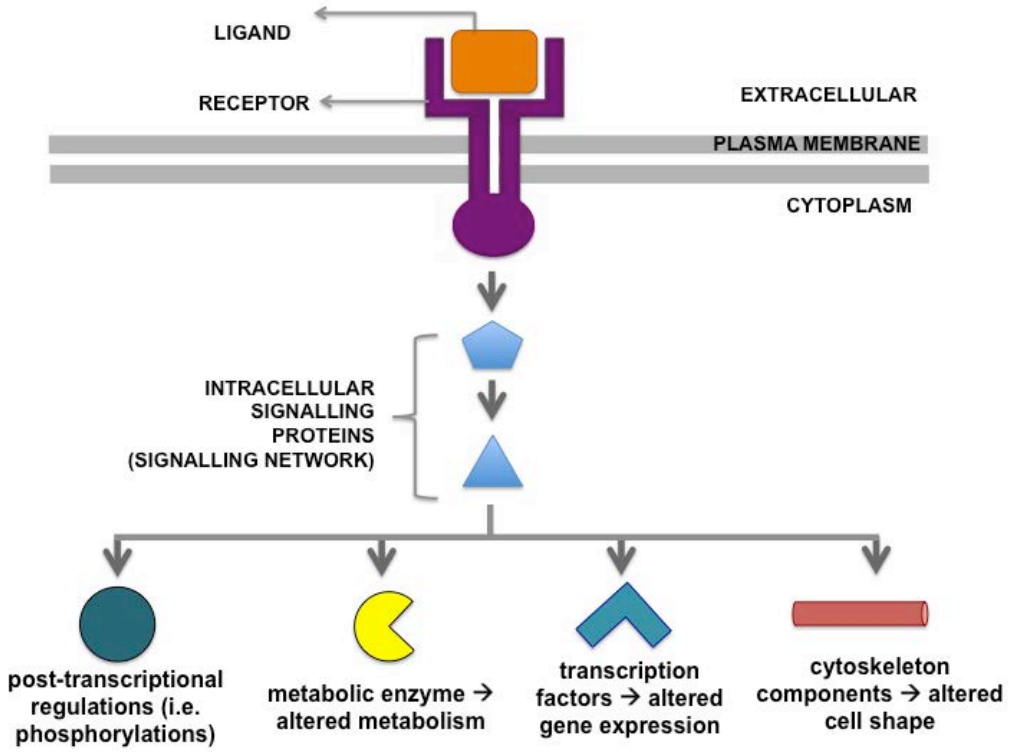

Figure 1.1. Diagram summarising the basic component involved in a signalling pathway activated by an extracellular compound. The ligand binds the receptor allocated in the plasma membrane that activates a signalling network mediated by several proteins, which will modified effector proteins what have an effect in the cell behaviour.

In plants, cell-cell signalling plays a central role in reproduction (further details discussed later in section 1.4). Particularly, an intricate regulatory signalling network mediates the pollen tube recognition and guidance in the stigma during fertilisation. For a review see Higashiyama and Takeuchi (2015). These studies in plants have been developed from concepts initially described for animal cells. Thus, studies investigating cell-cell communication and signalling networks between the sperm and the egg recognition have also been described in animals (Hoodbhoy and Dean, 2004).

An important characteristic of the signalling networks is its versatility. Even though they are specific for certain ligands, signalling network can be interconnected for key molecules, which allows to link two processes that may seem initially unrelated (Papin et al., 2005). Another characteristic of signalling networks, very relevant for this thesis, is that some of them have been conserved in highly diverged organisms. Thus, rather that generate a new signalling network *de novo*, there are several examples revealing that cells have adapted and optimised certain elements maintaining common basic components. This has identified universal and ancient components shared in signalling pathways in highly diverged cells. For instance, the two-component phospho-relay system, is present in bacteria (Kennelly and Potts, 1996), archaea (Leonard et al., 1998) and eukaryotes (Hwang et al., 2002). Another well-studied example is the MAP kinases signalling cascade, which is highly conserved in plants, animals and yeast. This cascade is activated by receptors that recognise pathogen-associated molecular pattern (PAMPs), which activate successive phosphorylation mediated by MAPK, leading to the activation of

transcription factors related with defence genes (Asai et al., 2002) or programmed cell death (Chang and Karin, 2001, Li et al., 2007).

Examples of these common signalling between diverged cells, relevant for this thesis, are detailed in the following sections.

1.1.1 Calcium response coupling conserved in diverged cells

Ca^{2+} is a commonly used second messenger in many signalling pathways. Numerous examples of Ca^{2+} involved in signalling pathways can be found in prokaryotic and eukaryotic cells. In animal cells, Ca^{2+} participates in fertilisation, cell growth, secretion, muscle contraction, neuronal signalling. Reviewed in (Berridge, 1993, Berridge et al., 1998). For instance, repetitive Ca^{2+} oscillations are essential to begin the fertilisation in mammals (Homa and Swann, 1994). Likewise, in plants, Ca^{2+} participates in a variety of mechanisms involved in cellular responses to the environment particularly abiotic stress responses. Reviewed by Trewavas and Malho (1998), Dodd et al. (2010).

Despite no specific Ca^{2+}-permeable channels have been characterised in plants (Swarbreck et al., 2013), there are numerous features of conserved Ca^{2+}-signalling components in plants including channels, pumps and Ca^{2+}-binding proteins. Sequence alignments of Ca^{2+}-transporter proteins between animal, plants and yeast revealed highly conserved channels. A number of ion channels that gate Ca^{2+} are present in plant and animal cells (**Figure 1.2**). These families have conserved key functional sites such as the calmodulin-binding domain and the cyclic-nucleotide-biding site (Nagata et al., 2004). These channels allow the transport of Ca^{2+} through the membrane after specific amino acids (i.e.

glutamate) have been bound to a receptor site in the channel. (Nagata et al., 2004).

The calmodulin family is a good example of proteins mediating several signalling pathways during cell development and responses to environmental stimuli, which have been described in plants and animals. Reviewed by Ranty et al. (2006).

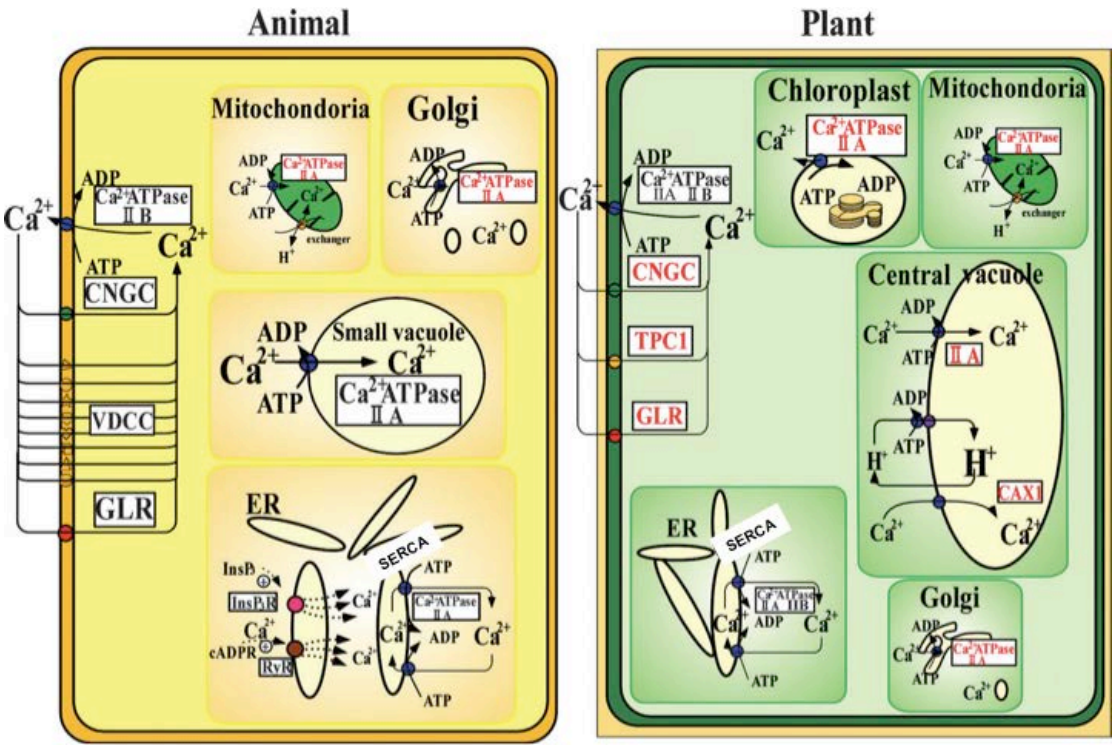

Figure 1.2 Diagram representing the conserved calcium transporters in animal and plant cells. $InsP_3$: inositol 1,4,5-triphosphate; cADPR: cyclic ADP-ribose; GLR: glutamate receptor; VDCC: voltage-dependent calcium channel; CNGC: Cyclic nucleotide-gated calcium channel; TPC1: two-pore channel; ER: endoplasmic reticulum. Receptors in red correspond to putative location. IP_3R: inositol 1.4.5-triphosphate receptor and RyR: ryanodine receptor.. Figure and legend adapted from (Nagata et al., 2004).

An increase in $[Ca^{2+}]_i$ is one of the principal cellular mechanisms to trigger Ca^{2+}-signalling pathways (Berridge and Taylor, 1988). Studies revealing the dynamics of Ca^{2+} at subcellular level can be found in animal cells over 40 years ago (Hagiwara, 1973, Hagiwara and Nakajima, 1966), whereas for plant, preliminary studies started in the early 80s (Dieter and Marme, 1980). Consequently, several techniques to study Ca^{2+} using live cell calcium imaging (Cannell et al., 1987) were developed initially for animal cells and later on optimised for plant cells. Initial studies carried out in neurons, contributed to the development of procedures to measure $[Ca^{2+}]_i$ in live cells by means of fluorescent dyes and microscopic analysis (Tsien, 1988). These studies provided valuable spatio-temporal information identifying where and when the Ca^{2+} increases occurred within a cell. This allowed demonstration that increases in $[Ca^{2+}]_i$ was a signal-response coupling to a variety of downstream alterations in the cell (Berridge, 1993). In plants, initial studies exploring the role of Ca^{2+} were carried out using live-cell Ca^{2+} imaging in guard cells (Gilroy et al., 1991). A similar experimental approach provided the first evidence revealing the importance of Ca^{2+} during the *Papaver* SI response (Franklin-Tong et al., 1993b).

Electrophysiological experiments such as patch clamping represents a powerful methodology to study Ca^{2+} signalling. Register of the conductance through a membrane as a consequence of an ion flux across that membrane, allows the functional characterisation of the channel associated with the current. Reviewed by Hamill et al. (1981), Sakmann and Neher (1984), Karmazinova and Lacinova (2010). Patch clamping was initially developed in animal cells, but has also been successfully used to study channels in plant cells (Maathuis et al., 1997).

These experiments provided crucial evidence in elucidating that the release of Ca^{2+} from the vacuoles was mediated by a channel, regulated by inositol 1,4,5-trisphosphate (Allen et al., 1995). Additionally, patch-clamp experiments in *Papaver* pollen protoplasts allowed confirmation that the *Papaver* SI response was mediated by a non-specific cation channel including Ca^{2+} and K^{+} (Wu et al., 2011).

Ca^{2+}, as it is one of the key hallmarks of the *Papaver* SI response (detail later in section 1.4.6.2.2 and 1.5) and a key aim for this thesis.

1.1.2 The role of actin cytoskeleton in conserved pathways in highly diverged species.

The actin cytoskeleton is conserved in highly diverged cells. It can be found in yeast, plant and animal cell (Alberts et al., 2008), and it is critical for functions related to cell size and shape, structural support, and subcellular organization of organelles. Moreover, the actin cytoskeleton participates in processes such as plasma membrane protrusion, cell adhesion, vesicle trafficking, cell division and signalling-response coupling (Alberts et al., 2008). Particularly, actin filaments (F-actin) are one of the main components of the cytoskeleton mediating signalling cascades in both plant and animal cells (Nelson et al., 2008). The importance of the actin cytoskeleton in animal cells will be presented in Chapter 5, and the role of the actin cytoskeleton in self-incompatibility in *Papaver* presented in sections 1.4.6.2.4.

In yeast, it has been established that actin cytoskeleton is fundamental for polarised growth (Ayscough et al., 1997), and mediating cellular signalling (Ho and Bretscher, 2001).

In mammalian cells, the actin cytoskeleton is essential for structures such as actin stress fibres and focal adhesions (Nobes et al., 1998, Narumiya et al., 1997). Actin stress fibres are bundles of actin, often anchored to focal adhesion, a site where a complex of proteins mediate crosstalk between the extracellular matrix and the actin cytoskeleton, and therefore a key mediator between external stimuli and intracellular signalling response (Wozniak et al., 2004). Actin stress fibres respond to the mechanical stimuli around the extracellular matrix, as well as biological stimuli such as toxins (Chardin et al., 1989). Studies monitoring F-actin configuration have established that proteins (*e.g.* Rho) can be activated by extracellular ligands triggering a signal transduction pathway including assembly of actin stress fibres (Hall, 1998). The role of actin stress fibres HeLa cells is detailed in Chapter 5.

In plants, the actin cytoskeleton has been described as a key component mediating signalling pathways (Staiger, 2000). For instance, in the plant-pathogen interaction, mechanical stimuli on epidermal cells generated by the attack of the pathogen, triggers actin cytoskeleton rearrangements.

Additional proteins, termed actin-binding proteins (ABP), coordinate the dynamics of the actin cytoskeleton in plant and animal cells. In plants, ABP participates in processes such as the self-incompatibility response in *Papaver* (Poulter et al., 2010) or operating as sensors of the cellular environment (Schluter et al., 1997). Actin-depolymerising factor (ADF/cofilin) is a well-studied ABP common between plant an animal cells. ADF is a central regulator in a

wide variety of processes (Bernstein and Bamburg, 2010). Interestingly, ABP can be regulated by [Ca^{2+}] (Wang et al., 2008), providing a robust link between the actin cytoskeleton dynamics and the Ca^{2+} signalling pathways described in 1.1.1.

Endocytosis and apoptosis/PCD are two cellular processes involving actin cytoskeleton conserved in yeast, animal and plant cells. Endocytosis requires remodelling of the cell cortex for the internalisation step and because actin cytoskeleton is a structural component of the cell cortex, it was not unexpected that proteins related with the actin cytoskeleton also participate in the membrane remodelling for endocytosis. Reviewed by Engqvist-Goldstein and Drubin (2003). Commons elements are shared in yeast, animal and plants in actin cytoskeleton mediating apoptosis/PCD (**Figure 1.3**). In animal cells, alterations (stabilising or destabilising) to the normal dynamic of F-actin by treatments with a F-actin-stabilising drug Jasplakinolide (Jasp) induced apoptosis via caspase activation (Odaka et al., 2000). Once apoptosis has been triggered, further alteration to the actin cytoskeleton can originate membrane blebbing (**Figure 1.3**). In yeast, alterations to the F-actin generated in response to environmental stimuli or intracellular signals (i.e. reactive oxygen species, ROS) lead to apoptosis (**Figure 1.3**). The actin cytoskeleton is also sensitive to increases in the oxidative status. Accumulation of ROS can reduce the dynamic capability of the cytoskeleton and therefore eventually leads to PCD (Dalle-Donne et al., 2001, Farah and Amberg, 2007). Stabilisation of F-actin using the drug Jasp induces apoptosis (Gourlay et al., 2004). Similarly, in plants, alterations to the dynamic of F-actin in response to extracellular stimuli, ROS, or Jasp lead to PCD (**Figure 1.3**). Further details with the role of F-actin, ROS in

PCD in plants, specifically during the *Papaver* SI response are in section 1.4.6.2 .

In addition to this relationship between apoptosis/PCD and the actin cytoskeleton dynamics, apoptosis/PCD can be triggered by other mechanisms detailed in the next section (1.1.3).

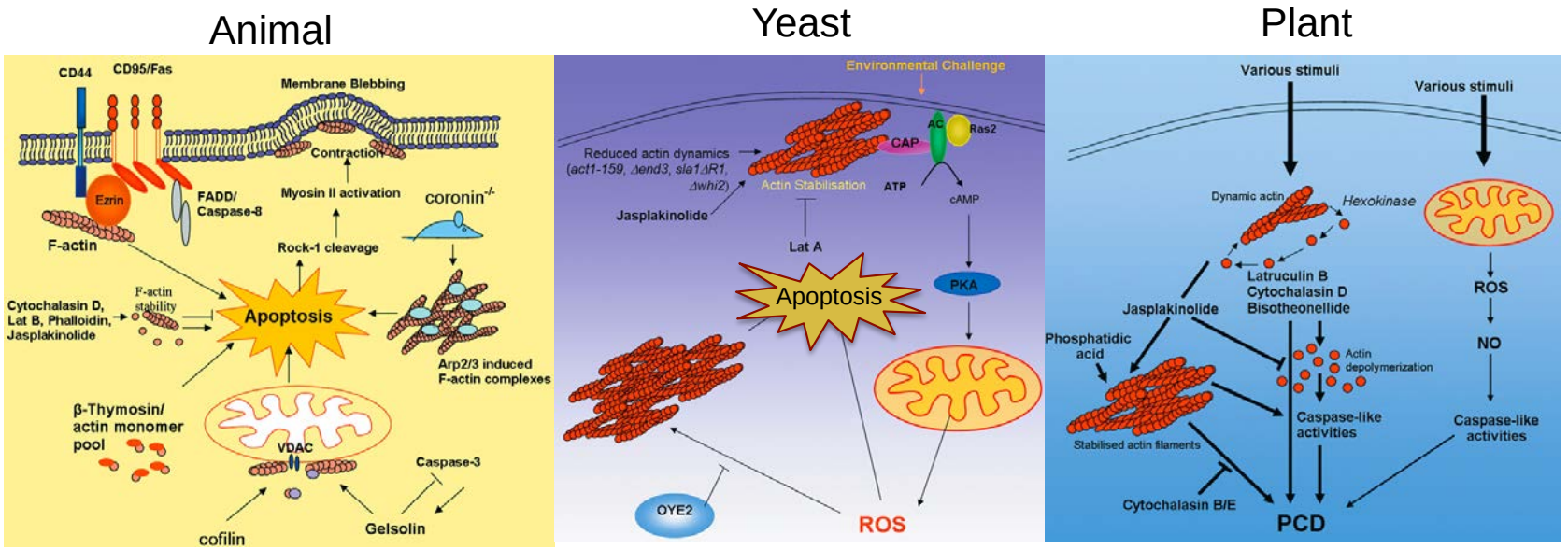

Figure 1.3. Diagram representing relationships between the actin dynamics and apoptosis/PCD in yeast, animal and plant cells. In **animal** cells CD95/Fas and CD44 death receptors that require actin to a functional assembling. Alterations in actin dynamics by means of treatments with actin-disrupting drugs (Jasp and CytD) or actin accessory proteins (cofilin, coronin, gelsolin) also lead to apoptosis. Some of these alterations can be via mitochondria. Once apoptosis has started, actin cytoskeleton facilitates membrane blebbing and the formation of apoptotic bodies. In **yeast**, actin stabilisation also leads to apoptosis. Also the abnormal production of ROS as a consequence of malfunctioning in the mitochondria leads to apoptosis. Actin cytoskeleton is also linked to cAMP signalling, which also can affect the actin dynamics. In **plants** cells, mitochondria and ROS production play a role in triggering PCD. Also Ca^{2+}, and NO mediate PCD. Moreover, actin dynamics also can trigger caspase-like activities and PCD in pollen. "This figure has been adapted from the originally published in Biochemical Journal. Franklin-Tong VE, Gourlay CW. A role for actin in regulating apoptosis/programmed cell death: evidence spanning yeast, plants and animals. Biochemical Journal. 2008; 413: 389.

1.1.3 Evolutionary role of apoptosis/PCD and its conservation between highly diverged cells

Processes such as DNA fragmentation (Nagase et al., 2003), or leakage of cytochrome *c* from the mitochondria into the cytosol (Balk et al., 1999) are some key diagnostic features of PCD. Additionally, caspases play a major role in apoptosis in animals. Plants have no true caspase gene homologues, but caspase-like protease activity has been reported and it is well established that PCD is present in plants (Bosch and Franklin-Tong, 2007) (further details in section 1.4.6.2.5) and yeast (Madeo et al., 1997).

Features of Ca^{2+}, actin cytoskeleton and apoptosis/PCD share similar elements between diverged species (**Figure 1.1**, **1.2** and **1.3**), suggesting that there are ancient pathways which have been adapted and optimised for new and different requirements, but there is a basic and fundamental core that has not been changed (**Figure 1.3**).

These identified conserved pathways sharing common elements between different cells makes it feasible to study genes, proteins or even metabolic pathways using a heterologous system.

1.2 The use of heterologous systems to study plant genes and proteins.

There are classical cellular systems with certain characteristics, which have transformed them into valuable model systems to study function of genes or proteins from other organisms.

Complementation analysis of an *E. coli* mutant with cDNA of *KAT1* channel from *Arabidopsis,* confirmed that KAT1 was a voltage-gated potassium channel (Uozumi et al., 1998). Further characterisation of the ion channel KAT1, using different heterologous model systems will be presented, here.

Yeast is widely used as a cellular model system. Moreover, it grows rapidly and reproduces by cell division (asexually) or fusion of two haploid cells (sexually). Therefore it can be maintained as either stable haploid or diploid, which is useful for genetic studies. Its genome has been sequenced and characterised mutants available (Giaever et al., 2002). Techniques such as functional complementation or patch-clamp experiments have been used to identify and characterise genes from other eukaryotic organisms. Patch-clamp is an electrophysiological technique that registers the currents in a membrane generated by the ion flux through a channel (Sakmann and Neher, 1984). Patch-clamp studies of KAT1 channel from *Arabidopsis* in expressed in yeast confirmed that KAT1 was mediating an inward current (Bertl et al., 1995). Further details regarding the use of *Saccharomyces cerevisiae* as a model system will be presented in Chapter 3 (section 3.1).

Among plants, *Arabidopsis thaliana* is the most used model system. It is small, can be grown in a glasshouse and has a short life cycle (about 8 - 10 weeks). The genome has been sequenced, annotated and there are mutants available. Protoplast represents a powerful tool to carry out functional characterisation of plant genes. Reviewed by in Yoo et al. (2007). Mesophyll protoplasts from *Nicotiana tabacum* have been used to confirm *in planta* that KAT1 from *Arabidopsis* is a potassium channel (Bei and Luan, 1998). Further details

regarding the use of *Arabidopsis* mesophyll protoplast will be presented in Chapter 3.

Mammalian cell lines such as HeLa, HEK or COS are robust cell models. They can be cultivated *in vitro* and transfected transiently or stably. Importantly, epithelial cells growth naturally attached to a surface, providing a major advantage for electrophysiological studies such as patch-clamp.

Patch-clamp of Chinese hamster ovary (CHO) cells expressing KAT1 channel from *Arabidopsis* also exhibited the inward currents previously described as a characteristic of the KAT1 channel (Szabo et al., 2000). Patch-clamp and live cell calcium imaging in animal cells are presented in Chapter 4 (section 4.1).

Relevant for this thesis, is the use of heterologous system to study self- and non-self cellular recognition.

1.3 Self and Non-self Recognition System in highly diverged organisms

Discrimination between self- and non-self is a strategy that can be found across highly diverged organisms. In animals, this discrimination process is normally referred as allorecognition and it is the fundamental base of the immune system. Reviewed by Dionne (2013)

In fungi (fungal mating types) recognition process is closely related to the reproduction process. A specialised region of the genome designated mating-type locus (*MAT*) establishes the cell type identity and its sequence is particular for each mating-type. In Saccharomyces cerevisiae, cells can be *MATa* or *MATα* according to the allele they have inherited. Mating between a- and α- is

possible and leads to an a-α- diploid that can undergo meiosis (Herskowitz, 1992). Reviewed by Fraser and Heitman (2004)

Ciona intestinalis is a hermaphroditic primitive chordate, which exhibits a self-incompatibility mechanism to prevent self-fertilisation. The current model includes two essential loci with specific expression in the egg and the sperm (Harada et al., 2008) allowing cognate identification and discrimination between the reproductive cells (Harada et al., 2008). Further studies have established that increases in $[Ca^{2+}]_i$ are mediating this incompatible response (Saito et al., 2012). This example share common elements with self-incompatible system in plants. For a review of similarities between self/non-self recognition system between plant and animal cells see Sawada et al. (2014).

1.4 Sexual Reproduction in Angiosperms

Flowering plants (angiosperms) are the most widespread group of plants. Angiosperm sexual reproduction begins when mature pollen lands, adheres on a stigma, hydrates and starts germinating. Concurrently a complex communication process between the stigma and the pollen grain (and later its pollen tube) begins and is another example of the importance of cell-cell communication. This process initially mediates the recognition and determines the stigma-pollen compatibility, and provides guidance of the pollen tube through the stigma and style towards its final destination, the ovule **(Figure 1.4.A)** (Dresselhaus and Franklin-Tong, 2013, Higashiyama and Takeuchi, 2015). Once the pollen tube has reached the ovule, it delivers the sperm cells, which carry out the double fertilisation process. This mechanism involves two

sperm cells and two female gametes, the egg cell and the central cell (**Figure 1.4.B**). The sperm cells first reach the synergids (**Figure 1.4.B**); one of them fuses with the egg cell generating the embryo, and the other sperm cell fuses with the central cell producing the endosperm **(Figure 1.4.C)** (Berger et al., 2008).

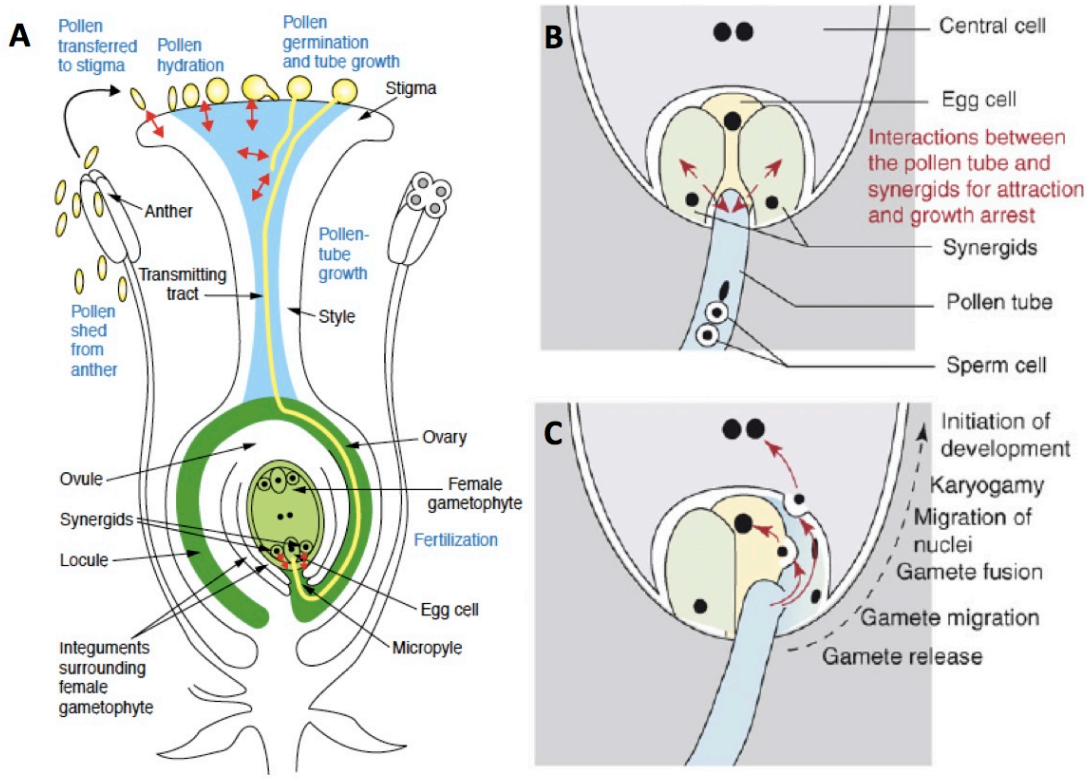

Figure 1.4. Schematic diagram of pollination and fertilisation processes in angiosperm. **(A)** Mature pollen is shed from the anthers. When it lands on a suitable stigma, it hydrates, germinates and begins to grow until it reaches the gametophyte. Red, double-headed arrows indicate some control points and signalling events (modified from Franklin-Tong, 2002). **(B)** Attraction and growth arrest of the pollen tube by the synergids. When the pollen tube reaches the vicinity of the female gametophyte, two synergids positioned on either side of the egg cell attract the pollen tube. After pollen tube arrival, direct interaction between the pollen tube and the synergids causes growth arrest of the pollen tube. **(C)** The double fertilisation process after pollen tube discharge. One of two sperm cell fuses with the egg cell to form the embryo, and the other fuses with the central cell to form the endosperm (kariogamy: the fusion of the male and female nuclei) Figure and legend have been adapted from Berger et al., 2008.

1.4.1 General Structure and Physiology of the Pollen tube

Pollen tube growth physiology has several distinctive aspects that make it an interesting system to study. Rapid growth in a highly polarised cell requires a tight regulatory network to coordinate crucial cellular processes involved in growth such as cytoskeleton dynamics, exocytosis and endocytosis **(Figure 1.5**) (Taylor and Hepler, 1997, Guan et al., 2013).

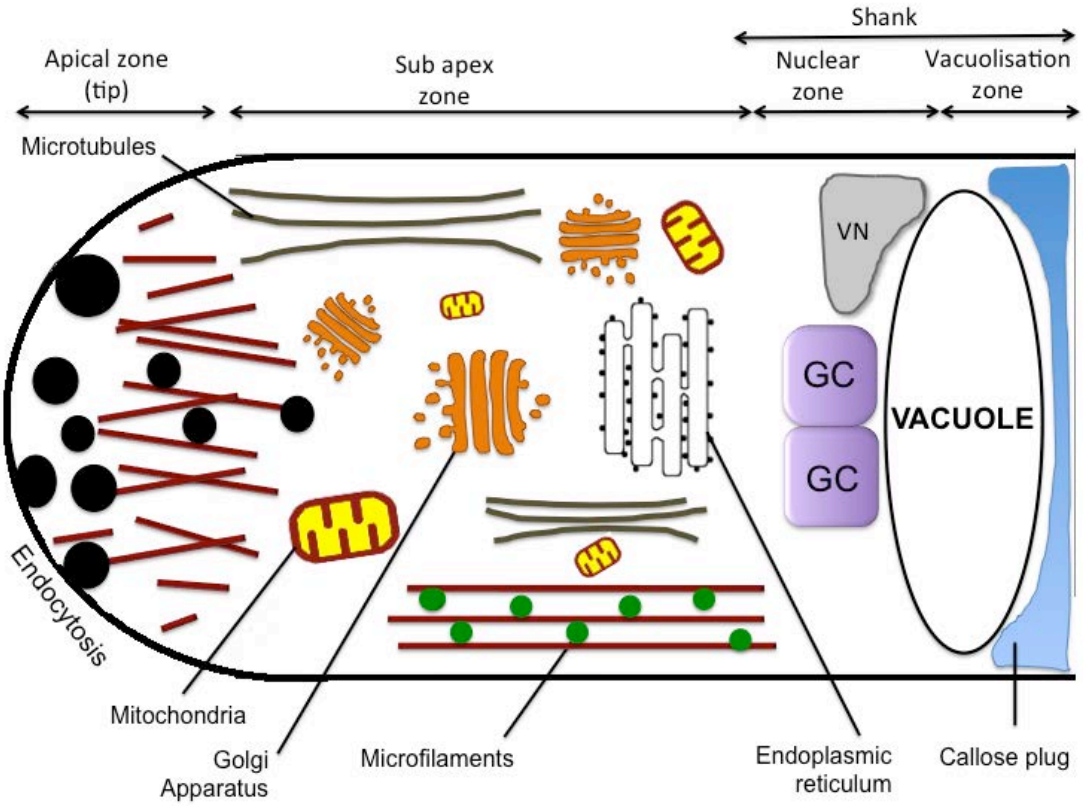

Figure 1.5. Diagram of the organisation and regulation of a normal pollen tube. Callose plugs separate viable streaming region of the cytoplasm from the highly vacuolated distal region. Streaming region can be divided according to its characteristics in: shank region, containing the generative cells (GC) and vegetative nucleus (VN), sub apex zone, where most of the organelles are confined, and the apical zone, which does not contain organelles and highly active in exocytosis processes.

Studies using *Lilium* and *Nicotiana* showed that pollen tube growth is a very dynamic process where the cytoskeleton plays a preponderant role (Miller et al., 1995). Additionally, studies in maize revealed a tight regulation at transcript level (Staiger et al., 1993). Reviewed by Taylor and Hepler (1997)

Considering structure and function, the pollen tube can be sub-divided to: shank, sub apical and apical region. The shank contains the sperm cells and vegetative nucleus and the sub apical region is rich in organelles. The apical region, which does not contain other organelles, is highly active in vesicle trafficking. Towards the back of the pollen tube, separated from the streaming region by callose plugs it is the vacuolated region (**Figure 1.5**) (Franklin-Tong, 1999, Guan et al., 2013).

Experiments staining F-actin in pollen revealed three different actin arrangements. Starting from the tip towards the base of the pollen tube: the apex, were virtually no F-actin are present; the collar, which is characterised by a dense mesh of actin filaments; and finally the sub-apex, zone containing actin arrays oriented parallel to the longitudinal axis of the cell (Geitmann et al., 2000).

Since pollen tube growth is a constant elongation, organelles and vesicles are constantly transported within the pollen tube. This trafficking represents a key feature of growing pollen tubes in angiosperms (Cardenas et al., 2005). This streaming relies on F-actin and it is fundamental for the distribution, accumulation and recycling of vesicles carrying cell wall materials, membrane protein, secretory proteins involved in the pollen tube growth (Cheung and Wu, 2008).

Disruption of the actin dynamics have a major inhibitory effect on pollen tube growth. A decline in the tip-focuses Ca^{2+} gradient (Cardenas et al., 2008, Gibbon et al., 1999), is also essential for pollen tube growth (Messerli and Robinson, 1997, Iwano et al., 2004, Hepler et al., 2012).

1.4.2 Food security and Plant Breeding

In angiosperm, the central cell participates in the double fertilisation process (**Figure 1.4**). The central cell is fertilised by one of the sperm cell to originate the endosperm (grain), a nutritious tissue that provides nutrients for the embryo development (Liu et al., 2010), but also are a commercial food crop. Therefore plant breeding technique a very important aspect of food security.

Especially relevant are staple cereals such as wheat or barley. Due to a constantly growing population and an economic system driven by market forces, food security faces the challenging goal to produce more without increasing the costs. Thus, agriculture and biotechnology have started to develop a variety of new tools in order to develop yield (Godfray et al., 2010, Moshelion and Altman, 2015).

Plant breeding is one of the fields where biotechnological tools have great potential. Heterosis and inbreeding depression are two key converse concepts underlying plant breeding. Heterosis (hybrid vigor), has been defined as : “phenotypic superiority of a hybrid over its parents with respect to traits such as growth rate, reproductive success and yield” (Lippman and Zamir, 2007). Charles Darwin described how hybrids display superior growth and fertility over their parents (Darwin, 1876), and Shull carried out initial systematic studies

focused in heterosis in maize (Shull, 1908). Opposite, inbreeding depression is the harmful effect (*e.g.* reduced survival or fertility) of offspring of related individuals, mainly associated to homozygosis. Inbreeding depression plays an important role in the evolution of outcrossing mating systems and in particular in crop breeding, because heterosis require intercrossing of inbreed lines (Charlesworth and Charlesworth, 1987, Charlesworth and Willis, 2009).

1.4.3 Breeding Technologies for Crop Production

Plant breeding involves several strategies. The traditional approach has been the identification and selection of suitable crosses between specific plants or lines to obtain a particular germplasm exhibiting any desirable characteristic. The current development of genomics, proteomics and metabolomics, has allowed complementing the traditional plant breeding strategies generating new alternatives. Reviewed by Tester and Langridge (2010). Here, we focused in the breeding of cereal crops, as a key objective addressed in this thesis (see section 1.5).

One of the most exploited new tools is the used of marker-assisted selection (MAS). MAS allows the identification and tracking of genetic regions that are associated with a desirable trait. This alternative to phenotypic selection is particularly useful for recessive genes that do not have an obvious phenotype are involved.

Another approach for crop breeding includes the generation of transgenic plants. It has been reported that maize plants overexpressing ZmNF-YB2, a transcription factor playing a role under water-limited conditions, exhibited an

increase in the yield of maize (Nelson et al., 2007). “Golden Rice” (Welsch et al., 2008), which does not represent an improvement in the yield, but has an improved nutritious quality, as it contains high levels of vitamin A. Genetically modified plants also contribute to the identification and characterisation of new genes. Therefore, despite the debate including political and social aspects, it is important to carry on with these studies. Moreover, so far, there is not scientific evidence suggesting hazards associated to transgenic plants (Nicolia et al., 2014). Additionally, new techniques such as marker-free transgenic plants represent a good chance to overcome some of the issues mentioned above (Woo et al., 2015).

A key goal in plant breeding is the generation of hybrids in order to exploit the advantages of heterosis. High-yielding hybrid varieties can increase the production in 15 -20%, which represent a major impact for the breeders. Chemical hybridising agents (CHA), cytoplasmic male sterility (and fertility restoration), and self-incompatibility are the main strategies used for the generation of hybrids, which allows to overcome the lack of hybrids due to the strong inbreeding nature of cereal crops such as wheat, rice and barley (Longin et al., 2012).

Cytoplasmic male sterility is a condition determined by plant mitochondrial genomes associated with a malfunction in the production of viable pollen. These plants are male sterile, however female fertility is not affected, and therefore male-sterile plants can set seed if they are pollinated with suitable pollen. The term cytoplasmic is due because the trait is maternally inherited with the mitochondrial genome (Eckardt, 2006). A male sterile line is convenient for breeders as these plants will not self-pollinate and therefore allows specific

crosses between the appropriate plants without the requirement to remove the male organs (emasculation), which is a time-consuming labour that increases the production cost of these hybrids. Although not currently in use due to its susceptibility to a fungal disease, maize *cms-T* is a popular example showing the potential of CMS. The male sterile maize Texas cytoplasm (*cms-T*) was massively used for the production of hybrid feed corn in the U.S representing over 85% of the production in 1970 (Crow, 1998). This maize did not require being detasseling in order to prevent self-pollination and therefore it was extremely popular among breeders. However, due to an epidemic fungal disease, the use of maize *cms*-T was terminated, and manual detasseling used again to prevent of self-pollination (Levings, 1993). Other examples of hybrid cereals are presented in **Table 1.1.** For a review on hybrid breeding in cereals see Longin et al. (2012)

Table 1.1. Table summarising examples of cereal hybrid plants.

Cereal	Name	Reference
Hybrid rice	Xieyou 9308 Lianyou Pei9	(Cheng et al., 2007)
Hybrid barley	HYVIDO®	(Syngenta, 2013)
Hybrid wheat	Probus	(Fossati and Ingold, 1970)

CMS has two disadvantages that have restricted its use. First, it requires fertility-restoration genes, which are not always available. And second, to maintain or propagate the pure lines can be a problem due to potential fertility issues. Because CMS lines are sterile, particular lines termed maintainer line is required to propagate the sterile line. Thus, there is a constant effort to discover new genes to carry on elucidating the mechanism underlying CMS at cellular

level. Based on *Arabidopsis* studies, the first gene related with male sterility in barley has been recently characterised (Fernandez Gomez and Wilson, 2014), opening new possibilities for barley breeding.

Self-incompatibility (SI) also represents a strategy for plant breeding tool as it allows preventing the self-pollination (detailed explanation regarding the SI mechanism will be presented in the next section). Since the 1950s hybrid varieties of commercial Brassica vegetable crops have been produced using an SI trait by growing two selected self-incompatible genotypes in alternate rows in an isolated field and harvesting hybrid F1 seeds from these crosses (Watanabe et al., 2000). There are examples of transferring SI between plants using traditional plant breeding techniques. Goring and collaborators reported the conversion of the naturally self-compatible cultivars of *Brassica napus* Topas and Regent, into self-incompatible ones, by transferring the *S*-locus from the self-incompatible *B. napus* rapifera Z-rutabaga line. Introgressing of the S-locus was achieved by repeated backcrossing using pollen from the self-incompatible variety and stigmas of the self-compatibles varieties (Goring et al., 1992).

1.4.4 Self-incompatibility

Incompatibility includes inter-specific and intra-specific incompatibility. Here we will focus in the homomorphic SI as it is more characterised and it is the more relevant for the purposes of this thesis.

Homomorphic SI is the main genetic mechanism that plants use to prevent self-fertilisation therefore encouraging outbreeding. SI is based on the self/non-self discrimination between male and female components. The system is controlled by a single locus, designated “S”, with multiple haplotypes (Takayama and Isogai, 2005). Each S-haplotype encodes for the male (expressed in the pollen) and the female (expressed in the stigmas) determinants, termed S-determinants. The interaction between male and female S-determinants (pollen-stigma) governs the self/non-self discrimination, controlling the viability of the fertilisation.

The pollen genotype is always haploid. However, as a result of two different strategies of pollen development, during the self/non-self recognition process, the pollen can behave as haploid or diploid. This has been used classify SI into two systems: 1) gametophytic SI (GSI), when the pollen phenotype is haploid, and 2) sporophytic SI (SSI), when the pollen phenotype is diploid (**Figure 1.6**). Furthermore, each system contains diverged molecular mechanisms, each one with particular characteristics (Rea and Nasrallah, 2008, Iwano and Takayama, 2012, Eaves et al., 2014).

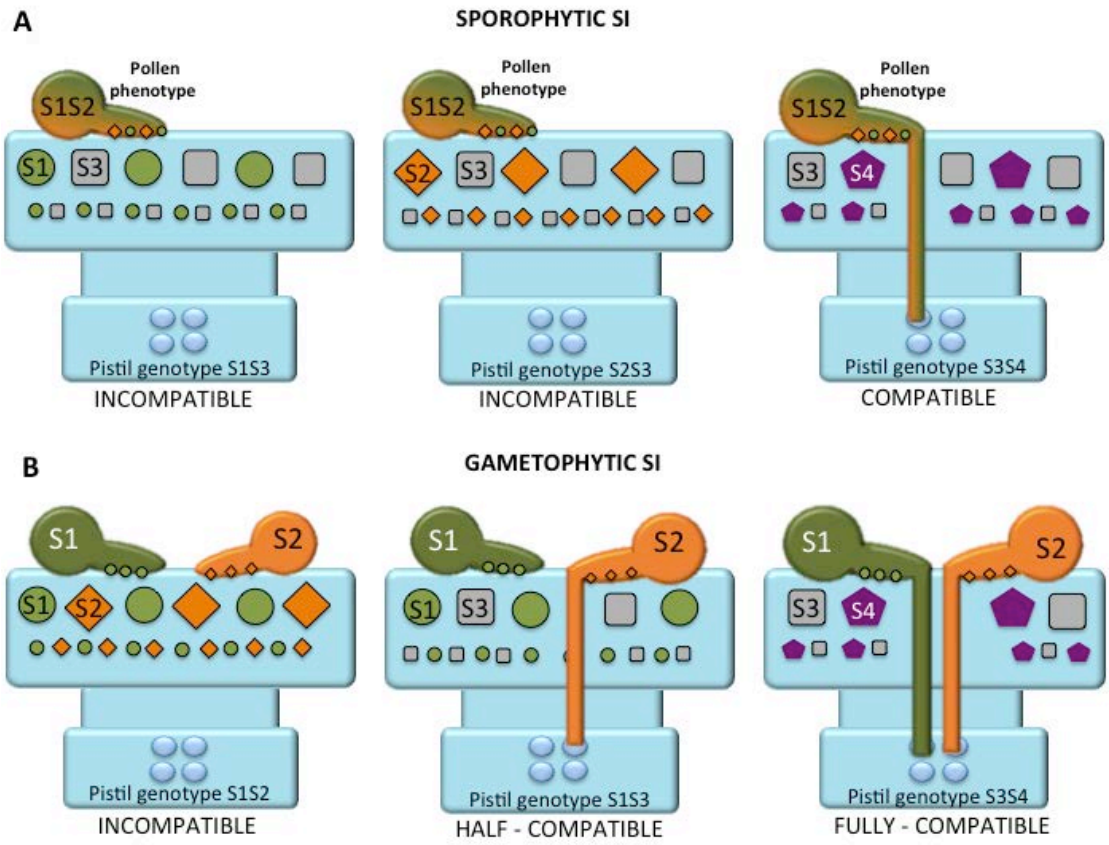

Figure 1.6. **Representation of the genetic control of SI.** According to the pollen phenotype, SI can be classified as sporophytic or gametophytic. (**A**) Sporophytic SI: pollen phenotype is the same as the patents diploid genotype. Thus, the pollen can germinate only in stigmas with both alleles different, generating two possible outcomes, compatible and incompatible. For instance, S1S2 pollen can only grow in a stigma with both alleles different such as S3S4. As soon as any of the alleles between pollen and stigma matches (Stigma S1S3 or S2S3), the recognition is incompatible and the pollen rejected. (**B**) Gametophytic SI: Pollen phenotype matches with its genotype (haploid). Thus, in this case there are three possible outcomes, fully compatible when lands in a stigma with both alleles different, incompatible when lands in a stigma sharing both alleles, and half-compatible, when only one of the alleles matches but the other is different. For instance, Pollen from a parental plant S1S2 will be either S1 or S2. This pollen will be fully compatible in a S3S4 stigma, incompatible in a S1S2 stigma and half-compatible in a S1S3 stigma, where pollen S1 will be inhibited, but pollen S2 will grow normally.

1.4.5 Sporophytic SI

The Brassicaceae family contains several economically important plants such as *Brassica napus* (rapeseed), *Brassica rapa* (turnip), *Brassica oleracea* (cabbage). SI in this family has been described as a sporophytic self-recognition system. The S-locus contains three genes: S-locus receptor kinase (SRK) (Takasaki et al., 2000, Silva et al., 2001), S-locus glycoproteins (SLG) (Kandasamy et al., 1989) and S-locus protein 11 (SP11, or S-locus cysteine-rich protein, SCR) (Takayama et al., 2001). The female component is SRK and is a membrane-spanning Ser/Thr receptor kinase that localises to the plasma membrane of stigmatic papilla cells. By means of gain-of-function-experiments, which showed that SRK alone determines the S-haplotype specificity and that SLG enhances the activity of SRK (Takasaki et al., 2000). By means of loss-of function and gain-of-function experiments it was demonstrated that SP11 - a cysteine-rich protein - is the male component (Schopfer et al., 1999). The binding of SP11 to SRK induces autophosphorylation of SRK, which stabilises the SRK in an active dimer form triggering the SI responses in the stigmatic papilla cell (Takayama et al., 2001).

It has been reported that additional proteins might act as positive mediators of the signal transduction downstream the SRK/SP11 interaction. One of them is the arm repeat-containing protein, ARC1 (Armadillo-repeat-containing 1), which is an E3 ubiquitin ligase that promotes the ubiquitination of proteins during the SI response (Mazzurco et al., 2001, Stone et al., 2003). And the other is the M locus protein kinase (MLPK), which is thought to enhance the signal produced by SRK after it's interaction with SCR/SP11 (Murase et al., 2004). Moreover,

studies in *Brassica napus* identified that ARC1 interact with Exo70A1, a protein that also was involved in the SI response (Samuel et al., 2009).

1.4.6 Gametophytic SI

Gametophytic SI has been reported in several families, however the mechanisms used are different. In this system, when the pollen genotype matches with the stigma genotype, an incompatible reaction occurs and no seed is set. Alternatively, a compatible reaction results in the setting of seeds when pollen genotype does not match the stigma genotype. Additionally, this system comprises a half-compatible situation, which is when half of the pollen contain a cognate allele, and therefore is rejected, but the other half of the pollen has a different allele and the pollen is compatible (**Figure 1.6**).

Solanaceae (*e.g. Nicotiana alata,* tobacco), Rosaceae (*e.g. Pyrus*, pear) and Scrophulariaceae (*e.g. Antirrhinum*, snapdragons) have a SI mechanism based in S-RNase activity to inhibit pollen growth. In Papaveraceae (*Papaver rhoeas*, poppy), PCD is triggered in pollen after several signalling cascade are triggered by a Ca^{2+} influx. Finally, in the Poaceae family (*e.g. Lolium perenne*, ryegrass) the SI mechanism is still unclear and currently is focus of several studies aiming to elucidate this system (Klaas et al., 2011).

1.4.6.1 Self-incompatibility in Solanaceae

In the Solanaceae, SI is activated by a non-self recognition strategy. In this system, the S-locus encodes a single female and multiple male S-determinants,

designated S-RNase and SLF (S-Locus F-box) or SFB (S-locus F-Box), respectively (Takayama and Isogai, 2005, McClure and Franklin-Tong, 2006). In addition, Petunia a collaborative non-self recognition system has been described. This system includes at least three types of divergent SLF proteins function as the pollen determinant, each recognizing a subset of non-self S-RNases (Kubo et al., 2010). In self-pollination, SLF does not interact with self-RNase, which causes degradation of RNA consequently inhibiting pollen tube growth. In cross-pollination, SLFs or proteins with SLF function interacts with non-self S-RNase, which detoxifies S-RNase and consequently, allowing the pollen tube growth (Iwano and Takayama, 2012). Several biochemical models have been proposed to explain the mechanism underlying this system (Hua et al., 2008). Even though most of the models explain the compatibility as the result of preventing the access for S-RNases to the pollen tube cytoplasm, they diverge in the mechanism, generating two main alternatives. One model suggests the S-RNases degradation while the other proposes the compartmentalisation of them. (McClure et al., 2011).

Moreover, it has been described the existence of non-S-specific factors, which are present in both pollen and pistil, playing a role in this SI response. For instance Sli (Phumichai and Hosaka, 2006) and SBP1 (O'Brien et al., 2004) are examples of proteins that have been proposed as pollen modifiers. On the other hand, 120K (Hancock et al., 2005) and HT-B (Goldraij et al., 2006) are proteins indicated as putative pistil factors.

1.4.6.2 Self-incompatibility in *Papaveraceae*

SI in *Papaver* is gametophitically controlled, by a single, multiallelic locus (Franklin-Tong and Franklin, 1993, Lawrence et al., 1978). The current model with the mechanisms described so far will presented in the following sections.

1.4.6.2.1 Model for PrpS and PrsS interaction

The essential components for the *Papaver* SI systems are: the male component, PrpS (*Papaver roheas* pollen *S* gene) and the female component, PrsS (*Papaver roheas* stigma *S* gene). These components are encoded by a single locus with multiple haplotypes, each haplotype encodes both male (PrpS) and female (*PrsS*) determinants (*S*-determinants). Self PrpS-PrsS interaction triggers signalling to the actin cytoskeleton, culminating in programmed cell death (**Figure 1.7**).

Initial studies aiming to identified the female *S*-determinant at molecular level started during the late eighties. A major breakthrough in elucidating the underlying mechanisms of the *Papaver* SI response was the development of an *in vitro* bioassay which allow to trigger the SI response in pollen germinated *in vitro* treated with different purified stigmatic fractions (Franklin-Tong et al., 1988). This *in vitro* bioassay revealed the first candidates for the female S-determinant and at the same time the beginning of its characterisation (Franklin-Tong et al., 1989). Several years after, the cloning, sequencing and characterisation of the female *S*-determinant was finally possible (Foote et al., 1994). Further analysis confirmed that the female *S*-determinant (S-protein,

later called PrsS) is a secreted protein of ~ 15 kDa coded by a single copy gene, highly polymorphic with a stigma-specific expression. Finally, functional analysis using the recombinant PrsS, purified from *Escherichia coli*, showed biological activity inhibiting pollen growth *in vitro* in a S-specific manner, confirming PrsS as the female S-determinant in *Papaver* (Foote et al., 1994).

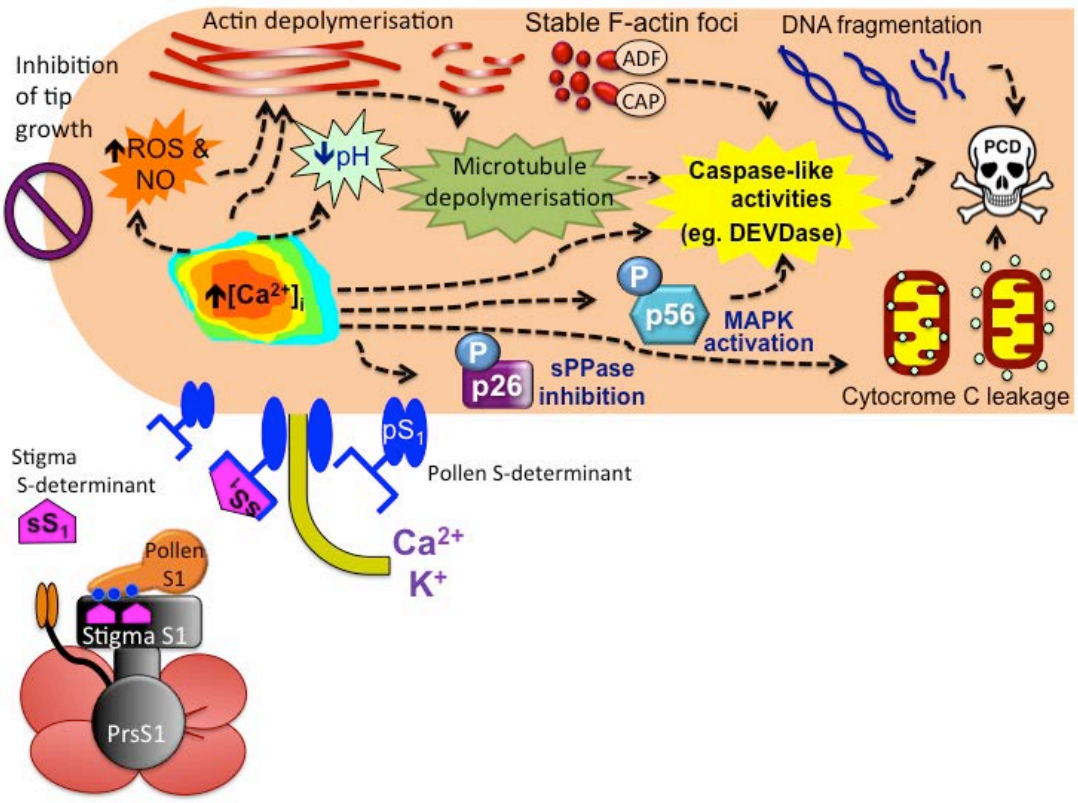

Figure 1.7. Schematic model of the SI response in *Papaver rhoeas*. The incompatible haplotype-specific interaction between stigmatic *S*-proteins (*e.g.* $PrsS_1$) and pollen *S*-receptors (*e.g.* PrpS1) induces a Ca^{2+} and K^+ influx in the cytoplasm of the pollen tube, triggering a signalling network, which arrest the pollen tube growth, and finally culminates in PCD. The events described so far participating in this signalling cascade are: cytosolic acidification, increase in ROS and NO species, sPPase inhibition and MAPK activation by phosphorylation, depolymerisation of actin and microtubule cytoskeleton leading to the formation of stable S-actin foci, activation of caspase-like activities and some particular evidence of PCD such as cytochrome C leakage and DNA fragmentation. "This figure has been adapted from the originally published in Biochemical Society Transactions. Eaves DJ, Flores-Ortiz C, Haque T, Lin Z, Teng N, Franklin-Tong VE. Self-incompatibility in *Papaver*: advances in integrating the signalling network. Biochemical Society Transactions. 2014; 42:370-6© copyright holder"

Identification and characterisation of the pollen *S*-determinant, PrpS, was achieved more than 10 years later. The transcript specifically expressed in the pollen during late anther development. This transcript encodes a ~20 kDa protein, encoded by a single-copy gene (Wheeler et al., 2009). Cloning of different alleles and sequence analysis revealed a high amino acid sequence divergence and no homology with other proteins (Wheeler et al., 2009). Moreover immunolocalisation analyses determined that PrpS localise in the pollen tube plasma membrane (Wheeler et al., 2009). Finally, functional analysis using knockdown lines of PrpS obtained by antisense oligonucleotide confirmed that PrpS is the male S-determinant in *Papaver* (Wheeler et al., 2009). Further analysis exploring putative structural topologies for PrpS and based on a 'topological homologue' have suggested that PrpS might be a Ca^{2+}-permeable channel (Wheeler et al., 2010). This topological homologue is a *Drosophila* protein, termed Flower, which has been described as a Ca^{2+}-permeable channel involved in the endocytosis of synaptic vesicles in neurons (Yao et al., 2009). Similar to PrpS, the Flower protein contains 3 or 4 transmembrane domains, and acidic amino acid residues in one of these transmembrane domains, which would form the pore and provide the channel selectivity (Yao et al., 2009). Interestingly, it has been demonstrated that the Flower protein is also involved in a cell-cell discrimination process, which leads to PCD of suboptimal cells among a population of growing cells (Rhiner et al., 2010).

Recently evidence obtained by means of whole-cell patch-clamp experiments of *Papaver* pollen, revealed that PrsS activates a nonspecific cation conductance in an S-allele-specific manner (Wu et al., 2011). These results confirmed that

the *Papaver* SI is a channel-mediated response, and even thought they did not confirm that PrpS was an ion/(Ca^{2+}) channel, it provided strong evidence supporting the current model.

In summary, the current model of the *Papaver* SI response has the characteristics previously described of a receptor-ligand interaction (see section 1.1), which allow the self/non-self recognition at the beginning of the *Papaver* fertilisation process. PrsS would act as a ligand, recognised by the plasma membrane receptor and Ca^{2+} channel, PrpS. PrpS-PrsS interaction is coupled to a Ca^{2+}-signalling pathway, whose targets and mechanism will be detailed in the following section.

Exploring the PrsS-PrpS interaction is a central aspect of this thesis. Particularly, try to determine the nature of PrpS as an ion channel. Further details of the aims of this thesis will be presented in section 1.5. The results exploring PrpS as a Ca^{2+} channel will be discussed and presented in Chapter 4.

1.4.6.2.2 The role of Ca^{2+} in *Papaver* SI

The first direct confirmation of Ca^{2+} involvement in *Papaver* SI, was investigated using confocal imaging by microinjecting pollen tubes with Ca^{2+}-sensitive dyes (Franklin-Tong et al., 1993b). Initially it was demonstrated that specifically after addition of incompatible stigma proteins fractions a transient increase in the level of $[Ca^{2+}]_i$ was induced followed by the inhibition of pollen tube growth (Franklin-Tong et al., 1993b), and could be mimicked by an artificially increasing [Ca^{2+}]i with caged Ca^{2+} (Franklin-Tong et al., 1993b). Later on, it was shown that this response was also triggered with the recombinant PrsS, which

indicated that special decorations of protein processing were not necessary (Franklin-Tong et al., 1995). Ratio imaging of $[Ca^{2+}]_i$ in *P. roheas* pollen, allowed quantification of the levels of $[Ca^{2+}]_i$ within the pollen tubes (Franklin-Tong et al., 1997). Exposure to incompatible S-protein resulted in rapid and dramatic alterations in Ca^{2+}_i levels. In the shank, variations levels increased above µM whereas in the tip a diminution of the tip-focused gradient was identified (Franklin-Tong et al., 1997). By means of using an ion-selective vibrating probe, it was established that the increase in the $[Ca^{2+}]$i were the result of a influx of Ca^{2+} from the extracellular medium (Franklin-Tong et al., 2002). As mentioned in previous section (1.4.6.2.3), patch-clamp experiments confirmed that the SI response is mediated by a cation channel (Wu et al., 2011). Therefore in the current model, this influx of Ca^{2+} would be mediated PrpS acting as a Ca^{2+} channel. Further details of the role of Ca^{2+} in *Papaver* SI will be presented in Chapter 4.

1.4.6.2.3 Phosphorylation in Poppy SI

In *Papaver*, protein extracts analyses revealed an S-specific increase in the phosphorylation of a 26-kD protein, termed p26 (Rudd et al., 1996). Further investigations revealed two inorganic pyrophosphatases, one cytosolic termed Pr-p26.1 and the other identified in the microsomal fraction, Pr-p26.2. Protein sequencing revealed a homology of p26.1 with the Family I sPPases (de Graaf et al., 2006). Two cDNAs sequences were cloned and expressed, Pr-p26.1a and Pr-p26.1b. Functional analysis confirmed sPPase activities revealed that

Ca^{2+} reduced its activity, describing a new mechanism for regulating sPPase activity in eukaryotes (de Graaf et al., 2006, Haque, 2015).

During the *Papaver* SI response a mitogen-activated protein kinase (MAPK) has been identified to be activated as result of phosphorylation (Tudor, 2009). Studies including in-gel kinase assays using substrate for MAPK, and specific antibodies, revealed that MAPKs were activated in a SI-specific manner (Rudd and Franklin-Tong, 2003). Further characterisation determined a 56 kDa protein, named p56, whose activation was Ca^{2+}-dependent and reached its peak of activation 10 min after SI induction (Rudd et al., 2003). Also it was established that inhibition of MAKP, prevented the decrease in viability as well as the activation of caspase-like activities (Li et al., 2007), which are key hallmarks of the *Papaver* SI response (**Figure 1.7**).

1.4.6.2.4 The role of actin during Poppy SI

Actin cytoskeleton plays a major role during pollen tube growth (section 1.4.1). In *Papaver*, untreated pollen growing *in vitro* showed well-structured actin filaments (F-actin) organised in bundles along the main axis of the pollen tube (**Figure 1.8.A**-**A.1**)**.** 5 min after SI induction F-actin exhibited alterations. The prominent bundles of F-actin started to disappear, so the F-actin mesh looked less organised (**Figure 1.8.B**-**B.1**). 60 min after SI induction, the F-actin arrangement has completely changed to F-actin foci forming a pattern speckles in the entire pollen tube (Geitmann et al., 2000) (**Figure 1.8.C**-**C.1**). Experiments *in vivo* exhibited similar alterations, providing the initial evidence of F-actin involved in the SI response (Geitmann et al., 2000). Quantification of the

fluorescent phalloidin bound to the actin, confirmed a significant reduction in the F-actin levels in pollen challenged with incompatible PrsS, demonstrating F-actin depolymerisation during SI response (Snowman et al., 2002) (**Figure 1.8**). Further details with the F-actin dynamics during the SI response will be presented in Chapter 5 (section 5.1)

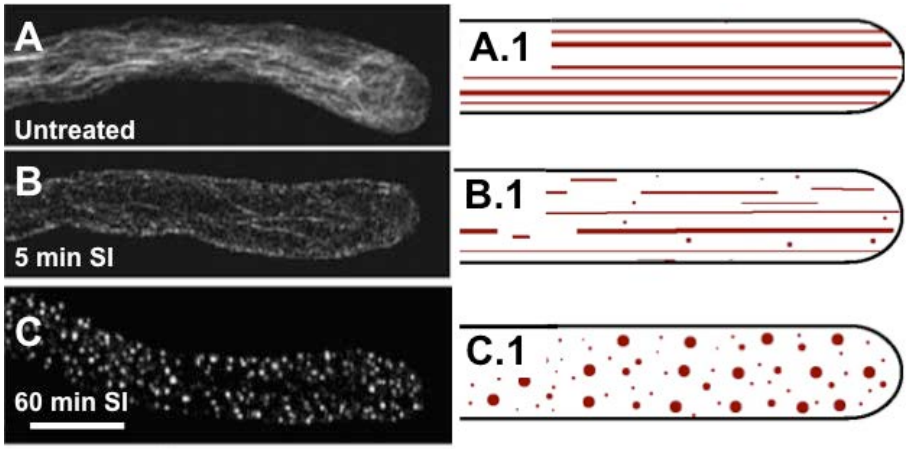

Figure 1.8 Rearrangements of the F-actin cytoskeleton during the *Papaver* SI response. F-actin cytoskeleton stained with Alexa-488-phalloidin **A:** Normal F-actin configuration in growing pollen. **A.1**: Diagram representing the F-actin filaments arrangement in a normal tube. Thick F-actin bundles oriented parallel to the longitudinal axis of the pollen tube. **B**: F-actin configuration a pollen tube 5 min after SI induction. **B.1**: Cartoon representing the F-actin arrangement during the early stages after SI induction. F-actin bundles started to disappear resulting in a diffuse appearance and a reduction in the intensity of the staining. **C**: F-actin cytoskeleton at later stage after SI induction. **C.1**: Diagram representing the lacking of F-actin arrangement in long filaments and predominantly organised in F-actin foci. Figure adapted from (Snowman et al., 2002).

Moreover, actin depolymerisation and punctate foci of F-actin were detected by increasing the $[Ca^{2+}]_i$ artificially, providing evidence to link the actin as a target for the Ca^{2+} signals present in the SI response (Snowman et al., 2002). Quantitative analysis established that the size of the punctate F-actin foci increases with time (Poulter et al., 2010). F-actin foci 3h after SI induction were highly stable structures. However F-actin foci showed to be dynamics structures, as its formation requires the assembly of new actin filaments rather than the aggregation of pre-existing filaments (Poulter et al., 2010).

Immunolocalisation analysis revealed two important actin-binding proteins (ABP) implicated in either the formation or stabilisation of the punctate actin structure: CAP and ADF. These proteins changed localisation under SI conditions, and both showed co-localisation with F-actin (Poulter et al., 2010). Further analyses by using Fourier transform ion cyclotron resonance mass spectrometry (FT-ICR-MS) showed a large amount of proteins involved in binding F-actin. Comparisons between SI and untreated samples, showed the main differences in 14-3-3 proteins, Ras-like proteins and heat shock proteins and chaperonines (Poulter et al., 2011, Haque, 2015).

Thomas et al (2006) determined that changes in actin filaments play a role initiating PCD (Thomas et al., 2006) (**Figure 1.4** and **Figure 1.7**). Details regarding this work as well as PCD as the final fate for incompatible pollen tube in *Papaver* will be presented section 1.4.6.2.5.

Microtubules have also been described as a target for the SI signals in *Papaver.* It was determined that microtubule depolymerisation occurred rapidly after SI induction (Poulter et al., 2008). Unlike actin, disruption of microtubule dynamics was not sufficient to trigger PCD. However, depolymerisation of both actin and microtubules are required to reach the normal levels of PCD in incompatible pollen tubes (Poulter et al., 2008).

1.4.6.2.5 Programmed Cell Death (PCD) in *Papaver* SI

Studies in *Papaver* showed that nuclear DNA fragmentation, a classic marker for PCD, occurred specifically by SI induction in incompatible pollen tubes (Jordan et al., 2000). Moreover, it was demonstrated that DNA fragmentation was inhibited by pretreatment with caspase-3 inhibitor I peptide, Ac-DEVD-CHO

(DEVD) (Thomas and Franklin-Tong, 2004). Several caspase-like activities are activated during Papaver SI response: DEVDase, VEIDase and LEVDase activities were detected using specific substrate and inhibitors (Bosch and Franklin-Tong, 2007, Poulter et al., 2011).

Thomas et al (2006) investigated whether alterations in actin dynamics can lead the pollen tubes into PCD. Pollen treated with jasplakinolide (Jasp), an actin-stabilising drug, alleviated PCD after exposures to incompatible PrsS. Additionally, artificial depolymerisation of actin filaments by treatments with LatB were enough to trigger PCD. Importantly, treatments with a caspase inhibitor (DEVD) could prevent DNA fragmentation induced by Jasp or LatB, confirming that the actin filament dynamics are sufficient to induce caspase-like activity and therefore PCD in *Papaver* pollen (Thomas et al., 2006) (**Figure 1.7**).

1.4.6.2.6 Cytosolic Acidification in Poppy SI

Cytosolic acidification as an early event of PCD it is well documented in animal cells (Gottlieb et al., 1995, Matsuyama et al., 2000). Bosch and Franklin-Tong (2007) monitored, using a pH-sensitive fluorophore, the intracellular cytosolic pH during *Papaver* SI. Normal growing pollen tubes exhibited pH values around 6.9, whereas SI induced pollen tubes showed a dramatically decrease reaching values of pH 5.5. In addition the determination of the pH dependence of the SI-induced caspase-like activities In *Papaver* showed maximal activity at pH 5.0 for DEVDase and VEIDase, with a significant decrease in the activity at values over pH 5.5 (Bosch and Franklin-Tong, 2007, Wilkins et al., 2015).

1.4.6.2.7 ROS and NO in poppy SI

Using live-cell imaging, rapid and transient increases in ROS and NO were visualised during the SI response in *Papaver* (Wilkins et al., 2011). Also, it was demonstrated that the ROS and NO increase is downstream of Ca^{2+} influx but upstream of SI-induced actin punctuate foci formation and activation of a DEVDase/caspase-3-like activity (Wilkins et al., 2015).

Figure 1.9 shows a diagram summarising the main events described in the previous section, which have been described participating in the *Papaver* SI response.

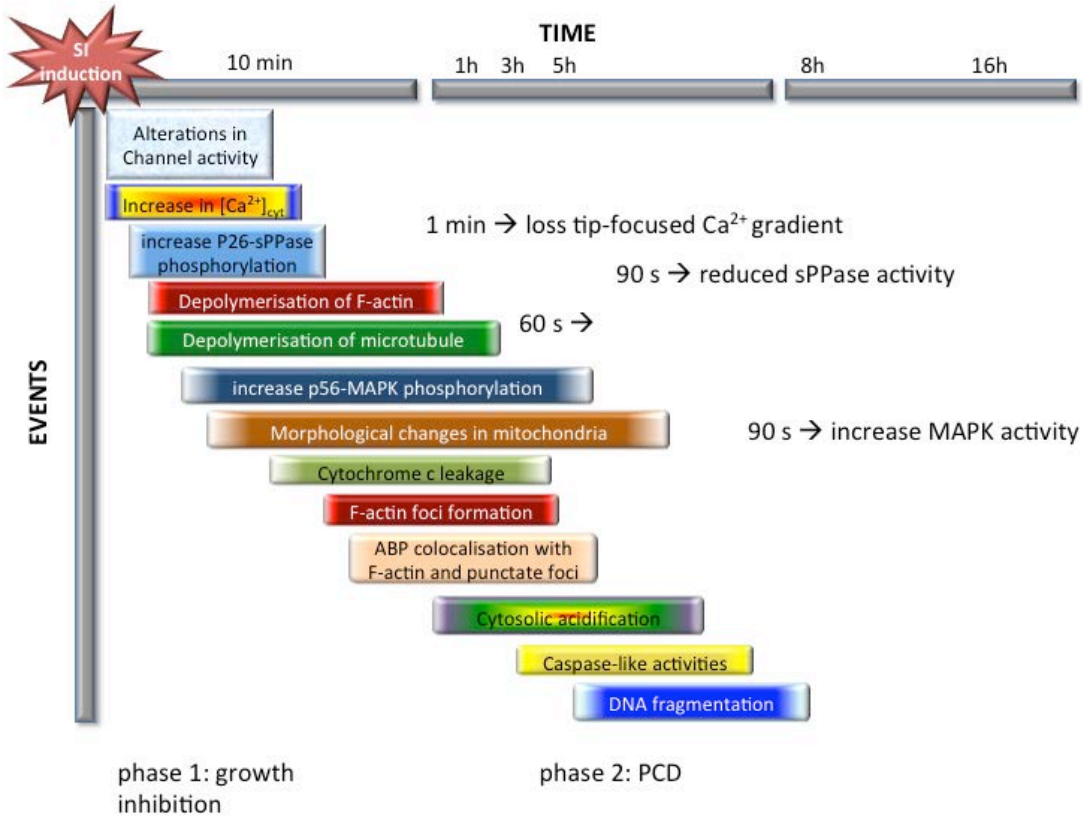

Figure 1.9. **Time-course events triggered during the *Papaver* SI response**. Early events can be clarified in a growth inhibition phase. This include increases in $[Ca^{2+}]_i$, cytosolic acidification, depolymerisation of actin filaments, inactivation of inorganic pyrophosphatases by phosphorylation. Subsequent events, which can be classified in a second phase are related with triggering PCD. This includes: F-actin foci formation, p56-MAP activation, cytochrome c leakage from the mitochondria into the cytosol, activation of caspases-like response, DNA fragmentation and morphological changes in the mitochondria.

1.4.7 Functional transfer of *Papaver* SI into *A. thaliana*

SI has the potential of improving the generation of F1 hybrid seeds (section 1.4.3). Transferring SI between plants using traditional crop plant breeding techniques relies on the sexual compatibility of the plants and/or some naturally occurring self-incompatible lines within a self-compatible species. So, to manipulate a SI system in terms of transferring it overcoming the sexual barrier, increases the biotechnological potential. Also, to go further in studying SI mechanism, the ability to transfer SI to a model self-fertile plant as *Arabidopsis thaliana* allows using a large number of genetic and molecular tools available for *Arabidopsis*.

Arabidopsis thaliana plants transformed with SRK-SCR genes from the self-incompatible crucifer *Arabidopsis lyrata* and *Capsella grandiflora* confer SI to *Arabidopsis thaliana* (Nasrallah et al., 2002, Nasrallah et al., 2004) However, even though the SI response is established in the transgenic *A. thaliana* SRK-SCR plants, the mechanism underlying the response might be different, as studies of the components involved in the SI cascade in Brassica species do not show the same participation in the SI response of transgenic *Arabidopsis thaliana* plants (Kitashiba et al., 2011).

The SI response in *Papaver* inhibits the pollen tube growth recruiting general and conserved mechanisms such cytoskeletal alterations and PCD mediating key signalling molecules such as Ca^{2+}. Because these mechanisms are not exclusively used for the SI response, and are conserved in highly diverged cells (section 1.1) it is plausible to attempt transferring the SI components from *P.*

rhoeas to other species, expecting that the same mechanisms involved in *Papaver* SI response are recruited in the transgenic organism.

Functional transfer of *Papaver* SI into *Arabidopsis* represents a major breakthrough, as they are highly diverged species. By means of an *in vitro* bioassay, it was previously demonstrated that the male *S-determinant* PrpS was functional when transferred into naturally self-compatible *Arabidopsis thaliana*. Pollen from *A. thaliana* plants expressing $PrpS_1$ (*$AtPpS_1$*) and $PrpS_3$ (*$AtPpS_3$*), exhibited remarkably similar alterations to the hallmark alterations and pathways described during the incompatible SI response in *Papaver* (de Graaf et al., 2012). Studies of the actin configuration, revealed actin alterations, particularly punctate actin foci formation, when PrsS was exposed to pollen expressing its cognate allelic combination (de Graaf et al., 2012). Viability assays of *$AtPpS_1$* and *$AtPpS_3$* pollen confirmed a reduction in viability after treatments with PrsS in a S-allele-specific manner (de Graaf et al., 2012). Moreover, *$AtPpS_1$* and *$AtPpS_3$* pollen pre-treated with the caspases inhibitor Ac-DEVD-CHO before the exposure to PrpS prevented cell death, indicating that PCD was involved in the reduction of viability, and also that PrsS was triggering a functional response, involving the same end mechanisms and molecular targets described in the *Papaver* SI. Additionally, treatments with recombinant $PrsS_1$ and $PrsS_3$ proteins specifically inhibited *$AtPpS_1$* and *$AtPpS_3$* respectively confirming that the response in *Arabidopsis* was allele-specific, another characteristic of the *Papaver* SI (de Graaf et al., 2012). These findings were the first strong evidence that PrpS was functional in highly diverted species (*Papaver rhoeas* and *A. thaliana* diverged ~140 million years ago) suggesting

that *Papaver* SI components can access and recruit signalling pathways of highly diverged cells (de Graaf et al., 2012).

Recently, the ultimate demonstration that PrpS and PrsS are functional in *Arabidopsis* was achieved by generating SI *A. thaliana in vivo* after transferring *Papaver* SI system (Lin, 2015). *Arabidopsis* stigmas expressing PrsS and pollinated with *Arabidopsis* pollen expressing PrpS, inhibited pollen tube growth in an allele-specific manner *in vivo* (Lin, 2015). Additionally, these pollinations resulted in shorter siliques and little to no seed production. Finally, co-transformation of self-compatible *A. thaliana* with PrpS and PrsS resulted in a self-incompatible *A. thaliana*, which exhibited normal growth and flowering in comparison with controls plants, but shorter siliques and no seed formation when they were left to set seeds naturally (Lin, 2015). This result represents a major breakthrough because despite functional SI has been successfully transferred between closely related species before, such as *Arabidopsis lyrata* (Nasrallah et al., 2002) and *Capsella grandiflora* (Boggs et al., 2009a) this is the first conclusive report where a SI system, in this case *Papaver* SI, can be functionally transferred into a highly diverged species *in vivo*. Moreover, this provides robust evidence suggesting that PrpS and PrsS can access and recruit components from the host cells to trigger a SI-like down stream response.

In the next section, the SI system from the Poaceae family will be presented. Barley belongs to this family, and is one of the species we attempted to transfer PrpS. Barley is self-compatible, and therefore this system is not functional, however it might represent valuable information for the generation of self-incompatible barley.

1.4.8 Self-incompatibility in Poaceae

Systematic studies regarding the SI *Poaceae* family - also called the true grasses - started several decades ago. (Lundqvist, 1954) carried out a detailed program of crosses aiming to elucidate the genetic bases behind mechanism of self-incompatibility in rye. Numerous studies during the past few decades have contributed in elucidating the mechanisms of SI in grasses (Heslop-Harrison, 1982). The current model comprises a multiallelic two-locus (*S* and *Z*) gametophytic system. Recognition of the same *S* and *Z* alleles during the pollen and pistil interaction triggers an incompatibility reaction and therefore fertilisation is prevented (Klaas et al., 2011, Yang et al., 2008).

Several attempts have been made to identify the *S* and *Z* components. Mapping studies have allowed locating the *S* and *Z* loci in *Lolium* (for a review, see Klass *et al* 2011) and *Hordeum bulbosum* (a SI wild relative of cultivated barley (Kakeda et al., 2008). However identification and confirmation of the genes remains unclear and only potential candidates are currently being analysed (Kakeda, 2009). **Table 1.2** summarises the main male and female components described for each SI system previously described.

Table 1.2. Identified S-determinant in different SI systems

FAMILIES	GENETIC CONTROL	MALE DETERMINANT	FEMALE DETERMINANT
Brassicaceae	SSI	SCR/SP11	SRK
Solanaceae, Rosaceae, Plantaginacear	GSI	SLF/SFB	S-RNase
Papaveraceae	GSI	PrpS	PrsS
Poaceae	GSI	?	?

1.5 Aims of this project

The work presented in this thesis addresses two main areas:

⇒ Important from an evolutionary perspective, we assessed whether PrpS could be functionally transferred into highly diverged heterologous systems. Based on the studies showing that some of the key mechanisms and cellular targets involved in the *Papaver* SI response are conserved and also present in diverged cells (section 1.1), and also the recent confirmation of functional transfer of *Papaver* SI into *A. thaliana* (section 1.4.7), it was decided to also attempt the functional transfer into *Saccharomyces cerevisiae* (Chapter 3), *Arabidopsis thaliana* protoplasts (Chapter 3), and HeLa cells (Chapter 4 and 5).

⇒ Relevant from a biotechnological perspective, we explored the feasibility of transfer *Papaver* SI into barley, aiming to exploit *Papaver* SI as a new tools for plant breeding. Converting self-compatible and economically relevant plant such as barley into a self-incompatible one has major potential for breeders reducing the costs in the production of F1 hybrids.

We aimed to evaluate the functionality of PrpS in these heterologous systems by monitoring the key hallmarks of the *Papaver* SI response. In HeLa cells, we evaluated: 1) alterations in the cytosolic Ca^{2+} levels ($[Ca^{2+}]_i$), 2) generation of currents through the plasma membrane, and 3) alterations in actin cytoskeleton. In barley, actin cytoskeleton in pollen grains, pollen tube growth and seed set were used as parameters to assess if SI was functional.

CHAPTER 2

MATERIALS AND METHODS

2.1 General Procedures

2.1.1 Production of recombinant *S*-proteins from *Escherichia coli*

Recombinant *S*-proteins were prepared as described in (Kakeda et al., 1998), according to procedures detailed in (Sambrook et al., 1989). This procedure was been systematically used in our laboratory and further details can be found in previous PhD thesis (Poulter, 2009).

2.1.2 *In vitro* SI bioassay

An *in vitro* SI bioassay has been developed and used in our laboratory for elucidating the cellular components and mechanisms underlying SI in *P. rhoeas* (Franklin-Tong et al., 1988, Foote et al., 1994). In this assay *Papaver* pollen is hydrated, germinated and grown *in vitro* in a glass Petri dish containing a suitable medium for its growth. The composition of this medium was 15.5% (w/v) sucrose, 0.01% (w/v) H_3BO_3, 0.001% (w/v) KNO_3, 0.01% (w/v) $Mg(NO_3)_2$•6H2O, 0.036% (w/v) $CaCl_2$ H_2O in Sterile Distilled Water (SDW). When solid medium was required, 1.2% (w/v) agarose was added. Pollen tubes were grown for 1 - 3 h before they were exposed to different treatments according to what is being evaluated. To trigger an *in vitro* SI response, recombinant PrsS (10 $\mu g.mL^{-1}$) is added to the pollen growing in the Petri dish, in an incompatible allelic combination.

Based on the previous assay, new SI bioassays were established in order to evaluate the functionality of the Poppy *S*-determinants in different cell types.

Different cells (*Arabidopsis* protoplasts, *Saccharomyces cerevisiae*, HeLa cells and barley pollen) expressing *PrpS* were exposed to recombinant incompatible PrsS, and then key features of the *Papaver* SI response were examined. These new bioassays have several variations depending on the evaluated trait and the cell type used as model. The modifications of each experimental design are detailed in the following sections: *Arabidopsis*, section 1.4.2; yeast, section 1.3.4; HeLa cells, section 1.4.4; barley, section 1.5.5.2.

2.1.3 Estimation of the protein concentration

Protein concentrations were determined by the colorimetric Bradford assay (Bradford, 1976) using Bio-Rad protein assay kit according to the manufacturer's instructions (Bio-Rad, UK).

2.2 Functional analysis of the Papaver *S*-determinants in *Arabidopsis thaliana* protoplasts

2.2.1 Seeds sterilisation and *in vitro* growth

Wild-type *A. thaliana* seeds were sterilised first with 1 mL of 70% (v/v) ethanol with a gentle shaking for two minutes and then washed with 1 mL of sterile distilled water (SDW). After 8 min incubation with 20% (v/v) of commercial bleach and 0.01% (v/v) Triton X-100, the seeds were washed four times (5 min) gentle shaking in 1 mL of SDW and a microfugation step to decant the seeds. Seeds were drained using a Whatman filter disk in a porcelain Buchner funnel

connected to a vacuum pump by means of a Kitasato flask. After dried on a laminar flow hood, seeds were sprinkled onto Murashige and Skoog plates (MS: 2.2 $g.L^{-1}$ MS powder, pH 5.6 - 5.8 and 1% (w/v) agar). Seeds were vernalised on plates at 4 °C for two days before transferring them to 22ºC.

2.2.2 Preparation and transfection of *Arabidopsis thaliana* leaf protoplasts.

Leaves from 3 weeks-old *Arabidopsis* seedlings were cut, transferred to a Petri dish and chopped with 10 mL of enzyme solution (0.5% w/v cellulose, 0.2% w/v macerozyme in K3 medium). After 3 h of incubation at room temperature in the dark, enzyme solution was removed without disturbing the leaves. The remaining tissue was gently swirled with 10 mL of K3 medium (1X B5 medium including vitamins, 5×10^{-4} $g.L^{-1}$ MES, 1×10^{-4} $g.L^{-1}$ myo-inositol, 0.25 $mg.L^{-1}$ NH_4NO_3, 0.75 $mg.L^{-1}$ $CaCl_2\bullet2H_2O$, 0.25 $mg.L^{-1}$ D-xylose, 0.4 mM sucrose, pH 5-6 - 5.8 adjusted with KOH) to release the protoplasts. protoplasts were filtered through a nylon filter into a sterile tube, which was left still for 1 h to allow the protoplasts to float to the top of the solution. The upper layer was transferred and gently mixed into a new tube containing 5 mL of K3 medium, before a new incubation of 40 min. Finally, the bottom layer was removed and the upper layer containing washed protoplasts was mixed with 1.5 - 5 mL of suspension solution (0.4 M mannitol, 20 mM $CaCl_2\bullet2H_2O$, 5 mM MES and pH 5.7).

For the protoplasts transformation, 5-25 µg of plasmid DNA were mixed with 250 µL of suspended protoplasts. Equal volume (DNA plus protoplasts) of PEG solution (250 - 275 µL) was added and gently mixed. After 30 min of incubation

at room temperature, 2 mL of K3 were added and incubated overnight at room temperature in the dark. Transient expression of GFP was evaluated by one and two days after transfection.

2.2.3 Genetic constructs for *A. thaliana* protoplasts transformation

A suitable genetic construct used for functional analysis of $PrpS_1$ in *Arabidopsis* somatic cells was generated and provided by Dr Javier Juarez-Diaz. Details in **Figure 2.1**

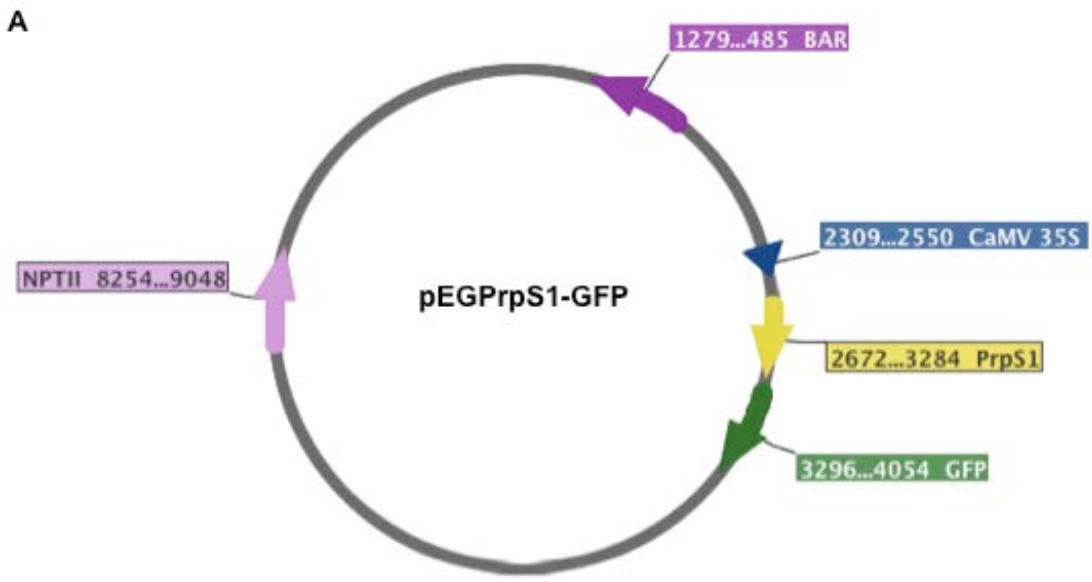

Figure 2.1 Genetic construct to assay the functionality of $PrpS_1$ in *Arabidopsis* leaf protoplasts. *$PrpS_1$* fused to GFP was cloned into the vector pEarlyGate103. Thus, *$PrpS_1$-GFP* was driven by the strong constitutive promoter Cauliflower mosaic virus35S RNA (CaMV35S), and transgenic plants selection based on the Basta herbicide resistance gene (BAR).

2.2.4 *In vitro* SI bioassay for *Arabidopsis thaliana* protoplasts

The treatments started with 200 µL of transformed protoplast. SI was induced by adding recombinant S proteins at a final concentration of 20 µg.mL^{-1}. For the sample with the caspase-3 inhibitor pretreatment, protoplasts were incubated with 100 µM of Ac-DEVD-CHO at 23°C for 1 h in dark. Viability assays were carried out 24 hours after exposure to PrsS using 0.05% Evans Blue staining as described in (Vatovec, 2012).

2.3 Functional analysis of the Papaver *S*-determinants in *Saccharomyces cerevisiae*

2.3.1 Standard procedures for yeast maintenance

Standards procedures for yeast culturing and handling were carried out according to the instruction manual of pYest-Dest52 Vector (Invitrogen) and the Yeast Protocols Handbook (Clontech).

2.3.2 Genetic constructs and yeast transformation

Suitable genetic constructs used for functional analysis of $PrpS_1$ in *Saccharomyces cerevisiae* were generated and provided by Dr Javier Juarez-Diaz. Details in **Figure 2.2.**

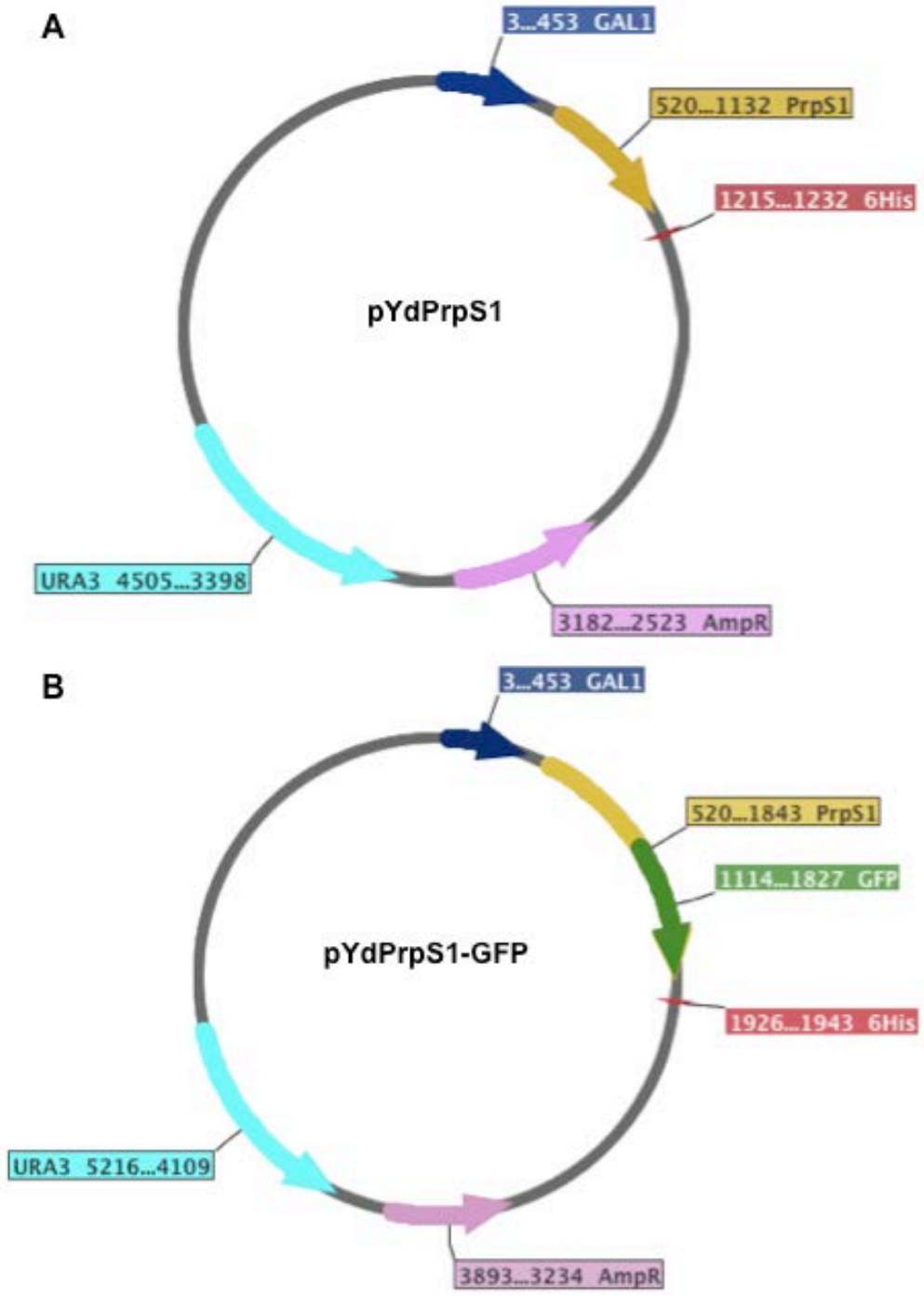

Figure 2.2 Genetic constructs to assay the functionality of $PrpS_1$ in the yeast *Saccharomyces cerevisiae*. *$PrpS_1$* alone and also *$PrpS_1$* fused to GFP were cloned into the vector pYES-DEST52 ($pYdPrpS_1$ and $pYdPrpS_1$-GFP respectively). *$PrpS_1$* and *$PrpS_1$-GFP* were driven by the yeast *GAL1* promoter for high-level, galactose-inducible protein expression. This vector also provides a 6xHis tag for detection and purification. It has *URA3* auxotrophic marker for selection of yeast transformants, and ampicillin resistance for selection in *E. coli.*

The yeast host strain selected was the *S. cerevisiae* IN*V*Sc1 (*MATa his3D1 leu2 trp1-289 ura3-52 MAT his3D1 leu2 trp1-289 ura3-52*), which is a diploid strain suitable for protein expression. IN*V*Sc1 requires uracil (Ura) to grow (Ura auxotroph), and therefore, it is compatible with the *URA3* auxotrophic marker in pYEST-DEST52, which allows the selection of yeast transformants in uracil-deficient medium.

Transformation procedure was carried out according to the LiAc (Lithium Acetate) method and the Yeastmaker™ Carrier DNA (Clontech) following the manufacturer instructions. Briefly, IN*V*Sc1 competent were prepared using a LiAc solution. Then, competent cells were incubated with a mix of the genetic construct to be transformed and the carrier DNA. After 30 min of incubation at 30ºC and shaking at 200 rpm, DMSO was added and the cells were heated shocked for 15 min at 4ºC, allowing the DNA to enter the cells. The cells were plated on appropriate SD medium (yeast nitrogen base without amino acids, yeast synthetic drop-out medium supplements without uracil, 2% (w/v) D-(+)-Raffinose, 2% (w/v) agar and pH 5.8). Finally, the plates were incubated at 30ºC during 3 days before the colonies appeared.

2.3.3 Protein extraction and western blot analysis for yeast

Protein extractions were carried out following the procedure detailed in the manufacturer manual of pYESDET52 vector (Invitrogen) based in the use of acid-washed glass beads to prepare the cell lysates.

Western blot analyses were carried out according to standard procedures using BioRad kit as described in detail in (Vatovec, 2012). SDS-PAGE were based in

protocol initially described by (Laemmli, 1970) and western blot in (Towbin et al., 1979). Briefly, 25 µm of total protein loaded in a 12.5% SDS-polyacrylamide gel and then proteins were transferred into a nitrocellulose membrane (Hybond-C, Amersham). The membrane was incubated with primary antibody, a monoclonal anti-GFP raised in mouse in a titration of 1:250 (Santa Cruz Biotechnology). The second antibody was a horseradish peroxidase-conjugated anti-mouse used in a titration of 1:1000. For the protein immunodetection, a protocol based in (Yakunin and Hallenbeck, 1998) was carried out using the reagents from GE Health Life Sciences.

2.3.4 *In vitro* SI bioassay for yeast

PrsS proteins were not dialysed, as it was determined that PrsS buffer (50mM Tris, 100mM NaCl and 2mM EDTA) did not have an effect in the growth curve.
Induction of PrpS expression was initiated by adding galactose to a culture at the start of the exponential phase. 3 - 4 h after the galactose induction, the SI treatment was started by adding PrsS (20 $\mu g.mL^{-1}$), and the absorbance at 600 nm was monitored at suitable time points. All the experiments were carried out at 30ºC (**Figure 2.3**). Dilutions of the culture were made to obtain Absorbance values between 0.3 and 0.9. Additionally, serial dilutions were carried out to obtain a number of colonies between 50 and 300 for the Colony-Forming Unit (CFU) counting.

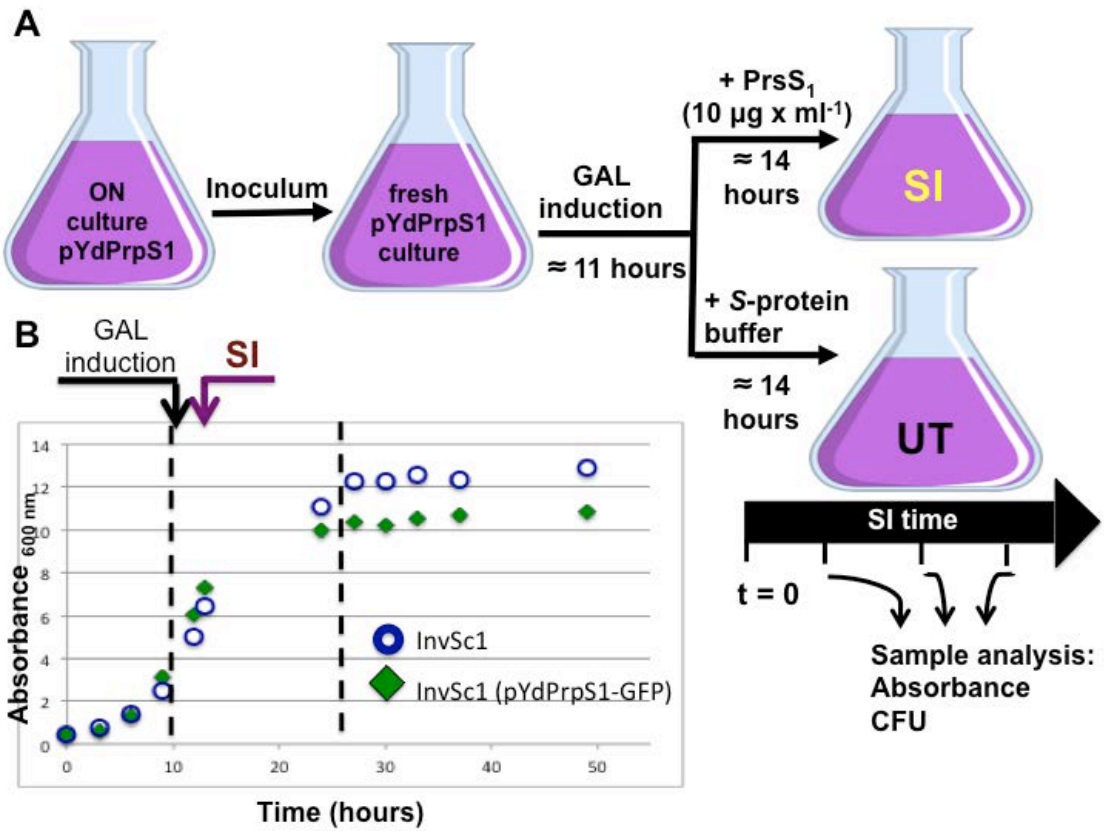

Figure 2.3 Summary of the experimental design to assess functional SI in *Saccharomyces cerevisiae.* A) Cartoon with the main steps and key time points during the SI bioassay of *S. cerevisiae*. An inoculum from a saturated overnight culture of InvSc1 transformed with pYdPrpS$_1$ or pYdPrpS$_1$-GFP was used to start a fresh sub-culture using Raffinose as a carbon source (Raffinose does not induce or repress GAL1 promoter). Approximately 10 - 11 hours after, GAL1 promoter was induced by adding 2% (w/v) galactose. One or two hours after the induction, incompatible PrsS$_1$ (20 µg.mL^{-1}) was added to the culture to evaluate SI. Finally, samples were taken at different time point to measure putative differences between the number of cells in the cultures challenged with PrsS (SI) in comparison with the control cultures treated with PrsS buffer (UT).

B) Typical phases of a cellular culture; lag phase during the first 10 hours, exponential phase between 11 and 25 hours and stationary phase over 25 hours. Despite InvSc1 transformed with pYdPrpS$_1$-GFP did not reach the same Absorbance during the stationary phase in comparison with InvSc1 wild type (suggesting a detrimental effect of the expression of PrpS$_1$-GFP), the time corresponding to the exponential phase, where the SI treatment was carried out, was the same for both cultures.

2.4 Functional analysis of the PrpS in mammalian HeLa cells.

2.4.1 Standard procedures for HeLa cells maintenance

Cells were grown under standard conditions: 37°C, 5% CO_2 in DMEM supplemented with 10% (v/v) FBS (Gibco), 1% penicillin/streptomycin mix (Sigma), and 1% (v/v) glutamine (Sigma).

Passing cell or sub-cultured procedure was carried out when culture confluence was about 75 - 80 according with standards procedures. The typical dilution for a 75-cm2 flask was 1:10 with a final volume of 10 - 12 mL. For a 6-well plate, the dilution considered was ~ 1: 2.7 in a final volume of 2 - 3 mL.

To freeze down cells, a 175-cm2 confluent flask was treated with 2 mL of trypsin. After 2 - 5 min incubation at 37 °C, 8 mL of fresh DMEM were added and the mixture transferred to a centrifuge tube. Cells were spin down at 80 - 100 x g for 5 minutes. The supernatant was removed and the pellet resuspended in 2 mL of freeze-down media (10% DMSO, 90% FBS). Finally, aliquots of 1 mL were transferred into cryogenic vials, and cells frozen down at -80 °C. For long-term storage it is recommended to transfer the cells into liquid nitrogen.

Frozen cells were thawed in a 37 °C bath and 1 mL vials were transferred into a 10 -12 mL of pre-warmed supplemented DMEM.

2.4.2 Genetic constructs

Transient transfected lines were generated with pEGFP-PrpS (**Figure 2.4.A**). For functional analysis, stable transfected lines were transfected with $PrpS_1$ in both, C-terminal (**Figure 2.4.C**) and N-terminal (**Figure 2.4.D**) respect to mCherry, generating HeLa-C-$PrpS_1$ and HeLa-N-$PrpS_1$ respectively. Cell line of HeLa transfected with pmCherryN1 (empty vector) (**Figure 2.4.B**) was used as a negative control of cells expressing mCherry without the gene of interest, HeLa-mCh.

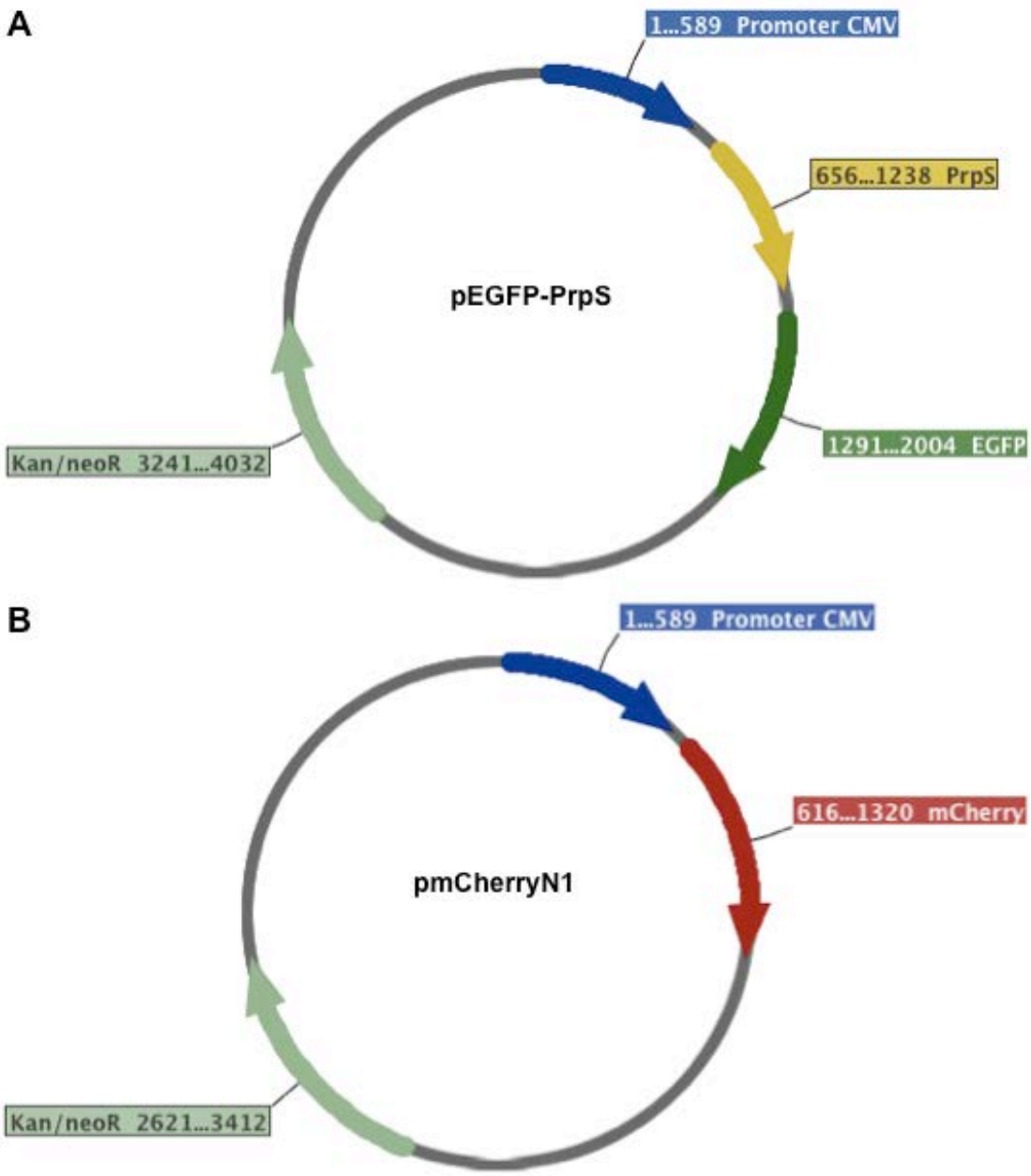
A
1...589 Promoter CMV
656...1238 PrpS
pEGFP-PrpS
1291...2004 EGFP
Kan/neoR 3241...4032
B
1...589 Promoter CMV
616...1320 mCherry
pmCherryN1
Kan/neoR 2621...3412

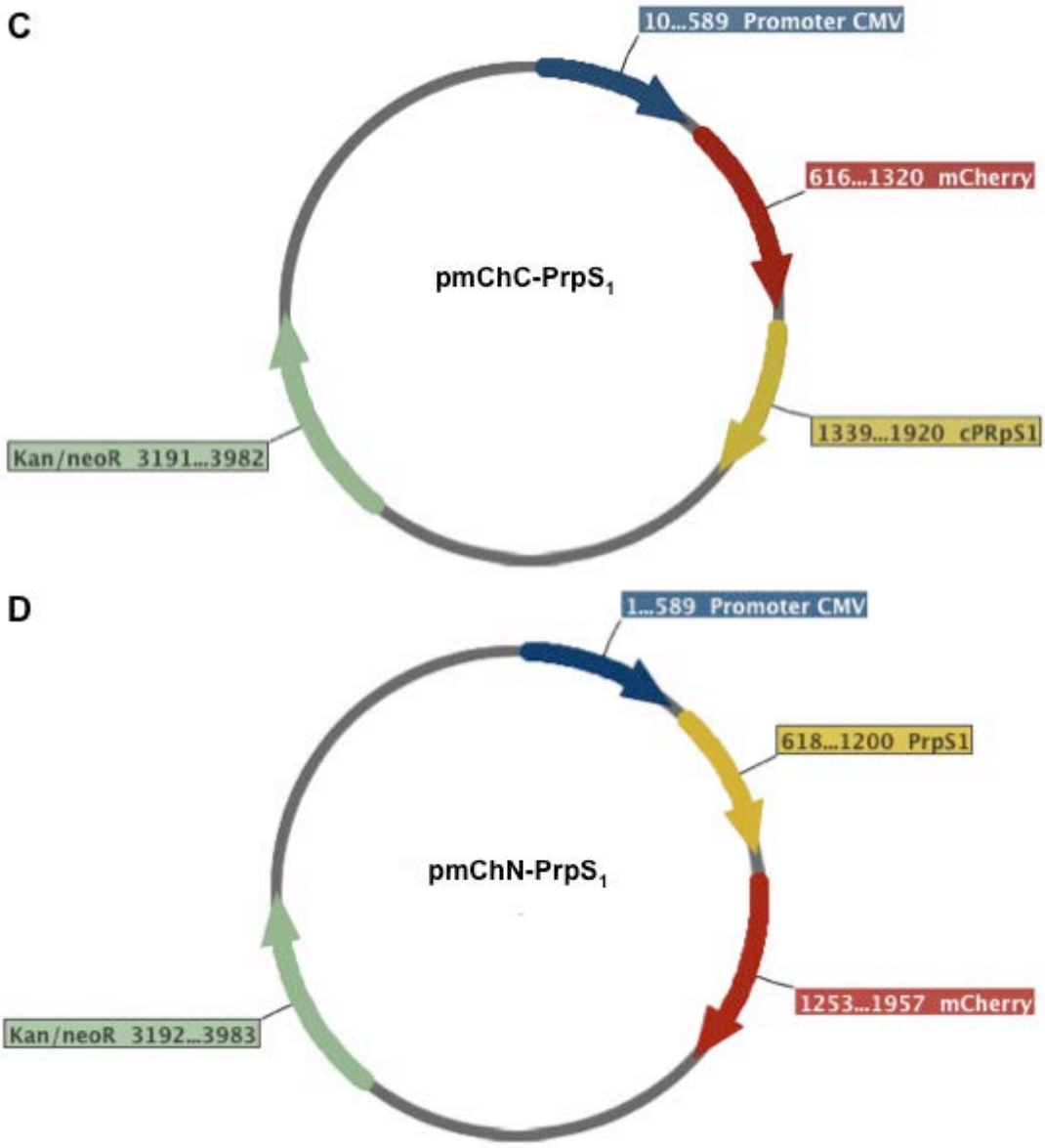

Figure 2.4 Genetic constructs to assay the functionality of *S*-determinants in HeLa cells. A) pEGFP-N1 is a 4.7 kb plasmid for expression in mammalian cells. It has the constitutive promoter cytomegalovirus (CMV) and provides Kanamycin resistance for bacterial selection and Neomycin as a selectable marker for mammalian cells. Three alleles *PrpS$_1$*, *PrpS$_3$* and alleles were independently cloned into pEGFP was termed pEGFP-PrpS$_1$ pEGFP-PrpS$_3$ and pEGFP- respectively. **B)** pmCherry-C1 is a 4.7 kb plasmid for expression in mammalian cells. It has the constitutive promoter cytomegalovirus (CMV) and mCherry as fusion tag protein. It provides Kanamycin resistance for bacterial selection and Neomycin as a selectable marker for mammalian cells. HeLa cells transfected with pmCherry-C1 were termed HeLa-mCh. **C)** Construct pmChC-PrpS$_1$ corresponds to *PrpS$_1$* cloned into pmCherry-C1. HeLa cells transfected with pmChC-PrpS$_1$ were termed HeLa-C-PrpS$_1$. **D)** Construct pmChN-PrpS$_1$ corresponds to PrpS$_1$ cloned into pmCherry-N1. HeLa cells transfected with pmChN-PrpS$_1$ were termed HeLa-N-PrpS$_1$. These constructs were generated and provided by Dr Andrew Beacham.

2.4.3 Standardisation and Optimisation of Cell Transfection

Three different parameters were assessed to the genetic transformations: 1) transfections reagents (Lipofectamine and GeneJuice), 2) The effect of the amount of DNA on the protein expression, and 3) the orientation (C- or N-terminal) of the fused tag protein respect to PrpS was also assessed. Constructs containing mCherry as a fusion tag (pmChC-$PrpS_1$ and pmChC-$PrpS_1$) were used to obtain the stably transfected cell lines used for the functional analysis of PrpS-mCh.

2.4.3.1 Transient transfections

Transfection efficiency was evaluated by counting the number of cells emitting fluorescence (GFP or mCherry) out of the total number of cells counted. Different transfection reagents have different transforming efficiencies depending on the constructs and the cells used for the transfection. Positively transfected cells exhibiting GFP emission were obtained with both transfection reagents. However, cells transfected with GeneJuice showed a more uniform expression pattern than cells transfected with Lipofectamine (data not shown). Therefore, GeneJuice was used to carry out the experiments described in this thesis.

For transfections with Lipofectamine 2000 (Invitrogen): 100 µL of serum-free DMEM were mixed separately with 0.1 - 10 µg of DNA, and 8 µL of Lipofectamine. Then, both mixes were combined and the 200 µL mix was incubated at room temperature for 5 minutes. Finally, the mixture was added to

a 6 well plate with 60% - 80% confluent cells and gently mixed. Reporter gene fluorescence was checked after 1 -2 days.

For the transfections using GeneJuice (Novagen): 100 µL of serum-free DMEM were mixed with 3µL of GeneJuice. After 5 minutes of incubation at room temperature, 0.1 - 10 µg of DNA was added to the GeneJuice serum-free mixture and mixed gently and incubated for 10 minutes at room temperature. The mixture was added to a 6 well plate with 60% - 80% confluent cells. After 2-8 hours, the transfection mixture was removed and replaced with supplemented DMEM. Reporter gene fluorescence was checked after 1 -2 days by microscopic analysis.

Transfection with constructs containing the three different alleles; $PrpS_1$, $PrpS_3$ and $PrpS_8$ fused to GFP (pEGFP-$PrpS_1$, pEGFP-$PrpS_3$, pEGFP-$PrpS_8$, respectively) were evaluated. Cells exhibiting GFP fluorescence (details in section 1.6) after transfections with pEGFP-$PrpS_8$ showed the lowest transformation efficiency (~ 15%), and transfections with pEGFP-$PrpS_3$ showed the highest efficiency (~ 40%). Transfections with pEGFP-$PrpS_1$ showed an efficiency ~ 30%.

Additionally, transfections were assessed with 0.25, 0.5 and 1 µg of pEGFP-$PrpS_1$ and pEGFP-$PrpS_8$ constructs. Consistent, with the previous result, pEGFP-$PrpS_8$ showed lower transfection efficiency in comparison with pEGFP-$PrpS_1$, but there was no improvement in the transfection efficiencies. However, the values obtained (over 30%) were high enough to carry on with the experiments to obtain stable-transfected lines.

2.4.3.2 Stable transfections

The protocol to obtain stable transfected lines begins with the same procedure described previously for transient transfections (section 2.4.3.1).

To evaluate the effect of the amount of DNA on transfection efficiency 0.1 and 1 µg of DNA were used. 1 µg of DNA exhibited the higher transformation efficiency (40%), whereas transfections using 0.1 µg of DNA exhibited 5% efficiency. When evaluating the mCherry tag positioning (N- or C-terminal with respect to mCherry), transfection efficiencies obtained using 1 µg of pmChN-$Prps_1$ and 1 µg pmChC-$PrpS_1$ were 30% for both constructs (**Figure 2.5**), indicating that the positioning of the mCherry tag did not have an effect on the transfection efficiency. **Figure 2.5.A** shows the mCherry emission from 16 cells transfected with pmChN-$PrpS_1$. **Figure 2.5.D** shows the mCherry emission from 12 cells transfected with pmChC-$PrpS_1$. Bright field panels are shown in **Figure 2.5** panels **C** and **E** respectively. The total number of cell in the field (needed to estimate the transfection efficiency), was obtained by overexposing the field in order to visualised all the cells, transfected and non-transfected. **Figure 2.5** panels **C** and **F** show these overexposed images. These are representative images of two independent transfections and three different fields for each transfection.

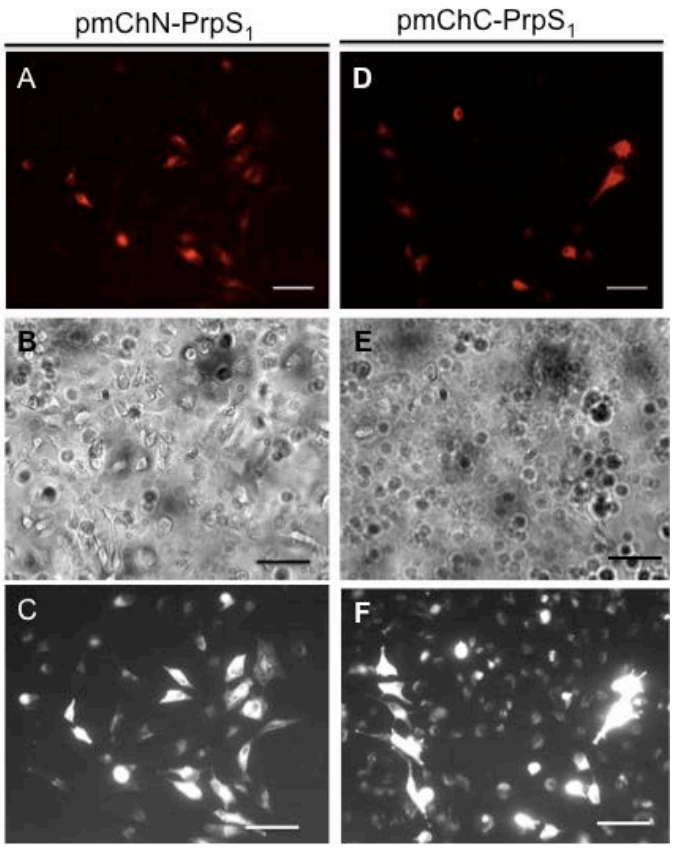

Figure 2.5 Evaluation of the effect of the mCherry tag positioning (N- and C- terminal) respect to $PrpS_1$ on transfection efficiency. A: Red fluorescence of HeLa cells transfected with pmChN-$PrpS_1$. Bright field is shown in panel **B**. Panel **C** shows the overexposed image. D: red fluorescence of HeLa cells transfected with pmChC-$PrpS_1$. Bright field is shown in panel **E**, and overexposed image in panel **F**. Images were taken using TRITC filters: excitation 550 nm, emission 572 nm. Scale bar: 50 μm

Once the transfections with the mCherry constructs were optimised, the procedure to obtain stable transfected cells was carried out. Integration of the DNA into the genomic DNA of the host is required to obtain stable transfected lines. Thus, after a transient transfection and in order to select the cells that have integrated the foreign DNA into its genomic DNA, it is necessary to expose the cells to an antibiotic pressure for several weeks. Both pmChN and pmChC vectors contain the marker gene neomycin phosphotransferase, which

confers resistance to G418 antibiotic (**Figure 2.4.C-D**). Therefore this antibiotic was used to select stable transfected lines.

The initial transient transfection was carried out as described previously in the section 2.4.3.1. After 1 - 2 days, the media was replaced by DMEM containing 600 $\mu g.mL^{-1}$ of G418 antibiotic. Media containing antibiotic was replaced every 3 - 4 days and after 2 weeks the first isolated colonies were observed. One week later, after the colonies reached ~2 mm diameter, they were picked and transferred individually to a 6 well plate. At this stage antibiotic concentration was reduced to 400 $\mu g.mL^{-1}$. Once the colony started to proliferate, the cells were checked for mCherry expression by fluorescence microscopy.

Once the colony had reached 80% confluence, the cells were transferred to a 10 -12 mL culture in order to carry on with the proliferation allowing the production of enough cells to freeze an aliquot, and carry on with the experiments for the functional analysis.

2.4.4 Live cell calcium imaging: monitoring alterations in $[Ca^{2+}]_i$ during SI response

Live cell calcium imaging was used to monitor $[Ca^{2+}]_i$ levels of the cells. Modifications to the SI bioassay protocol described in section 2.1.2 were made in order to optimise this experimental design. These experiments were designed and carried in collaboration with Dr Steve Publicover from the University of Birmingham. With the guidance of Dr Publicover and base on some previous studies using a similar approach (Thomas et al., 2000, Wyrsch et al., 2013) a suitable experimental design was optimised.

HeLa-C-PrpS$_1$ cells were grown in a multi well plate containing sterilised coverslips (no bigger than 25 mm^2) placed on the bottom of the well so that the cells grew in a monolayer over the coverslip. Then coverslip was transferred and mounted onto a perfusion chamber. The cells were labelled with Fluo-4 (1-5 mM), and incubated at 37°C for 35 - 40 minutes. Afterwards, the cells were washed and the chamber was positioned on the microscope (Nikon Eclipse). The arrangement of the perfusion chamber and the microscope stage plate insert is shown in the **Figure 2.6**. Fluorescence images were taken using FITC filter: excitation 492 nm, emission 519 nm. The collected images were analysed using the Andor iQ3 software.

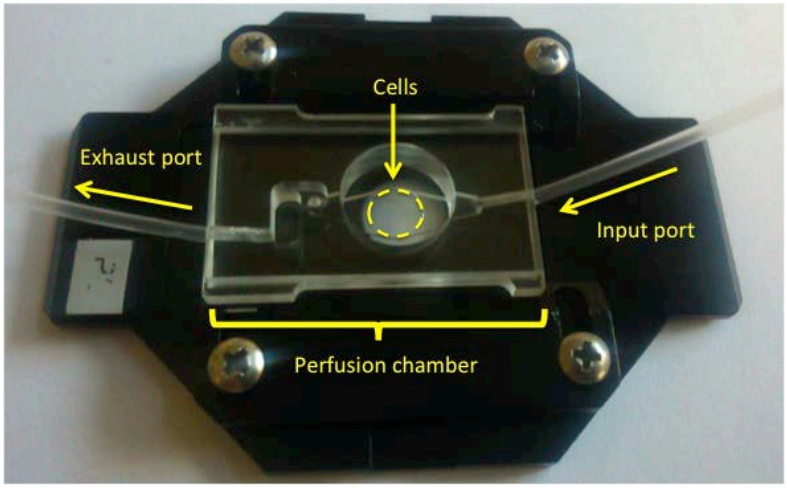

Figure 2.6 Set up for Live-cell calcium imaging. The input port was connected to a syringe tube, which acts as reservoir, containing the solution that will go through the chamber. The exhaust port was connected to the waste container.

The experiments were started by adding FluoBrite for several minutes at a flow rate of 1.5 mL.min^{-1}. For the different treatments, the solution on the reservoir was replaced. The timing and order for exposing the cells to the different treatments are indicated in the results section corresponding to each

experiment. $PrsS_1$ and $PrsS_8$ were added in a concentration of 20 µg.mL^{-1}. Histamine (100 µM) was used to increase $[Ca^{2+}]_i$.

2.4.4.1 Buffer exchange of PrsS

Recombinant PrsS purified from *E. coli* was exchanged to DMEM or FluoroBrite DMEM media (Gibco®) using Zeba™ Spin Desalting Columns, 7K MWCO (Thermo) following the manufacturer's instructions. Concentration of PrsS was estimated as described in section 2.1.3.

2.4.5 Assessing the electrophysiological activity in HeLa cells during the SI response

Patch clamp procedure was used to measure the electrophysiological activity of the cells during SI response. Variations to the SI bioassay protocol described in section 2.1.2 were necessary for each experimental approach. These experiments designed and carried out in collaboration with Dr Steve Publicover (University of Birmingham, UK) and Dr H. Rheinallt Parri and Dr Robert Sims (University of Aston, Birmingham UK).

HeLa-$PrpS_1$ and HeLa-mCh (empty vector) cells (**Table 4.1**) were grown in a monolayer on sterilised coverslip (9mm diameter, thickness No 1). The coverslip were placed in a perfusion chamber and visualised in an Eclipse FN1 microscope (Nikon, Japan). The arrangement for the path-clamp in these cells is shown in **Figure 2.7.**

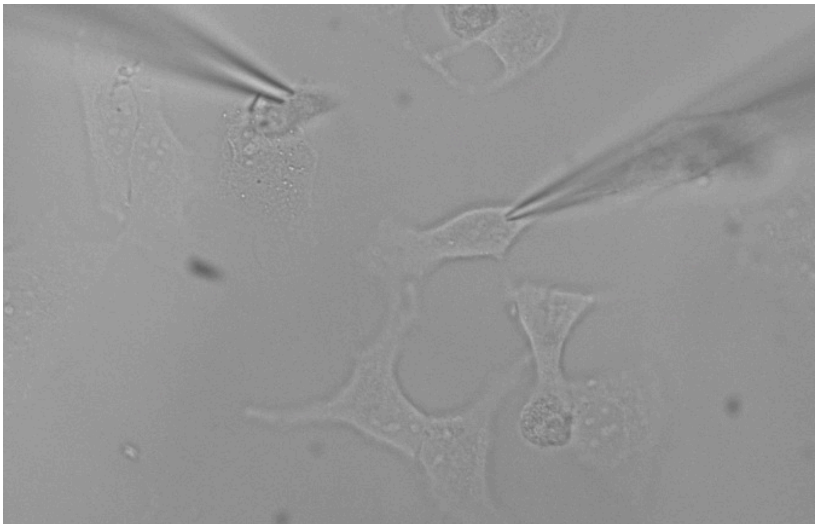

Figure 2.7. Bright field image of the setup used for patch-clamp experiments. The chamber and manipulators were mounted on a moveable top plate platform (MP MTP-01, Scientifica, UK), and the chamber was perfused at 1-2 mL.min-1 with an isotonic, physiologically-representative bath solution comprising: NaCl (126 mM), $NaHCO_3$ (26 mM), KCl (2.5 mM), KH_2PO_4 (1.25 mM), $MgSO_4$ (1 mM), $CaCl_2$ (2 mM), glucose (10 mM), bubbled with 95:5 O_2:CO_2. Recording electrodes and injection micropipettes were prepared with a Model P-97 micropipette puller (Sutter Instruments, USA). Recording electrodes contained a solution comprising: $KMeSO_4$ (120 mM), HEPES (10 mM), Na_2ATP (4 mM), GTP (0.5 mM), EGTA (0.1 mM), adjusted to pH 7.3 with KOH and osmolarity 280-290 mOsm. They had resistance 4-5.5 MΩ in the bath solution, and whole cell patches were formed on healthy cell bodies. Healthy cells were identified visually under bright field as firmly attached to the coverslip, with smooth, well-defined edges, and lack of blebbing. Patched cells were voltage clamped at -70 mV unless otherwise stated, and data where the series resistance changed by >20% or where the holding current at -70 mV became more negative than -500 pA were excluded. A micropipette containing either solution was placed at a distance of 50-200 µm, with tip (~10-20 µm diameter) directed at the recording cell. Solution was pressure injected from this micropipette towards the cell and care was taken not to mechanically disturb the target cell with excessive flow.

Currents were recorded using an Axon Instruments Multiclamp 700B amplifier, digitised with a Digitdata 1322A, and acquired and analysed online using Clampex 9.2 software (all Molecular Devices, USA). Additional offline analysis was through Clampfit 9.2 software (Molecular Devices, USA), and SigmaPlot (Systat Software Inc., USA).

2.4.6 Time-lapse experiments

For the time time-lapse experiments, cells were imaged using bright field microscopy. Images were taken every 5 minutes during 7 - 8 hours in a 24-well plate. For the SI treatments, cells were exposed to 20 $\mu g.mL^{-1}$ of PrsS in FluoroBrite DMEM.

2.4.7 Study of the actin configuration in HeLa cells during the SI response

F-actin was stained using Alexa Fluor® 488 phalloidin (Thermo) and then examined under the microscope. Phalloidin binds selectively to F-actin and Alexa Fluor® 488 provides green fluorescence (excitation/emission 495/518 nm) for visualisation.

For the SI bioassay, HeLa-C-$PrpS_1$, HeLa-mCh and untransfected HeLa cells (Hela-wt) were grown as described in section 2.4.1. SI was triggered by adding 20 $\mu g.mL^{-1}$ during 3 h unless otherwise stated in the results section for a particular experiment.

2.4.7.1 Fixation and actin staining and of HeLa cells attached to a coverslip

Cells were washed with PBS, and then fixed with PFA 4% (w/v) for 5 minutes. After 3 washes with PBS, the cells were permeabilised with 0.1% (v/v) Triton X-100 in PBS. After three washes with PBS the cells were stained with 488-

phalloidin during 40 minutes, protected from light and at room temperature. Finally, three additional washes with PBS were carried out before mounting the coverslips over a drop of ProLong® anti-fade reagent (Thermo) onto a slide.

2.4.7.2 Fixation and F-actin staining of “floaters” HeLa cells

Based on the procedure described above (2.4.6.1) but carried out in a microfuge tube and with less wash steps, in order to maximise the number of cells in the sample, F-actin of floater cells was stained. Cells were recovered by pipetting off the media after treatment and washed once with PBS. cells were fixed with 4% PFA during 5 minutes. Afterwards, the cells were centrifuged 4 minutes at 100 x g, the supernatant was removed and cells permeabilised by adding 10 µL of 0.1% (v/v) Triton X-100 in PBS. After one wash with PBS, cells were stained with 488-phalloidin during 40 minutes at room temperature. After one final wash, the sample was mounted onto a slide using mounting media ProLong®. For every wash, cells were centrifuged 4 minutes at 100 • g and resuspended in 20 µL, except for the last wash where 10 µL were used to resuspended the cells

2.4.8 Quantification of floaters cells

Floating cells were collected by pipetting off the media after 3h of treatment, plus one wash with PBS. Next, cells were centrifuged during 4 minutes at 100.g and resuspended in 10 µL of PBS. Then, an aliquot was taken and mixed

in a 1:1 proportion with 0.4 % (v/v) tryphan blue (Gibco®). Cells were counted using a Neubauer haemocytometer (BS.748, Hawksley).

2.5 Functional analysis of the Papaver *S*-determinants in *Hordeum vulgare* (barley)

2.5.1 Genetic constructs for PrpS

Genetic constructs for assessing the functionality of PrpS in barley were generated previous to the start of this thesis (**Figure 2.8**). The transformations of barley plants with these genetic constructs were also carried out before this thesis at the John Innes Centre, UK (JIC).

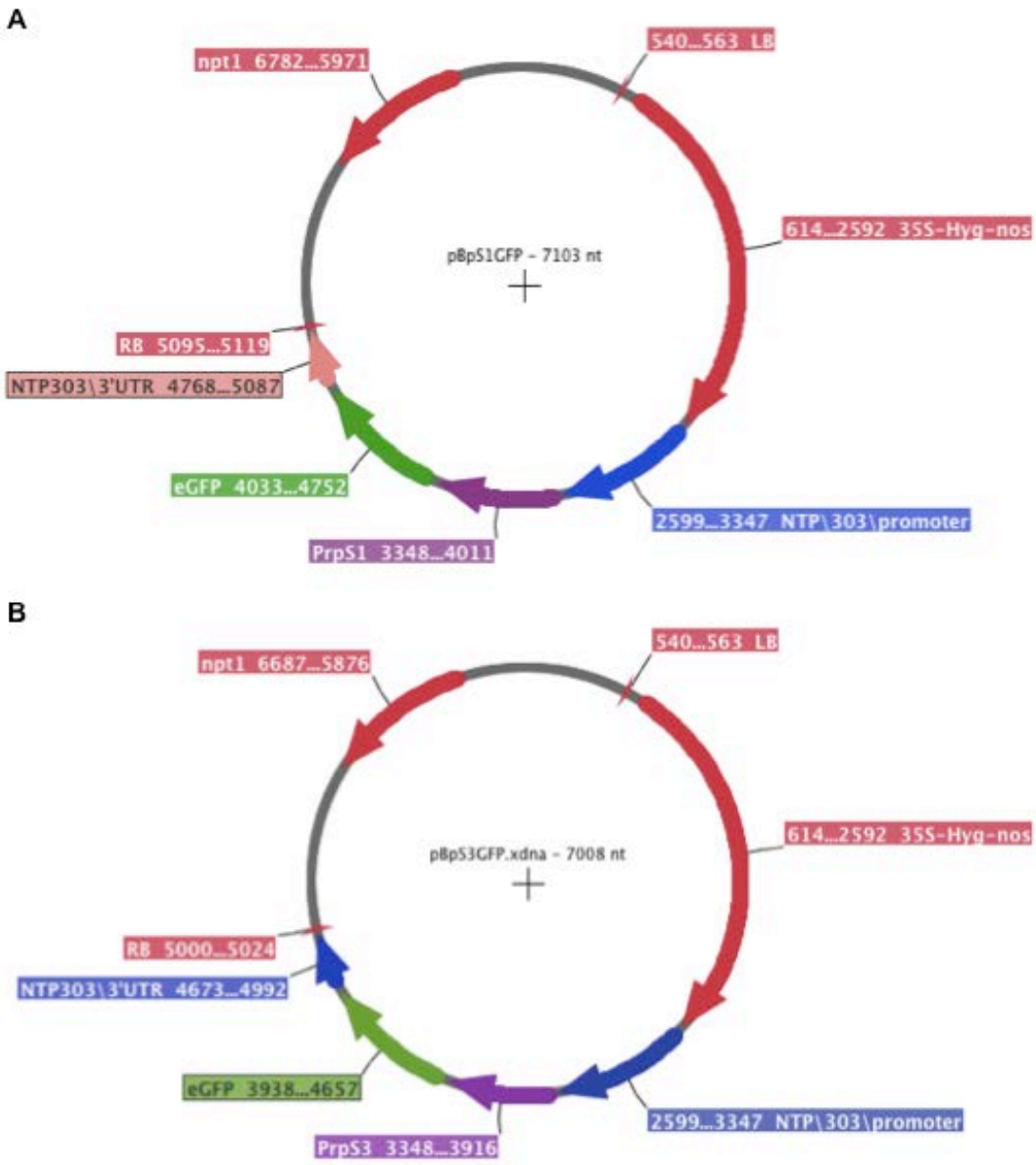

Figure 2.8 Genetic constructs used to evaluate the functionality of PrpS in barley. **A:** $PrpS_1$-GFP driven by the NTP303 promoter cloned in pBract202. **B:** $PrpS_3$-GFP driven by the NTP303 promoter cloned in pBract202.

2.5.2 Generation of genetic constructs for barley transformation

General protocols are detailed in **Table 2.1.** PCR reactions regarding gene cloning were carried out using KOD polymerase (Merk) as this enzyme has proofreading activity. For routine PCR Red DNA Polymerase (Thermo) was

used. Digestion, ligation, DNA and RNA purifications, RT-PCR were carried out according to the manufacturer. *E. coli* transformation were done by heat shock, whereas *A. tumefaciens* transformation by electroporation as described in (Sambrook et al., 1989).

Table 2.1. **General molecular biology procedures used during the work with barley.**

KOD (Novagen) PCR (high fidelity)	Standard PCR (Thermo Scientific)
Reaction mix: 1X KOD buffer 0.2 mM dNTPs 1 mM MgSO4 0.3 µM primer FWD 0.3 µM primer REV 0.75 µL template DNA 0.5 µL KOD Polymerase Water to complete 25 µL Cycle programme Step 1: 95 °C - 1 min Step 2: 95 °C - 20 s Step 3: 59 °C - 10 s Step 4: 70 °C - 15 s Step 5: step 2 to 4 25 times Step 5: 70 °C for 3 min.	Reaction mix: 1X ReddyMix™ buffer 0.4 µM PrsS primer forward 0.4 µM PrsS primer reverse 1 µL template DNA 1 µL REDTaq Polymerase Water to complete 25 µL Cycle programme Step 1: 95 °C - 1 min Step 2: 95 °C - 30 s Step 3: annealing - 1 min Step 4: 72 °C - 1m Step 5: step 2 to 4 30 times Step 5: 72 °C for 5 min.
DIGESTION	LIGATION
Reaction mix: 1X buffer NEB 4 0.5 - 1 restriction enzyme 1 µL of plasmid DNA or 4 µL of PCR product Water to complete 10 µL ON incubation at room temperature Double digestions were carried out with both enzymes at the same time.	1X T4 DNA Ligase Buffer 50-100 ng of plasmid DNA 50-100 ng of insert DNA 1 µL of T4 DNA ligase Water up to 20 µL. ON incubation at 15 °C
DNA purification	Gel purification
DNA miniprep: Wizard® DNA purification kit (Promega). DNA maxiprep: QIAGEN Plasmid Plus Maxi Kit	For gel extraction and clean up of DNA, the QIAquick GeL Extraction Kit was used.
RNA extraction	RT-PCR
RNA extractions were carried out from leaves according to the protocol provided by RNeasy Mini Kit (Quiagen). Integrity of the RNA was evaluated by 1% (w/v) agarose gel in a RNase-free	SuperScript® II Reverse Transcriptase kit (Invitrogen) was used for the cDNA synthesis according to the manufacturer instructions. RT-PCR mix:

electrophoresis tank prepared with DEPC treated TBE buffer. Finally, samples were treated with DNase I RNAse-free (Thermo).	5 - 10 µL RNA sample 1 µL dNTPs mix (10 mM each) 1 µL oligo(dT) (500 µg.mL^{-1}) Water to complete 12 µL This mix was heated at 65ºC for 5 min, and then placed in ice. Afterward, the following components were added: 4 µL 5X First-Strand Buffer 0.1 M DTT 1 µL RNase inhibitod RNasin® (Promega) New incubation at 42ºC for 2 min before adding 1 µL SuperScript II RT. Finally the 20 µL mix were incubated at 42ºC for 50 min, before inactivate the reaction at 70ºC for 15 min.
Transformation *E. coli*	Transformation of *A. tumefaciens*
2 µL of plasmid DNA or 4 µL of ligation reaction 50 µL aliquot of competent cell 30 minutes incubation on ice Heat shock: 42ºC for 40 s 5 minutes on ice Add 300 µL of SOC medium (2% w/v tryptone, 0.5% w/v yeast extract, 10 mM NaCl, 2.5mM KCl, 10 mM MgCl2, 10mM MgSO4 and 20 mM glucose) 1 h at 37 °C on a rotary shaker at ~200 rpm. Plate the cell on LB-agar plate with the appropriate selective antibiotic and grown overnight at 37ºC.	100 ng BsS1 or B202 100 ng pSoup 40µl of electrocompetent cells Mix in an electroporation cuvette Electric shock: 25µF Capacitance, 200 Ω Resistance, 2.4V Voltage Incubate at 4 °C for 2-5 min add 500 µL of LB-broth media Transfer into a 1.5 mL microfuge tube Incubated at 28 °C during 2 h Plate the cell on LB-agar plate with the appropriate selective antibiotic and grown overnight at 37ºC during 2-3 days. Note: use media, cuvettes etc, pre-cooled.
E. coli culture	*A. tumefaciens* culture
Liquid cultures of E. coli were grown for ~16 h at 37 °C on a rotary shaker at ~200 rpm. Solid cultures were carried out in 1% (w/v) agar plates ~16 h at 37 °C.	Liquid cultures of *A. tumefaciens* were grown for ~16 h at 28 °C on a rotary shaker at ~200 rpm. Solid cultures were carried out in 1% (w/v) agar plates for 3-4 days at 28 °C.

The primers design and analysis was done using the tool OligoAnalyzer, available online in the website of the Integrated DNA Technologies (http://eu.idtdna.com/site). Primer list is detailed in **Table 2.2**. For in silico restriction digest analysis, the free online available software Webcutter 2.0 was used. (http://rna.lundberg.gu.se/cutter2/).

Table 2.2- List of primers used for the barley related work.

Primer name (direction)	Sequence (5' → 3')	Observations / Comments
$PrsS_1$ (FWD)	AAAAAACCCGGGATGAACATATTTTATGTTATTGTGCTGCTATCG	For $PrsS_1$ cloning in pBract211. *XmaI* restriction site is underlined.
$PrsS_1$ (REV)	AAAAAAACTAGTTCAGGTTCGACCTTCCTTCCTTTCTTTCTTTATC	For $PrsS_1$ cloning in pBract211. *SpeI* restriction site is underlined.
CONSTANS (FWD)	ATTGTGCCAACAAGATAGATCG	Barley single copy gene used as a control of the genomic DNA extraction quality.
CONSTANS (REV)	AAAGGCAAATAATCTGGTCTGC	
HYG (FWR)	AATTCAGCGAGAGCCTGACC	Primers were used for determined the presence of the selectable marker gene (Hyg) in barley lines
HYG (REV)	CCGTCAGGACATTGTTGGAG	
***Hv*ACTIN (FWD)**	ATGATCGGCATGGAGTCTTC	Primer used to amplify the actin gene in barley. Used for control of suitable DNA.
***Hv*ACTIN (REV)**	GCTGAGTGAGGCTAGGATGG	

Maps of the BsS1 and B202 constructs are presented in Chapter 6, section 6.2.1.1. All the genetic constructs were checked by sequencing using the Genomics Lab services at University of Birmingham (Applied Biosystems). Additionally, the integrity of BsS1 after transformation into *Agrobacterium* was confirmed by a double digestion of plasmid preparation with XmaI/SpeI (data not shown).

2.5.3 Transformation and regeneration of transgenic barley lines

Since barley genetic transformation is a genotype-dependent procedure, the cultivar used in this thesis is Golden Promise as is the most responsive genotype to genetic transformation (Harwood et al., 2009). The vector

pBract211 was selected as it has been previously used for barley plants transformation. This features a T-standard region containing the *hpt* gene conferring resistance to hygromycin. pBract vectors are based on pGreen (Hellens et al., 2000) and further details can be found at the Bract website (http://www.bract.org). Bract vectors need to be co-transformed into *Agrobacterium* with the helper plasmid pSoup, which carries the trans-acting replicase gene (*RepA*) essential for the origin of replication of pGreen in *Agrobacterium*.

Transformations were carried out according to the optimised procedure developed in Dr Wendy Harwood's laboratory (Harwood et al., 2009). Briefly, immature seeds were collected and sterilised by treatments with ethanol and sodium hypochlorite. Immature embryos (IE) were isolated and 25 plated scutellem side up on a callus induction medium plate and storage ON in dark at 23 - 24ºC (details with the media composition in **Table 2.3**). *Agrobacterium* culture containing the appropriated genetic construct BsS1 or B202 were used to inoculate the embryos. After 3 days of co-cultivation, the embryos were transferred to fresh callus induction plates containing hygromycin and Timentin. During the initial 2 weeks the plates were maintained in dark conditions at 23°C. Then, embryo and callus were transferred every two weeks to fresh callus induction media and incubated in light conditions. After 6 weeks on callus induction, the embryo-derived callus were transferred to transition medium. The embryos were incubated in low light conditions at 23ºC during 2 weeks. During this stage, callus developed green areas and small shoots. Next, embryo-derived tissue, were transferred to new deep Petri dishes containing regeneration medium where the incipient green tissue and roots developed into

noticeable organs. Once the shoots and roots have developed, the plantlets were transferred to glass culture tubes containing callus induction media without dicamba. Finally, after 1 or two weeks, rooted plants with long leaves were ready to be transferred to soil and acclimatised to the greenhouse conditions.

Table 2.3 Media used during the transformation and regeneration process

Media	Components
Callus induction	4.3 $g.L^{-1}$ MS plant salt base (Duchefa M0221) 30 $g.L^{-1}$maltose 1.0 $g.L^{-1}$ casein hydrolysate 350 $mg.L^{-1}$ myo-inositol 690 $mg.L^{-1}$ proline 1.0 mg/L thiamine HCl 2.5 $mg.L^{-1}$ Dicamba 3.5 $g.L^{-1}$ Phytagel 1X callus induction vitamin mix
100X callus induction vitamin mix	100 $mg.L^{-1}$ thiamine HCl 35 $g.L^{-1}$ myo-inositol 69 $g.L^{-1}$ proline. This solution was filter sterilised and stored at 4ºC
Transition	2.7 $g.L^{-1}$ MS modified plant salt base (without NH_4NO_3) (Duchefa M0238) 20 $g.L^{-1}$ maltose 165 $mg.L^{-1}$ NH_4NO_3 750 $mg.L^{-1}$ glutamine 100 $mg.L^{-1}$ myo-inositol 0.4 $mg.L^{-1}$ thiamine HCl 2.5 $mg.L^{-1}$ 2,4-dichlorophenoxy acetic acid (2,4-D) 0.1 $mg.L^{-1}$ 6-benzylaminopurine (BAP) 3.5 $g.L^{-1}$ Phytagel 1X transition induction vitamin mix
Regeneration	2.7 $g.L^{-1}$ MS modified plant salt base (without NH_4NO_3) 20 $g.L^{-1}$ maltose 165 $mg.L^{-1}$ NH_4NO_3 750 $mg.L^{-1}$ glutamine, 100 $mg.L^{-1}$ myo-inositol 0.4 $mg.L^{-1}$ thiamine HCl 3.5 $g.L^{-1}$ Phytagel 1X regeneration induction vitamin mix
100X transition and regeneration vitamin mix	40 $mg.L^{-1}$ thiamine HCl 10 $g.L^{-1}$ myo-inositol. This solution was filter sterilised and stored at 4ºC

Both hygromycin (Roche) at 50 $mg.L^{-1}$ as the selective agent, and Timentin (Duchefa) at 160 $mg.L^{-1}$ to remove *Agrobacterium* were added to the media. The pH was adjusted to 5.8 with NaOH. Vitamin mix solutions were added after autoclave media with the other components. Additional copper (1.25 $mg.L^{-1}$ $CuSo_4 \bullet 5H_2O$) was added to induction and transition media.

After acclimatisation, genomic DNA extractions from barley leaves were carried out based in a protocol previously tested for barley (Edwards *et al*., 1991). This DNA was used for the screening of the transgenic lines by means of PCR for the *hyg* marker gene.

The transformation efficiency was calculated as the number of independent embryos regenerating plants on transition medium. Embryos regenerating plants starts to green up during transition medium and are more evident in the regeneration medium.

2.5.4 Handling of barley plants: emasculation and pollinations.

Transgenic barley lines were grown in glasshouse conditions under a 16h light/8h dark period at 22 °C. As part of the training to gain practical experience in barley related techniques, a visit to the JIC was carried out in the laboratory of Dr Wendy Harwood. During this visit, training regarding procedures such as emasculation, pollination by hand, and pollen collection were carried out.

For the emasculation of barley flowers, the spikes selected exhibited the awns emerged from the flag leaf around 2 - 3 cm. This normally ensured premature anthers, which were removed without releasing pollen. Once the three anthers per flower were removed, the stigmas were left on the plant until they were mature and receptive to receive pollen. For the pollinations, good quality pollen

was obtained from anthers on the point of dehiscence. Mature pollen was assessed by triggering shedding of the pollen after a gentle tap. Then, this anther was used to carry out the pollination by tapping on the surface of the stigma.

2.5.4.1 Pollen Collection and Germination

For the pollen collection, 30 - 40 anthers with mature pollen were placed into a 1.5 mL microfuge tube containing 500 µL of barley germination media (see table 2.4). After gently agitation for 5 - 10 sec, pollen was released from the anther in the liquid media. The pollen in suspension was carefully transferred into a new microfuge tube using a pipette with a cut tip, leaving the anthers or any debris in the previous tube. Then, pollen was incubated at 21 - 23ºC.

Table 2.4 Recipes for barley pollen germination *in vitro*.

Recipe 1 (Chakrabarti et al., 1976)	Recipe 2 (Kakeda K, personal communication)
20 - 25% (w/v) Sucrose	20% (w/v) sucrose
10 µg.mL^{-1} H_3BO_3	5 µg.mL^{-1} H_3BO_3
30 - 40 µg.mL^{-1} $CaNO_3$	700 µg.mL^{-1} $CaNO_3$
10 µg.mL^{-1} EDTA	10% PEG 4000
pH 7 adjusted with NaOH	
Agar and phytoagar (0.5, 1 and 2 % (w/v)) were evaluated as solidifying agents when solid media was required	

2.5.4.2 Viability assays

Pollen was incubated with 0.05% of Evans blue for 5 - 10 min. After three washes with barley germination media (water was also evaluated), 20 - 30 µL

were mounted in a microscope slide and visualised using bright field microscopy. Unstained pollen was considered alive, and dark stained pollen dead.

FDA is a chemical that becomes fluorescent when taken up by metabolically active viable-pollen. For the FDA staining, FDA was added to a sample of freshly collected pollen to a final concentration of 5 $\mu g.mL^{-1}$ and incubated protected from light at room temperature for 3 - 5 min. Then one wash was carried out to decrease background signal. Finally, 20 - 30 µL were mounted in a slide or 50 µL in a glass bottom petri dish, and visualised under the fluorescence microscope using the FITC filter: excitation 492 nm, emission 519 nm. Pollen exhibiting noticeable fluorescence emission was viable whereas pollen exhibiting faint fluorescence emission was considered dead.

2.5.4.3 Germination and culture of barley plantlets *in vitro*

Seeds were submerged ON in sterile water at room temperature. Next day, the seeds were transferred to bleach (37% v/v) and incubated for 2h with agitation. Finally, the seeds were washed three times with sterile water and placed in MS plates with hygromycin. The washes were carried out in a laminar flow cabinet and using sterilized forceps. These method was adapted from a protocol developed in the laboratory of Prof. Russell Goddard (Valdosta State University, USA) (Inatomi and Slaughter, 1971).

2.5.5 SI bioassay for barley pollen

Before development of the SI bioassay for transgenic barley pollen, a protocol for visualisation of F-actin needed to be standardised as F-actin configuration is a key feature to evaluate whether there is a SI-like response.

2.5.5.1 Actin labelling with Rhodamine-Phalloidin of barley pollen

The protocol for staining barley actin filaments was optimized from the method standardised for poppy pollen (Geitmann et al., 2000), and *Lotus japonicus* (Tansengco et al., 2004).

First an additional cyclohexane treatment was essential for pollen coat removal, allowing F-actin staining. The procedure includes collecting mature pollen by vortexing the anthers in cyclohexane and then centrifuging the mixture. After the spin the pollen coat will remain in the cyclohexane phase and pollen grains are confined to the pellet.

Pollen grains collected as described in section 2.5.4.1, were treated with 400 µM maleimidobenzoyl N-hudroxysuccinimide (MBS) for 6 min and then fixed with 2% (v/v) paraformaldehyde (PFA) during 1.5 h at 4 °C. Then, for removing the PFA, the samples were centrifuged at 3,600 rpm for 1 minute, the supernatant was removed and the pollen grains resuspended in 200 - 400 µL of TBS. This washing procedure was repeated three times. Afterwards, samples were incubated with TBS plus 0.1 % Triton for 1 h to permeabilise the pollen grain. Tubes were stained with 66 nM Rhodamine-phalloidin and samples were incubated for 16 h at 4 °C. Finally, 10 µL of pollen sample were mounted with 5 µL of Vectashield (with DAPI) and sealed with nail polish once the cover slide

was placed. Images were captured using the Nikon Eclipse TE300 (details in section 2.6)

2.5.5.2 *In vitro* SI bioassay for barley

Once the pollen was collected and its viability assessed, 20 $\mu g.mL^{-1}$ of incompatible PrpS protein was added to the sample and incubated 16 h at 23 °C. Afterwards, the actin labelling protocol was carried out as described in section 2.5.5.1.

2.5.5.3 Pollinations of barley plants and pollen tube staining

Immature barley flowers were emasculated removing the anthers by a small incision in the awn, leaving the immature stigma protected by the awn. Stigmas were pollinated once the stigma reached its mature stage (characterise by a feathery appearance of its papilla cells).

For the semi-*in vivo* pollinations, the mature stigmas were cut from the barley plant and placed in a petri dish containing solid germination media. Then freshly collected pollen was sprinkled by tapping the anther on the stigma. Finally, the stigmas were incubated ON in a chamber at 23ºC. For the pollen tube staining, after ON incubation the pollinated stigmas were submerged in an aniline blue solution, and incubated at least during 5 hours for staining and soften (ON was

also used). Finally the stigmas were placed on a microscope slide and squashed with a coverslip for visualisation using UV illumination.

For the *in vivo* pollinations, the procedure was similar as described above for the semi-*in vivo* pollinations, but in this case the mature emasculated stigmas were pollinated and left in the plants for seed set.

2.6 Imaging

2.6.1 Confocal laser Scanning Microscopy

Images were captures with the Zeiss LSM 710 system. **Table 2.5** details confocal microscope acquisition set up.

Table 2.5 Parameters used for imaging acquisition

Parameter	Value
Frame size	1024 x 1024
Line Step	1
Averaging Number	2
Averaging Bit depth	16 Bit
Size interval	1 µm

Images were collected using the software ZEN 2010 and edited using ImageJ software (Schneider et al., 2012).

2.6.2 Fluorescence

Epifluorescence images were captured with a Nikon Eclipse Tε300 microscope. The setup includes a charge-couple device as image sensor. NIS-Element software and edited in ImageJ.

2.7 Statistical analysis

Statistical analyses were carried out using the statistical software “R” (R Development Core Team, 2013). Differences were considered significant at $P < 0.05$. The specific used is details in each experiment in the results section.

CHAPTER 3

Functional Analysis of Papaver *S*-determinants in *Arabidopsis thaliana* protoplasts and *Saccharomyces cerevisiae*

3.1 Introduction

Papaver SI response was successfully transferred into *Arabidopsis in vivo* (Lin, 2015), establishing that PrpS-PrsS interaction is functional in highly diverged cells (Chapter 1, section 1.4.7). Moreover, studies investigating the *Papaver* SI response have revealed that several of the pathways and mechanism involved in the SI response, including Ca^{2+} signalling, actin cytoskeleton, and PCD, are universal signalling pathways conserved among most eukaryotic cells (Chapter 1, sections 1.4.6.2 and 1.1).

Previous studies attempting functional transfer of SI have been done in pollen and stigmatic cells. So, the next step and one of the aims of this thesis, was to further evaluate the versatility of *Papaver* SI system assessing whether PrpS and PrsS can be functional in somatic/vegetative cells. Considering that PrpS-PrsS interaction could trigger alterations involving universally conserved cellular components, which are not restricted to reproductive cells, it was feasible to evaluate whether PrpS was functional in highly diverged heterologous model systems, as this would represent a major advantage to study the *Papaver* SI response.

The plant model *Arabidopsis thaliana* (Chapter 1, section 1.2) was used for the first attempt to transfer the *Papaver* SI into leaf protoplasts. Protoplasts represent a versatile single plant cell system, but are derived from vegetative tissue. So, evidence of functional PrpS in this system would indicate that this system is not restricted to sexual cells (pollen and stigma) and will have other advantages detailed later. Arabidopsis, protoplast isolation and transfection protocols have been previously established, a major advantage in comparison

with *Papaver* where genetic manipulation is not possible. One step further was to evaluate whether PrpS was functional in a more diverged unicellular organism *Saccharomyces cerevisiae* (yeast). This model system has been extensively used to identify and characterise plant genes and protein (Chapter 1, section 1.2). Moreover, cultivation, manipulation and experiments in yeast were expected to be easier and quicker in comparison to *Papaver.*

Since *Arabidopsis* is the model system employed to study plants, a functional assay to study *Papaver* SI using *Arabidopsis* protoplast, has a major potential as the vast amount of information and resources available for *Arabidopsis* would become available for the studies of *Papaver* SI. This includes for instance, the use of relevant *Arabidopsis* mutants, to explore the pathways described so far for the *Papaver* SI response. Moreover, isolation and transfection procedures of *Arabidopsis* leaf protoplasts have been established, and rapid, allowing a high-throughput scale of experiments (Yoo et al., 2007). For yeast, there is a large library of mutant available, which is a powerful tool for functional analysis of genes. Studies based in the analysis of relevant mutant could provide robust and valuable data finding the links and integrating the pathways involved in during the *Papaver* SI response. Complementation analysis using plant genes in mutant yeast has also made a major contribution identifying important genes of plant (Mowla et al., 2006, Minet et al., 1992). Further details in Chapter 1, section 1.4.

Our aims were to evaluate whether PrpS was functional in both *Arabidopsis* mesophyll protoplasts, and *Saccharomyces cerevisiae*. Based on the evidence denoting common pathways and mechanism between plant cells and yeast, including actin cytoskeleton, and PCD, we expected that PrpS could trigger a

"*Papaver* SI-like response", recruiting the cellular components from the host cell and exhibiting similar alterations to the ones described during the *Papaver* SI, particularly cell death.

The functional evaluation of PrpS in *Arabidopsis* protoplasts consisted of the isolation of mesophyll protoplasts and transient transfection with vector expressing PrpS. If treatment with incompatible PrsS were able to trigger a "*Papaver* SI-like response", a reduction in the viability of the protoplasts was expected, as a consequence of the activation of PCD. For yeast, a stably transformed yeast expressing PrsS was challenged with incompatible PrsS. If PrpS was functional, we expected a reduction in the growth rate of yeast.

3.2 Results

3.2.1 Previous studies of the Papaver *S*-determinants in *Arabidopsis thaliana* mesophyll protoplasts expressing $PrpS_1$

Work prior to this thesis, aimed to explore whether PrpS was functional in *Arabidopsis* mesophyll protoplasts. Protoplasts from a stably transformed *A. thaliana* line with $PrpS_1$ driven by the CaMV35S promoter (At-35S:$PrpS_1$) were challenged with incompatible $PrsS_1$. These experiments did not reveal a *S*-specific reduction in the viability or caspase activity in protoplasts after treatments with incompatible $PrsS_1$, suggesting that PrpS was not triggering a response that includes cell death and therefore not functional in *Arabidopsis* mesophyll protoplasts (Vatovec, 2012). Next, transient experiments by Dr Javier Juarez-Diaz and Dr Andrew Beacham used transfections of *Arabidopsis*

mesophyll protoplasts with constructs designed to express $PrpS_1$ and $PrpS_8$ fused to GFP (pEGPrpS_1-GFP and pEGPrpS_8-GFP). **Figure 3.1** shows the viability of protoplasts transfected, and tested under different PrsS treatments. Promisingly, treatment with incompatible cognate PrsS generated a significant decrease in the viability of protoplasts transformed with pEGPrpS_1-GFP (**Figure 3.1.A**) and pEGPrpS_8-GFP (**Figure 3.1.B**). This suggested that the protoplast were responding specifically to the incompatible cognate combination of PrsS. However, these data was not conclusive as the differences were not as marked as results with *A. thaliana* pollen expressing PrpS (de Graaf et al., 2012). In the experiments with protoplasts, the viabilities before any treatment (0 h) were between 70 - 75%, whereas in the experiments with pollen, the viabilities were over 90%. Moreover, the decrease in the viability was smaller in the experiments with protoplasts compared to the experiments with *Arabidopsis* pollen. Additionally, protoplasts experiments did not explore whether caspases-like activities, a hallmark of the *Papaver* SI response, were involved in the decrease of the viability.

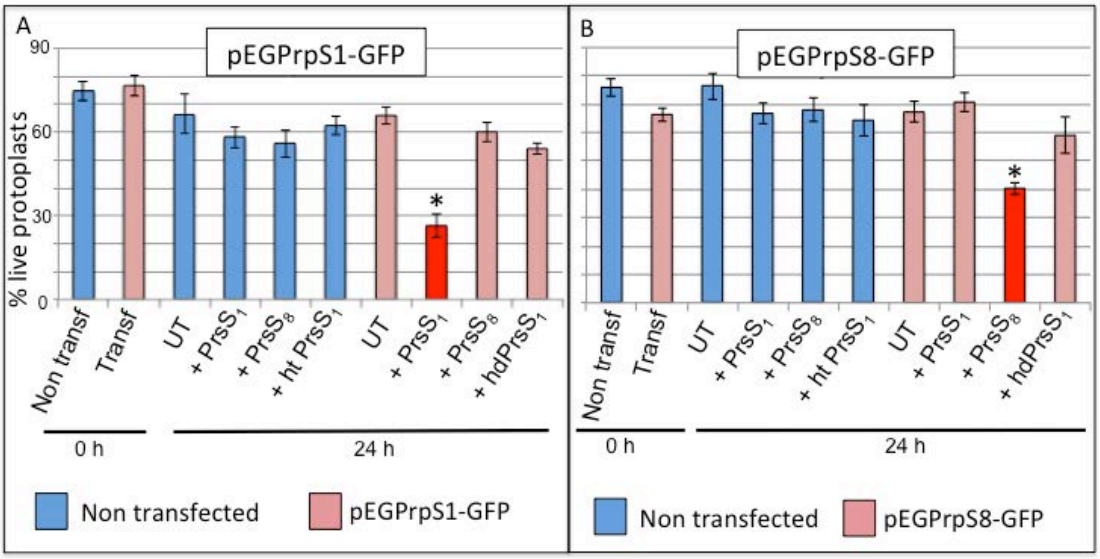

Figure 3.1 Evaluation of the viability of protoplasts expressing PrpS challenged with incompatible PrsS. A: protoplasts transfected with 53S::$PrpS_1$-GFP**. B:** protoplasts transfected with 35S::$PrpS_8$-GFP. **Blue bars**: non-transfected protoplasts. **Pink bars**: transfected protoplasts. **UT**: Untreated (exposed to buffer only). Treatments with $PrpS_1$: **+ $PrsS_1$**. Treatments with $PrsS_8$: **+$PrsS_8$**. Control treatment with heat-denatured proteins: **+$hdPrsS_1$**, and **+$hdPrsS_8$**. Viability was measured by using Evans blue staining. Values are the mean of four independent replicates. Error bars: SEM. These experiments were carried out in collaboration with Dr Javier Juarez-Diaz and Dr Andrew Beacham**.** Unpublished data.

Even though these preliminary data suggested a *S*-specific decrease in the viability of the protoplast expressing $PrpS_1$-GFP and $PrpS_8$-GFP, additional repeats and further studies were necessary to obtain reliable and conclusive data. In this thesis we present the continuation of these experiments.

3.2.2 Transferring *PrpS* into *A. thaliana* mesophyll protoplasts: transient transfection efficiency of *$PrpS_1$-GFP* and pattern expression analysis based on fluorescence of $PrpS_1$-GFP.

The plasmid used for the transient transfection is detailed in Table 3.1

Table 3.1 Genetic construct used to assay the functionality of $PrpS_1$ in *Arabidopsis* mesophyll protoplasts. This construct was provided by Dr Javier Juarez-Diaz

Name	Details	Observations
pEGPrpS1-GFP	*$PrpS_1$* fused to GFP ($PrpS_1$-GFP) cloned into pEarlyGate103.	pEarlyGate103 has the constitutive promoter CaMV 35S.

Firstly, aiming to maximise the transfection efficiency, transfection using pEGPrpS1-GFP were carried out with three different concentrations of DNA. The GFP signal was used to assess the number of cells transfected with PrpS1-GFP. Fluorescence emission was observed after all the transfections, however the transfections rates were equally low compared to the values previously reported (Vatovec, 2012). Transfections using 5 µg of DNA exhibited efficiencies of 7 % (**Figure 3.2**.**A** and **B**). Transfections with 10 and 15 µg of DNA revealed similar efficiencies of 15 % (**Figure 3.2**.**C** and **D**), which was higher than the efficiency using 5 µg of DNA. Therefore 10 µg of DNA were used for the following experiments. Background levels of autofluorescence are shown in (**Figure 3.2**.**E** and **F**).

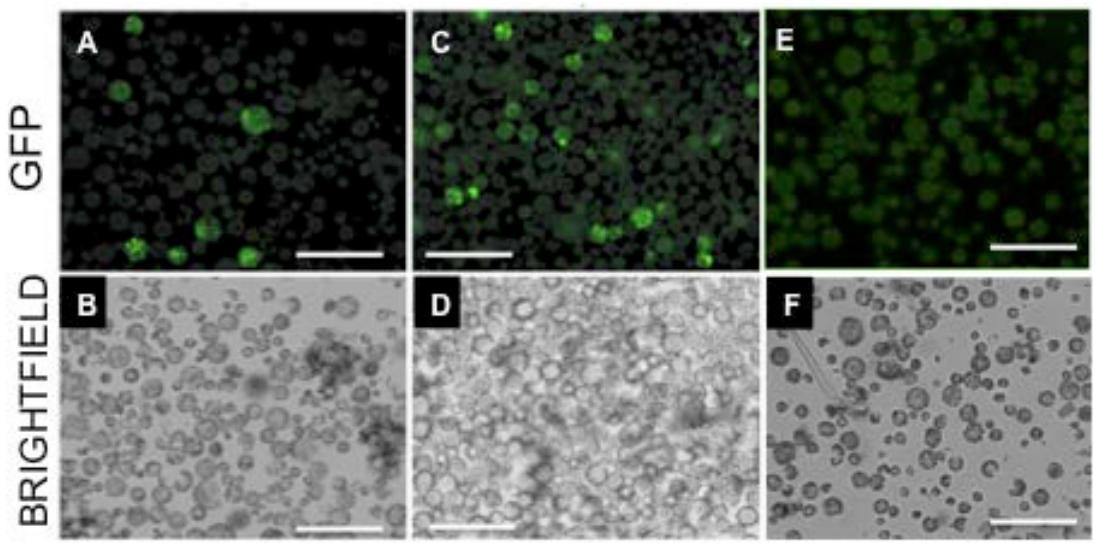

Figure 3.2. **Representative images of transfection efficiency with different amount of 35S::PrpS$_1$-GFP. A, B**: Protoplasts transformed with 5 µg of DNA (7 % efficiency). **C, D**: Protoplasts transformed with 10 µg of DNA (15 % efficiency). Fluorescence images were taken using the FITC filter: excitation 492 nm, emission 519 nm. Scale bar = 150 µm.

Based in studies in *Papaver* pollen, it was expected that PrpS$_1$-GFP was targeted to the plasma membrane and therefore the fluorescence emission of PrpS$_1$-GFP would be predominantly associated with the protoplast plasma membrane. However, the of pattern expression denoting the subcellular localisation of PrpS$_1$-GFP was not homogeneously distributed in the protoplasts. GFP signal appeared restricted to very bright areas and absent in others areas, forming a speckle pattern within the protoplasts, whereas other areas of the same protoplast did not exhibit an evident signal (**Figure 3.3**). The GFP signal did not seem to be distributed at the edge of the cell as expected if PrpS$_1$-GFP was targeted to the plasma membrane. Moreover, the intensity of the signal also varied between protoplasts within the same population. Using the software ImageJ to estimate the intensity of the signal, protoplast showed in **Figure 3.3.A** had a 25% higher intensity in the signal in comparison with the protoplast in **Figure 3.3.B**. Our interpretation was that this heterogeneous

pattern expression in the fluorescence was a consequence of abnormalities during the synthesis and/or the processing of $PrpS_1$-GFP during the secretory pathway, probably due to the overexpression of the $PrpS_1$-GFP.

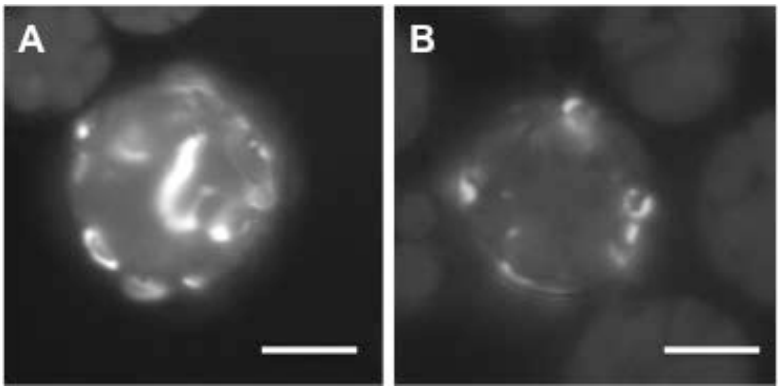

Figure 3.3. **GFP expression of 35S:$PrpS_1$-GFP in *A. thaliana* protoplast**. **A and B**: protoplasts from the same population exhibiting heterogeneity in both distribution and intensity of the GFP signal. (n = 90 after three independent transfections) Fluorescence images were taken using the FITC filter: excitation 492 nm, emission 519 nm. Scale bar = 15 µm.

These results did not reveal the expected membrane-associated pattern expression of -GFP. Thus, the bright areas restricted to specific regions might be indicating the accumulation of -GFP in subcellular organelles such as endoplasmic reticulum or Golgi apparatus. This heterogeneity in the fluorescence will be discussed and analysed further in Chapter 4 (4.2.1), where similar results of were obtained in mammalian HeLa cells. Despite the *Arabidopsis* protoplast being different to HeLa cells, we thought that similar issues might be originating this heterogeneous and unexpected pattern distribution.

3.2.3 Functional Analysis of *A. thaliana* mesophyll protoplasts transfected with -GFP

Even though the expression of GFP did not appear as expected, we thought enough GFP might be reaching the plasma membrane. Therefore experiments to assess the functionality of PrpS in the protoplasts expressing GFP were carried out. The *in vitro* SI bioassay for protoplasts was adapted based in the *in vitro* SI bioassay previously established for *Papaver* and *Arabidopsis* pollen (Chapter 2, section 2.2.4). If $PrpS_1$ was functionally expressed in the protoplasts, it was expected that the challenge with incompatible $PrsS_1$ would trigger a SI-like response, leading to a PCD, causing a decrease in the viability of these protoplasts. The viability of protoplasts was monitored using 0.05 % Evans Blue staining (Chapter 2, section 2.2.4).

Additionally and aiming to confirm that the decrease in the viability was a consequence of PCD (as it has been established in *Papaver*), an assay to determined if caspase-like enzymes were involved was carried out. This assay comprised the use of Ac-DEVD-CHO, a caspase 3-like inhibitor (Chapter 2, section 2.2.4), which should prevent the decrease in the viability if the protoplast were dying as a consequence of PCD. Thus, protoplasts were incubated with 100 µM of Ac-DEVD-CHO (caspase-3 inhibitor) at 23°C for 1 h in dark before the exposure to $PrsS_1$. After treatment the viability of protoplasts was evaluated using Evans blue staining.

Figure 3.4 shows the percentage of live protoplasts under different conditions (n = 4). The average viability of the untreated samples was 63%. The percentage of live protoplast in the control situation of protoplasts exposed to

the caspase inhibitor Ac-DEVD-CHO alone (DEVD) was 62%, which was not significantly different compared to the untreated sample (p-value 0.999). This result confirmed that the pretreatment with the caspase inhibitor did not have an effect in the viability of the protoplasts. In the SI combination (i.e. protoplasts expressing were exposed to incompatible $PrsS_1$), the percentage of live protoplast exhibited a significant reduction compared to both untreated sample (p-value 0.0073) and the control of exposure to Ac-DEVD-CHO alone (p-value 0.0148). Moreover, the viability was also significantly lower in comparison with the treatment when protoplast were pre-treated with Ac-DEVD-CHO and then exposed to incompatible $PrsS_1$ (p-value 0.03861). This suggested that treatments with were causing a reduction in the viability of *Arabidopsis* protoplasts. Interestingly, the pre-treatments with Ac-DEVD-CHO prevented the decrease in the viability of the protoplast after treatments with $PrsS_1$, and the viability value was 60%, which was not statistically different to the untreated (p-value 0.9954) and the control of treatment with Ac-DEVD-CHO alone (p-value 0.9998), suggesting that the decrease in the viability was mediated by caspase-like activity, and therefore that was triggering a "*Papaver* SI-like response" in *Arabidopsis* protoplasts.

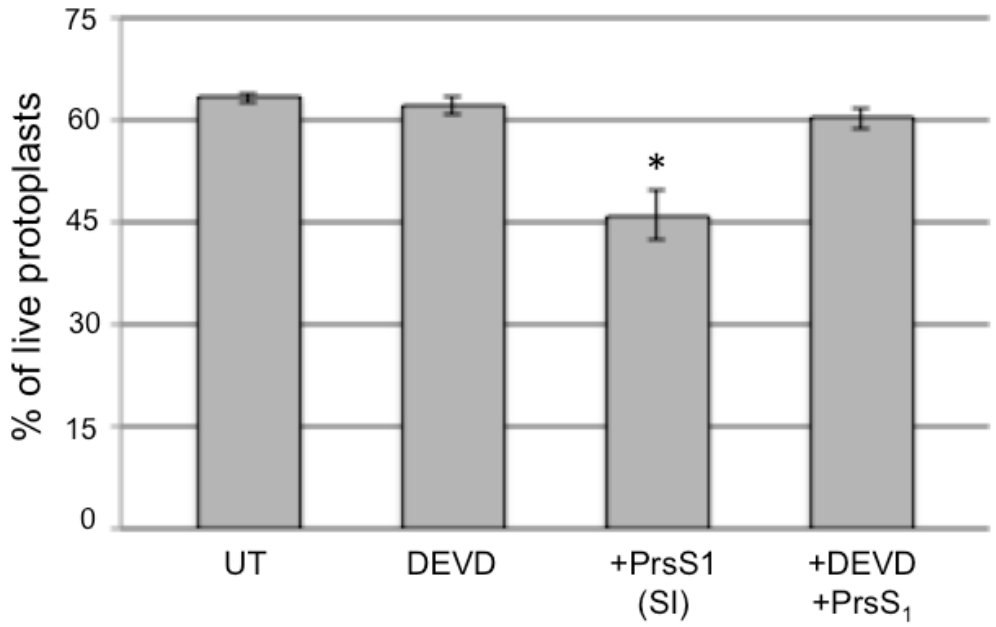

Figure 3.4. Viability assay in *A. thaliana* protoplast expressing $PrpS_1$-GFP exposed to incompatible $PrsS_1$. UT: untreated, transfected protoplast only exposed to W5 buffer (control). DEVD: transfected protoplasts exposed to 100 μM Ac-DEVD-CHO treatment. +PrsS1: transfected protoplast exposed to $PrsS_1$ (SI condition). +DEVD+PrsS1: protoplasts transfected with $PrpS_1$-GFP pre-treated with caspase-3 inhibitor, Ac-DEVD-CHO. The bars represent the mean of four replicates. 100 protoplasts were counted for each treatment. Error bars are SEM. Statistically significant difference is indicated with * ($p<0.05$). These experiments were carried out with Dr Javier Juarez-Diaz and Dr Andrew Beacham.

All together, these data suggested that Papaver SI can be functionally transferred to non-reproductive plant cells. However, even though the differences between the incompatible treatments and the controls were statistically significant, they were not as dramatic as expected considering experiments carried out in *Arabidopsis* pollen expressing PrpS (de Graaf et al., 2012). Therefore it is not possible to make categorical conclusion regarding the functionality of PrpS in *Arabidopsis* mesophyll protoplasts.

The technical reason for this lack of clear cut between the SI treatments and the controls were likely to be a combination of: 1) lower viability values in the untreated samples, consequence of the protoplast isolation and transfection

protocols, 2) low transfection efficiencies, and 3) heterogeneity in the expression of PrpS-GFP, suggesting issues in the synthesis and/or targeting of $PrpS_1$-GFP.

Our next attempt was for functional transfer of PrpS using yeast as a heterologous model system, provide an alternative to avoid some of the potential issues mentioned above regarding the protoplasts.

3.2.4 Studies of the Papaver *S*-determinants in *Saccharomyces cerevisiae*

The aim addressed in this section was to evaluate whether PrpS was functional in yeast. The experimental design included the stable transformation of yeast with $PrpS_1$-GFP and then generates the SI conditions by adding incompatible $PrsS_1$ to a liquid cell culture. If $PrpS_1$ was functional in yeast, is was expected that the exposure to incompatible $PrsS_1$ triggered a "*Papaver* SI-like response" including PCD, causing a decrease in the viability of yeast. The viability of the cell population was monitored by both measuring the growth rate of the culture Absorbance, 600 nm), and counting the colony-forming unit (CFU) (Chapter 2, section 2.3.4).

3.2.5 Genetic constructs

Two genetic constructs suitable for yeast and generated by Dr Javier Juarez-Diaz were used for the functional studies carried out during this thesis. These constructs were generated using pYES-DEST52 vector, which contains the

GAL1 promoter for inducible expression by galactose, and also contains *URA3* as auxotrophic marker for selection of transformants. The yeast strain selected for the transformation was InvScI, which is a *ura3*$^{-}$ mutant, which means that in minimal media without uracil, it can only grow if it has been complemented by the transformation with a construct containing the *URA3* gene. *PrpS$_1$* cloned in pYES-DEST52 was named pYdPrpS$_1$. The construction containing *PrpS$_1$* fused to *GFP* (PrpS$_1$-GFP) cloned in pYES-DEST52 was named pYdPrpS$_1$-GFP. (Chapter 2, section 2.3.2). A summary table with the main characteristics in presented in **Table 3.2.**

Table 3.2 Yeast strain and genetic constructs used to carry out the functional evaluation of PrpS on yeast.

Name	Details	Observations
InVSc1	Yeast strain suitable for selection with pYES-DEST52	Diploid yeast strain with *ura3* genotype (Ura^{-}). Therefore in minimal media lacking of uracil, it only grows when complemented by pYES-DET52.
pYdPrpS$_1$	InvSc1 transformed with *PrpS$_1$* cloned into pYES-DEST52	pYES-DEST52 carries the *GAL1* promoter for inducible expression in *S. cerevisiae. GAL1* promoter is repressed by glucose and induced by galactose. Raffinose does not induce or repress this promoter. Also contains *URA3* as auxotrophic marker for selection of transformants.
pYdPrpS$_1$-GFP	InvSc1 transformed with *PrpS$_1$* fused to *GFP* (PrpS$_1$-GFP) cloned into pYES-DEST52	

Yeast transformation was carried out using the Yeastmaker™ DNA carrier and the Lithium acetate method (Chapter 2 section 2.3.2).

3.2.6 Determining the growth stages timing and the effect of alternative carbon source on *S. cerevisiae*.

Before any experiment assessing the functionality of PrpS and PrsS in yeast, the key time points in the growth curve of yeast (lag, exponential and stationary phase) and the effect of different carbon sources on this growth needed to be determined. The experimental design to evaluate whether PrsS has an effect on yeast expressing PrpS, was based on monitoring the yeast growth, assuming that a *Papaver* SI-like response would result in a slower growth rate in comparison with the controls, as PCD was triggered in the cells exposed to incompatible PrsS. Therefore it was important to determine the time of the exponential growth of InSc1, and to collect data during this stage, as it was expected that differences in the growth rate would be evident during this period. Additionally, different carbon sources were evaluated to rule out any potential abnormalities in the growth rate due to the carbon source. This was especially important as the induction of the *GAL1* promoter and the concomitant transcription of $PrpS_1$ or $PrpS_1$-GFP could have affected intrinsically the yeast physiology and therefore its growth rate.

Figure 3.5 shows the growth curve of yeast under different conditions. The exponential phase began after ≈10 h, and lasted until 25 h when a deceleration stage reached the stationary phase (≈40 h). The untransformed cultures of InvSc1 reached significant higher absorbance values growing in both glucose and galactose in comparison with the yeast expressing PrpS (p-value 0.03795). This indicated that InvSc1 could grow similarly well using both sugars.

Additionally, the fact that under the same growth conditions, untransformed yeast reached higher values in comparison with pYdPrpS$_1$ and pYdPrpS$_1$-GFP suggested that the expression of PrpS$_1$ and PrpS$_1$-GFP had an effect in the yeast growth. Further statistical analysis did not reveal a significant difference between pYdPrpS$_1$ and pYdPrpS$_1$-GFP (p-value 0.4971), suggesting that the expression of PrpS$_1$ and PrpS$_1$-GFP did not have a differential impact in the yeast.

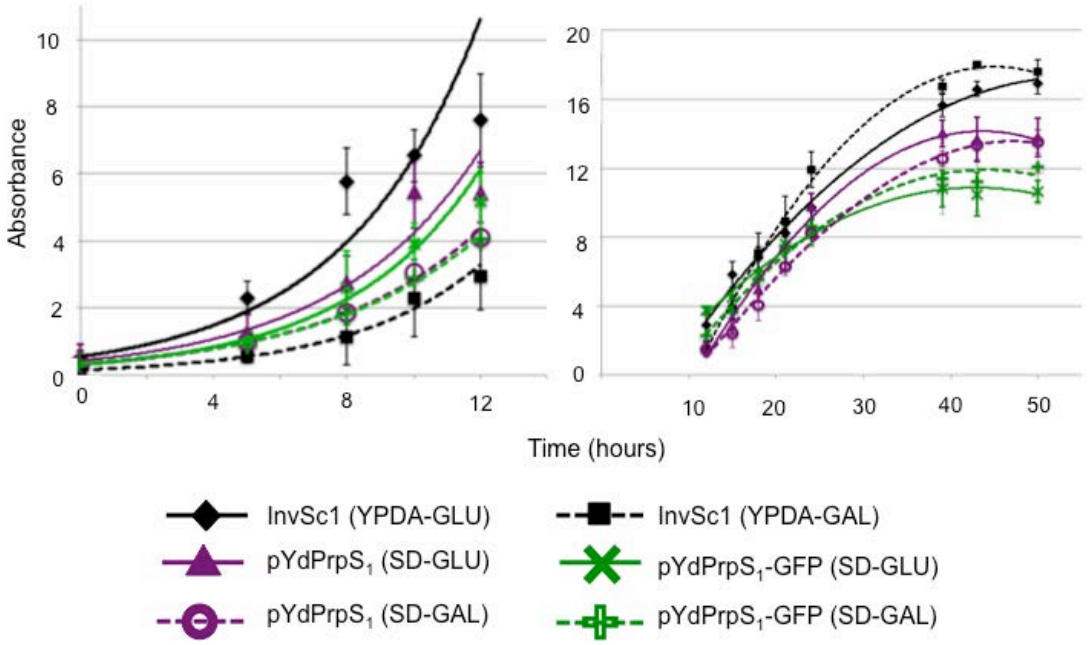

Figure 3.5 Growth curves of yeast strain InvSc1 transformed with PrpS$_1$ and PrpS$_1$-GFP in glucose (GLU) and galactose (GAL). YPDA: Yeast peptone dextrose adenine is a complete media for yeast growth. SD: Yeast minimal media used together with dropout supplement without uracil for selecting transformants yeast. Black diamond solid line: untransformed InvSc1 growing in YPDA-glucose. Black square dashed line: untransformed InvSc1 growing in YPDA-galactose. Purple triangle solid line: pYdPrpS$_1$ growing in SD-glucose. Purple circle dashed line: pYdPrpS$_1$ growing in SD-galactose. Green cross solid line: pYdPrpS$_1$-GFP growing in SD-glucose. Green "plus" sign dashed line: pYdPrpS$_1$-GFP growing in SD-galactose. Absorbance was monitored at 600 nm. Values are the mean of two experiments (n = 2). Errors bars: SEM.

These experiments showed that the expression of PrpS and PrpS$_1$-GFP had a limiting effect in the growth rate to *S. cerevisiae*. However, this effect did not

affect the exponential growth phase timing, which was still between 10 and 20 h.

Aiming to minimize any effect of the *GAL1* promoter on the growth rate due to the expression of $PrpS_1$ or $PrpS_1$-GFP, a new growth curve using raffinose as a carbon source was determined. Unlike the sugars evaluated previously, glucose (which repress) or galactose (which induce), raffinose does not have any effect upon the expression of the genetic construct. This allowed a more precise control in starting the promoter induction because it reduces the lag that is produced when the promoter is induced from a repressed state.

The growth parameters using raffinose were similar to the ones described previously using glucose and galactose (**Figure 3.5**). The exponential stage was between 10 and 20 hours for all the conditions. Statistical analysis only revealed significant differences at 37 h and 49 h between the non-transformed yeast (i.e. IncSc1) and the yeast expressing PrpS (i.e. pYdPrpS1 and pYdPrpS1-GFP) (p-value 0.0414 and 0.0409). Thus, consistently with the previous experiment, untransformed InvSc1 reached the highest values of absorbance (~13) during the stationary phase after 40 h of culture (**Figure 3.6**). $pYdPrpS_1$ and $pYdPrpS_1$-GFP yeast exhibited similar growth curve reaching the stationary phase after 30 hours of culture with absorbance values between 11 and 12 (**Figure 3.6)**.

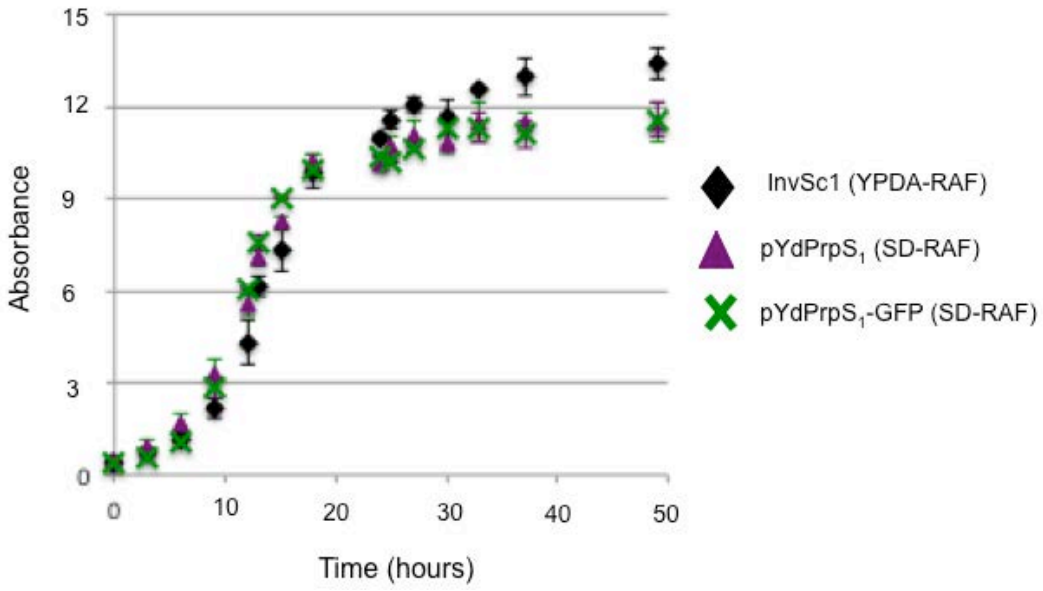

Figure 3.6 Growth curves of InvSc1 in raffinose. YPDA: Yeast peptone dextrose adenine is a complete media for yeast growth. SD: Yeast minimal media used together with dropout supplement without uracil for selecting transformants yeast. Black diamond: untransformed InvSc1 growing in YPDA-raffinose. Purple triangle: pYdPrpS$_1$ growing in SD-raffinose. Green cross: pYdPrpS$_1$-GFP growing in SD-raffinose. Values are the mean of three replicates. Error bars: sem. (n = 3). Values were analysed with ANOVA and Tukey post-test.

These results confirmed that the exponential growth stage was between 10 and 20 hours. They also suggested, similarly to the previous experiment, that the expression of PrpS$_1$ and PrsS$_1$-GFP had an effect in the physiology of the yeast, as the untransformed yeast reached higher absorbance in the stationary phase in comparison with pYdPrpS$_1$ and pYdPrpS$_1$-GFP, which exhibited similar values between them.

3.2.7 Evaluation of the pattern expression of PrpS$_1$-GFP in yeast.

The protein expression of PrpS$_1$-GFP in pYdPrpS$_1$-GFP was evaluated by both GFP emission and western blot. Importantly, western blot analysis allowed an estimation of the timing of the expression of PrpS$_1$-GFP.

Representative images of the GFP emission of pYdPrpS$_1$-GFP are shown in **Figure 3.7**. A noticeable GFP signal was detected in 70% of the cells, which displayed a range in the intensities of GFP emission in cells from the same culture (**Figures 3.7 A** and **C**). Moreover, there were also a 30% of pYdPrpS$_1$-GFP cells where the GFP signal was not detected (**Figures 3.7 A** - **D**). Because the small size of yeast cells, and constant movement despite they were on a coverslip, good quality images were challenging to obtain. This made it difficult to analyse the patterns expression of GFP signal within the cell. The images obtained suggested heterogeneity of expression with some regions exhibiting higher GFP emission whereas other areas of the same cell the emission was not detected (**Figure 3.7 C**). A comparison between the fluorescence image and its corresponding bright field image (**Figures 3.7 A** and **C**) indicated that the GFP emission was not delineating the edge of the cell, which suggested that PrpS$_1$-GFP was not associated to the plasma membrane as expected. To confirm that the fluorescence detected in pYdPrpS$_1$-GFP was not background fluorescence from the yeast, we monitored the fluorescence of pYdPrpS$_1$, which does not express GFP. No signal was detected at exposure times lower than 2 s. A negligible background emission was visible after 3 s of exposure, which represents a dramatic overexposure time**. Figure 3.7.E** shows representative images of the background emission after 5 second of overexposure.

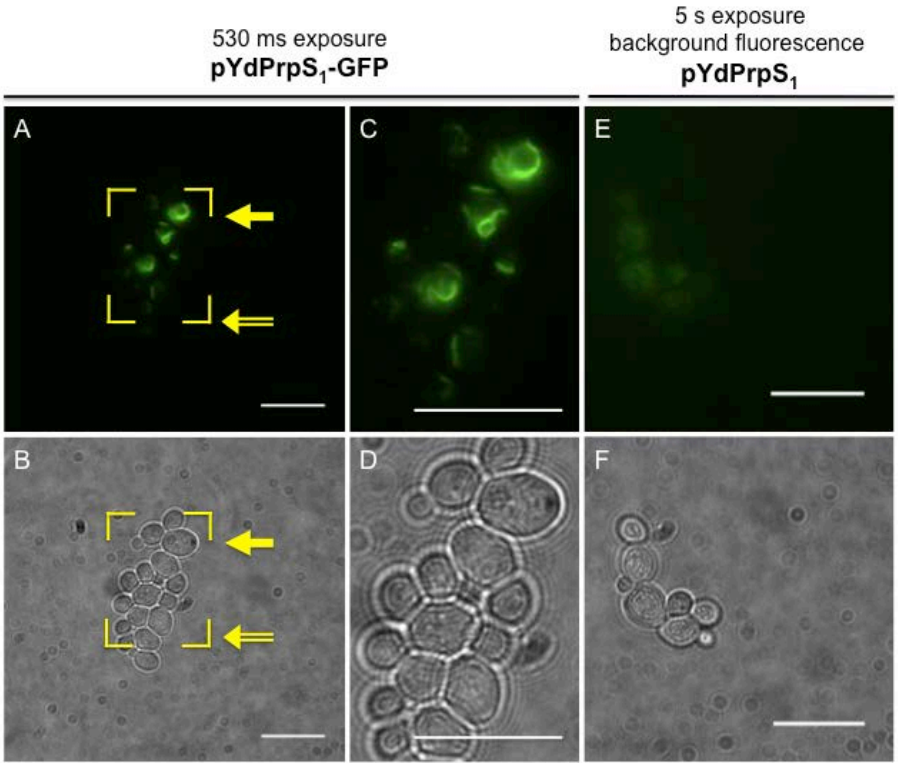

Figure 3.7. Heterogeneity in the GFP emission of pYdPrpS$_1$-GFP. A: GFP signal of pYdPrpS$_1$-GFP after 530 ms of exposure. **B**: bright field of panel A. The single line arrow indicates a cell exhibiting noticeable GFP fluorescence. The double line arrow indicates an area with several cells, which did not exhibit GFP signal. **C**: magnification corresponding to the yellow square indicated in A. **D**: bright field of panel C. **E**: background fluorescence of pYdPrpS$_1$ overexposed during 5 s. **F**: bright field of panel E. Fluorescence images were taken using TRITC filter: excitation 492 nm, emission 519 nm. Scale bar:12 µm.

These results confirmed that yeast transformation was successfully carried out and that PrpS$_1$-GFP was expressed in pYdPrpS$_1$-GFP. Moreover, fluorescence analysis between pYdPrpS$_1$-GFP and pYdPrpS$_1$, confirmed that the GFP fluorescence correspond to a real signal from PrpS$_1$-GFP as pYdPrpS$_1$ with did not exhibited fluorescence. Additionally, heterogeneity in the fluorescence of pYdPrpS$_1$-GFP, suggested that PrpS$_1$-GFP was not properly expressed and/or targeted to the plasma membrane.

Western blot analysis was carried out to allow to confirm expression and timing for PrpS$_1$-GFP expression. This would provide valuable information to ensure a

suitable time exposure to PrpS during the *in vitro* SI bioassay. **Figure 3.8.A** shows a coomassie staining gel with 50 µg of protein extraction from pYdPrpS$_1$-GFP at different times. At 0 to 3 h, the protein pattern of bands remained constant. At later time points (23 and 27 h) the bands corresponding to proteins with a size larger than 55 kDa decreased in comparison with the early time points. This was especially dramatic for proteins between 100 and 250 kDa, where proteins of this size were not detected at 23 and 27 h.

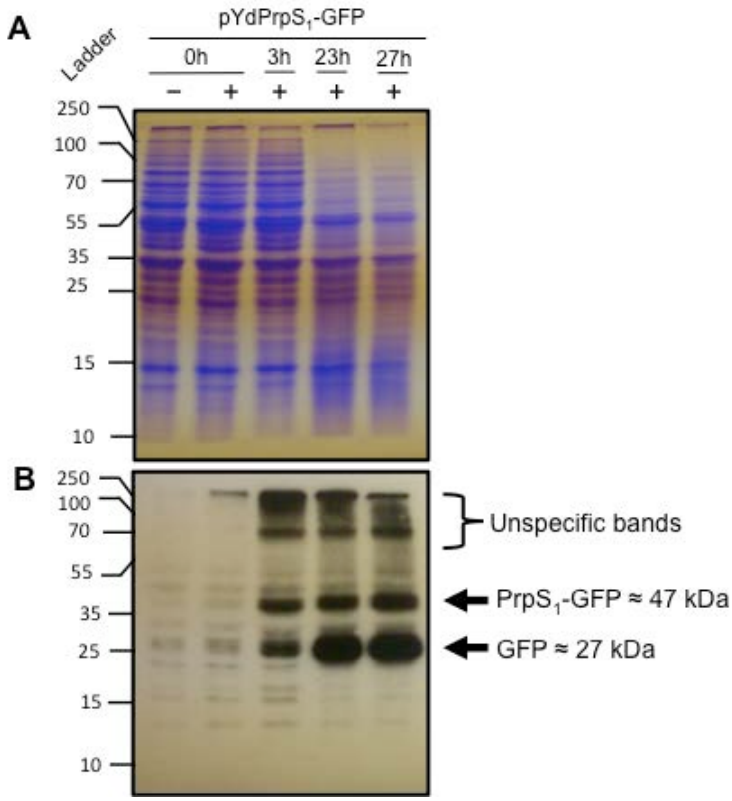

Figure 3.8 PrpS$_1$-GFP protein is expressed and detected in transformants yeast pYdPrpS$_1$-GFP. The expression of PrpS$_1$-GFP protein was assessed at different time points after induction of the *GAL1* promoter by the addition of 2% galactose to the media. **A:** Coomassie blue staining shows the protein concentration of yYdPrpS$_1$-GFP taken without (-) and with galactose induction (+) at 0 h and 3, 23 and 27 h after induction (+). B: Western blot against GFP detected a band of the expected size (PrpS1-GFP of ≈ 47 kDa).

Western blot using GFP antibody to detect PrpS$_1$-GFP protein (≈ 47 kDa) extracts at the time points previously mentioned, revealed a band at 3 h. This

band was also present at 23 and 27 h (**Figure 3.8.B**). Additionally, there was a band at ≈ 27 kDa, which could correspond to GFP alone, and would indicate that $PrpS_1$-GFP was being cleaved. Also, unspecific bands corresponding to a high molecular weight (between 70 and 250 kDa) were detected. This result confirmed the expression of $PrsS_1$-GFP in pYdPrpS_1GFP and allowed us to identify that 3 h after induction, the protein was already expressed at high levels.

Together the growth curve and the $PrpS_1$-GFP expression analysis were used to design the SI bioassay experiments. The growth curve revealed that the exponential time was in between 10 and 20 h and the western blot confirmed that 3 h after induction $PrsS_1$-GFP was already expressed in the cells. Thus, the induction was carried out at 10 -11 h of culture (when it was expected that the culture was starting the exponential phase of growth), and the SI treatment 3 - 4 h after (when PrpS was well expressed in the cells). For details see Chapter 2, section 2.3.4.

3.2.8 Functional analysis of $PrpS_1$ and $PrpS_1$-GFP in yeast

The *in vitro* SI bioassay the *GAL1* promoter was induced at 10 - 11 h. Then SI treatments started 3 - 4 h after the induction by the addition of recombinant PrsS. The SI bioassay was carried out with both pYdPrpS_1 and pYdPrpS_1-GFP. If PrpS was functional in yeast, it was expected that PCD would be triggered in pYdPrpS_1 and pYdPrpS_1-GFP after the addition of incompatible $PrsS_1$ to the culture. As a consequence of this PCD in the cultures exposed to PrsS, it was expected that the growth curve would exhibit a lower slope in comparison with

the control cultures exposed to PrsS buffer alone. Similarly, it was expected a lower number of CFU in the cultures challenged with incompatible $PrsS_1$ in comparison with the controls exposed to PrsS buffer alone.

The induction of PrpS started at 10 h by adding galactose. Three hours later, SI treatments began with the addition of incompatible $PrsS_1$. Absorbance values did not exhibit any significant difference between the samples treated with the incompatible $PrsS_1$ (incompatible, SI) and the control samples exposed to S-protein buffer alone (**Figure 3.9.A**). Absorbance of ~4 at 14 h in untreated and incompatible samples did not exhibited significant differences (p-value 0.8771). At this time point the Absorbance values were the same in comparison with the values of Absorbance at 10 h, which was probably a consequence of the addition of $PrsS_1$ and PrsS buffer, and therefore a dilution of the cultures. Absorbance values of ~8 at 15 h, ~9 at 17.5h, ~12 at 20 h, and ~17 at 36 h did not exhibited significant differences between untreated and incompatible cultures (p-values of: 0.9901, 0.9101, 0.2513, and 0.8391 respectively).

The counting of colony-forming unit (CFU) did not exhibit significant differences between pYdPrpS$_1$ exposed to incompatible $PrsS_1$ and the controls exposed to S-protein buffer alone (**Figure 3.9.B)**. After 1 h incompatible and untreated cultures did not exhibit significant differences and both had CFU values ~ 1.3×10^8, (p-value 0.8438). At 2.5 h both cultures remained without significant differences with CFU values ~ 2.0×10^8 (p-value 0.9294). For the later time points 5 h and 23 h both cultures remained unaltered exhibiting values ~ 2.0×10^8 without significant differences between untreated and incompatible cultures (p-values 0.9284 and 0.8293 respectively).

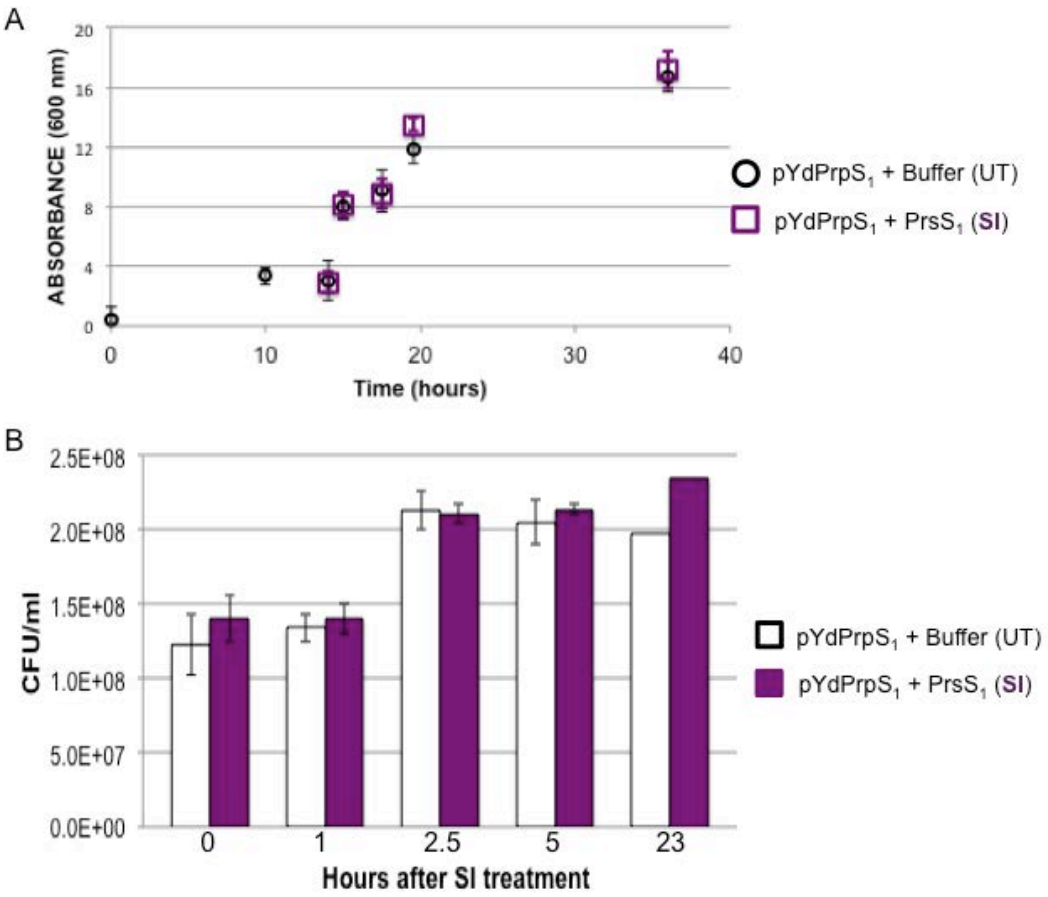

Figure 3.9 Functional analysis of the effect of PrsS on yeast expressing $PrpS_1$. The Colony-forming Unit (CFU) of pYdPrpS1 was monitored after exposure to PrsS during the exponential growth phase. **A**: Growth curve of $pYdPrpS_1$ monitored by the Absorbance. Galactose induction was done at 10 hours and SI induction 2 hours after. Black circle: $pYdPrpS_1$ exposed to S-protein buffer alone (untreated). Magenta square: $pYdPrpS_1$ exposed to incompatible PrsS1 (SI). ANOVA analysis was used to compare the means of three independent experiments. **B**: Counting of CFU. White bars: $pYdPrpS_1$ exposed to S-protein buffer alone (untreated). Magenta bars: $pYdPrpS_1$ exposed to incompatible $PrsS_1$ (SI). Student's T-test was carried out to compare the means of two experiments. Time point corresponding to 23 h has only one value. Errors bars: SEM.

These results did not reveal differences between control cultures of $pYdPrpS_1$ exposed to S-protein buffer alone and $pYdPrpS_1$ cultures exposed to incompatible $PrpS_1$. This data suggested that $PrpS_1$ did not trigger a reduction in the viability of yeast, suggesting that $PrpS_1$ was not functional in yeast.

Next, similar experiments were carried out monitoring the Absorbance and CFU of $pYdPrpS_1$-GFP exposed to incompatible $PrsS_1$ and its respective control of exposure to PrsS buffer alone. Unlike $pYdPrpS_1$ culture, $PrpS_1$-GFP protein

expression was confirmed in pYdPrpS$_1$-GFP culture, by both microscopy of GFP emission, and western blot analysis. Thus, in these experiments we knew that PrpS was at least being expressed. **Figure 3.10.A** shows Absorbance values of the control culture (i.e. pYdPrpS$_1$-GFP exposed to PrsS buffer only), and the incompatible combination (i.e. pYdPrpS$_1$-GFP exposed to incompatible PrsS$_1$). Galactose induction was carried out at 11 h where the Absorbance was ~5. One hour after, the SI treatment started with the addition of PrsS$_1$. At this point, a small decrease in the Absorbance (~ 4) was measured, but this was likely to be due to a dilution effect because of the addition of PrsS$_1$ as it also occurred after the addition of S-protein buffer alone (untreated control). Absorbance of ~4.5 at 13 h did not reveal significant differences between incompatible culture and controls. (p-value 0.1501). For the following time points the Absorbance between incompatible and control cultures were similar and significant differences were not detected. Absorbance of: ~5.5 at 15.5 h (p-value 0.6188); ~6.5 at 18 h (p-value 0.2433; ~10 at 27 h (p-value 0.1690); and ~11 at 39 h (p-value 0.6191).

Figure 3.10.B shows the counting of the CFU of the control culture (i.e. pYdPrpS$_1$-GFP exposed to PrsS buffer only), and the incompatible combination (i.e. pYdPrpS$_1$-GFP exposed to incompatible PrsS$_1$). At 0 and 1 h, both cultures had around 6.0×10^7 CFU without significant differences (p-value 0.0949 and 0.4905 respectively). For later time points measured (2.5, 5, 15 and 27 h) the number of CFU increased and remained constant to between 8.0×10^7 and 1.0×10^8 without differences between the cultures exposed to PrsS buffer alone and the cultures exposed to incompatible PrsS$_1$ (p-values 0.710, 0.291, 0.249, 0.925 respectively).

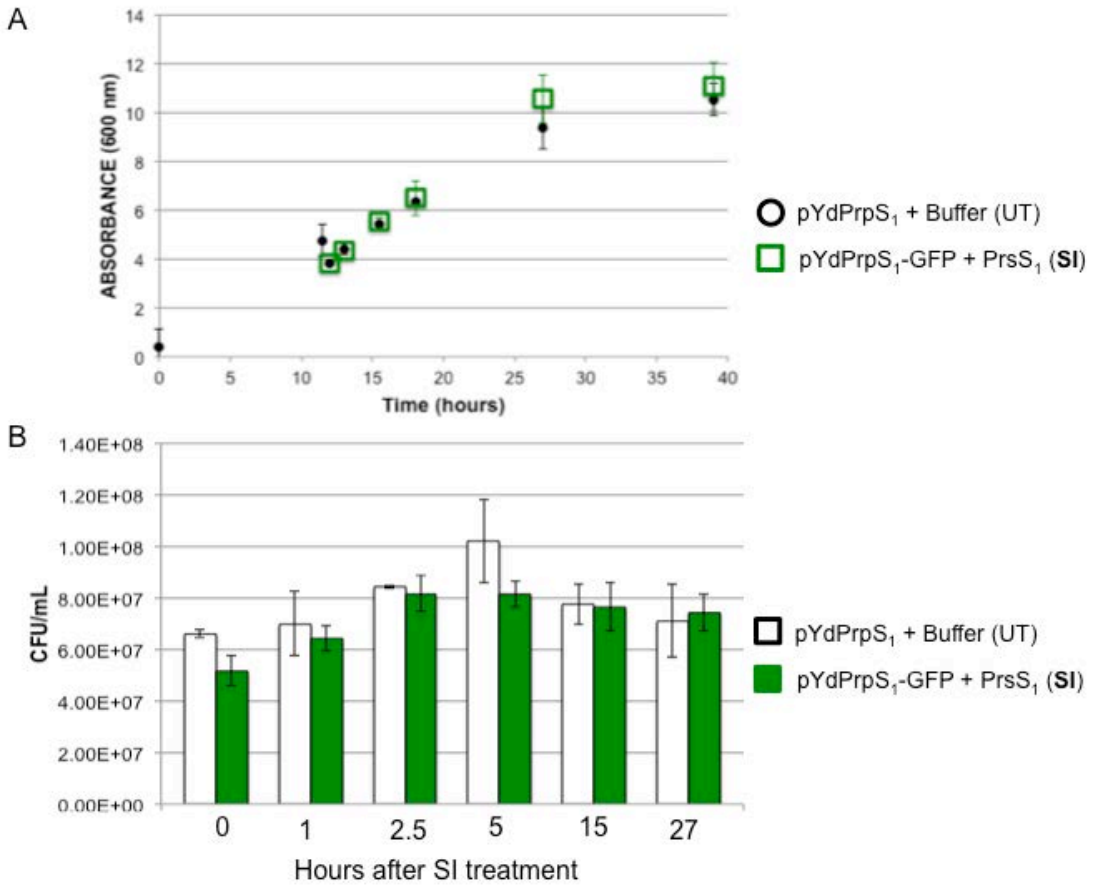

Figure 3.10. Functional analysis of the effect of $PrsS_1$ on yeast expressing $PrpS_1$-GFP. The Colony-forming Unit (CFU) of pYdPrpS_1-GFP was monitored after exposure to PrsS during the exponential growth phase**.** **A**: Growth curve of pYdPrpS_1-GFP monitored by the Absorbance. Galactose induction was done at 11 hours and SI induction 1 h after. Black circle: pYdPrpS_1-GFP exposed to S-protein buffer alone (untreated). Green square: pYdPrpS_1-GFP exposed to incompatible $PrsS_1$ (SI). **B**: Counting of CFU. White bars: pYdPrpS_1-GFP exposed to S-protein buffer alone (untreated). Green bars: pYdPrpS_1-GFP exposed to incompatible $PrsS_1$ (SI). In A and B: ANOVA analysis was carried out using three independent experiments. Errors bars: SEM.

Results from both pYdPrpS_1 and pYdPrpS_1-GFP showed similar tendencies without differences when comparing incompatible combination versus untreated cultures. These data showed that PrsS treatments did not have a detrimental effect neither in the growth rate nor in the CFU, suggesting that $PrpS_1$-GFP was not functional in yeast.

3.3 Discussion

In this Chapter we presented an attempt to transfer the *Papaver* SI system into two different single cellular model systems: *Arabidopsis thaliana* mesophyll protoplasts and *Saccharomyces cerevisiae.*

Arabidopsis protoplasts expressing $PrpS_1$-GFP*,* exhibited a decrease in the viability after treatments with incompatible $PrsS_1$. Interestingly, pretreatments with the caspase-3 inhibitor Ac-DEVD-CHO could prevent the increase in dead protoplast after the exposure to incompatible $PrsS_1$. These results suggested that PrpS was functional in *Arabidopsis* protoplasts leading to PCD in response to incompatible PrsS. However, these results did not provide a categorical conclusion because the differences were not so clear as the differences obtained when PrpS was transferred into *Arabidopsis* pollen (de Graaf et al., 2012). In these experiments, the *Arabidopsis* pollen viability decreased 70% after exposure to incompatible PrsS (de Graaf et al., 2012), whereas in *Arabidopsis* protoplast, the viability decreased only 25%. Also considering the experiments carried out previous to this thesis (Vatovec (2012), Juarez-Diaz and Beacham, unpublished data) the viability values of the controls were around 60% and therefore any difference compared to the incompatible combination was not clear.

Low transfection efficiency was a constant problem in the experiments using protoplasts. It has been reported that efficiencies greater than 50% can be reached (Yoo et al., 2007), however, we could not obtain efficiencies higher than 25 - 30%. A small number of protoplasts transfected in the sample used for the functional analysis, could explain the small differences in the viability test. If

only a minority of protoplasts is transfected in a population, any potential response, and therefore difference with the controls, will be minimised. A strategy to avoid this problem would be generate stable transformed transgenic plants and then carry out the protoplast isolation protocol with this transgenic plants.

Another alternative to explain the small difference between SI treatments and the controls, is that PrpS was not properly targeted, probably due of faulty processing during the secretory pathway. This could include misfolding of PrpS, or PrpS trapped in any organelle of the endomembrane system such as endoplasmic reticulum or Golgi apparatus, and/or failure in the subcellular destination. It has been reported that PrpS localises in the plasma membrane in *Papaver* pollen tube (Wheeler et al., 2009). A predominant membrane localisation was maintained when PrpS was expressed in pollen from *A. thaliana* (de Graaf et al., 2012). Thus, it was expected a similar distribution in *Arabidopsis* protoplasts, with a fluorescence signal mainly delimited at the edge of the circular shape of the protoplasts. However, the microscopic analysis of the GFP emission (**Figure 3.2**) supports revealed a heterogeneity distribution of $PrpS_1$-GFP emission, supporting the possibility of issues during the secretory pathway (further discussed in Chapter 4). Since PrpS was fused to GFP it is possible that GFP tag was affecting the protein function and/or subcellular localisation as it has been reported in other studies (Rappoport and Simon, 2008).

Despite these experiments being inconclusive, they provided preliminary evidence suggesting that PrpS can be functionally transferred to vegetative cells. The reduction in the viability of protoplasts expressing $PrpS_1$ after

exposure to incompatible $PrsS_1$, and the prevention in dead after pre-treatment with caspase inhibitor, suggests that PrpS-PrsS interaction is triggering a "*Papaver* SI-like response" in *Arabidopsis.* This would suggest that the *Papaver* SI system does not require a specific mechanism used by reproductive cells. Moreover PrpS and PrsS would be enough to recruit the cellular components from the host cells, and activate universal signalling pathways described to be involved in the *Papaver* SI response and conserved among diverged cells (Chapter 1, section 1.1).

Saccharomyces cerevisiae transformed with PrpS and PrpS-GFP did not reveal a decrease in the growth rate or the CFU as expected. These results have two main interpretations. One of them is that PrpS is not functional in yeast. Since yeast is more evolutionary diverged from *Papaver* than *Arabidopsis,* a feasible conclusion is that there were evolutionary restrictions, which could have prevented to PrpS-PrsS to access and/or recruit the cellular components of the yeast. The other alternative is that due to experimental reasons, the *in vitro* SI bioassay was not suitable to evaluate the functionality of PrpS. Similar to the situation mentioned previously with the protoplasts, experimental problems comprise potential issues in the biosynthesis of PrpS in yeast during the secretory pathway. Misfolding of PrpS or failure in the PrpS destination are some possibilities. An alternative explanation could be that the response (assuming that there was one) included a slow decrease in the viability, which was compensated for the growth rate of yeast. Thus, the number of yeast cells dying does not have an impact in the total population, which exhibited a sustainable growth due to its rapid generational time (doubling every 1.5 - 2 h). Another alternative as a consequence of malfunctioning during the synthesis or

targeting of PrpS, could be that even though all the cells were transformed with PrpS, there was a heterogeneity in the expression of PrpS. This could imply that only a fraction of the cells were properly expressing functional PrpS, and therefore exhibited a response. Thus, any potential functional response would have been diluted by the non-responsive cells.

Monitoring a different key hallmark from the *Papaver* SI response such as actin cytoskeleton, represents a feasible alternative to evaluate weather PrpS is triggering a “SI-like” response. Actin cytoskeleton has been studied in yeast (Gourlay and Ayscough, 2005), therefore it represent a feasible approach for future studies.

In the following chapters our attempt to evaluate the functionality of PrpS in another cellular model, mammalian HeLa cells. Some of the traditional hallmarks of the *Papaver* SI response will be monitored in HeLa cells expressing PrpS during the exposure of PrsS.

CHAPTER 4

Functional Analysis of *Papaver* Male *S*-determinant PrpS in Mammalian Cells: Calcium Response and Electrophysiological Activity

4.1 Introduction

Chapter 1 (section 1.1.1) described how Ca^{2+} is a central molecule participating in a wide variety of conserved signalling pathways in highly diverged cells. Moreover, it was been established and well documented that Ca^{2+} plays a major role in the *Papaver* SI response. These alterations are triggered after the recognition of "self" male (PrpS) and female (PrsS) determinant (*S*-determinants), which generated an incompatible response (Chapter 1, section 1.4.6.2). Alterations in the $[Ca^{2+}]_i$ are one of the earliest and first studied events in the SI response, where increases in $[Ca^{2+}]_i$ where detected in *Papaver* pollen tubes micro-injected with Ca^{2+}-sensitive dyes (Franklin-Tong et al., 1993a). These alterations were S-allele specific and comprise a transient increase of the $[Ca^{2+}]_i$ (Franklin-Tong et al., 1996, Franklin-Tong et al., 1997) causing the loss of the tip-focused calcium gradient necessary for the normal growth of the pollen tube (Holdaway-Clarke et al., 1997). These transient increases started with a very rapid increase (within the range of seconds) of up to 10-fold increase from the basal levels (Franklin-Tong et al., 1996, Franklin-Tong et al., 2002, Franklin-Tong et al., 1997). Studies using an ion selective vibrating probe determined that an influx of extracellular Ca^{2+} was involved in the increase of the $[Ca^{2+}]_i$ (Franklin-Tong et al., 2002). Patch-clamp experiments using *Papaver* pollen protoplasts, confirmed that a SI-induced current was induced in the pollen grain plasma membrane specifically after treatments with the incompatible cognate PrsS (Wu et al., 2011) (Chapter 1, section 1.4.6.2). This SI-activated conductance was permeable to both divalent and monovalent cations such as Ca^{2+} and K^+ respectively (Wu et al., 2011). This duality in the

permeability does not rule out PrpS as a channel, as other channels have been described in this situation (Hess et al., 1986, Oosawa, 1989). However, other properties such as the conductance activation at resting potential or the lack of sensitivity to pH does not resemble the Ca^{2+}-permeable channels described in plants so far (Wu et al., 2011), suggesting that PrpS involves a new type of channel or channels, which needs to be further investigated.

The virtually immediate initiation of the *Papaver* SI response, suggests that PrpS-PrsS interaction might be a receptor-ligand interaction, activating a Ca^{2+}-signalling pathways. According to the current model PrpS might be a Ca^{2+} channel mediating the Ca^{2+} influx during the *Papaver* SI response (Chapter 1, section 1.4.6.2.1). However its functional characterization still needs to be confirmed.

Originally, when only alleles of PrsS had been identified and cloned, the SI bioassay used to identify the mechanisms involved in the *Papaver* SI response, was restricted to the use of poppy pollen containing endogenous PrpS. However, once alleles of PrpS were identified and cloned (Wheeler et al., 2009), PrpS could be transformed into a heterologous system. *Arabidopsis* was successfully transformed with *Papaver* SI system (Chapter 1, section 1.4.7). *Arabidopsis* pollen expressing PrpS exhibited an equivalent SI response, in comparison to the response in *Papaver*, including F-actin foci formation and PCD, when it was exposed to incompatible recombinant PrsS (de Graaf et al., 2012). Remarkably, it has been recently demonstrated that both PrpS and PrsS are functional *in vivo*, converting a self-compatible and highly diverged lineage such as *A. thaliana*, into a self-incompatible one just by transferring the *Papaver* S-determinants (Lin, 2015).

The fact that PrsS and PrpS are not only functional but also able to trigger SI in a heterologous system, suggests that the *S*-determinants have the capacity of recruiting cellular components from the host cell for downstream effects such as actin alterations and PCD. This has prompted the idea of exploring the versatility of the *S*-determinants, and establishing if they can be functionally transferred in to a more evolutionarily distant cell line.

Animal and plant cells are highly diverged, however they still share some characteristics that provide support to make this attempt of transfer of *Papaver* SI into mammalian cells feasible. Much of the *Papaver* SI studies have taken inspiration from classic animal cell-cell communication and signalling studies. This is also the case for the techniques; for instance, the initial studies suggesting that Ca^{2+} was an important molecule involved in the SI response in *Papaver* were carried out using live cell calcium imaging (Franklin-Tong et al., 1993b), which is a techniques that was initially developed in animal cells (Tsien, 1988, Haugland et al., 2002).

Increases in the $[Ca^{2+}]_i$ and F-actin alterations are *Papaver* SI hallmarks especially relevant for this thesis, as functional similarities have been described in animal cells and particularly mammalian cells. Calcium influx is one of the earliest events of the *Papaver* SI response and it is essential for the activation of downstream events. Moreover, it was established that F-actin foci formation was induced after increases in $[Ca^{2+}]_i$, providing evidence for a link between Ca^{2+} and F-actin (Snowman et al., 2002). Additionally, ABP (ADF and CAP) were also identified mediating the *Papaver* SI response leading to PCD (Poulter et al., 2010). In animal cells, Ca^{2+} also represents a key molecule mediating different signalling pathways (Lipscombe et al., 1988, Berridge, 1993, Berridge

et al., 1998) (Chapter 1, section 1.1.1). Moreover, the family of actin depolymerizing factor (ADF)/cofilin proteins has emerged as a connecting point in the cell physiology, providing a link between Ca^{2+} and actin cytoskeleton (Bernstein and Bamburg, 2010). Additionally, it has been demonstrated that ADF/cofilin also plays a regulatory role during the initiation of apoptosis in mammalian cells (Chua et al., 2003).

These common components between plant and animal cells suggest evolutionary conservation (previously discussed in Chapter 1 section 1.1), which might allow the use of mammalian cells as a heterologous system to characterise further the proteins and signalling pathways triggered during the *Papaver* SI response. Therefore, an attempt to assess whether the poppy SI *S*-determinants are functional in mammalian cells emerges as ambitious, but feasible challenge to investigate further the *Papaver* SI response. Moreover, this would allow us to explore whether it was possible that a plant system can operate in an animal cell system, which is relevant in an evolutionary context providing potential new resources to study conserved signalling pathways in diverged cells.

The experimental design comprised of an *in vitro SI* bioassay, with mammalian cells expressing PrpS, subsequently exposed to incompatible PrsS. If PrpS was functional, it was expected that the cells showed similar alterations to the ones described for the *Papaver* SI (Chapter 1, section 1.4.6.2).

In this chapter we have focused on the cell transfection with *PrpS* and subsequent analysis of HeLa cells expressing PrpS fused to GFP by microscopic analysis of GFP emission. Additionally, we present functional analyses using live-cell calcium imaging, monitoring the $[Ca^{2+}]_i$ of HeLa cells

expressing PrpS during the SI bioassay. Using patch clamp experiments on *Papaver* pollen Wu et al. (2011) established that a non-specific cation current was mediating the *Papaver* SI response. Thus, we used a similar approach on HeLa cells aiming to assess the proposed nature of PrpS as an ion channel (details in Chapter 1, section 1.4.6.2.1). Using patch-clamp experiments, we monitored the membrane currents of HeLa cells expressing PrpS exposed to incompatible PrsS.

4.2 Results

Data from both transient, and stably transfected HeLa cell lines with *PrpS* will be presented. Since transient transfections are a rapid procedure, they were used to standardise and optimise the transfections and determine the subcellular localisation of PrpS (Chapter 2 section 2.4.3.1). The use of stable transfected mammalian cell lines is a common method used to evaluate gene function (Kim and Eberwine, 2010). Thus, stable transfected lines were generated (Chapter 2 section 2.4.3.2) and functional analyses of PrpS were evaluated.

A summary with the genetic constructs and cell lines used during this chapter are presented in Table 4.1. For further details in Chapter 2, section 2.4.2.

Table 4.1. Genetic constructs and cell lines generated for PrpS analysis in HeLa cells. These constructs were provided by Dr Andrew Beacham.

Cell line	Genetic construct	Description / Observations
N/A	pEGFP-PrpS *CMV*::*PrpS$_x$-GFP* (x = alleles 1, 3 & 8)	Plasmid pEGFP has the promoter CMV promoter and EGFP as a C-terminal fusion tag protein. It was used to generate transient lines for expression analysis of $PrpS_1$, $PrpS_3$ and $PrpS_8$.
HeLa-mCh	pmChN (*CMV*::*mCherry*)	Plasmid pmCherryN1 (Clontech) contains the CMV promoter and mCherry (mCh) as a fusion tag protein. It was used to generate stable lines and represents the negative control (empty vector) for functional analysis.
HeLa-C-PrpS$_1$	pmChC-$PrpS_1$ (*CMV*::*PrpS$_1$-mCh*)	Plasmid pmCherryN1 (Clonetech) contains the CMV promoter and N-terminal mCherry (mCh) as a fusion tag protein. Stable line with $PrpS_1$ was generated and used for functional analysis.
HeLa-N-PrpS$_1$	pmChN-$PrpS_1$ (*CMV*::*mCh-PrpS$_1$*)	Plasmid pmCherryC1 (Clonetech) contains the CMV promoter and C-terminal mCherry (mCh) as a fusion tag protein. Stable line with $PrpS_1$ was generated to compare transfection efficiencies with pmCherryC1.

Only transient transfections were carried out with pEGFP vector, and therefore cell lines were not generated with this plasmid. Function analyses were not carried out with HeLa-N-$PrpS_1$ as preliminary studies did not exhibit any response with this cell line.

4.2.1 Characterisation of the subcellular localization of PrpS-GFP in HeLa cells

PrpS subcellular localisation in *Papaver* pollen has been described mainly associated with the plasma membrane, however, immunolocalisation analysis also showed some PrpS signal within the pollen tube (Wheeler et al., 2009, Poulter, 2009). Therefore, confirming the subcellular localisation of PrpS in HeLa cells was relevant to confirm both protein expression, and also, to confirm that PrpS exhibited the same subcellular localisation (associated with the plasma membrane) in mammalian HeLa as it does in *Papaver* pollen.

Confocal microscopy using HeLa cells transiently transfected with pEGFP-$PrpS_1$ and pEGFP-$PrpS_3$ (C-terminus fusion to GFP) was used to assess the subcellular localisation of $PrpS_1$-GFP and $PrpS_3$-GFP respectively. Representative images of the pattern of GFP emission of HeLa-$PrpS_1$-GFP and HeLa-$PrpS_3$-GFP are shown in **Figure 4.1**.

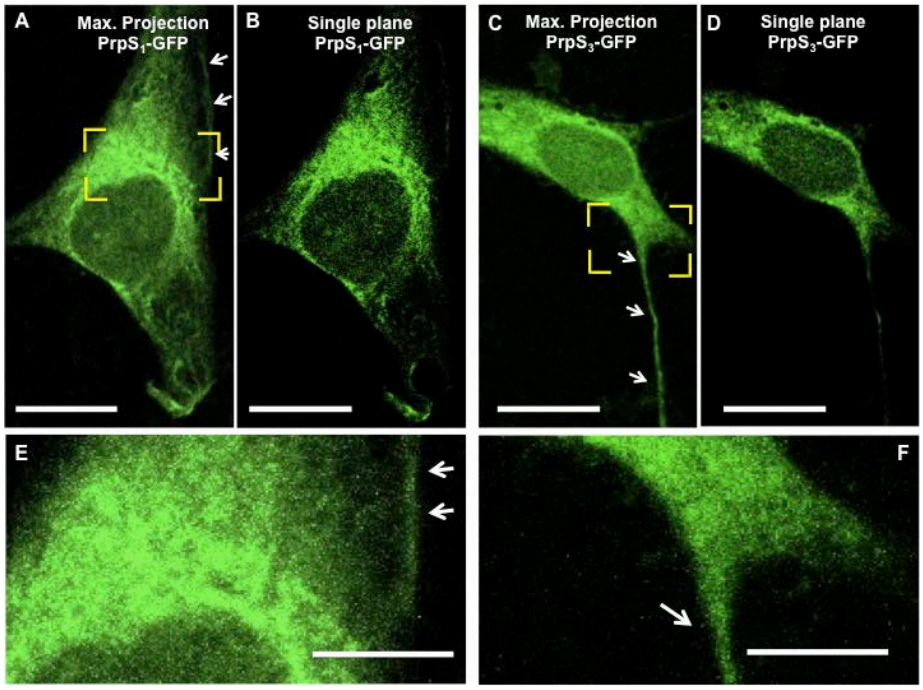

Figure 4.1 Representative confocal images of the GFP fluorescence in HeLa cells transformed with pEGFP-PrpS. (A) Maximum projection stack of a fixed HeLa cell expressing $PrpS_1$-GFP. White arrows indicate emission on the edge of the cell suggesting that at least some $PrpS_1$-GFP might be reaching the plasma membrane. **(B)** Single plane of the fixed HeLa cell showed in (A). This image shows the reticulated pattern expression of the GFP emission. **(C)** Maximum projection stack of a fixed HeLa cell expressing $PrpS_3$-GFP. White arrows indicate GFP emission in a cell projection such as pseudopodium or lamellipodium. **(D)** Single plane of HeLa cell fixed showed in (C). Reticulate patterns expression of the GFP emission. **(E)** Magnification of the yellow rectangle indicated in (A). Shows the differential intensity of the emission and also the putative plasma membrane (white arrows). **(F)** Magnification of the yellow rectangle indicated in (C). Shows a detailed section of the membrane projection. Fluorescence in all the images were taken with Argon 488 nm laser and collecting the emission between 500 - 540 nm. Scale bar in A-D = 25 µm and in E, F = 11 µm.

The distribution of the GFP signal was neither wholly associated with nor predominantly associated to the plasma membrane as expected. The distribution was not homogeneous in the cell, which exhibited a circular area in

the centre of the cell with lower signal surrounded by an area with a reticulate pattern and high emission of GFP (**Figure 4.1.A-D**). Magnifications of these images show in detail the differences in the intensity of the emission with a lower and a higher area as well as a signal distribution on the edge of the cell, which might correspond to $PrpS_1$-GFP reaching the plasma membrane (**Figure 4.1.E**). However, because the signal was too broad to be just plasma membrane, based on this data it was not possible to conclude that PrpS-GFP located on the plasma membrane. Similarly, a magnification of the cell expressing $PrpS_3$-GFP (**Figure 4.1.F**) shows a detail of the cell projection, probably a pseudopodium or lamellipodium, with a sharply delineated GFP signal.

Unfortunately we did not carry out experiments to directly evaluate whether PrpS-GFP was associated to the plasma membrane, Golgi apparatus (GA) or endoplasmic reticulum (ER). This would have helped us to assess the distribution of the fusion protein better. However, after comparison with representative images of HeLa cells labelled with a Golgi-specific protein and with a nuclei stain (Gill et al., 2010), it seems reasonable to consider, based on the similarities, that the central zone with the lower fluorescence emission correspond to the nuclei, and the adjacent zone with high signal correspond to GA or ER. Since the synthesis of secretory and membrane proteins is carried out in the ER in an intimate interaction with the GA (Nelson et al., 2008) it is reasonable to consider that the high levels of expression in these cells, is the result of an overexpression of PrpS-GFP causing alterations in the normal functioning of the secretory pathway, particularly in organelles such as ER or GA.

We decided to evaluate using smaller amounts of DNA for the transfections as this might reduce total expression and focus the pattern of expression to the expected distribution along the edge of the cell. Three different amounts of DNA were tested (0.25, 0.5 and 1.0 µg), but the pattern expression was the same in all the cases, suggesting that the concentration of DNA used was still too high, or that the amount of DNA did not have an effect modulating the expression pattern of PrpS.

These data suggest that PrpS-GFP is localising in the internal organelles such as ER or GA and therefore was not efficiently transported to nor limited to the plasma membrane. Despite problems with the expression of PrpS and the fact that we could not clearly observe distribution at the plasma membrane, we decided to carry on with the functional analysis assuming that some of PrpS was reaching the plasma membrane.

4.2.2 Stable transfection of HeLa cells with PrpS-mCherry: characterisation of PrpS-mCherry subcellular localization and pattern expression

Initially, transient transfections with pmChN-PrpS_1 and pmChC-PrpS_1 were used to test whether the location of mCherry tag (N- or C-terminal respect to PrpS) would make a difference to transfection efficiency or mCherry expression pattern. Transfections with pmChC-PrpS_1 showed a slightly higher of transfection efficiency (28%) in comparison with pmChN-PrpS_1, with a 20% (details in Chapter 2 section 2.4.3.2).

Small proportions of transiently transfected cells integrate the foreign DNA into the genomic DNA, resulting in replication of the transgene. So not all the cells express the transgene. However, under the selective pressure of the encoded antibiotic, selection to maintain just the cells that carry the gene for antibiotic resistance, plus the cassette containing *PrpS* on the chromosome, which after proliferation will generate a stable, transfected line. For robust functional analysis we generated stable PrpS-mCherry lines to carry out the functional analysis. Although, transfection efficiencies were low, they were considered high enough to attempt obtaining stably transfected HeLa cell lines.

Figure 4.2 shows a colony obtained from stable transfected cells after antibiotic selection (Methods in Chapter 2, section 2.4.3). This type of colony expands in a concentric manner, with more cells concentrated in the centre, as they grow on top of each other whereas on the edge they form the typical monolayer of epithelial cells. The entire isolated colonies were picked from both mCherry constructs pmChN-PrpS_1 and pmChC-PrpS_1 transformants (**Figure 4.2**), at the proliferation stage to isolate and establish the stably transfected cell line.

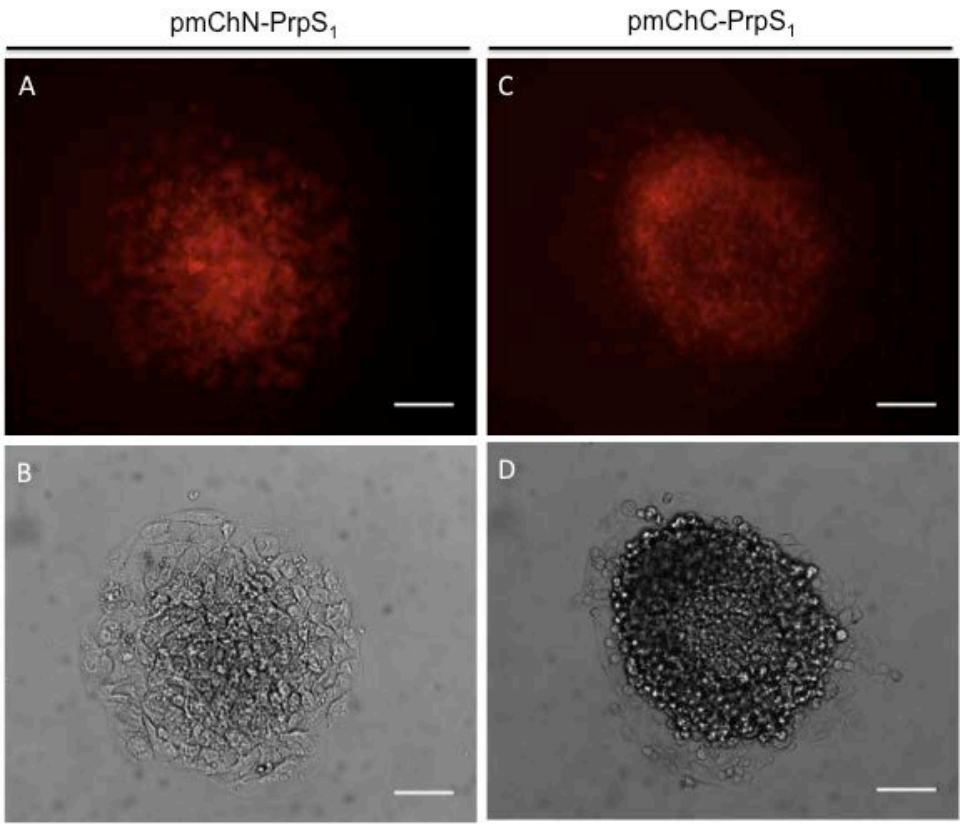

Figure 4.2. Representative images of the stable transfected colonies expressing PrpS-mCh. A colony growing in a circular shape was an important criterion to ensure selection of a clonal cell line. Stable transfected colonies were successfully generated expressing either N-terminal or C-terminal mCherry fused $PrpS_1$. HeLa-N-$PrpS_1$ cells, mCherry fluorescence of (**A**) and bright field (**B**). HeLa-C-$PrpS_1$ cells, mCherry fluorescence (**C**) and bright field (**D**). Fluorescence images were taken using TRITC filter: excitation 550 nm, emission 580 nm. Scale bar: 100 µm.

Similar to the expression patterns obtained for the GFP constructs, fluorescence signal form the mCherry fusion protein was not confined to the border of the cell (**Figure 4.3**). There was a non-homogeneous speckled pattern observed within the cells, with some areas exhibiting very high emission and other areas where the emission was not detected. **Figure 4.3.A** shows representative HeLa-C-$PrpS_1$ cells. **Figure 4.3.B** shows that cells had different levels of expression; the cell on the left exhibited the fluorescence limited to a small area of the cell whereas the fluorescence emission from the cell on the

right was covering a larger area of the cell. Four representative HeLa-N-PrpS_1 cells (N- or C- terminal) are shown in **Figure 4.3.C**. Two cells on the left showed an obvious signal, but the emission exhibited from the two cells on the right was just noticeable (**Figure 4.3.D**).

This suggested that PrpS-mCherry, like the PrpS_1-GFP was not membrane expressed in these cells, denoting potential issues in the synthesis, movement and/or destination of PrsS-mCherry during the secretory pathway. Thus, the bright speckled pattern is likely due to abnormal accumulations of the fusion protein in membrane organelles such as ER or GA. The range in the intensity of the fluorescence signal among the cells was unexpected, as all the cells should have originated from a single stably transfected cell and therefore exhibit the same pattern. One explanation is that they did not originate from a single cell. Alternatively, another parameter such as the aging of the cells, could account for differing total accumulations of PrpS-mCh.

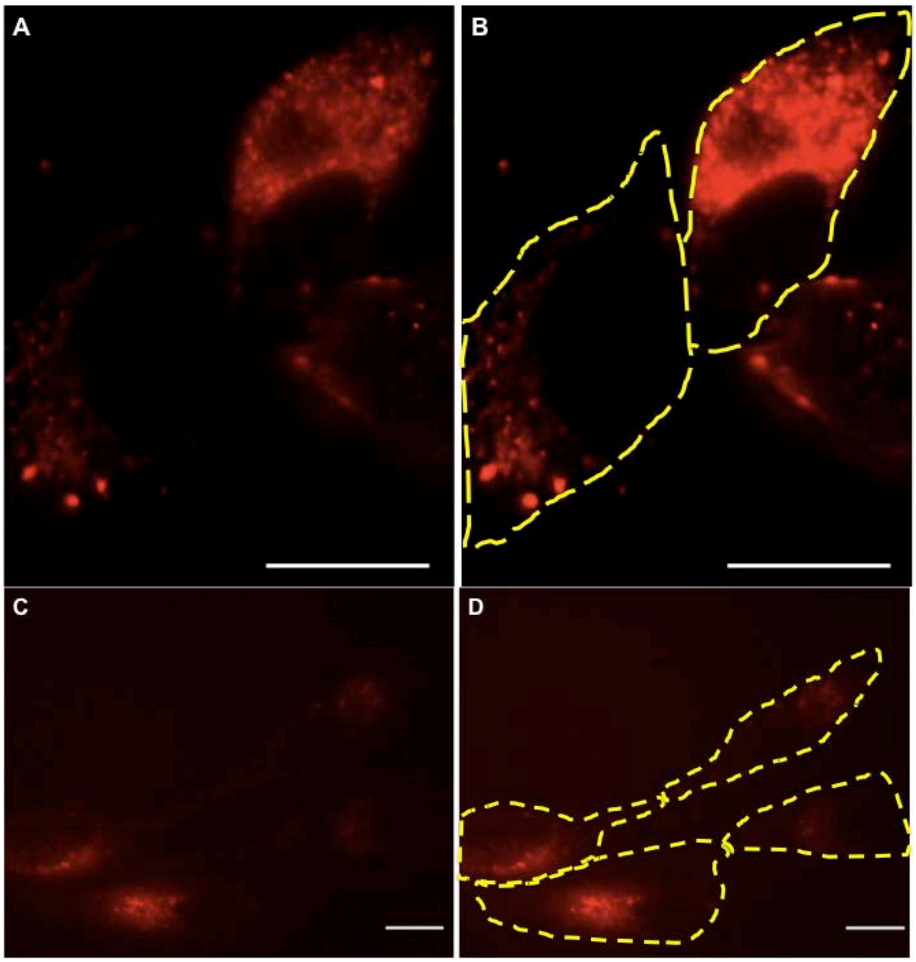

Figure 4.3 Differential intensities of expression of pmChC-PrpS$_1$. Epifluorescence microscopy of stable colonies transfected with PrpS$_1$ with a C-terminal (A and B) and N-terminal (C and D) mCherry tag. As it was expected for a stable transfected cell line, all the cells emitted fluorescence, however the intensity was not homogeneous neither within the cells neither among them. Yellow dashed lines show the edge of the cells determined by overexposing the pictures. Fluorescence images were taken using TRITC filter: excitation 550 nm, emission 580 nm. Scale bar = 15 µm.

Detection of mCherry fluorescence demonstrates that PrpS$_1$-mCh is expressed in these cells, but was likely to be localised in organelles such as ER or GA. Optimising the expression of PrpS1-mCh towards the plasma membrane could be attempted by using weaker promoter, expecting that lower expression helps overcoming the potential issues of PrpS-mCh during the secretory pathway. Additionally, the use of a signal peptide to PrpS-mCh to the plasma membrane could also be an alternative approach (Stern et al., 1997).

However, as the imaging analysis confirmed that the HeLa cells were at least expressing PrpS-mCherry we decided to examine if some of the protein was functional testing whether the cells responded to the addition of PrsS.

4.2.3 Functional analysis: Does PrpS trigger alterations in the intracellular calcium concentrations ($[Ca^{2+}]_i$)?

Having shown that PrpS-mCherry is expressed in HeLa cells, our next aim was to assess whether PrpS, was functional in HeLa cells. Here we monitored and compared the $[Ca^{2+}]_i$ levels in HeLa-C-PrpS_1 cells before and after addition of incompatible PrsS_1 mimicking the SI conditions. Based on the experiments carried out in *Papaver* pollen (Franklin-Tong et al., 1997), we decided that live-cell calcium imaging was a suitable technique for our purposes, as it monitors the $[Ca^{2+}]_i$ of a living cell in real time, allowing us to assess the effect of PrsS on HeLa cells expressing PrpS. Additionally, monitoring $[Ca^{2+}]_i$ by means of a fluorescent calcium-ion-sensitive probe was a practical approach that had already been used in mammalian in HeLa cells (Wyrsch et al., 2013) . Considering all these, we expected that if PrpS was functional in HeLa cells, an increase in the $[Ca^{2+}]_i$ levels would be triggered within seconds after the exposure to incompatible PrsS. Moreover, similar to *Papaver*, we expected that the increase in $[Ca^{2+}]_i$ should be triggered exclusively after treatments with incompatible PrsS_1, and $[Ca^{2+}]_i$ levels remain constant after treatments with compatible PrsS_3 or PrsS_8.

Fluo-4 is calcium sensitive probe, which emission increases when intracellular calcium levels $[Ca^{2+}]_i$ increase (Gee et al., 2000, Haugland et al., 2002). We

selected Fluo-4, due to its high sensitivity in comparison with others fluorescent Ca^{2+} indicators (Thomas et al., 2000). Fluo-4 emission is in green, therefore we used the stable lines of PrpS fused to mCherry (red emission) to avoid fluorescence overlap (see **Table 4.1** for details).

HeLa-C-$PrpS_1$ (see **Table 1**, section 2.4.1) cells were grown on a coverslip in a multi well plate, transferred to a perfusion chamber and loaded with the fluorescent probe Fluo-4. The loaded cells were then exposed sequentially to recombinant $PrpS_1$ (incompatible) and $PrsS_8$ (compatible) whilst $[Ca^{2+}]_i$ was monitored using live-cell calcium microscopy (Method in Chapter 2, section 2.2.1 and 2.4.4). **Figure 4.4** shows a live cell calcium imaging experiment. A time-course summary of procedures during the experiment is detailed in **Figure 4.4.A**. **Figures 4.4.B** shows a graphic with the relative values of the fluorescence intensities of the cells during the experiment, and **Figure 4.4.C** shows the fluorescence intensity, represented in each HeLa-C-$PrpS_1$ cell loaded with Fluo-4 during the exposure to recombinant $PrsS_1$ and $PrsS_8$.

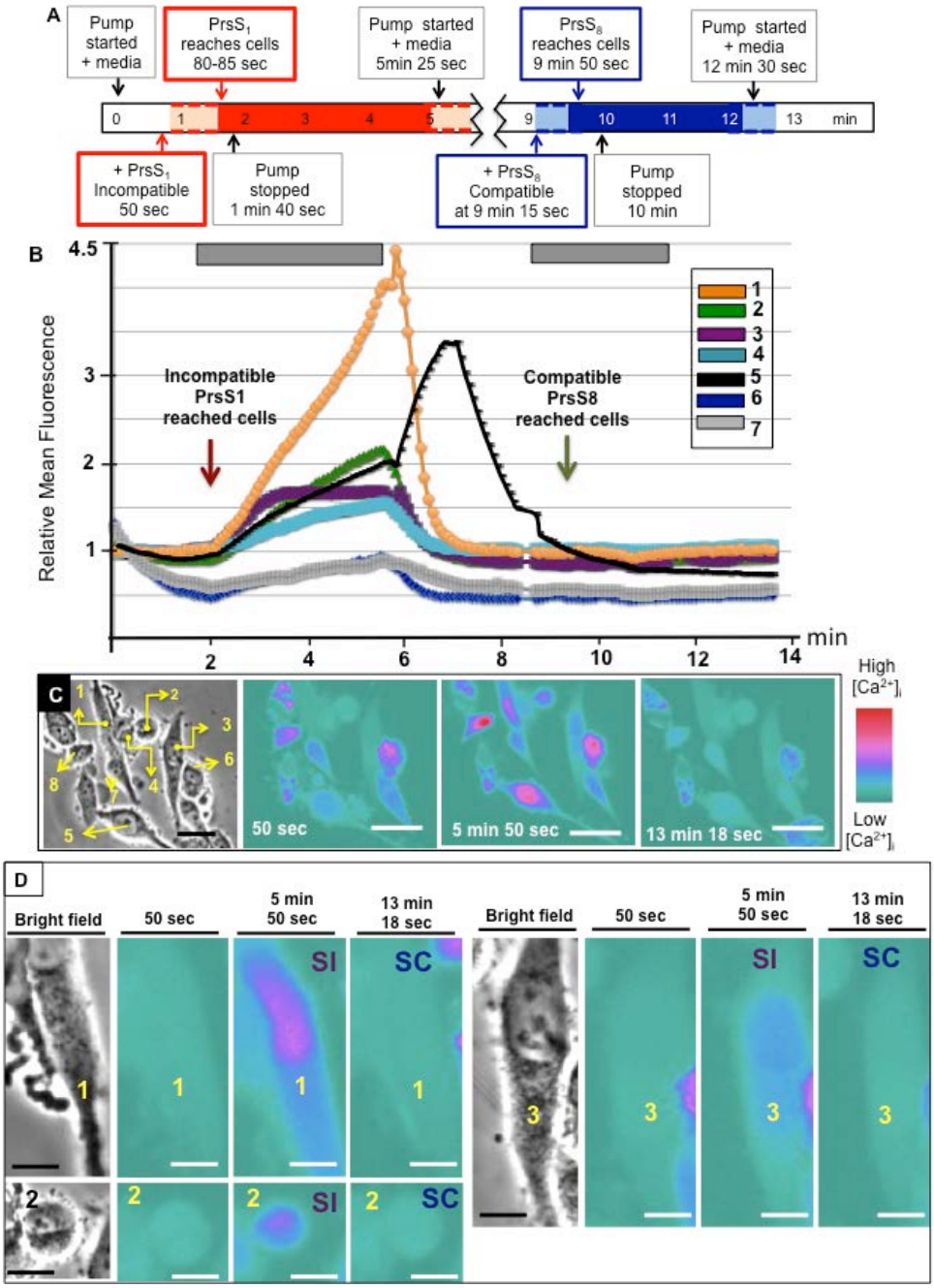

Figure 4.4. Live-cell calcium imaging monitoring $[Ca^{2+}]_i$ of HeLa-C-PrpS$_1$ during SI bioassay. **A)** Cartoon with a timeline summarising the time course with the treatments used during this experimental design. Solid red and blue colours represent the time of effective exposure of PrsS to the HeLa-C-PrpS$_1$. Pale red and light blue represents the time corresponding to the "dead space" tubing between the reservoir and the chamber with the cells. The media used correspond to DMEM FluoroBrite. **B)** Graphic representation of the normalised data corresponding to the fluorescence values obtained during the SI bioassay. Each trace corresponds to one of the cells as labelled section in panel (C)**:** cell 1 in orange, cell 2 in green, cell 3 in magenta and cell 4 in turquoise, cell 5 in black, cell 6 in dark blue and cell 7 in grey. Grey rectangles on top represent the application of the respective PrsS protein. **C)** Pseudo-coloured images showing HeLa-C-PrpS$_1$ cells loaded with the fluorescent calcium dye Fluo-4 and their fluorescence emission. Cells before (50 sec), during SI treatment (5 min 50 sec) and after washing out (13 min 18 sec). Bottom right panel corresponds to the bright field identifying the cells. Scale bar = 20 µm. Fluorescence images were taken using FITC filter: excitation 492 nm, emission 519 nm. **D)** Magnification in detail the temporal and spatial response of cell 1, cell 2 and cell 3 during the time points detailed in (C). Scale bar = 7 µm.

The experiment started with the addition of media alone at a flow rate of 1.5 $mL.min^{-1}$. Recombinant $PrsS_1$ (incompatible with $PrpS_1$) was added to the reservoir 50 seconds after, reaching the chamber between 30 - 35 seconds later. At this point the timing of the calcium alterations (if any) were uncertain, as there was likely a lag time between $PrsS_1$ exposure to $PrpS_1$ before triggering a response. Therefore the pump was stopped between 1 min 40 sec and 5 min 25 sec, in order to allow an increase in the exposure time between PrpS and PrsS, with the intention of maximising the possibility of triggering a measurable response (**Figure 4.4.A**).

At two minutes, after starting the registering of fluorescence, 8 cells showed simultaneous increases in $[Ca^{2+}]_i$. These cells labelled from No. 1 to 8 in **Figure 4.4.C**, bright field panel. Cells 1 to 7 were analysed further, but the analysis of cell number 8 was not possible due to the movement of the cell during the experiment. This movement did not allow to the software used to monitor the fluorescence to obtain the trace of the emission. Quantification of the emission by means of the relative fluorescence of the seven analysed cells, showed an increase in $[Ca^{2+}]_i$. There was variation in both the magnitude and the temporal dynamics of the increases (**Figure 4.4.B**). Cell No. 1 showed a 4.5-fold increase, whereas cell No. 2 a 2-fold increase. Cells No. 3 and 4 only showed a 0.5-fold increase. Cells No. 1, 2 and 4 displayed a gradual increase starting around two minutes after the beginning of the experiment, and reaching a peak in $[Ca^{2+}]_i$ just before six minutes. Cell No. 3 was the quickest reaching its maximal emission (just after minute three), and then its emission remained constant until $PrsS_1$ was washed out the chamber (5 min 25 sec) (**Figure 4.4.B**). Cell No. 5 reached the second highest rise reaching almost 3.5-fold

increase. Particularly cell No. 6, but also cell No. 7 seemed to have had a considerable increase based on the colorimetric scale (**Figure 4.4.C**), however the quantification analysis revealed that these cells only had a 0.5-fold increase. This was because the $[Ca^{2+}]_i$ were already high in these cells at the beginning of the experiment. Moreover, before these cells were exposed to PrsS, their $[Ca^{2+}]_i$ were not stable, and they were decreasing during the first two minutes of the experiment. Once the cells have reached this peak, all the cells, except cell No. 5, exhibited a steep reduction in the fluorescence emission, reaching basal levels at seven minutes after the beginning of the experiment. This decrease coincides with the media replacement, and therefore when $PrsS_1$ was removed from the chamber, suggesting that the increases in $[Ca^{2+}]_i$ were triggered as a consequence of the exposure to $PrsS_1$.

A detailed image of the temporal and spatial increase in the $[Ca^{2+}]_i$ for cell 1, cell 2 and cell 3 is shown in **Figure 4.4.D**. The increase in $[Ca^{2+}]_i$ seemed to have reached its peak in the centre of the cell, however, this interpretation is relative, as the thickness of the cells were not measured, and therefore the pattern of emission could be due to the shape of the cell rather than an response associated with a subcellular localisation. **Figure 4.4.D** also shows that the levels of $[Ca^{2+}]_i$ return to the basal levels after washing $PrpS_1$ out with media, indicating that this increase in $[Ca^{2+}]_i$ was a transient alteration, which represents further evidence supporting that this was a real response.

It is important to consider that the Ca^{2+} is involved in many physiological processes at cellular level, and therefore physiological responses vary between cells. This could explain spontaneous unexpected fluctuations in the Ca^{2+} levels can be ascribed to the metabolic activity of the individual cells. This is an

explanation for cells No. 6 and No. 7 exhibiting higher calcium levels at the beginning of the experiment. Also, it provides an explanation for the delay in the $[Ca^{2+}]_i$ decrease in cell No. 5 (**Figure 4.4.B**). In addition, differences of Fluo-4 loading into the cells, or in the amount of PrpS-mCh expressed on the plasma membrane, can also explain the heterogeneity in the magnitudes of the $[Ca^{2+}]_i$ increase.

Recombinant $PrsS_8$ (compatible with $PrpS_1$-mCh) was added to the cells at resting $[Ca^{2+}]_i$ at 9 min 15 sec, reaching the chamber around 9 min 50 sec. The pump was again stopped between 10 minutes until 12 minute 30 sec exposing the cells to $PrsS_8$. Finally the pump was started at 12 min 30 sec and the cells were washed with media (**Figure 4.4.A**). **Figure 4.4.B** shows that the levels of $[Ca^{2+}]_i$ remained constant at basal levels throughout exposure to $PrsS_8$ protein.

These results indicate that the alterations in $[Ca^{2+}]_i$ were specific for incompatible $PrpS_1$, as no $[Ca^{2+}]_i$ increase was detected during compatible $PrsS_8$ challenge. This is important evidence because specific alteration of $[Ca^{2+}]_i$ during incompatible PrsS challenge is a crucial characteristic of the allelic *S*-specificity in the *Papaver* SI response. This result represented the first evidence that PrpS was functional in HeLa cells by showing that HeLa cells expressing $PrpS_1$ exhibited increases in $[Ca^{2+}]_i$ exclusively after the exposure to incompatible $PrsS_1$.

To confirm that the lack of response to the compatible $PrsS_8$ exposure was a result of the allelic specificity and not because cells were inactivated after exposure to incompatible $PrsS_1$, in the next experiment, we changed the sequence of PrsS addition, and added compatible $PrsS_8$ first, and incompatible $PrsS_1$ afterwards. We also kept the pump moving, to give a more gentle flow

(and therefore less turbulence), which improved the imaging of the cells. However, it also reduced the time of exposure to PrsS. As the flow rate was 1 $mL.min^{-1}$ we calculated that the cells were exposed PrsS for 21 seconds approximately (**Figure 4.5.A**). At this flow rate, it was expected that PrsS reached the chamber around 30 sec after its addition to the reservoir, depending on the amount of media remaining in the reservoir. In this experiment, also a treatment with histamine was included to confirm that the cells were responsive and increases in calcium properly detected.

Histamine is an amine mediating several physiological processes in the cell. In mammalian cells, cellular effects of histamine are mediated *via* G-protein coupled receptors, followed by the generation of inositol-1,4,5-triphosphate (IP3), which causes an increase in $[Ca^{2+}]_i$. It has been reported that histamine treatments activates the MAPK signalling pathways, and it is expected that PCD is triggered in cells exposed to histamine (Beermann et al., 2014). Thus, treatments with histamine are a robust control that increases the $[Ca^{2+}]_i$ providing strong evidence the cells are responsive and properly loaded. However due to its broad physiological effect, interpretations about the dynamics of the $[Ca^{2+}]_i$ after the treatments with histamine do not have biological significance.

Eight HeLa-C-$PrpS_1$ cells labelled with Fluo-4 were selected for further analysis. After preliminary examination, three cells revealed stable $[Ca^{2+}]_i$ before any treatment, these cells were selected for further analysis. The level of relative fluorescence showing changes in the $[Ca^{2+}]_i$ in these cells is presented in **Figure 4.5.B**, and the images detailing the cells labelled from No.1 to 3 as well as the colorimetric images representing the $[Ca^{2+}]_i$ are shown in **Figure 4.5.C**.

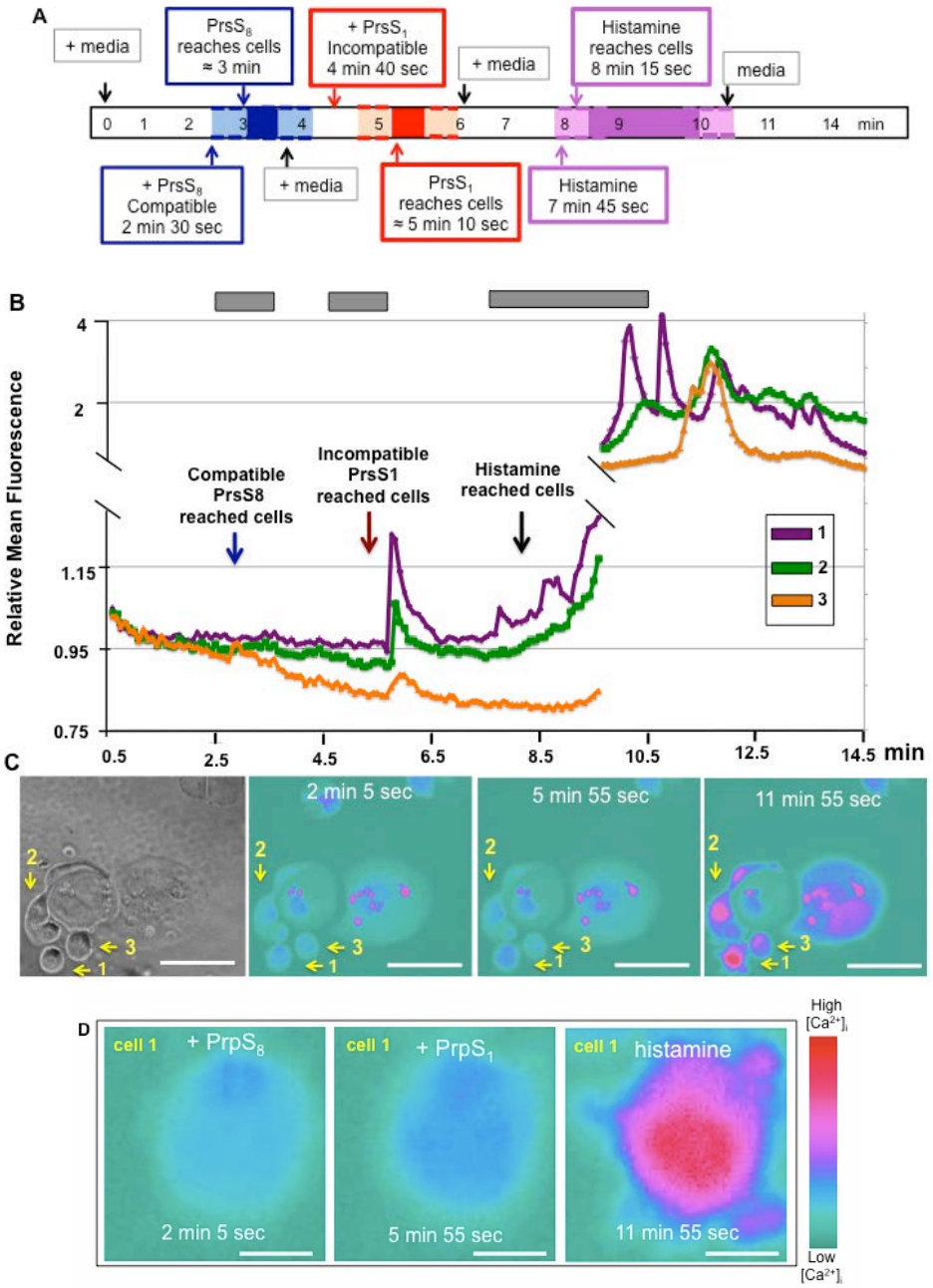

Figure 4.5. **Live-cell calcium imaging monitoring $[Ca^{2+}]_i$ of HeLa-C-PrpS$_1$ during a SI bioassay. A)** Cartoon with a timeline summarising the time course with the treatments used during this experimental design. Solid red, blue and magenta colours represent the time of effective exposure of PrsS to the HeLa-C-PrpS$_1$. Pale red, light blue and light magenta represent the time corresponding to the "dead space" tubing between the reservoir and the chamber with the cells. The media used correspond to DMEM FluoroBrite. **B)** Graphic representation of the normalised data corresponding to the fluorescence values obtained during the SI bioassay. Each trace corresponds to the fluorescence levels of the individual cells: cell 1 in magenta, cell 2 in green and cell 3 in orange. Grey rectangles on top represent the application of the respective PrsS**. C)** Pseudo-coloured images showing HeLa-C-PrpS$_1$ cells loaded with the fluorescent calcium dye Fluo-4 and their fluorescence emission. Cells before (2 min 50 sec), during SI treatment (5 min 50 sec) and after washing out (13 min 18 sec). Fluorescence images were taken using FITC filter: excitation 492 nm, emission 519 nm. Left panel corresponds to the bright field identifying the cells. Scale bar = 50 µm. **D)** Insert with images corresponding to a magnification showing in detail the temporal and spatial increase in the $[Ca^{2+}]_i$ of cell No.1 during the key points in the experiment. Sale bar = 10 µm.

The experiment started with addition of media alone (**Figure 4.5.A**). Once the fluorescence levels were stable, $PrsS_8$ (compatible) was added to the reservoir at 2 min 30 sec reaching the cells around 3 minutes. Cells No.1 and No.2, exhibited no obvious alterations in fluorescence when $PrpS_8$ reached the chamber or after. However, cell No.3 showed a very small increase (0.04-fold), at 3 minutes, which could indicate a nonspecific response to the $PrsS_8$ exposure. Then, $PrsS_1$ (incompatible) was added at 4 min 40 sec, reaching the cells around 5 min 10 sec. Cell No.1, and cell No.2 exhibited a very rapid increases in the fluorescence of a 0.24-fold and 0.14-fold respectively at 5 min 45 sec (**Figure 4.5.B**). This increase was transient, and before 7 min, the calcium levels were similar to the levels before the increase. Also at 5 min 45 sec, cell No.3 displayed a very small increase (0.05-fold), similar to the one described after the addition of $PrsS_8$, supporting the fact that this cell was displaying an unspecific alteration (**Figure 4.5.B**). Therefore, cell No.3 provides a useful reference to compare background alterations with alterations that represents and actual response. Finally histamine was added at 7 min 45 sec and reached the cells at 8 min 15 sec. As it was expected, all three cells responded with an increase in fluorescence. Cell No.1 exhibited a 2.5-fold increase and both cell No.2 and No.3 with a 2-fold increase, confirming that all the cells were responsive and $[Ca^{2+}]_i$ alterations effectively detected. **Figure 4.5.C** shows the cells monitored during this experiments, bright field (left panel) as well as the pseudo-coloured images of these cells representing the $[Ca^{2+}]_i$ (three panels on the right). A magnification of cell No.1 during the experiments, shows that the 0.24-fold increase in the $[Ca^{2+}]_i$ after exposure to incompatible $PrsS_1$ corresponds to a homogeneous increase within the cell with a minor

change in the colorimetric scale (**Figure 4.5.D**). In contrast, the treatment with histamine resulted in a dramatic increase with a peak in the centre of the cell (**Figure 4.5.D**), confirming that the cells were responsive and the fluorescence denoting changes in $[Ca^{2+}]_i$.

Data presented in **Figures 4.4** and **4.5** shows six cells that fulfil all the requirements to obtain a reliable measurement (such as the cell remained still during the experiment, or the $[Ca^{2+}]_i$ were stable at the beginning of the experiment), however, in addition to the experiments presented here, a further six independent similar repeats were carried out. In total six repeats were carried out; five of them included treatments with both $PrsS_1$ (incompatible) and $PrsS_8$ (compatible), and one of them included the exposure of $PrsS_1$ only. Measurement of all the cells exhibiting changes in the $[Ca^{2+}]_i$ were summarised according to the magnitude of the increase of $[Ca^{2+}]_i$ in **Figure 4.6.**

Looking at the data as a whole, experiments including the exposure to $PrsS_1$ (incompatible) and $PrsS_8$ (compatible) comprised a total of 63 cells. Alterations after $PrsS_1$ included: two cells exhibited the largest $[Ca^{2+}]_i$ increases between 3- and 3.9-fold, and four cells between 2- and 2.9-fold increase. Five cells showed between 1- and 1.9-fold increase, whereas the majority of the cells (n = 40 cells) displayed an increase between 0.1- and 0.99-fold increase in the $[Ca^{2+}]_i$. Finally, nine cells showed between 0.01- and 0.09-fold increase, and 3 cells exhibited alterations smaller than 0.01-fold (**Figure 4.6**). For these alterations (i.e. smaller than 0.01-fold) there was not an obvious peak in the Fluo-4 signal. Therefore, in order to obtain a reference value, the average of fluorescence over to the time PrsS was expected to be exposed to the cells was used. This value was compared with the average fluorescence corresponding to the time

just before the exposure to PrsS. For the alterations monitored after exposure to $PrsS_8$: most of the cells (n = 40 cells) showed an increase in $[Ca^{2+}]_i$ smaller than 0.01-fold, followed by 22 cells with an increase between 0.01- and 0.99-fold. Only one cell showed an increase between 0.1- 0.99-fold (**Figure 4.6**). These data indicated that there was a difference in the peak increases in $[Ca^{2+}]_i$ depending on the exposure to $PrsS_1$ or $PrsS_8$. The majority of the cells (63%) exhibited an increase between 0.1- and 0.99-fold in the $[Ca^{2+}]_i$ after exposure to $PrsS_1$, whereas after the exposure to $PrsS_8$ most of the cells (also 63%) exhibited alterations smaller than 0.01-fold.

Chi-square test comparing the frequencies of the magnitudes of the increases in the $[Ca^{2+}]_i$ after exposure to incompatible $PrsS_1$ and compatible $PrsS_8$, confirmed that the magnitudes in the $[Ca^{2+}]_i$ increases were significantly higher after treatments with incompatible $PrsS_1$ ($p<0.05$).

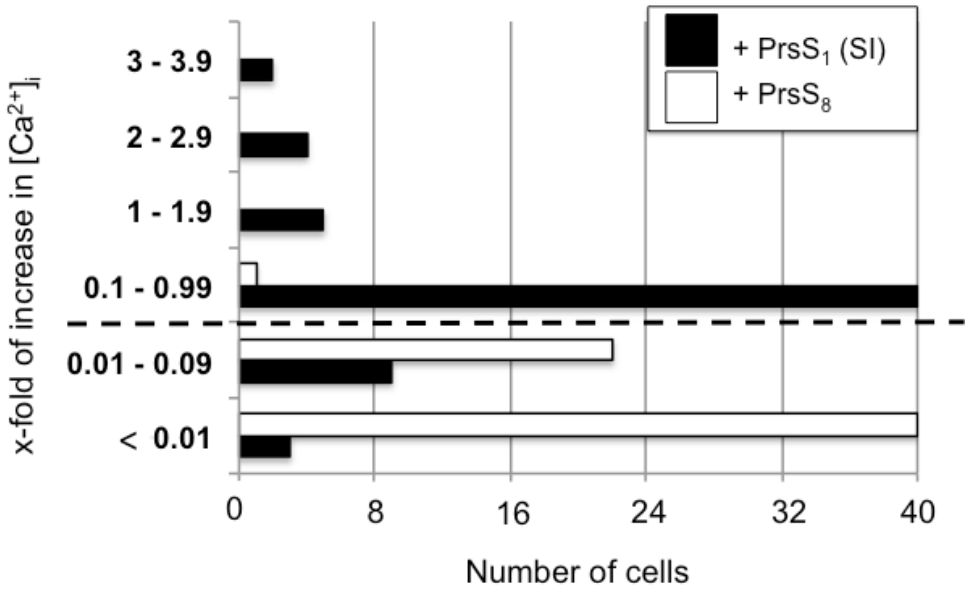

Figure 4.6 Chart summarising the number of cells and the magnitude of the increase in $[Ca^{2+}]_i$ in independent experiments. Black bars represent increase in calcium of HeLa-C-$PrpS_1$ cells after exposure to incompatible $PrsS_1$. White bars represent increase in calcium of HeLa-C-$PrpS_1$ after exposure to compatible $PrsS_8$. Chi-square test indicated significant difference between response to $PrsS_1$ (black bars) and $PrsS_8$ (white bars) ($p<0.05$). For values below the dotted line, the differences between a potential peak and the background signal were not clear.

All together, this provides an overall picture of the conditions and results observed in this experiment, providing further evidence suggesting that $PrpS_1$ was functional in HeLa cells. Thus, a “SI-like” reaction was triggered in HeLa-C-$PrpS_1$ specifically after challenge with $PrsS_1$, which included increases in $[Ca^{2+}]_i$.

It was of considerable interest to note that the majority of the cells after the exposure to incompatible $PrsS_1$, exhibited alterations in the shape (i.e. rounding up). This could represent a response itself and it will be discussed further in the discussion of this chapter.

4.2.4 Does a plasma membrane channel mediate PrpS-PrsS “SI response”?

In addition to using HeLa-C-$PrpS_1$ as a system to determine functional SI signal by measuring $[Ca^{2+}]_i$ during the SI bioassay, having HeLa-C-$PrpS_1$ cells also provided the opportunity to investigate whether PrsS-PrpS interaction triggered Ca^{2+} influx. Additionally this allowed us to determine the nature of PrpS, which previous evidences had suggested correspond to an ion channel (see Chapter 1, section 1.4.6.2.1). By means of patch-clamp experiments of HeLa-C-$PrpS_1$ we addressed the key question: Is PrpS a “receptor-channel” itself? If PrpS is the channel involved in the SI-induced $[Ca^{2+}]$ influx, it was expected that after exposure to PrsS, the PrpS-PrsS interaction generate a *S*-specific current. An additional control consisted in the exposure of $PrsS_1$ and $PrsS_8$ protein to HeLa cells expressing mCherry only, without $PrpS_1$ (HeLa-mCh), in which case no current generation was expected. The experimental is detailed in Chapter 2,

section 2.4.5. Briefly, HeLa-C-PrpS_1 and HeLa-mCh cells (**Table 4.1**) were grown on a coverslip, which was transferred to the patch clamp chamber. The experimental design consisted of a two-pipettes arrangement. One of the pipettes was used to patch the cell and the other applies the different treatments. These experiments were carried out in collaboration with Dr Rheinallt Parri and Dr Robert Sims at University of Aston.

4.2.4.1 Does PrsS_1 trigger a current in HeLa-C-Prps$_1$ cells?

Patch clamp experiments were carried out in whole-cell configuration on HeLa-C-PrpS_1 cells. The holding voltage was set to -70 mV, a value consistent with mammalian cell membrane potential under physiological conditions. Once the cell exhibited a stable register of membrane current, PrsS was applied. **Figure 4.7.A** shows the current generated after three consecutive treatments of approximately 5 seconds each with incompatible PrsS_1. In the first treatment, the current increased from -290 pA until -510 pA (difference of 220 pA). After returning to basal levels, once PrsS_1 was washed off, a second application of PrsS_1 reactivated the current from -320 pA until -680 pA (difference of 360 pA). In the last application, PrsS_1 triggered an inward current from -380 pA until -850 pA (difference of 470 pA). Even though in this particular experiment the magnitude of the differences exhibited an incremental decrease during the sequential treatments, this was not a clear trend in the other four independents replicates carried out. These experiments confirmed, as expected, an inward current stimulated almost immediately after the addition of PrsS_1. Once the exposure to PrsS_1 was removed this current rapidly decayed reaching basal

levels before the next application within the following 10 seconds. To test if this current was specifically generated for incompatible $PrsS_1$, we next carried out patch-clamp experiments in HeLa-C-$PrpS_1$ cells exposed to $PrsS_8$ (**Figure 4.7.B**). Using a comparable scale of current with the experiment showed in **Figure 4.7.A**, **Figure 4.7.B** shows small and transient inward current generated after three consecutive treatments of approximately 5 seconds each with compatible $PrsS_8$. These currents were at least 10-fold smaller than the currents generated in the previous experiments with the incompatible combination, suggesting an allele-specific response for cognate PrsS, which is another characteristic of the *Papaver* SI response. This is further evidence supporting an authentic SI-like response in HeLa-C-$PrpS_1$ cells.

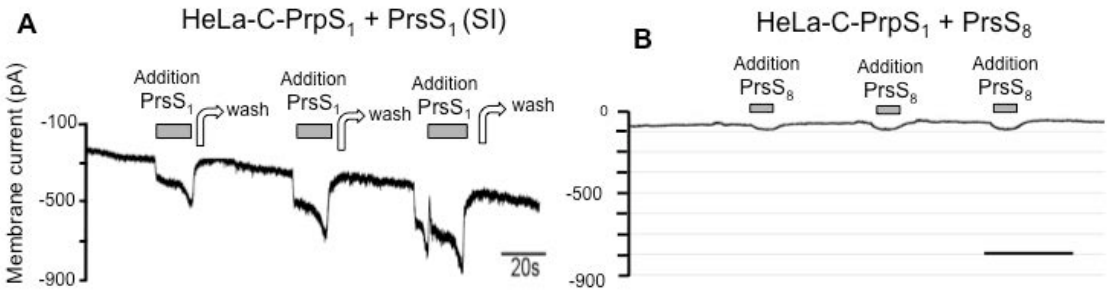

Figure 4.7 Membrane current records of HeLa-C-$PrpS_1$ cells in whole-cell patch clamp configuration exposed PrsS. A: Register of HeLa-C-$PrpS_1$ cells-clamped and exposed to incompatible $PrsS_1$. This experiments was carried out in 4 independents cells, with a total of 11 applications of $PrsS_1$. **B:** Register of HeLa-C-$PrpS_1$ cells-clamped and exposed to compatible $PrsS_8$. The grey boxes indicate the application of $PrsS_1$. This experiments was carried out in 4 independents cells, with 13 applications of PrsS in total.

This suggests that PrpS is functional in HeLa cells, as PrpS-PrsS interaction is triggering ligand-gated channel activity.

The next control was the addition of media alone. This experiment allowed to confirmed that the current generated was not due to unspecific

mechanoreceptors, which could be activated as a result of the physical contact between the media or any solution and the cell. **Figure 4.8** shows the current record of HeLa-C-PrpS$_1$ during two treatments with media alone. It is clear that there were no currents generated as a consequence of technical procedure of application the solution.

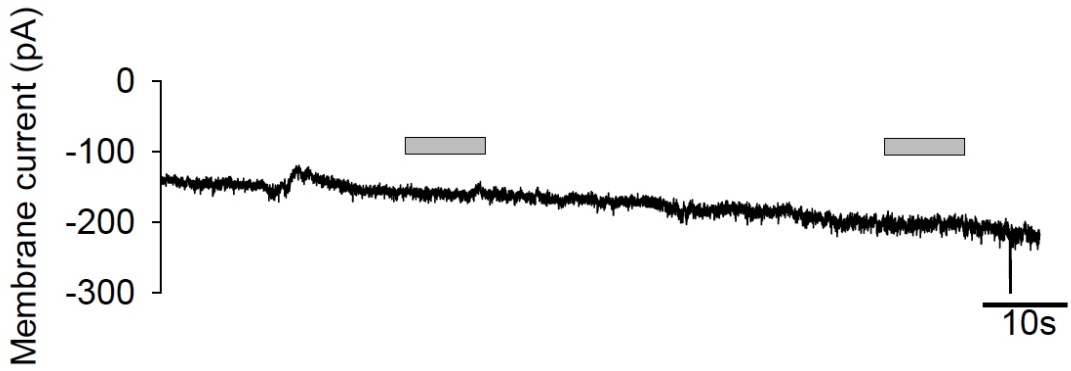

Figure 4.8. Membrane current records of cells in whole-cell patch clamp configuration exposed to media alone. Register of HeLa-mCh cells-clamped and exposed to PrsS$_1$. This experiment was carried out in 1 cell with 2 applications of media. The grey boxes indicate the application of media.

Together, these experiments suggested that PrpS was functional in HeLa cells, and that PrpS-PrsS interaction was triggering a current through the plasma membrane. The next, challenge was to evaluate whether this current was specific for cognates PrpS-PrsS interaction.

4.2.4.2 Is PrsS the channel triggering a current in HeLa-C-mCh?

An important control were patch-clamp experiments of HeLa cells expressing mCherry only (HeLa-mCh cells), so they had no PrpS expression, exposed to PrsS. This would allow us to evaluate if PrpS was the responsible of the current

generated after exposure to PrsS and therefore if PrpS was acting as an ion channel.

Unexpectedly, a negative current was also stimulated when the HeLa-mCh cells were exposed to PrsS (**Figure 4.9**), suggesting that PrsS itself stimulated channel activity in HeLa cells. However, this current was much smaller compared to the incompatible combination (i.e. HeLa-C-$PrsS_1$ exposed to $PrsS_1$). To provide a graphic comparison, **Figure 4.9.A and C** show the current generated in HeLa-mCh exposed to $PrsS_1$ and Prs_8 respectively, using a similar scale used in **Figure 4.9**. After this comparison, it is evident that HeLa-mCh exposed to PrsS generated a small current. **Figure 4.9.B** shows a magnification of current shown in **Figure 4.9.A**. After the first treatment the current increased from -43 pA until -54 pA (difference of 11 pA). The second application stimulated the current from -42 pA until -62 pA (difference of 20 pA). The third treatment from -62 pA until 86 pA (24) and the final exposure triggered and increase from -84 pA until -105 pA (difference of 21 pA). The current generated in HeLa-mCh after exposure to $PrsS_1$, did not exhibit an obvious return to the values before the treatment, however, this current still exhibited transient characteristics, as after the treatment with $PrsS_1$, the current stopped increasing and tended to stabilise. This was probably due to a deficient quality in the seal of the patch clamp, and/or an unhealthy cell. **Figure 4.9.D** shows a magnification of current shown in **Figure 4.9.C** generated in HeLa-mCh after six consecutive treatments with $PrsS_8$. The first treatment triggered a current from -20 pA until -50 pA (difference of 30 pA). Between the second and the fifth treatments the current generated was around 55 pA. Before the last treatment,

which generated a current from -10 until -50 (difference of 40 pA), the current exhibited a noticeable decrease, probably due an unhealthy cell.

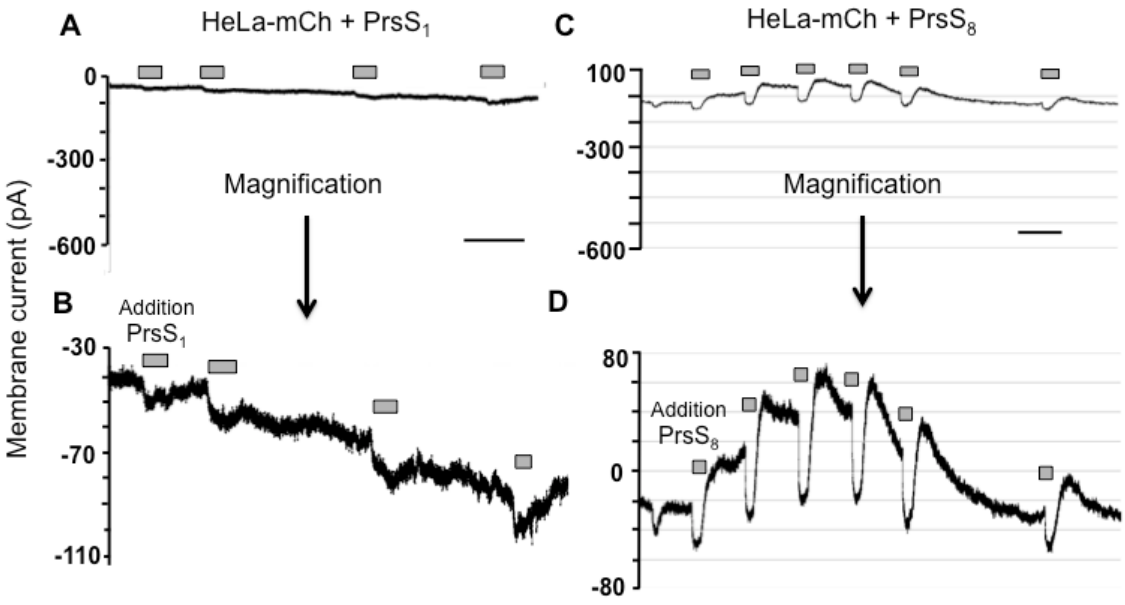

Figure 4.9. Membrane current records of HeLa-mCh cells in whole-cell patch clamp configuration exposed to PrsS. A) Register of HeLa-mCh cells (empty vector) to $PrsS_1$. **B)** Magnification of trace showed in A. This experiments was carried out in 3 independents cells, with 13 applications of PrsS in total. **C)** Register of HeLa-mCh cells (empty vector) exposed to $PrsS_8$. **D)** Magnification of trace showed in C. This experiments was carried out in 1 cell, including 6 applications of PrsS in total. The grey boxes indicate the application of PrsS. Scale bar = 20 sec.

Unfortunately the small currents generated in HeLa-mCh after exposure to PrsS did not allow confirm if PrpS was an ion channel, as they revealed that HeLa can naturally sense and respond to PrsS.

All together, these results confirmed that $PrpS_1$ was triggering a large inward current in HeLa-C-$PrpS_1$ cells, and even though PrsS itself seemed to generate a small current in HeLa cells, the incompatible combination of HeLa-C-$PrpS_1$ exposed to $PrsS_1$ showed currents up to 10-fold higher. This suggested that

PrpS was functional in HeLa cells and that the current generated was a real response exhibiting allelic-specificity for the incompatible combination.

Because the currents in these graphs depend on the electrical properties of each cell linked with its physiological status, comparisons between these graphs do not represent conclusive data. Aiming to obtain comparable data, the current-voltage (I-V) relationships were needed. The results of these experiments will be presented in the next section.

4.2.4.3 Characterisation of the currents generated after the interaction of PrpS-PrsS in HeLa cells: Current-Voltage (I-V) experiments

I-V curves provided more robust data to compare currents between different cells, as the electrical conditions of the cells were standardised by the electrophysiological setup and the measurements correspond to differences between established parameters. Also, these experiments allow the parameters of the current (*e.g.* reversal potential) to be determined, which provide valuable information regarding the ion channel mediating that current. HeLa-C-PrpS_1 and HeLa-mCh were patched and the current measured after the exposure to PrsS_1 and PrsS_8 whilst a voltage ramp protocol (from -90 to +30) was applied (further details in Chapter 2 section 2.4.5)

Figure 4.10.A shows the average current induced in four independent repeats of HeLa-C-PrpS_1 cells exposed to PrsS_1. Cell currents were very variable at negative potentials, including large currents over 150 pA at potentials around -80 mV. The reversal potential was around 8 mV, and at more positive potentials, the currents between the replicates were more similar reaching a

maximum of 11 ± 8 pA at 30 mV (n = 4). **Figure 4.10.B** shows the average current induced in three independent repeats of HeLa-mCh cells exposed to $PrsS_1$. The currents in the replicates were very similar. At -90 mV the inward currents reached a maximum of -33 ± 12 pA. The reversal potential was around -55 mV, and the outward current reached a maximum of 33 ± 9 pA at 20 mV (n = 3). **Figure 4.10.C** shows the average current induced in two independent repeats of HeLa-$PrpS_1$ cells exposed to compatible $PrsS_8$. At -90 mV the inwards current reached a maximum of -37 ± 8 pA. The current shifted to positive values around -40 mV, and the outward currents reached a maximum of 10 ± 13 pA at 30 mV (n = 2). **Figure 4.10.D** shows a single experiment corresponding to HeLa-mCh cells exposed to $PrsS_8$. At -90 mV the inward current reached a maximum of -21 pA. In this experiment the current does not shift to positive values reaching to -0.4 at 30 mV (n = 1).

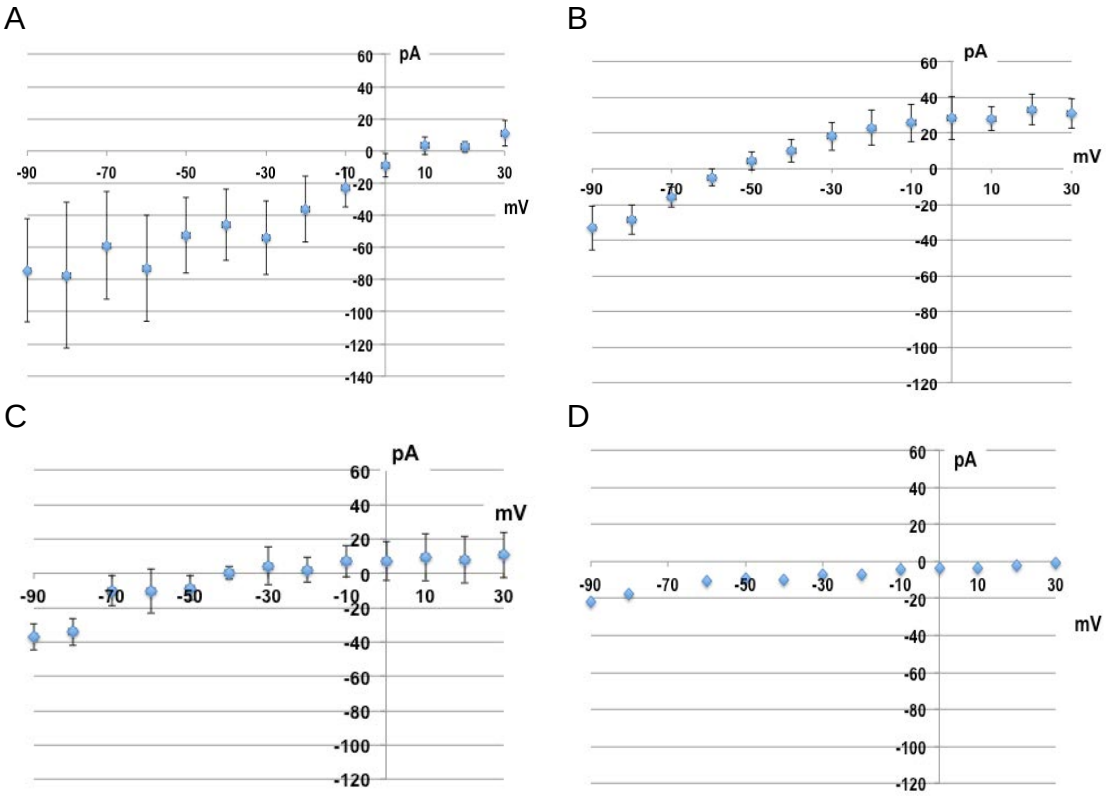

Figure 4.10. I-V curves for the PrsS-induced currents in different lines of transgenic HeLa cells. A) HeLa-C-PrpS_1 cells treated with incompatible PrsS_1 (result = ± SEM; n=4). **B)** HeLa-mCh cells treated with PrsS_1 (result = ± SEM; n=3). **C)** HeLa-C-PrpS_1 cells treated with PrsS_8 (result = ± SEM; n=2. **D)** HeLa-mCh cells treated with PrsS_8 (n=1).

Analysis and comparisons of the currents stimulated after the exposure of PrpS_1 and PrpS_8 to both HeLa-C-PrpS_1 and HeLa-mCh cells revealed that they were different. The most relevant values to describe and interpret the currents are summarised in **Table 4.2**

Table 4.2 Summary with the main values of the PrpS-induced currents.

Condition	Cell line + Treatment	Mean max. inward	Mean max. outward	Reversal potential
(SI)	**HeLa-C-PrpS$_1$ + PrsS$_1$** (n = 4)	-77 ± 45 pA (at -80 mV)	10 ± 7 pA (at -30 mV)	8 mV
Control empty vector"	**HeLa-mCh + PrsS$_1$** (n = 3)	-33 ± 12 pA (at -90 mV)	33 ± 9 pA (at 20 mV)	-55 mV
Compatible control	**HeLa-C-PrpS$_1$ + PrsS$_8$** (n = 2)	-37 ± 8 pA (at -90 mV)	10 ± 13 pA (at 30 mV)	-40 mV
Control empty vector"	**HeLa-mCh + PrsS$_8$** (n = 1)	-21 pA	-0.4 pA (at 30 mV)	Current did not reach positive values

Differences were evident between currents stimulated after applications of $PrsS_1$ to both HeLa-C-$PrpS_1$ cells (incompatible), and HeLa-mCh cells (control). The currents at positive potentials, for the incompatible combination exhibited values around 10 pA, whereas in the control reached over 30 pA. The comparisons at negative potentials were not so clear as there were high variations between the replicates. Nonetheless, the inward currents in the incompatible combination (-77 pA) were more than 2-fold higher in comparison with the currents generated in the control using HeLa transformed with the empty vector (-33 pA). The reversal potential was also different in the incompatible combination reaching 8 mV, and considerably higher to the control, which exhibited reversal potential -55 mV.

Currents stimulated after the exposure of HeLa-C-$PrpS_1$ to $PrsS_8$ reached a maximum efflux of 10 pA and a maximum influx of -37 pA. The reversal potential was -40 mV. The current in the control of HeLa-mCh exposed to $PrsS_8$ did not exhibit an efflux at any potential (therefore a reversal potential could not be calculated), reaching a minimal influx of -0.4 pA. The maximal influx was -21

pA. Unfortunately, we did not have enough time to carry out more replicates for the treatments with $PrsS_8$, in order to obtain robust data to carry out more reliable comparisons.

Interestingly, the control HeLa-mCh exposed to $PrsS_1$ and HeLa-C-$PrpS_1$ cells exposed to $PrsS_8$ exhibited similar values for maximum influx, and reversal potential, and these values were different in comparison with the incompatible combination of HeLa-C-$PrpS_1$ cells exposed to $PrsS_1$. This differential response between the incompatible condition with the control treatments, shows that transgenic HeLa cells can sense the PrsS protein, as there is a specific and strong response when HeLa-C-$PrpS_1$ were exposed to incompatible $PrsS_1$. The response included a greater than 2-fold larger influx current in comparison with the controls of HeLa-C-$PrpS_1$ exposed to compatible $PrsS_8$, and HeLa-mCh exposed to $PrsS_1$. Moreover the reversal potential shifted from clearly negative potentials in the controls, until a positive potential in the incompatible combination.

Assuming that the current stimulated after the application of $PrpS_1$ on HeLa-mCh is a background current, we attempted to obtain the current values corresponding exclusively to the $PrpS_1$ by subtracting this current to the current obtained in the incompatible combination of HeLa-C-$PrpS_1$ exposed to $PrsS_1$. **Figure 4.11.A** shows the resultant current after this. The inward current reached a maximum value of -68 pA at -60 mV. The outward current reached 30 mV at 20 mV and the reversal potential was around -8 mV. **Figure 4.11.B** shows the subtracted current normalised by the capacitance ($pA \times pF^{-1}$), which to compensate for variation in cells size by assessing current density. After this

correction the maximum influx was -17 pA × pF^{-1}, the maximum efflux was 7.6 pA × pF^{-1}, and the reversal potential was -9 pA × pF^{-1}.

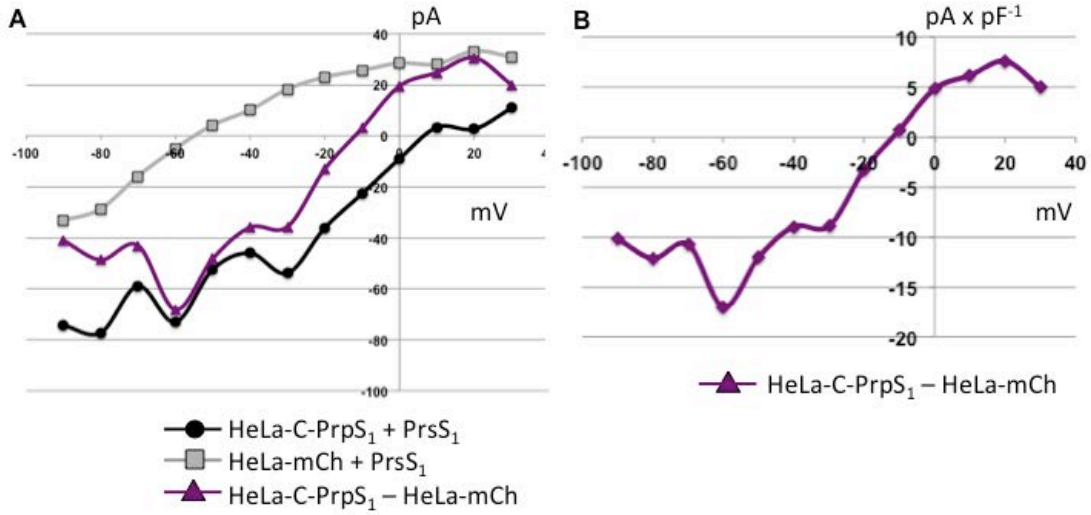

Figure 4.11. I-V curve resulted after the subtraction of the currents stimulated for PrsS1 treatments. A: the grey line shows the control combination of HeLa-mCh treated with $PrpS_1$. The black correspond to the incompatible combination of HeLa-C-$PrpS_1$ exposed to $PrsS_1$. The magenta line represents the putative current corresponding to $PrpS_1$ obtained after the subtraction of black and yellow currents. **B:** Subtracted current between HeLa-C-PrpS1 exposed to $PrsS_1$ and HeLa-mCh exposed to $PrsS_1$ normalised to capacitance (pA x pF^{-1}). A capacitance of 4 pF estimated for HeLa cells.

As the outward current is apparently absent at -90 mV and increases at more positive values, it is reasonable to consider that it corresponds to a characteristic potassium current. Interestingly, this was the major current observed in the studies in *Papaver* pollen protoplast (Wu et al., 2011). Also, the reversal potential described in *Papaver* pollen protoplast for the SI-induced current was around 10 pA × pF^{-1} (Wu et al., 2011), which is relatively close to 0 pA × pF^{-1} suggesting that it is was a nonselective channel. Remarkably, the corrected reversal potential obtained for HeLa-C-$PrpS_1$ exposed to incompatible PrsS1 was of -9 pA × pF^{-1}, which can be considered relatively close to 0 pA × pF^{-}1, suggesting again that the current measured correspond to a nonselective ion channel.

4.3 Discussion

Transfection efficiency and expression pattern of PrpS in HeLa cells

The secretory pathway involves biosynthesis and trafficking of protein between the ER through the GA to finally arrive to the cell surface or hydrolytic compartments (vacuoles in plants and lysosomes in animals cells) (Vitale and Raikhel, 1999). A quality control system in the ER ensures the production of properly folded and assembled structures (Trombetta and Parodi, 2003). When this quality control system detects anomalies in the biosynthesis, the protein is retained in the ER and eventually destined to the cytosol for degradation by the ubiquitin proteasome pathway (Trombetta and Parodi, 2003). Overexpression of proteins, particularly foreign ones, can be sensed as an abnormality, leading to a similar cellular fate of protein aggregates (Garcia-Mata et al., 1999). This quality control system relies on several chaperones with different specificities and roles (Vitale and Raikhel, 1999). Since PrpS is a plant protein, it is possible that the quality control machinery, particularly chaperones in HeLa cells do not recognise and fold properly the PrpS, resulting in the retention the PrpS in the ER. Moreover, because *PrpS* is driven by the cytomegalovirus (CMV) promoter, PrpS is overexpressed, and consequently has additional risk of being directed to non-functional protein aggregates.

GFP fluorescence was observed in the entire cell, and not confined at the edge of the cell. The mCherry signal that was not homogenous in the cell, and some cells exhibited a speckled pattern, which could be non-functional aggregates of PrpS. Although the mCherry signal corresponding to PrpS-mCherry was expected to be observed mainly on the peripheral region of the cell, the fact the

mCherry signal was detected in the cytoplasmic region was not completely unanticipated. Immunolocalisation studies of PrpS in *Papaver* pollen tubes showed that PrpS localises mainly to the pollen tube plasma membrane, but some signal was also detected inside the pollen tubes, which was expected because PrpS needs to be synthesised and then transported before reaching the plasma membrane (Poulter, 2009).

One of the most likely explanations for the wide range of results obtained in both calcium and electrophysiology experiments could be that the levels of PrpS reaching the membrane were low and not uniform in the plasma membrane. In this context, it was surprising to obtain data, suggesting that the functional studies worked, given the odd overloaded cellular distribution of PrpS. Thus, the fact that the cells were responsive to the exposure to $PrsS_1$, suggests that enough $PrpS_1$ reached the plasma membrane to interact with $PrsS_1$ to trigger a response including alterations in $[Ca_{2+}]_i$ and electrophysiology.

To improve this system, future studies could aim to decrease the total overexpression, and therefore the putative miss-targeting of PrpS-mCh. The use of a different genetic construct including a weaker promoter, which allow evaluating whether a lower expression would change the subcellular localisation of PrpS-mCh towards a peripheral localisation (Colosimo et al., 2000). Another option would be to design a new genetic construct, including a suitable destination peptide could also contribute to improve the folding and cellular destination of PrpS (Stern et al., 1997). Additionally, evaluate if growing the cell culture at lower temperature has an impact reducing the expression levels of PrpS and consequently improving its localisation.

Calcium alterations observed in HeLa-C-PrpS1 cells

HeLa-C-PrpS_1 cells exhibited transient increases in the $[Ca^{2+}]_i$ exclusively after the exposure to incompatible PrsS_1, suggesting that PrpS is functional in HeLa cells and can trigger similar alterations to the ones described for the *Papaver* SI response.

The increases in $[Ca^{2+}]_i$ in HeLa-C-PrpS_1 during the SI bioassay were smaller than the increases reported during *Papaver* SI. In poppy increases of over 10-fold in the $[Ca^{2+}]_i$ have been reported after the exposure to incompatible PrsS (Franklin-Tong et al., 1993b, Franklin-Tong et al., 1996), whereas the highest increases we obtained here with HeLa-C-PrpS_1 cells was 3.5-fold. However, these were preliminary experiments and the systems were not properly optimised for expression in HeLa cells. Nonetheless, the increases were transient and exhibited *S*-specificity for the cognate allelic combination PrpS-PrsS, which are two characteristics of the *Papaver* SI response. Together, these results suggests that the $[Ca^{2+}]_i$ increase represent an actual response, and therefore the first evidence that PrpS is functional in a highly diverged system as mammalian HeLa cells.

Using a similar experimental design in animal cells, it has been demonstrated that increases in $[Ca^{2+}]_i$ have a cellular response. Studies in human fibroblasts using Ca^{2+}-responsive dyes showed that increases in the cytosolic $[Ca^{2+}]_i$ were essential in cytoskeleton rearrangement for the cell adhesion (Ko et al., 2001). This example is also a relevant for our work as provide evidence of a connection between Ca^{2+} signalling pathway and the cytoskeleton, which is also exhibited in the *Papaver* SI response.

PrpS triggers currents in transgenic HeLa cells

PrsS-PrpS interaction triggered a current in HeLa cells. This was an inward current mediated by a putative cationic non-specific channel and generated specifically in the incompatible allelic combination of HeLa-C-$PrpS_1$ exposed to $PrsS_1$. Analysis of I-V relationship revealed that the inward current stimulated in the incompatible combination of HeLa-C-$PrpS_1$ cells treated with $PrsS_1$ was more than 2-fold the average of the currents triggered by $PrsS_1$ on HeLa-mCh, or the other control combination of HeLa-C-$PrpS_1$ after exposure to $PrsS_8$. This supports the idea that $PrpS_1$ is triggering an authentic SI response as a consequence of the PrsS-PrpS interaction. This agrees with the larger increase in $[Ca^{2+}]_i$ detected in the incompatible combination in comparison with the compatible combination in the calcium-imaging experiments. Additionally, in terms of the reversal potential, the fact that the current obtained after the subtraction of HeLa-C-PrpS1 cells and HeLa-mCh cells after exposure to $PrsS_1$ exhibited a reversal potential relatively close to 0 mV suggests that the current registered is mediated by a non-specific channel, similar to the situation described in *Papaver* pollen protoplast (Wu et al., 2011). Other similarities between the *Papaver* pollen protoplast and the data obtained here for HeLa-C-$PrpS_1$, is that the inward current was larger than outward current, and that the currents were transients, as they stopped rapidly on washout of $PrsS_1$. Despite the fact that more replicates are needed to have a stronger interpretation and conclusion, the analysis of some of the currents showed that there was a two-component response; a relatively immediate inward current, and a slower outward current. The presence of the outward current interferes with the inward current, making its analysis very challenging. However, considering that

experiments showed little outward current, the reversal potential was observed at negative potentials (were it sodium or calcium it should reverse at positive voltages given our internal / external ionic concentrations), suggesting that it is a nonspecific cation current, which agrees with previous electrophysiological studies in *Papaver* pollen protoplasts (Wu et al., 2011).

All together, increases in the $[Ca^{2+}]_i$ and alterations in the plasma membrane currents, strongly suggests that exposure of HeLa expressing PrpS to PrsS is enough to trigger a specific “SI-like” response in animal cell.

Heterogeneity in the response of HeLa-C-PrpS$_1$ cells to incompatible PrpS$_1$

There was a wide range in the magnitude of the Ca^{2+} responses. Some cells exhibited large alterations (of several fold), whereas other cells did not show any or very modest alterations. This range in the responses could be a consequence of the issues mentioned earlier (section 4.2.1.2) regarding the expression of the protein and even though our data suggested that some of PrpS is reaching the plasma membrane, the pattern of expression, it also suggests overload expression of PrpS. Considering that we are overexpressing a plant protein, PrpS, in a heterologous highly diverged system, it is reasonable to think PrpS is misfolding, and PrpS may be stuck in subcellular organelles such as ER or GA. Nevertheless, our data indicates that enough PrpS gets to the plasma membrane as there was a functional response.

Another possibility, based on the heterogeneity of the expression of PrpS-mCh, is that the line generated and used for the experiments (HeLa-C-PrpS$_1$), was a mix of more than one clone. In this case, the population of cells used to carry

out the experiments would not be a single clonal line explaining the diversity in the responses. Thus, heterogeneity in the responses can be ascribed to several possibilities.

Another possibility to be considered for future experiments is the use of a ratiometric dye, which provide quantitative measurements of Ca^{2+} concentrations, and therefore further interpretations regarding the concentration and the spatio-temporal characteristics of the increases in $[Ca^{2+}]_i$.

HeLa cells as a model cell system to characterise PrpS

We chose HeLa cells as a model system for these investigations for several reasons. From a technical point of view, HeLa cells have several advantages in comparison with any plant cell. The patch clamp procedure in animal cells, particularly HeLa cells, has several advantages in comparison with plant cells. HeLa cells grow rapidly, with a doubling time of around 24 h. Since they are epithelial cells, they normally grow in a monolayer attached to a surface. Also, as all the animal cells, they do not have a cell wall. This is a major advantage, as the plasma membrane has to be exposed to the electrode for recording the current during the patch clamp. Therefore if there is a cell wall, like in plant cells, this has to be removed. Cell wall removal can be done by chemical treatments, producing protoplasts (see Chapter 3 for details). Protoplasts are not ideal because in addition to its fragility, it is difficult to maintain them immobile to carry out the patch clamp as they round up into spheres, which float. Also the cell wall regenerates over time so there is a limited frame of time to use them. Another option to remove the cell wall is to use laser-assisted

procedures, which is highly challenging and not a practical proposition here (Henriksen and Assmann, 1997, Very and Davies, 2000).

The stimulation of currents in the negative controls of HeLa-mCherry cells treated with $PrsS_1$ indicated that there is a nonspecific response, which generates a background current. However, the currents generated in the incompatible SI combination were at least 2-fold larger in comparison with the background currents, suggesting that there was a SI-specific current. Nonetheless, the generation of background currents opens up the possibility that PrsS is triggering channel activity in HeLa cells, which is interesting in its own right as a plant ligand could activate mammalian channels, but also, makes further analysis very problematic because it would be very challenging to dissect the current and identify what is a channel response and what is the nonspecific response of the HeLa cells. This makes it impossible to assign the currents measured to PrpS, and therefore does not demonstrate that PrpS is a channel protein in this animal cell environment.

Based on the promising results obtained from the functional analysis which show a cellular response, but considering the drawbacks described above, using mammalian cells as a model to study *Papaver* SI appears to be a feasible approach. It needs to be pursued further and optimised or have all the components required. The identification of an alternative cell line, which does not exhibit a background current after exposure of PrsS is fundamental to successfully characterise $PrpS_1$ to demonstrate functionality of PrpS in highly heterologous cellular system, and determine if PrpS itself acts as a channel.

Can cell movement represent a biological response?

During the SI bioassay carried out here, it was observed that some HeLa-C-$PrpS_1$ cells exhibited a rounded up phenotype, and/or floated off from the coverslip where they were growing. This was consistently observed after the cells were exposed to $PrsS_1$ (incompatible), but not $PrsS_8$ (compatible), suggesting that is an effect of the addition of incompatible PrsS. An interesting possibility is that this movement was an attenuated response to the PrsS exposure, and therefore a consequence of a stimulated pathway downstream of the alterations of calcium in the HeLa-C-$PrpS_1$ cells. Is has been reported that extracellular Ca^{2+} has an effect on HeLa cell adhesion and morphology. By manipulations in Ca^{2+}, HeLa cells modulated its spreading and attachment capacities (Crawford and Jacobson, 1998). Moreover, cytoskeleton configuration plays an important role in cell adherence. Several proteins (including the small GTPase Rho) have been described as key regulators in processes such as cell adhesion and contraction (Narumiya et al., 1997). Therefore it is feasible that alterations in actin caused by increases in Ca^{2+} caused cells to be less firmly attached, and consequently prone to be disturbed when exposed to the flow of media going through the chamber during the SI bioassay. Based on these data, and considering that actin has been described as a cellular target during the *Papaver* SI response, we have explored the possibility of alterations in the actin cytoskeleton of HeLa-C-$PrpS_1$ exposed to incompatible $PrsS_1$. This is presented in Chapter 5.

CHAPTER 5

Functional Analysis of PrpS using HeLa Cells: Investigation of Actin Configuration during SI

5.1 Introduction

Chapter 4 showed studies on transgenic HeLa cells expressing PrpS (HeLa-C-$PrpS_1$), describing $[Ca^{2+}]_i$ alterations and channel activity in response to PrsS. To obtain additional data in order to determine whether PrpS is functional in HeLa cells, we carried out further studies, this time focusing on a different key hallmark of the *Papaver* SI response, the actin cytoskeleton.

As mentioned in Chapter 1 (section 1.1.2) the cytoskeleton is a highly dynamic structure, fundamental for cell physiology. In plants and animal cells, responses to stimuli can involve dramatic rearrangements of the cytoskeleton. It is well established that the actin cytoskeleton and accessory proteins, such as actin-binding proteins (ABPs), play a fundamental role mediating signalling transduction cascades (Staiger, 2000, Smertenko et al., 2010, Thomas et al., 2009). The associations between actin cytoskeleton, ABPs and cascade signalling comprise a diverse range of processes. Auxin and plant growth (Li et al., 2014, Hussey et al., 2006), pathogen response (Song et al., 2012), intracellular communication (Wang et al., 2014), and pollination (Sudo et al., 2013).

The integrity of F-actin is essential for pollen tube growth (Staiger et al., 2010). Therefore abnormalities in the F-actin of pollen tubes, such as actin depolymerisation and F-actin foci formation produced during the *Papaver* SI response, have a concomitant impairment in the pollen tube growth, viability, and ultimately the fertilisation process (Geitmann et al., 2000, Poulter et al., 2010).

PrpS-PrsS interaction triggers a signalling pathway in pollen, which involves actin depolymerisation and actin foci formation (Geitmann et al., 2000, Snowman et al., 2002, Poulter et al., 2010), leading to PCD (Thomas and Franklin-Tong, 2004, Thomas et al., 2006) (details in Chapter 1, section 1.4.6.2).

Dramatic changes in the actin configuration during *Papaver* SI were monitored by staining the actin cytoskeleton with Rhodamine-phalloidin after exposure to recombinant incompatible PrsS (Geitmann et al., 2000). Further microscopic analysis aimed to characterise and quantify the formation of the F-actin foci also provided evidence regarding the participation of actin-binding proteins ADF and CAP during this process (Poulter et al., 2010) (details in Chapter 1, section 1.4.6.2.4). Moreover it was established that actin alterations play a functional role in the viability of the cell, as they trigger a caspase-3-like activity, leading to PCD (Thomas et al., 2006) (details in Chapter 1 section 1.4.6.2.5).

The actin cytoskeleton is a highly-conserved structure, which plays a critical role in a wide variety of cellular processes in plant and animal cells (Chapter 1, section 1.1.2). Studies have also focused on the regulation of actin cytoskeleton dynamics. Throughout the last decades, a series of actin-binding protein (ABPs) have been discovered. Reviewed in (Lee and Dominguez, 2010).

In non-muscular cells, the major contractile structures are stress fibres. In non-motile cells, especially endothelial and some cancer cell lines, these structures are prominent thick and relatively stable bundles of actin filaments (Cramer et al., 1997) crosslinked by α-actinin (Goldman et al., 1975); Reviewed in (Tojkander et al., 2012). It was first demonstrated in fibroblasts that stress fibre had contractile properties (Kreis and Birchmeier, 1980), and despite the

mechanism underlying the formation of these structures is not completely understood, there is consensus in that they play a role in cell adhesion and morphogenesis (Pellegrin and Mellor, 2007, Tojkander et al., 2012)

As stress fibres are part of focal adhesions, they can also play a role in signalling and mediating the response of the cell to external stimuli. Focal adhesions are specialised sites of adhesion linking the cytoskeleton and the extracellular matrix with the surface on which the cells are growing (Burridge et al., 1997, Horwitz et al., 1986). Cells modify focal adhesions according to changes in the physiology status of the cell at molecular level, and physical forces acting in the extracellular matrix (Wozniak et al., 2004). The extracellular matrix has an effect in the activation of protein kinases such as Scr (a family of protein tyrosine kinases) and FAK (focal adhesion kinase), which have a role in several processes including cell motility (Ilic et al., 1995), proliferation (Zhao et al., 1998), and adhesion signals (Frame et al., 2002). Thus, it has been proposed that focal adhesions play a role regulating the physiology of the cell, and coupling environmental stimuli with intracellular signalling.

Based on their morphology and association with focal adhesions, stress fibres can be classified into four main groups: ventral, and dorsal stress fibres, transverse arcs and the perinuclear actin cap (Tojkander et al., 2012). Ventral stress fibres are attached to focal adhesions at both ends. (Small et al., 1998, Chen, 1981). Dorsal stress fibres are attached to focal adhesions at one end only. They are not involved in the filament contraction, but they seem to contribute to the assembly of other types of stress fibres (Heath and Dunn, 1978, Tojkander et al., 2011). Transverse arcs are bundles of actin that form

beneath the dorsal surface of cells (Heath, 1983). They do not form focal adhesions, but the connect with dorsal stress fibres.

In this chapter we describe studies assessing the actin configuration and morphology alterations of transgenic HeLa cells after SI induction, to evaluate if further functional evidence of *Papaver* SI response in mammalian HeLa cells, by monitoring changes in F-actin configuration and/or cellular shape might be stimulated. F-actin staining and visualisation is a well-established protocol for mammalian cells, including HeLa cells. The functional data presented in Chapter 4, showed that $[Ca^{2+}]_i$ increases, and plasma membrane current alterations were stimulated more dramatically after exposure to incompatible $PrsS_1$, and negligible increases in $[Ca^{2+}]_i$ as well as smaller currents were generated after the compatible (i.e. HeLa-C-$PrpS_1$ cells exposed to $PrsS_8$) and control (*e.g.* HeLa-mCh cells exposed to $PrpS_1$) combinations. Together, this suggested that PrpS was functional in HeLa cells, but also that HeLa cells could have an innate physiological respond to PrsS. Therefore, we wanted to explore whether other cellular targets described in the *Papaver* SI response were also affected in HeLa-C-$PrpS_1$ after the exposure to incompatible $PrsS_1$ and compatible $PrsS_8$. Thus, we assessed the hypothesis of actin alterations in HeLa-C-$PrpS_1$ cells after the exposure to incompatible $PrsS_1$ as part of a *Papaver* SI-like response in mammalian HeLa cells.

As mentioned in Chapter 4 (section 4.1), studies carried out to elucidate the mechanisms *Papaver* SI response had been inspired by studies and techniques initially developed in animal cells. Thus, most of these studies to monitor the F-actin cytoskeleton utilised dye *e.g.* rhodamine phalloidin, and fluorescent-

conjugated antibodies (Panchuk-Voloshina et al., 1999) have been primarily developed for animal cells and later on adapted for other cell types.

As a reminder, **Table 5.1** summarises the constructs and cellular lines used for the functional analyses presented in this Chapter.

Table 5.1. Genetic constructs and cell lines generated for PrpS analysis in HeLa cells. These constructs were provided by Dr Andrew Beacham.

Cell line	Genetic construct	Description / Observations
HeLa-mCh	pmChN (*CMV*::*mCherry*)	Plasmid pmCherryN1 (Clontech) contains the CMV promoter and mCherry (mCh) as a fusion tag protein. It was used to generate stable lines and represents the negative control (empty vector) for functional analysis.
HeLa-C-PrpS$_1$	pmChC-PrpS$_1$ (*CMV*::*PrpS$_1$-mCh*)	Plasmid pmCherryN1 (Clonetech) contains the CMV promoter and N-terminal mCherry (mCh) as a fusion tag protein. Stable line with PrpS$_1$ was generated and used for functional analysis.

5.2 Results

In this chapter we investigated whether the F-actin configuration of HeLa-C-PrpS$_1$ exhibited alterations after treatments with incompatible PrsS$_1$.

As mentioned in the introduction, the actin cytoskeleton plays a role in the cell shape and cell adherence. Therefore, in addition to visualising the actin cytoskeleton, experiments assessing the number of HeLa-C-PrpS$_1$ cells floating off after exposure to incompatible PrsS$_1$, as well as monitoring cell shape during the SI bioassay were carried out.

5.2.1 Effect of incompatible $PrsS_1$ on the adherence of HeLa-C-$PrsS_1$ cells

Preliminary experiments assessing the actin configuration of HeLa-C-$PrpS_1$ cells consistently revealed two tendencies after SI challenge. First, after the actin staining protocol there was an evident reduction in the number of cells attached to the coverslip, and second, the number of cells exhibited morphological changes, particularly rounding up and reduction in size. This suggested that the SI treatment was having an effect on the cells.

Because F-actin is an integral component of the focal adhesion (structure mediating cell adhesion), it was reasonable to assume that the decrease in the number of adherent HeLa-C-$PrpS_1$ cells after treatments with incompatible $PrsS_1$ was a consequence of alterations in the actin cytoskeleton. Before looking for actin alterations, our first challenge was to investigate this reduction in the number of cell attached after exposure to PrsS. Time-lapse experiments were carried out to confirm that the cells under treatments with incompatible $PrsS_1$ were becoming detached from the coverslip and floating off into the media (**Figure 5.1**). The experimental design was similar to the one used in the experiments presented in Chapter 4 (see Chapter 2, section 2.4.6). Briefly, a monolayer of HeLa-C-$PrpS_1$ or HeLa-mCh (control) cells were grown in a multi-well plate on a coverslip. SI treatments were generated by adding incompatible $PrsS_1$. For the compatible control, cells were exposed to $PrsS_8$, and for the untreated control the cells were exposed to media (DMEM) only. Additional controls were HeLa-mCh cells exposed to $PrsS_1$, $PrsS_8$ and media only.

This population of cells floating off into the media was termed “floaters”. As the actin staining protocol involves media removal and several washing steps, these experiments allowed us to assess cell adherence.

Cells before any treatment (untreated) were the control used as a reference for each treatment. Untreated HeLa-C-PrpS_1 cells are shown in **Figure 5.1.A** and **5.1.D**, whereas untreated HeLa-mCh cells in **Figure 5.1.G** and **Figure 5.1.J**. After seven hours of exposure to PrsS_1, HeLa-C-PrpS_1 (**Figure 5.1.B** and **5.1.E**) did not exhibit obvious differences in the number of cells attached to the surface compared to the controls, but some of the cells attached had started to exhibit morphological alterations (**Figure 5.1.E**). For HeLa-mCh cells, after seven hour of exposure to PrsS_1 the number of cells remained relatively constant (**Figure 5.1.H**), however minor morphological alterations were observed (**Figure 5.1.K**) in comparison with the untreated HeLa-mCh cells (**Figure 5.1.J**). After media removal and washing procedure, the situation in terms of the number of cells attached to the surface was completely different for HeLa-C-PrpS_1 versus HeLa-mCh cells. After the media removal, HeLa-C-PrpS_1 cells (**Figure 5.1.C**) exhibited a noticeable decrease in the number of cells attached in comparison with the same population of cells before the media removal and washing procedure. In contrast, the number of HeLa-mCh cells remained similar (**Figure 5.1.I**) in comparison with the same population before the media removal and washing procedure (**Figure 5.1.H**). The few HeLa-C-Prps$_1$ cells still attached to the coverslip after incompatible treatment and washing (**Figure 5.1.F**) also showed major changes in their shape, particularly rounding up and a decrease in size. These changes in morphology and size were also observed, but in a lesser extent, in control HeLa-mCh (empty vector)

exposed to $PrsS_1$ (**Figure 5.1.L**). These images are representative of two independent recorded time-lapse experiments. The phenomenon of “floaters” was observed in three more independent experiments (total n = 5).

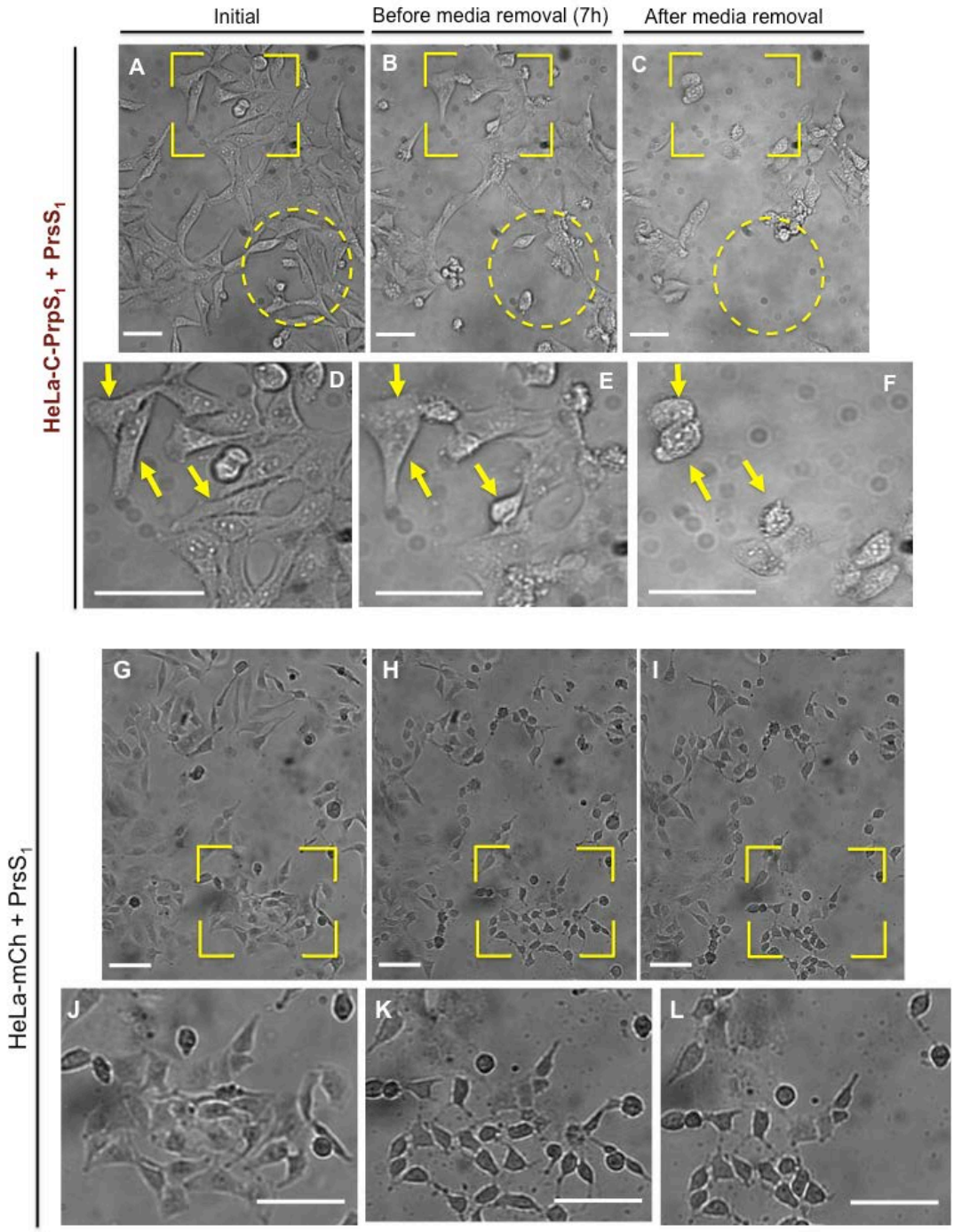

Figure 5.1. **Time-lapse experiments to evaluate alterations in transgenic HeLa cells exposed to PrsS**. Incompatible combination HeLa-C-Prps$_1$ exposed to 20 µg.mL^{-1} of PrsS$_1$, at 0h (**A**), 7h before (**B**) and after media removal and wash (**C**). Magnification area corresponding to the yellow square indicated in (A), (B) and (C) are shown in panels (**D**), (**E**) and (**F**). Control combination of HeLa-mCh cells (transformed with empty vector) exposed to 20 µg.mL^{-1} of PrsS1, at 0h (**G**), 7h before (**H**) and after media removal and wash (**I**). Magnification area corresponding to the yellow square indicated in (G), (H) and (I) are shown in panels (**J**), (**K**) and (**L**). Indicated in a dashed lines circle, a group of cells that completely disappear after the treatments and washing procedure. These are representative images of two independent experiments for each combination (Total n = 5). Scale bar: A - E = 20 µm, and G -L = 40 µm.

These experiments showed that there was a population of HeLa-C-PrpS_1 cells stimulated to detach as a result of the exposure to PrsS_1. Importantly, the reduction in the number of adherent cells was noticeable for the incompatible combination of HeLa-C-PrpS_1 cells challenged with incompatible PrsS_1, whereas in the control combination of HeLa-mCh cells exposed to PrsS_1 the number of adherent cells appeared to remain constant, suggesting an actual response to the challenge with PrsS_1. The reduction in the number of cells after incompatible treatment and washing procedure, revealed a clear difference between the treatments. The reduction in size and rounding up phenotype was more dramatic in the incompatible treatment HeLa-C-PrpS_1 exposed with PrsS_1. Similar alterations, but to a lower extent, were also observed in the control treatment of HeLa-mCh exposed to PrsS1. Therefore, initially we focused in the characterisation of the population of cells floating off, as this was the most consistent difference between the treatments.

We next investigated the population of “floaters” to confirm our observations of HeLa-C-PrpS_1 cells exhibiting poor adherence and reduction in size in response to incompatible PrsS_1. We investigated whether the population of “floaters” in the incompatible treatment (HeLa-C-PrpS_1 challenged with PrsS_1) exhibited any distinctive feature in size and/or shape compared to the “floaters” in the controls (HeLa-C-PrpS_1 exposed to media alone). It was expected that HeLa-C-PrpS_1 challenged with PrsS_1 presented a higher number of “floaters” cells, and also that these cells were smaller.

Figure 5.2 shows analysis of the HeLa-C-PrpS_1 cells exposed to incompatible PrsS_1 (**Figure 5.2.A-F**) or media alone (**Figure 5.2.G-L**) as a control. Fluorescence microscopy revealed that the “floaters” HeLa-C-PrpS_1 cells were

expressing the fusion protein $PrpS_1$-mCherry (**Figure 5.2** panels **A**, **D**, **G** and **J**). Consistent with previous experiments, HeLa-C-$PrpS_1$ cells treated with 20 $\mu g.mL^{-1}$ of incompatible $PrsS_1$ were smaller (**Figure 5.2** panels **B** and **E**) in comparison with the controls where the same cell line HeLa-C-$PrpS_1$ cells were treated with media (**Figure 5.2** panels **H** and **K**) were larger. The merged images (**Figure 5.2** panels **C**, **F**, **I** and **L)** allowed the identification of the cells, as there was some debris on the slides. An estimation using these data indicates that the number of "floaters" HeLa-C-PrpS1 after treatments with incompatible $PrsS_1$ was between 3- and 5-fold higher than in the controls.

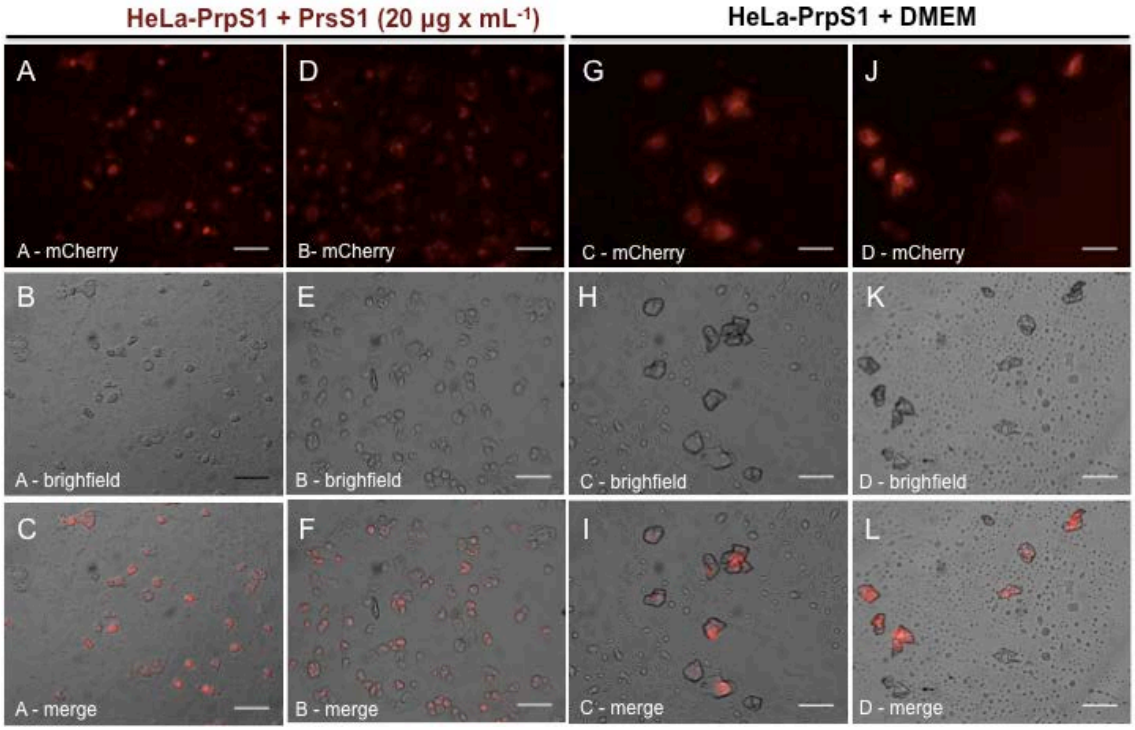

Figure 5.2. Population of HeLa-C-$PrpS_1$ floaters examined under the microscope after 3 hours of treatment. HeLa-C-$PrpS_1$ treated with incompatible $PrsS_1$: mCherry emission (**A** and **D**), bright field (**B** and **E**), merge (**C** and **F**). HeLa-C-$PrpS_1$ treated with DMEM (control): mCherry emission (**G** and **J**), bright field (**H** and **K**), merge (**I** and **L**). Images were taking using TRITC filter: excitation 550 nm, emission 572 nm. These images were obtained using the same magnification. Scale bar = 20 µm. These are representative images from one experiment with two replicates for test situation.

This experiment confirmed that treatments of HeLa-C-PrpS_1 cells with PrsS_1 had a correlation with an increase in the number of “floaters” exhibiting mCherry signal as well as a reduction in their size. Having confirmed that the reduction in the number of cells attached to the coverslip was a consistent trend and that it was associated with the incompatible combination of HeLa-C-PrsS_1 challenged with PrsS_1, our next goal was to quantify the number of cells floating into the media, “floater” cells.

5.2.2 Quantification of HeLa-C-PrpS_1 cells floating off during the SI bioassay

To obtain quantitative data, we systematically counted the cells that floated off the coverslip after treatments with incompatible PrsS_1 and compatible PrsS_8. Treatments with PrsS were done at different concentrations aimed to generate a dose response relationship. Thus, three different HeLa cell populations: Hela-wt (nontransfected, wild type HeLa cells) and two stably transfected lines, HeLa-C-PrpS_1 and HeLa-mCh cells, were exposed to three different concentrations (5, 10 and 20 $\mu g.mL^{-1}$) of incompatible PrsS_1. In addition, to test the potential allele-specificity of the response HeLa-C-PrpS_1 cells were exposed to compatible PrsS_8 at these concentrations (n = 3 for each combination, except for HeLa-C-PrpS_1 treated with PrsS_1 with n = 4). After the treatment, the number of “floaters” was counted. The only test that exhibited a statistically significant difference in the number of floating cells was the incompatible combination of HeLa-C-PrpS_1 cells challenged with 20 $\mu g.mL^{-1}$ of PrsS_1 (**Figure 5.3**) (p-value < 0.001, n = 4). At this concentration of PrsS_1, on average 3×10^5

floaters were observed for the incompatible combination, which was almost 3-fold higher compared to all the other combinations including untransfected HeLa cells (HeLa-wt), and HeLa-mCh exposed to 20 $\mu g.mL^{-1}$ of $PrsS_1$ (p-value = 0.00011 and 0.00051 respectively), and the compatible control of HeLa-C-$PrsS_1$ exposed to 20 $\mu g.mL^{-1}$ of $PrsS_8$ (p-value = 0.00071), which exhibited around 1.2×10^5 "floaters" cells on average. The number of "floaters" cells for untreated samples was around 1×10^5 for all the cell lines evaluated (HeLa-C-$PrpS_1$, HeLa-mCh and HeLa-wt). For treatments with 5 $\mu g.mL^{-1}$ of PrsS the average of floaters cells was also around 1×10^5 except for HeLa-C-$PrpS_1$ treated with $PrsS_1$ with 1.5×10^5 cells. For treatments with 10 $\mu g.mL^{-1}$ of PrsS the average of floaters cells was slightly higher with values around 1.5×10^5 for all the treatments.

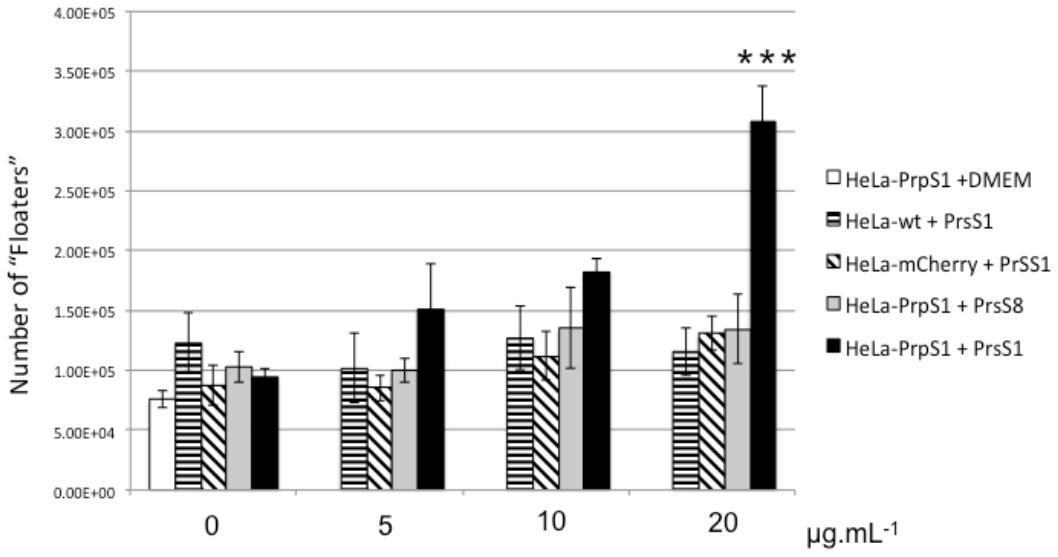

Figure 5.3. **Quantification of the dose-response effect of PrsS on different HeLa cell lines.** Number of HeLa cells floating off after 3h of treatment with PrsS at different concentrations. HeLa-C-$PrpS_1$ treated with incompatible $PrsS_1$ (black bars). Control of HeLa-C-$PrpS_1$ treated with DMEM only (white bars). Nontransfected "wild type" HeLa cells (HeLa-wt) treated with $PrpS_1$ (horizontally dashed bars). HeLa cells expressing mCherry without $PrpS_1$ (HeLa-mCh) treated with PrsS1 (diagonal dashed bars), and HeLa-C-PrpS1 treated with compatible $PrsS_8$ (grey bars). The values are mean ± SEM; n=3, except HeLa-C-$PrpS_1$ with n=4. The star represents significant difference after one-way ANOVA. The p-values for treatments of HeLa-C-$PrpS_1$ cells treated with 20 $\mu g.mL^{-1}$ were: 0.00011 for HeLa-wt exposed to PrsS1, 0.00051 for HeLa-mCh and 0.00071 for HeLa-$PrpS_1$ treated with $PrsS_8$.

Table 5.2 summarises the p-values for the combinations of each lines at different concentrations of PrsS.

Table 5.2. P-values of the comparison between cellular lines at different concentrations of $PrsS_1$ and $PrsS_8$.

Line : treatment compared to →	Line : treatment	p-value
(UT) HeLa-wt : 0 µg.mL $PrpS_1$		
	HeLa-wt : 5 µg.mL $PrpS_1$	1
	HeLa-wt : 10 µg.mL $PrpS_1$	1
	HeLa-wt : 20 µg.mL $PrpS_1$	1
(UT) HeLa-mCh : 0 µg.mL $PrpS_1$		
	HeLa-mCh : 5 µg.mL $PrpS_1$	1
	HeLa-mCh : 10 µg.mL $PrpS_1$	1
	HeLa-mCh : 20 µg.mL $PrpS_1$	0.999
(UT) HeLa-$PrpS_1$: 0 µg.mL $PrsS_8$		
	HeLa-$PrpS_1$: 5 µg.mL $PrsS_8$	1
	HeLa-$PrpS_1$: 10 µg.mL $PrsS_8$	0.999
	HeLa-$PrpS_1$: 20 µg.mL $PrsS_8$	0.998
(UT) HeLa-$PrpS_1$: 0 µg.mL $PrpS_1$		
	HeLa-$PrpS_1$: 5 µg.mL $PrpS_1$	0.986
	HeLa-$PrpS_1$: 10 µg.mL $PrpS_1$	0.558
	HeLa-$PrpS_1$: 20 µg.mL $PrpS_1$	0.00014 ***

Statistically highly significant difference denoted with *** ($p<0.001$)

These experiments revealed that 20 $\mu g.mL^{-1}$ of $PrsS_1$ was the only concentration that showed statistically significant differences among all the treatments and combinations. Therefore 20 $\mu g.mL^{-1}$ was established as a suitable concentration to generate a SI-like response. Moreover 20 $\mu g.mL^{-1}$ is a concentration previously used in our laboratory to generate a response in heterologous system such as *Arabidopsis* pollen expressing PrpS (de Graaf et al., 2012). These data provide good evidence suggesting that poppy PrpS is functional in HeLa cells and their interaction with PrsS triggers a response, which affects the adherence of the HeLa cells.

5.2.3 Studies of the actin cytoskeleton of HeLa-C-PrpS_1 after exposure to incompatible PrsS_1 in the SI bioassay.

Having established that exposure to PrsS_1 triggered detachment from the coverslip, we decided to examine the cells and characterise them focusing on the F-actin configuration. Thus, as mentioned in the introduction of this chapter actin cytoskeleton in HeLa cells, particularly stress fibres are important for cell attachment, and therefore it was feasible to consider that issues in the cell adherence could be related to alterations in the actin cytoskeleton. Analysis of the actin cytoskeleton was particularly relevant because actin cytoskeleton is a major cellular target during the *Papaver* SI response (see Chapter 1 section 1.4.6.2.2). Thus, monitoring the actin cytoskeleton was potentially a powerful tool to evaluate if PrpS and PrsS were triggering an SI response similar to the *Papaver* response in HeLa cells. It was expected that the actin cytoskeleton in HeLa-C-PrpS_1 cells might undergo alterations when incompatible PrsS_1 was added. Here we describe the analysis of the actin cytoskeleton of HeLa-C-PrpS_1 cells exposed to PrsS_1.

The protocol to stain F-actin cytoskeleton of epithelial (such as HeLa) cells is well standardised for adherent animal cells. However the staining of the "floaters" cells was extremely challenging because the protocol include several washing steps with buffer solutions. These steps are trivial if the cells are firmly attached to a surface, so the cells can be easily washed and rinsed. However for the "floater" population, we had to collect the cells in a microfuge tube, and rely on centrifugation steps to harvest the cells and wash them without loosing them. The centrifugation had to be as gentle as possible to maintain the

integrity of the cells, the pellet generated was not firmly attached to the bottom of the tube and a considerable number of cells were lost every time the buffer was removed. We optimised a protocol in order to stain floaters cells (Chapter 2 section 2.4.7), so it was possible to obtain images of the actin cytoskeleton of some HeLa-C-PrpS_1 cells, which floated off after treatments with incompatible PrsS_1.

Because mCherry has a red emission, in these experiments, 488-phalloidin (emission in green) was used to stain the F-actin and analyse the actin configuration. Alexa-488 phalloidin is a dye that selectively labels F-actin (Haugland et al., 2002, Panchuk-Voloshina et al., 1999). See **Table 5.1** at the start of this chapter for details of the genetic constructs.

Figure 5.4 shows representative actin cytoskeleton staining of untreated HeLa cells exposed to media (DMEM) only. Numerous, stress fibres were observed in both HeLa-mCh cells (**Figure 5.4.A**) and HeLa-C-PrpS1 cells (**Figure 5.4.B)**. The stress fibres appeared more defined in HeLa-mCh cells (**Figure 5.4.A**) in comparison with HeLa-C-PrpS_1 cells (**Figure 5.4.B, C**). The F-actin in HeLa-C-PrpS_1 exhibited irregularities in the staining with some areas brighter than others, suggesting that the expression of PrpS_1 might have an impact in the actin configuration of HeLa-C-PrpS_1 cells.

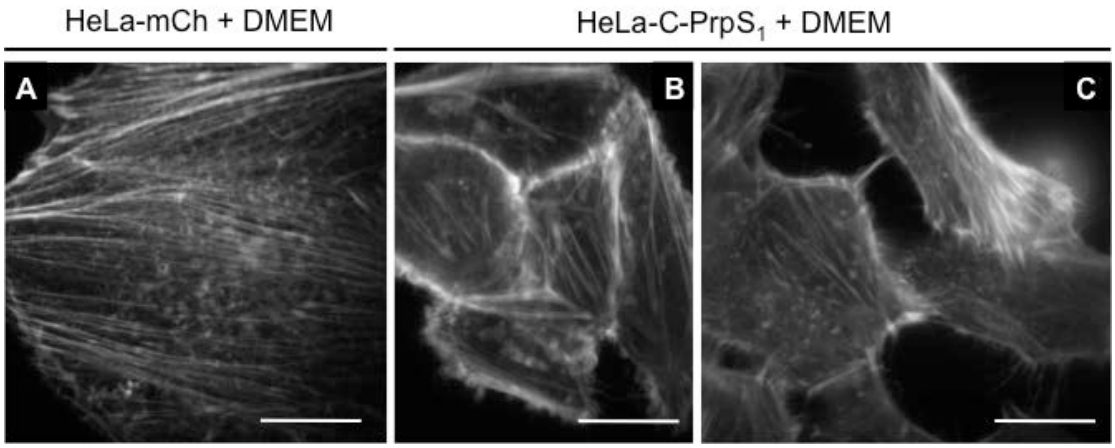

Figure 5.4. Epifluorescence images of F-actin staining of HeLa cells using 488-phalloidin. Representative images of the F-actin of untreated HeLa cells exposed to media (DMEM) only. **A:** HeLa-mCh cells. **B** and **C:** HeLa-C-$PrpS_1$ cells. Actin stress fibers were prominent in all the assessed cells. Images were taking using FITC filter: excitation 490 nm, emission 520 nm. Scale bar = 25 µm.

From this it was apparent that HeLa-C-$PrpS_1$ cells has a slightly altered actin configuration in untreated cells probably due to the overexpression of $PrpS_1$. However, we could still see if there was a change after the addition or PrsS.

A dose-response experiment was carried out to assess whether there was a correlation between the actin configuration and the concentration of PrsS. **Figure 5.5** shows representative images of various actin cytoskeleton configurations exhibited in both untreated cells, and also in cells during the treatments with incompatible $PrsS_1$. **Figure 5.5.A and Figure 5.5.B** shows actin cytoskeleton of HeLa-mCh and HeLa-C-$PrpS_1$ respectively, treated with media alone (untreated cells). These cells exhibited abundant, long stress fibres crossing the cell. As shown in **Figure 5.4**, the F-actin in HeLa-C-$PrpS_1$ exhibited a slightly more uneven actin staining in comparison with HeLa-mCh. **Figure 5.5.C, D** and **E** shows the rounding up cells and also that the effect of $PrsS_1$ was dose-dependant; HeLa-C-$PrsS_1$ treated with 5 µg.mL^{-1} still exhibited several noticeable stress fibres (**Figure 5.5.C**). The stress fibres were less

prominent in HeLa-C-PrsS_1 treated with 10 µg.mL^{-1} (**Figure 5.5.D**) and practically non-existent after treatments with 20 µg.mL^{-1} (**Figure 5.5.E**). So, there was a clear dose-response effect. This supports the hypothesis that stress fibres in HeLa-C-PrpS_1 cells are affected by exposure to incompatible PrsS_1. Finally, **Figure 5.5.F** and **G** shows F-actin in "floaters" HeLa-C-PrpS_1 cells after treatments with 20 µg.mL^{-1} of PrsS_1. Some cells had very short, disorganised stress fibres (**Figure 5.5.F**). Strikingly, the most extreme alterations revealed a speckled pattern in some areas of the cells (**Figure 5.5.G**). This spotted pattern resembles, to some extent, the F-actin foci described as a hallmark of the *Papaver* SI. These cells also were smaller and stress fibres were completely absent (**Figure 5.5.G**).

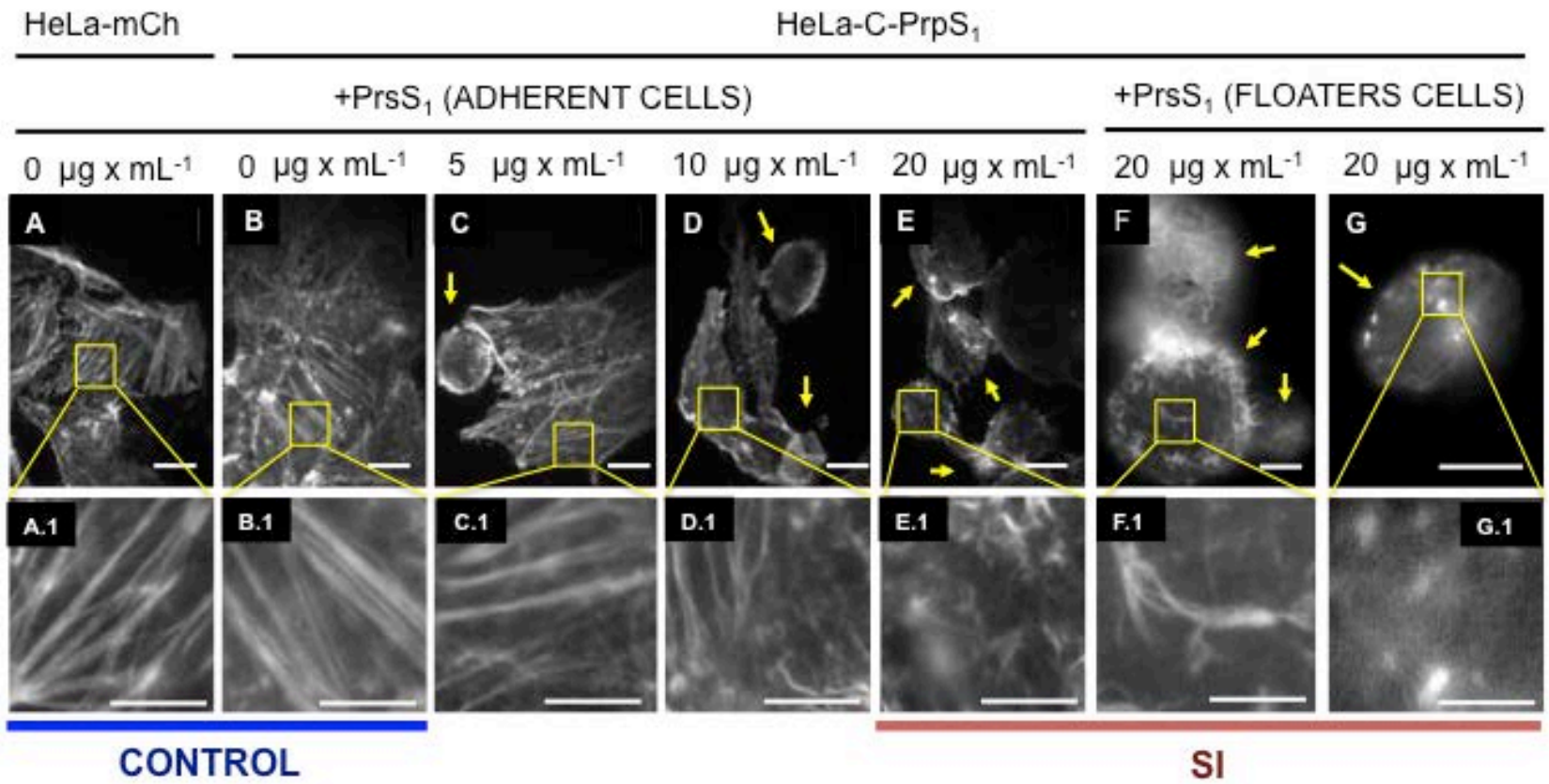

Figure 5.5 Representative epifluorescence images exhibiting a gradient in the actin cytoskeleton alterations during SI conditions. A: HeLa cells expressing mCherry only and exposed to media alone (control) **B**: HeLa-C-PrpS_1 cells treated with media alone (control). C: HeLa-C-PrpS_1 cells treated with 5 µg.mL^{-1} of PrsS_1. **D**: HeLa-C-PrpS_1 cells treated with 10 µg.mL^{-1} of PrsS_1 **F**: HeLa-C-PrpS_1 cells treated with 20 µg.mL^{-1} of PrsS_1 **E**: HeLa-C-PrpS_1 cells treated with 20 µg.mL^{-1} of PrsS_1. Two independent experiments, with two replicates each.120 cells were analysed, 30 cells in each treatment**. F** and **G**: "floaters" HeLa-C-PrpS_1 cells treated with 20 µg.mL^{-1} of PrsS_1. Area highlighted in the yellow square is presented magnified in the respective panel below each picture. Yellow arrows indicate cells that exhibited rounding up. Images were taking using FITC filter: excitation 490 nm, emission 520 nm. One experiment with two replicates, 15 floaters HeLa-C-PrpS_1 cells were imaged. Scale bar: A-G= 10 µm A.1 - G.1 = 5 µm.

These results provide strong evidence that $PrsS_1$ has an effect on the F-actin organisation of HeLa-C-$PrpS_1$ cells. In adherent cells, the most consistent trend was the correlation between the concentration of PrsS and the disappearance of stress fibres. At treatments with 5 $\mu g.mL^{-1}$ of $PrsS_1$, the stress fibres were still visible in most of the cells, however at 20 $\mu g.mL^{-1}$ the stress fibres had completely vanished. In the "floaters", the lack of stress fibres was consistent in all the 15 cells observed.

A more detailed comparison between representative images of the actin cytoskeleton of "floaters" HeLa-C-$PrpS_1$ cells during contrasting treatments is shown in **Figure 5.6**. Seven "floater" HeLa-C-$PrpS_1$ cells were stained for actin, and imaged after exposure to media alone (untreated). In all the cells, the signal did not show evident structures (see **Figure 5.6.A)**. The bottom section of the cells in **Figure 5.6.A** was the only area where faint structures that could correspond to a disorganised arrangement of actin filaments could be visible (**Figure 5.6.B**). In the case of HeLa-C-$PrpS_1$ cells after treatments with 20 $\mu g.mL^{-1}$ of incompatible $PrsS_1$, 15 "floater" cells were stained and successfully imaged. Eight of them exhibited a speckled pattern with noticeable bright dots (see **Figure 5.6.C** and **5.6.D)**.

In terms of the F-actin alterations, increasing concentration of PrsS, generated a progressive reduction in the number of stress fibres, which we interpret as a detrimental effect in cell adherence, eventually leading to the detachment of the cells from the coverslip. The most intense response was in the "floaters", which lacked of stress fibres and had structures which resemble the actin foci formed during the *Papaver* SI response.

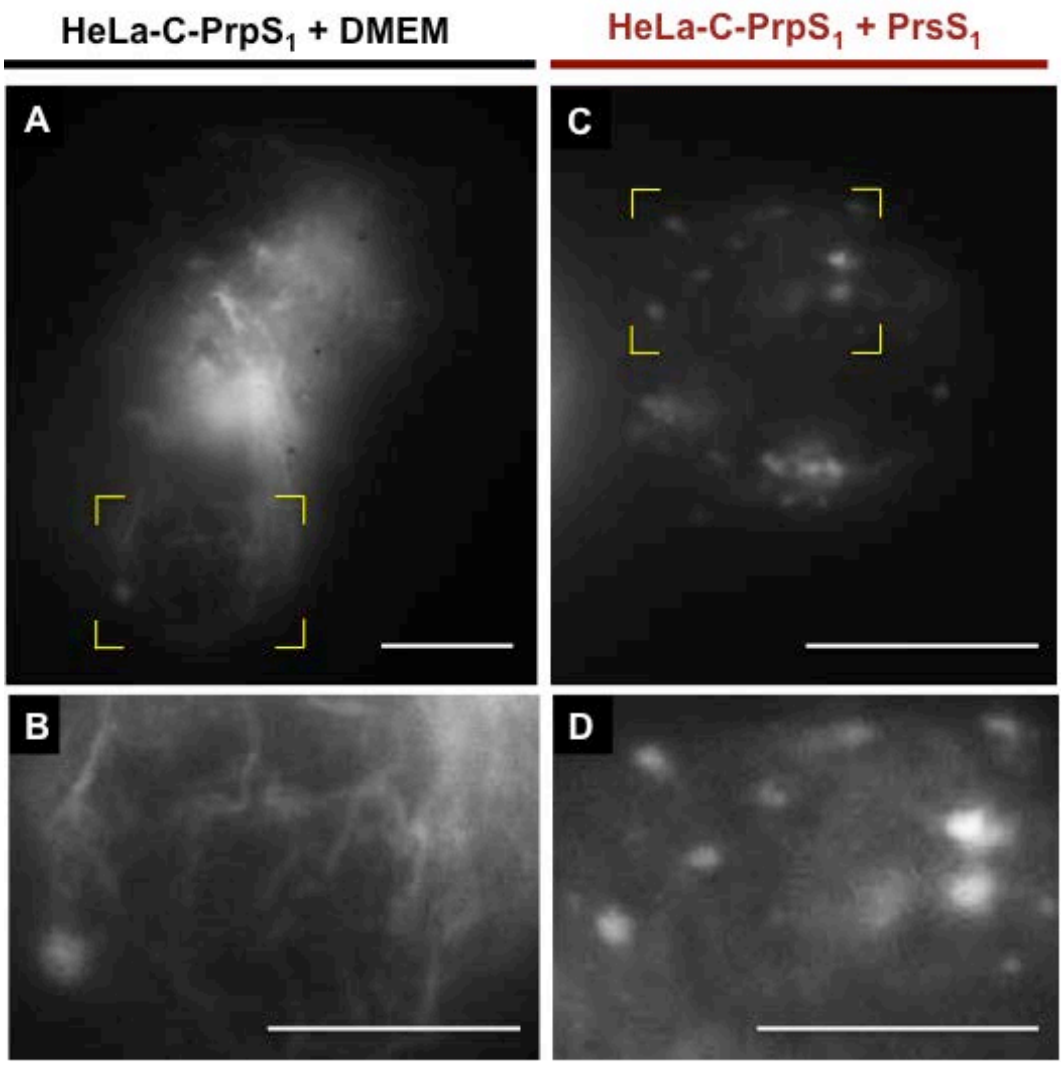

Figure 5.6. Epifluorescence imaging monitoring the F-actin cytoskeleton of "floaters" HeLa cells. Comparison of the F-actin configuration stained with 488-phalloidin in two different treatments. A: control treatment of HeLa-C-PrpS$_1$ exposed to media (DMEM) alone. **B**: Magnification of the yellow square detailed in A. Images from two experiment with two replicates **C**: incompatible treatments of HeLa-C-PrpS$_1$ exposed to 20 µg.mL^{-1} of PrsS$_1$. **D**: Magnification of the yellow square detailed in C. Images were taking using FITC filter: excitation 490 nm, emission 520 nm. Images from one experiment with two replicates. Scale bar: A and C = 10 µm, B = 20 µm and D = 15 µm.

As expected, "floaters" exhibited the most dramatic alterations, such as reduction in size and the lack of stress fibres (see also section 5.2.4). These experiments suggested that the response of HeLa-C-PrpS$_1$ cells to the exposure of PrsS$_1$ triggers F-actin rearrangements resembling the F-actin foci described during the *Papaver* SI response.

5.2.4 Characterisation and analysis of the actin cytoskeleton of "floaters" HeLa-C-PrpS_1 cells

The population of "floaters" cells was one of the more dramatic alterations in the actin cytoskeleton of HeLa-C-PrpS_1 cells responding to the exposure of incompatible PrsS_1. Therefore it was especially relevant to analyse the cytoskeleton of "floaters" cells. Importantly in the following experiments, HeLa cells expressing mCherry only without PrpS_1 (HeLa-mCh) was included as negative control. This control is robust, as these cell lines express mCherry protein tag, allowing to assess any potential unspecific effect due to the expression of mCherry.

In total, after several attempts optimising the protocol for actin staining of "floaters" cells (see in section 5.2.3), 33 cells were stained and imaged for all the different treatments. For HeLa-C-PrpS_1, 14 "floater" cells after treatments with incompatible PrsS_1, and 7 "floater" cells after exposure to media alone were obtained. For HeLa-mCh, 9 "floater" cells after treatments with PrsS_1, and 3 "floater" cells after exposure to media alone were obtained. **Figure 5.7** shows representative images of the actin cytoskeleton of "floater" HeLa-C-PrpS_1 cells and HeLa-mCh cells after 3 h of exposure to 20 $\mu g.mL^{-1}$ of PrsS_1. **Figure 5.7.A** and **B** shows representative images of the actin cytoskeleton of 8 "floaters" HeLa-C-PrpS_1 exposed to incompatible PrsS_1. **Figure 5.7.C** shows the representative F-actin configuration of the other 4 "floater" HeLa-C-PrpS_1 cells. **Figure 5.7.D** and **E** shows representative images of the actin cytoskeleton of 5 "floaters" HeLa-mCh exposed to PrsS_1. These cells did not present definite bright dots. Three HeLa-mCh cells exhibited F-actin similar to **Figure 5.7.F**, with

a speckled pattern, and one cell exhibited a blurred staining without speckled pattern. Additional controls of “floater” HeLa-C-PrpS_1 and HeLa-mCh after exposure to media (DMEM) alone were also carried out. In this condition, 6 “floater” HeLa-C-PrpS_1 cells exhibited a blurred actin staining (like **Figure 5.6.A)**, and one exhibited a speckled pattern. For HeLa-mCh, 2 “floaters” cells exhibited actin staining similar to Figure **5.7.C**, and one cell exhibited an unclear staining.

In terms of size, 10 out of 14 HeLa-C-PrpS_1 cells exposed to incompatible PrsS_1 exhibited a diameter smaller than 20 μm, whereas for the control of HeLa-mCh cells exposed to PrsS_1, 6 out of 9 cells exhibited diameter larger than 20 μm. These preliminary data suggest that the incompatible combination (i.e. HeLa-PrpS_1 exposed to PrsS_1) also reduces the cell size.

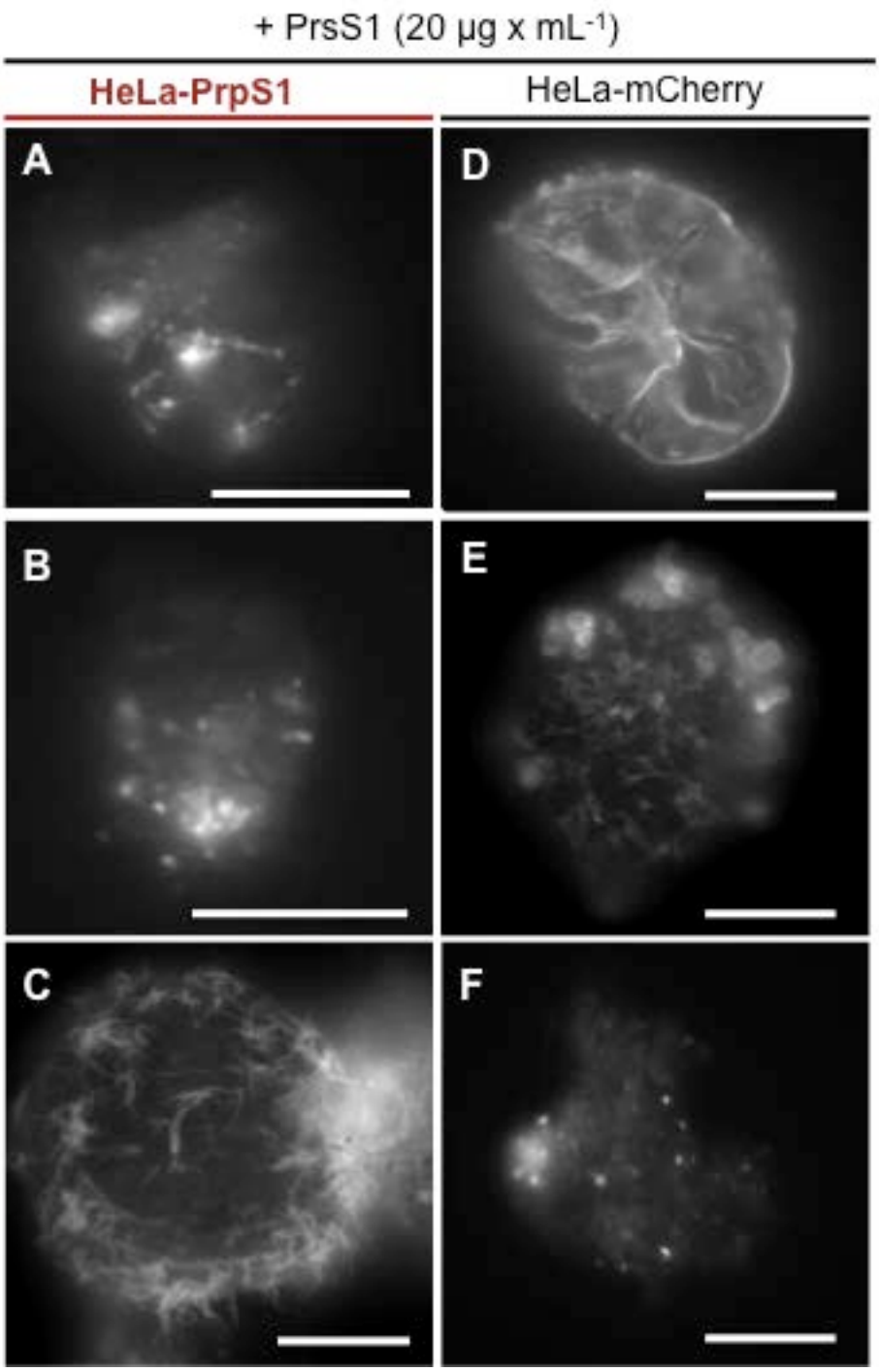

Figure 5.7. Representative images of the actin configuration of floaters cells. **A, B** and **C**: HeLa-C-PrpS$_1$ cells exposed to 20 µg.mL^{-1} of incompatible PrsS$_1$. **D**, **E** and **F**: HeLa-mCh cells exposed to 20 µg.mL^{-1} of PrsS$_1$ (control). Treatments were carried out for 3 h. Images were taking using FITC filter: excitation 490 nm, emission 520 nm. Scale bar = 10 µm.

A summary of formation on all the “floaters” previously described is presented in **Table 5.3** grouped according the cell diameter, and the presence of an actin speckle pattern similar to the F-actin foci described in *Papaver*.

Table 5.3 Summary of the counting of the actin status of the floaters cells after different treatments.

	+PrsS$_1$		**+ DMEM**		Total cells
	HeLa-C-Prps$_1$ (SI)	**HeLa-mCh**	**HeLa-C-Prps$_1$**	**HeLa-mCh**	
Cell diameter					
< 20 µm	**10**	3	-	-	13
> 20 µm	**4**	6	7	3	20
Imaged cells	**14**	9	7	3	33
F- Actin					
Cells with speckled pattern, “actin foci”	**8**	3	1	-	12

Although this is a small data-set, there was a clear trend among these cells. In terms of actin cytoskeleton, 67% (8 out of 12) cells exhibiting a speckled pattern resembling the F-actin foci during the SI in *Papaver* were “floaters” HeLa-C-PrpS$_1$ challenged with incompatible PrsS$_1$. Regarding the size, 76% (10 out of 13) of the cells with a diameter smaller than 20 µm were “floaters” HeLa-C-PrpS$_1$ cells challenged with incompatible PrsS$_1$. Moreover, 80% (16 out of 20) of the cells with a diameter larger than 20 µm were controls. Moreover the SI combination exhibited 14 “floater” cells, and in total 19 “floater” cells were obtained from the three control conditions analysed, which represent an average of ~6 “floater” per control condition.

The size of the “floaters” HeLa-C-PrpS_1 cells after exposure to incompatible PrsS_1 was consistently smaller than the “floater” cells in controls. Interestingly, most of the cells exhibiting a speckled pattern after the actin staining were also “floaters” HeLa-C-PrpS_1 cells after exposure to incompatible PrsS_1.

The visualisation of structures that resemble the F-actin foci described in *Papaver* SI, and the fact that these structures were predominant in the incompatible combination, represent a promising breakthrough in this work, suggesting that PrpS is functional in HeLa cells and responsive to cognate PrsS.

5.2.5 Characterisation and functional analysis of the adherent cells

The response of HeLa-C-PrpS_1 cells to PrsS involved a dose-dependant response rather than a discrete “all or nothing” response (**Figure 5.3**). Having analysed the extreme response in the floaters cells, we also analysed the cells that remained attached to the coverslip after treatment with incompatible PrpS_1.

5.2.5.1 Dose-response effect on the actin cytoskeleton of cells attached to the surface after exposure to PrsS_1

As preliminary data suggested that this effect could be associated with alterations in the actin stress fibres (section 5.2.3, **Figure 5.5**), which might be the reason for an eventual loss of adherence. Here, we present further data exploring the dose-response effect on the F-actin configuration of cells that remained attached to the coverslip after treatment with PrsS. We assessed the

correlation between the exposure to incompatible PrsS and F-actin alterations based on the integrity of the stress fibres.

It was expected that the actin stress fibres in HeLa-C-PrpS_1 cells would gradually disappear with the exposure to increasing concentration of incompatible PrsS_1. In other words, higher concentration of incompatible of PrsS_1 should result in less actin stress fibres, whereas cells treated with lower concentrations of PrsS_1 should retain more stress fibres.

Figures 5.8.A, **B** and **C** show representative images of at least 60 cells analysed in three independent experiments. These images show untreated HeLa-C-PrpS_1 cells that grew normally and exhibited typical arrangement of F-actin, which includes noticeable bundles of stress fibres in HeLa cells. Detail shown in **Figure 5.8.A1**, **B1** and **C1** showed numerous F-actin stress fibres, in several cells crossing along the main axis of the cell, similar to the arrangement described for normal epithelial HeLa cells growing on a rigid surface (Tojkander et al., 2012). These actin stress fibres showed predominantly a parallel distribution, but also, some branching points where the fibres extended in an angled direction.

Cells exposed to 5 $\mu g.mL^{-1}$ of PrsS_1 were similar in shape and size to the controls (**Figure 5.8.D**). These cells exhibited numerous stress fibres similar to the controls (**Figure 5.8.D.1**). Cells exposed to 10 $\mu g.mL^{-1}$ of PrsS_1 did not exhibit obvious changes in shape or size compared to the controls (**Figure 5.8.E**). However actin stress fibres were less prominent and restricted to specific areas of the cells (**Figure 5.8.E.1**). Cells exposed to 20 $\mu g.mL^{-1}$ of PrsS_1 revealed the typical changes in shape (rounding up) and size (smaller cells) observed in the SI-like response HeLa-C-PrpS_1 previously (section 5.2.1),

in comparison with the controls (**Figure 5.8.F** and **5.8.G**). In these cells the stress fibres were indistinguishable and the actin arrangement was a diffuse mesh (**Figure 5.8.F.1** and **5.8.G.1**), instead of the distinct actin stress fibres displayed in the cells exposed to lower concentration of $PrsS_1$ and especially in the controls of HeLa-C-$PrpS_1$ exposed to media (DMEM) alone. The images for treatments with 5, 10 and 20 $\mu g.mL^{-1}$ of $PrsS_1$ are representative of at least 30 different cells, in two independent experiments. Because adjacent HeLa cells growing *in vitro* tend to overlap, especially along their edges it was not possible to obtain the exact number of cells analysed based on the actin staining. Additional staining with dyes such as DAPI (to stain the nucleus) should have been used to identify and count individual cells in a precise way.

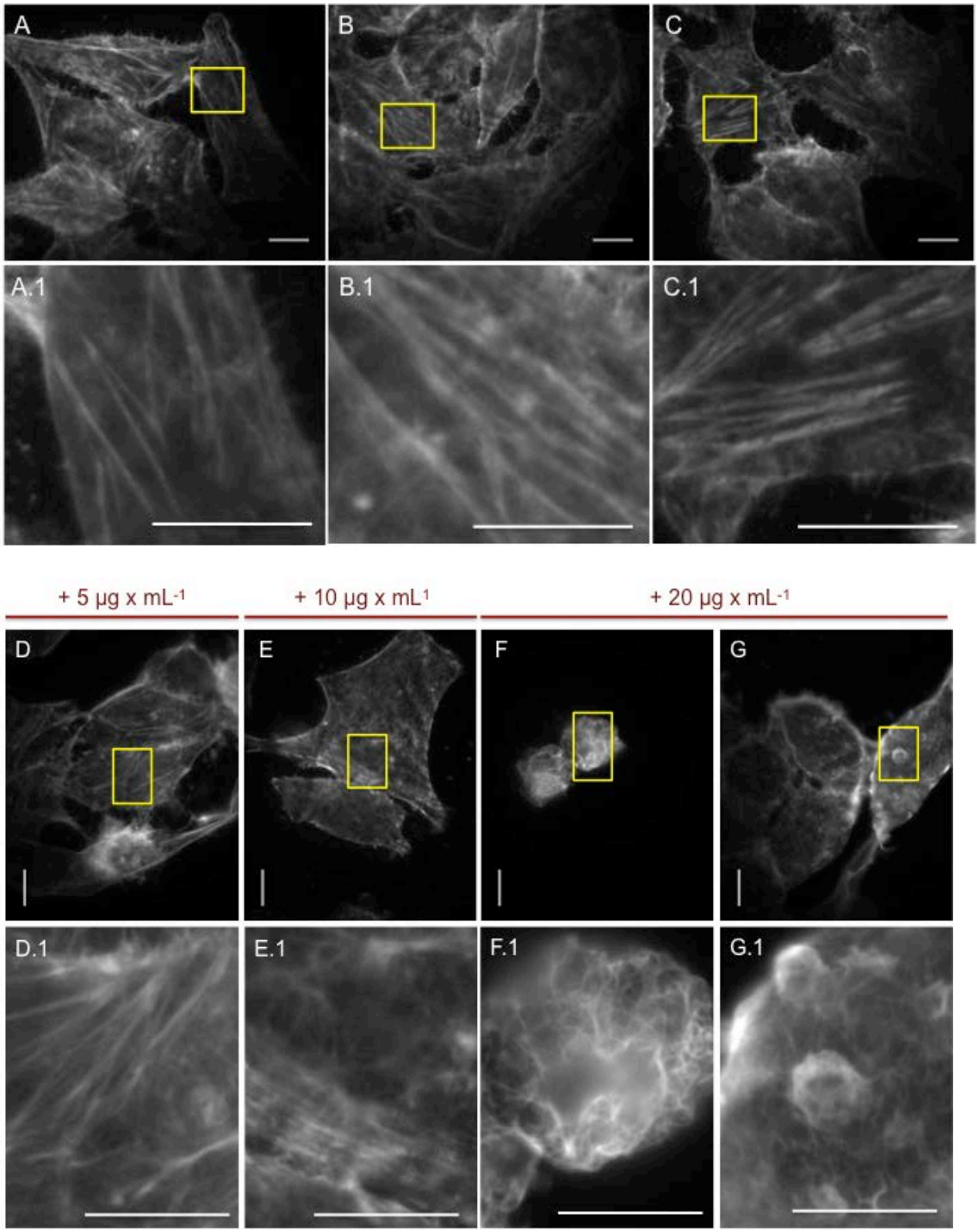

Figure 5.8. **Representative images of F-actin stained with 488-phalloidin of HeLa-C-PrpS_1 exposed to three different concentrations of incompatible PrsS_1.**

A, **B** and **C**: Untreated HeLa-C-PrpS_1. Magnification of the highlighted yellow square is presented in the panel below **A.1**, **B.1** and **C.1**, respectively. **D**: HeLa-C-PrpS1 cells exposed to 5 µg. mL^{-1} of PrsS_1. **E**: HeLa-C-PrpS1 cells exposed to 10 µg.mL^{-1} of PrsS_1. **F** and **G**: HeLa-C-PrpS_1 cells exposed to 20 µg.mL^{-1} of PrsS_1. Magnification of the highlighted yellow rectangle is presented in the panel below **D.1**, **E.1, F.1** and **G.1** respectively. Images were taking using FITC filter: excitation 490 nm, emission 520 nm. Scale bar A-G = 10 µm and A.1 - G.1 = 6 µm.

This result indicates that there is a dose-dependant alteration to the organisation of F-actin of HeLa-C-PrpS_1 cells exposed to incompatible PrsS_1. This effect includes: (1) a decrease in the number of actin stress fibres, (2) reduction in the size and (3) a rounding-up phenotype. A dose-dependant response, represent strongly suggests that the alterations are a real cellular response.

5.2.5.2 Are the actin alterations in HeLa-C-PrpS_1 cells after PrsS_1 treatments allele-specific?

Another important characteristic of the poppy SI is allele specificity. So, we next addressed the question whether there is a differential response after HeLa-C-PrpS_1 cells exposed to PrsS_1 (incompatible) and PrsS_8 (compatible). It was expected that HeLa-C-PrpS_1 cells exposed to incompatible PrsS_1 exhibit stress fibres disappearance while treatments PrsS_8 should reveal no alterations, similar to untreated controls. However, based on our results obtained from our electrophysiological experiments (Chapter4, section 4.2.3.2), it was expected that HeLa-C-PrpS_1 cells might exhibit some alterations after exposure to PrsS_8, but perhaps to a lesser extent that the alterations after treatments with incompatible PrsS_1.

HeLa-C-PrpS_1 cells were exposed to 20 µg.mL^{-1} of PrsS_1 (incompatible) and in parallel to 20 µg.mL^{-1} of PrsS_8 during the 3 h before F-actin staining. Untransfected HeLa cells (HeLa-wt) were also included as a control.

Untransfected HeLa cells (HeLa-wild-type, termed HeLa-wt) treated with media alone exhibited predominant and numerous actin stress fibres (**Figure 5.9.A**, **B**

and **C**). Similarly HeLa-C-Prps$_1$ cells exposed to media alone looked similar to the untreated controls (**Figure 5.9.D**, **E** and **F**).

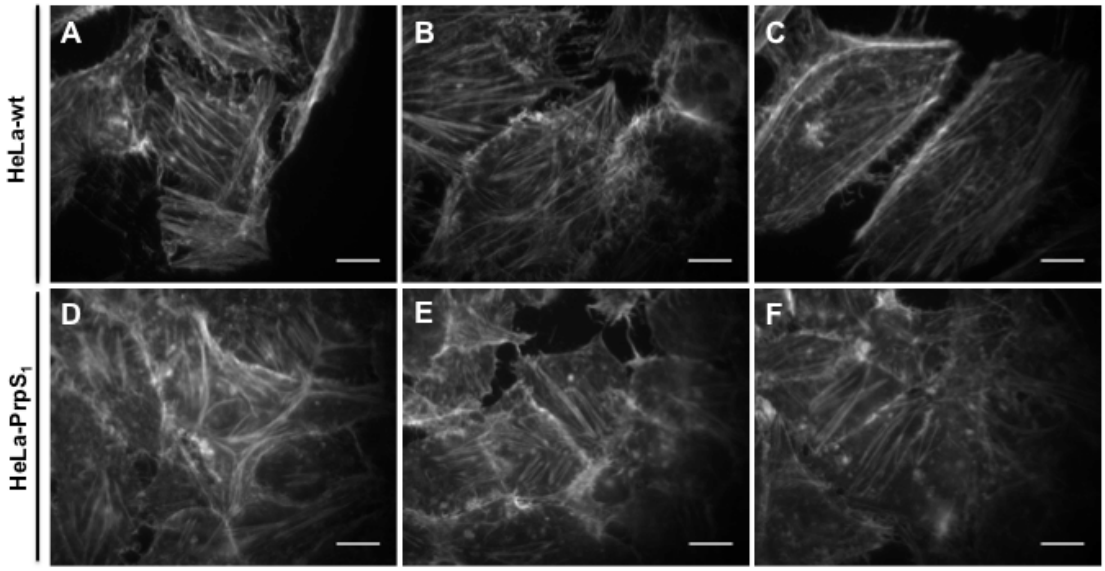

Figure 5.9 F-Actin using 488-phalloiding of HeLa cells exposed to media only (untreated). **A**, **B** and **C**: non-transfected wild type HeLa cells (HeLa-mCh). **D**, **E**, **and F**: HeLa cells expressing PrpS$_1$ (HeLa-C-PrpS$_1$). These are representative images of at least 40 different cells imaged in two independent experiments with two replicates each. Scale bar = 10 µm.

In terms of cellular shape and size the results in this experiment were consistent with previous data. A representative image of 40 HeLa-C-PrpS$_1$ cells analysed after exposure to 20 µg.mL^{-1} of PrsS$_1$ exhibiting rounding up and reduction in size is shown **Figure 5.10.A**. In contrast, the cell controls with no PrpS, (HeLa-wt) cells did not exhibit alterations in size or shape after treatment with 20 µg.mL^{-1} of PrsS$_1$ (**Figure 5.10.B**). Similarly, HeLa-C-PrpS$_1$ cells treated with 20 µg.mL^{-1} of compatible PrsS$_8$ did not exhibit evident change in morphology or size (**Figure 5.10.C**). In terms of the actin stress fibres, both HeLa-C-PrpS$_1$ cells exposed to PrsS$_8$ and HeLa-wt cells exposed to PrsS$_1$ cells exhibited stress fibres (**Figure 5.10.B.1** and **5.10.C.1** respectively), whilst HeLa-C-PrpS$_1$

cells exposed to incompatible $PrpS_1$ did not show stress fibres and the actin arrangement was an actin mesh without a clear organisation (**Figure 5.10.A.1**) These data provide further evidence that actin alterations in HeLa-C-$PrpS_1$ are part of a SI-like response, as these actin alterations were allele-specific. Despite the compatible combination of HeLa-C-$PrpS_1$ cells challenged with $PrsS_8$, exhibited a reduction in the number of actin stress fibres, these fibres were still present in some cells. However, the absence of actin stress fibres in the incompatible combination of HeLa-C$PrpS_1$ cells exposed to $PrsS_1$ was very dramatic.

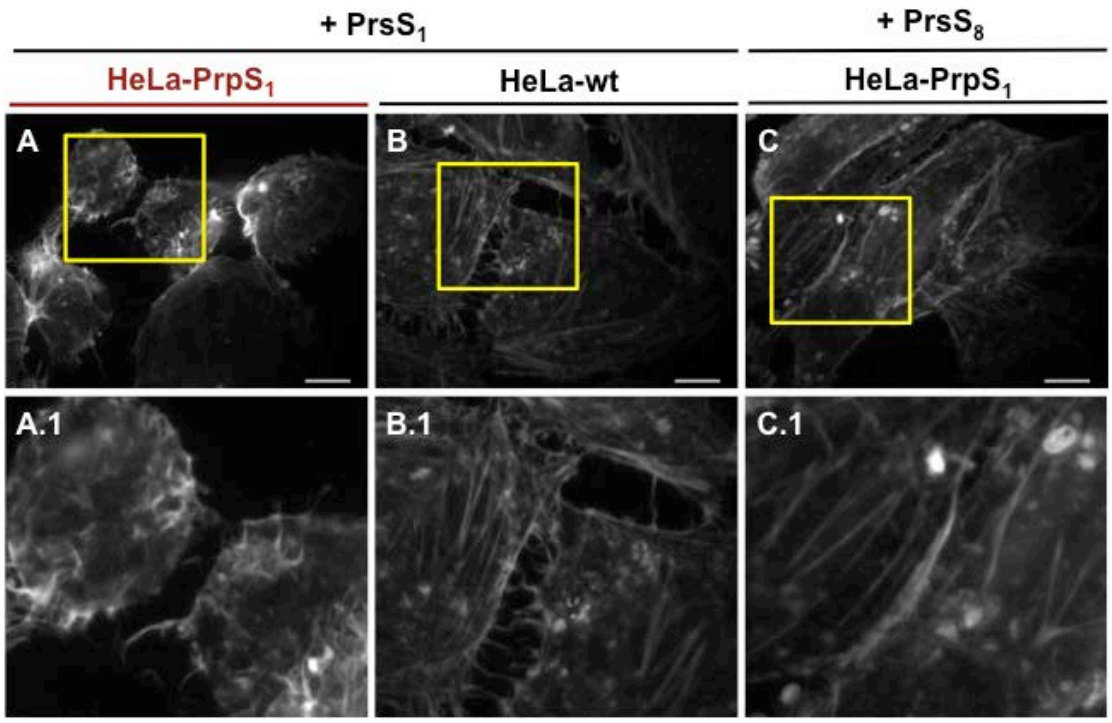

Figure 5.10. Evaluation of the allele-specificity of the actin alterations triggered by $PrsS_1$ on HeLa-C-$PrsS_1$ and HeLa-wt. **F-actin staining using 488-phalloiding. A**: HeLa-C-$PrpS_1$ cells treated with 20 µg.mL^{-1} of $PrsS_1$. **B**: nontransfected wilt type (HeLa-wt) cells treated with 20 µg.mL^{-1} of incompatible $PrsS_1$. **C**: HeLa-C-$PrpS_1$ cells treated with 20 µg.mL^{-1} of compatible $PrsS_8$. Magnification of the highlighted yellow rectangle is presented in the panel below **A.1**, **B.1,** and **C.1** respectively. Images from 30 analysed cells were obtained from two independent experiments with two replicates each. Images were taking using FITC filter: excitation 490 nm, emission 520 nm. Scale bar = 10 µm.

We next evaluated the effect of incompatible $PrsS_1$ and compatible $PrsS_8$, but this time with the additional control of HeLa cells expressing mCherry without $PrpS_1$ (HeLa-mCh). This control is important because it provides robust evidence that allows us to ascribe that the effect on the actin alterations is due to $PrpS_1$, ruling out a nonspecific effect as a result of the transfection, the expression of mCherry and/or PrsS addition.

Representative images of untreated HeLa-C-$PrpS_1$, HeLa-mCh and HeLa-wt cells (n = 15 each) are shown in **Figure 5.11.A**, **B** and **C** respectively. These cells exhibited normal acting stress fibres crossing the cell along the main axis of the cell. The F-actin of HeLa-wt appeared slightly more even in comparison with HeLa-C-$PrpS_1$ and HeLa-mCh cells. This suggest that the expression of either $PrpS_1$-mCh or just mCherry might have a minor effect on the actin cytoskeleton. Considering these results, the integrity of the actin stress fibres was the most consistent feature to analyse differences among the cells, as the presence of other putative structures such as bright specks varied. **Figure 5.11.E** shows HeLa-C-$PrpS_1$ cells treated with incompatible $PrsS_1$ (n=30). These cells exhibited round-up phenotype and a reduction in size compared with the controls of HeLa-mCh cells treated with incompatible $PrsS_1$ (**Figure 5.11.F**) and HeLa-wt cells treated with incompatible $PrsS_1$ (**Figure 5.11.G**), which exhibited numerous, noticeable and well-arranged actin stress fibres crossing the cell (n=15). **Figure 5.11.D** shows HeLa-C-$PrpS_1$ cells treated with 20 $\mu g.mL^{-1}$ of compatible $PrsS_8$ (n=30). These cells displayed less noticeable actin stress fibres in comparison with the other controls of HeLa-mCh and HeLa-wt exposed to $PrsS_1$. Nonetheless, magnification of the images revealed that HeLa-C-$PrpS_1$ exposed to incompatible $PrsS_1$ was the only treatment

where actin stress fibres were completely absent (**Figure 5.11.E.1**). HeLa-C-$PrpS_1$ treated with compatible $PrsS_8$ exhibited actin stress fibres (**Figure 5.11.D.1**), even though the cellular shape showed alterations. The other two controls HeLa-mCh (**Figure 5.11.F.1**) and HeLa-wt (**Figure 5.11.G.1**) presented a very organised, distinctive arrangement of actin stress fibres. The use of HeLa-mCh as a control, confirmed that the effect of PrsS on F-actin is not a consequence of PrsS itself on the HeLa cells and PrpS is necessary to reach the dramatic alterations.

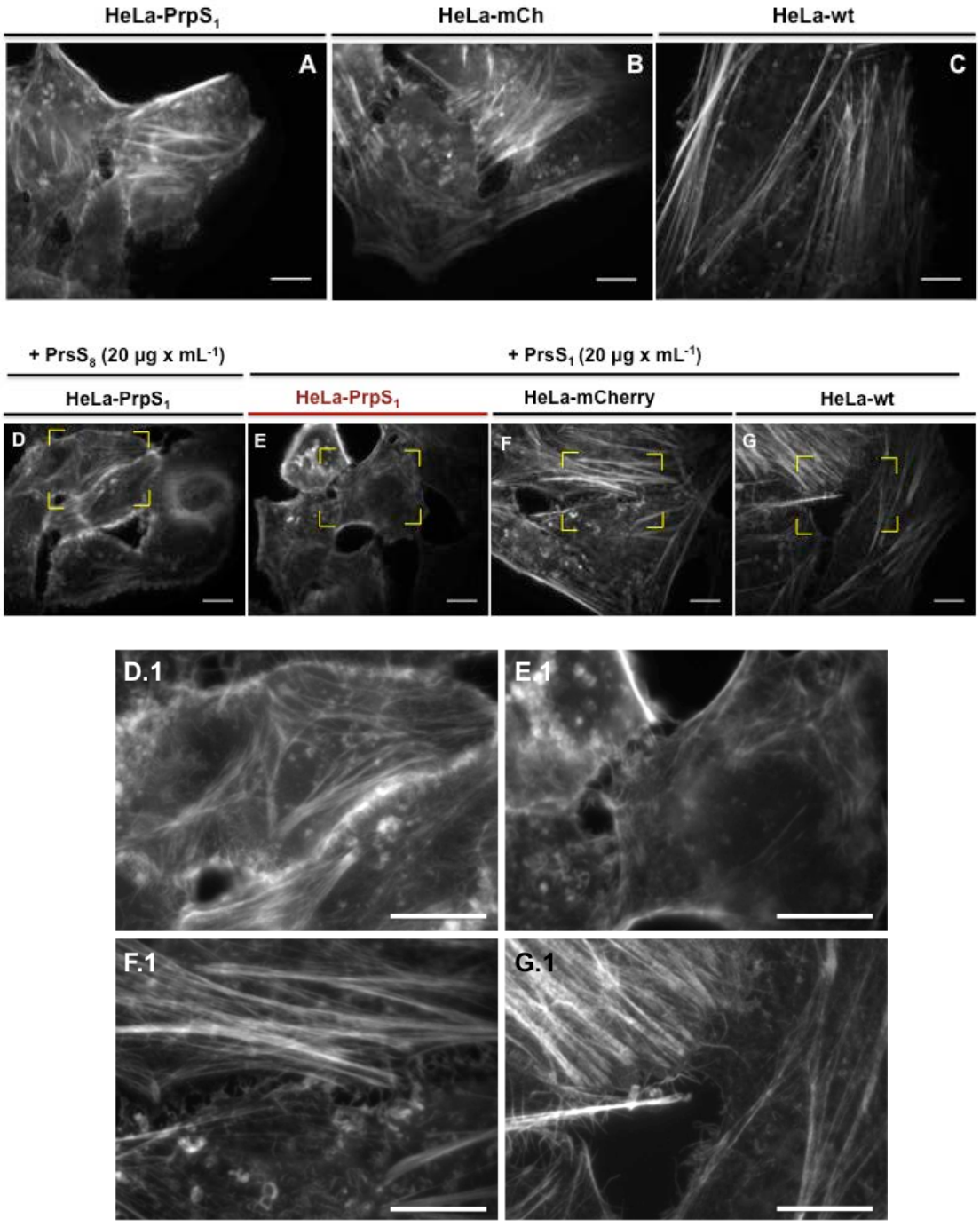

Figure 5.11. **Evaluation of the *S*-specificity of the F-actin alterations during treatments with $PrsS_1$ and $PrsS_8$ on HeLa-C-$PrpS_1$, HeLa-mCh and HeLa-wt.** Representative images of F-actin obtained using 488-phalloiding staining. **A**: HeLaC-$PrpS_1$ cells untreated (n=15 cells). **B**: HeLa-mCh cells untreated (n = 15 cells). **C**: HeLa-wt cell untreated (n=15 cells). **D**: HeLa-C-$PrpS_1$ cells exposed to compatible $PrsS_8$ (n=30 cells). **E**: HeLa-C-$PrpS_1$ cells exposed to incompatible $PrpS_1$ (n=30 cells). **F:** HeLa-mCh cells exposed to incompatible $PrpS_1$ (n=15 cells). **G**: HeLa-mCh cells exposed to incompatible $PrpS_1$ (n=15 cells). Magnification of the highlighted yellow rectangle is presented in the panel below **D.1**, **E.1, F.1** and **G.1** respectively. 15 cells were analysed for each condition. Images were taking using FITC filter: excitation 490 nm, emission 520 nm. Scale bar = 10 µm.

The dramatic loss of actin stress fibres in the incompatible combination of HeLa-C-PrpS_1 exposed to PrsS_1 suggested that there is an allele specific effect, which strongly support that the F-actin alterations are part of a real response to cognate PrsS. Thus, these data agree with the data from the calcium and electrophysiology experiments suggesting that PrpS is functional in HeLa cells, and that the exposure to incompatible PrsS triggers a *Papaver* "SI-like" response.

5.2.5.3 Timing of the actin alterations triggered after the exposure of incompatible PrsS

Once we had evaluated that there was an effect on the actin cytoskeleton of HeLa-C-PrpS_1 cells after treatments with PrsS_1, the next question was how quick the changes in morphology occurred, and especially the loss of actin stress fibres, which was the most consistent trait associated with the exposure to incompatible PrsS in adherent HeLa-C-PrpS_1 cells. First we considered the time course established for actin alterations during poppy SI. In *Papaver* pollen actin alterations were reported within minutes, reaching F-actin foci stage after several hours after triggering SI (Geitmann et al., 2000, Snowman et al., 2002, Poulter et al., 2010). Earlier HeLa cells experiments revealed that actin alterations were evident 3 h after incompatible treatment; so, this time-point was included as a positive control where actin alterations were expected. We wanted to assess the actin configuration at several time-points after treatment with incompatible PrsS_1. However, due to technical problems, only 1 h and 3h time-points assessed.

Figure 5.12 shows representative images of at least 15 cells from one experiment. Just before the treatment (t = 0) both cell lines, HeLa-C-PrpS_1 and HeLa-wt cells exhibited numerous and prominent actin fibres (**Figure 5.12.A** and **5.12.D** respectively). 60 min after challenge with PrsS_1, some HeLa-C-PrpS_1 cells have started to undergo morphological changes (**Figure 5.12.B**), which by 3 h showed a noticeable rounding up phenotype (**Figure 5.12.C**). HeLa-wt cells 60 min after SI, did not show obvious alterations in the shape or size (**Figure 5.12.C**). Visualization in more detail revealed that actin stress fibres were already less noticeable 60 min after incompatible PrsS_1 (**Figure 5.12.B.1**) and these fibres have disappeared by 3h (**Figure 5.12.C.1**). In contrast, in the control of HeLa-wt, the actin stress fibres were visible still 60 min (**Figure 5.12.E.1)** and 3 h (**Figure 5.12.F.1**) after treatments with PrsS_1.

These results indicated that the actin stress fibres began disappearing prior to 60 minutes. Further time-points are needed to identify how quickly these alterations begin. As alterations in *Papaver* are visible within minutes, it is expected that this might be similar in these cells.

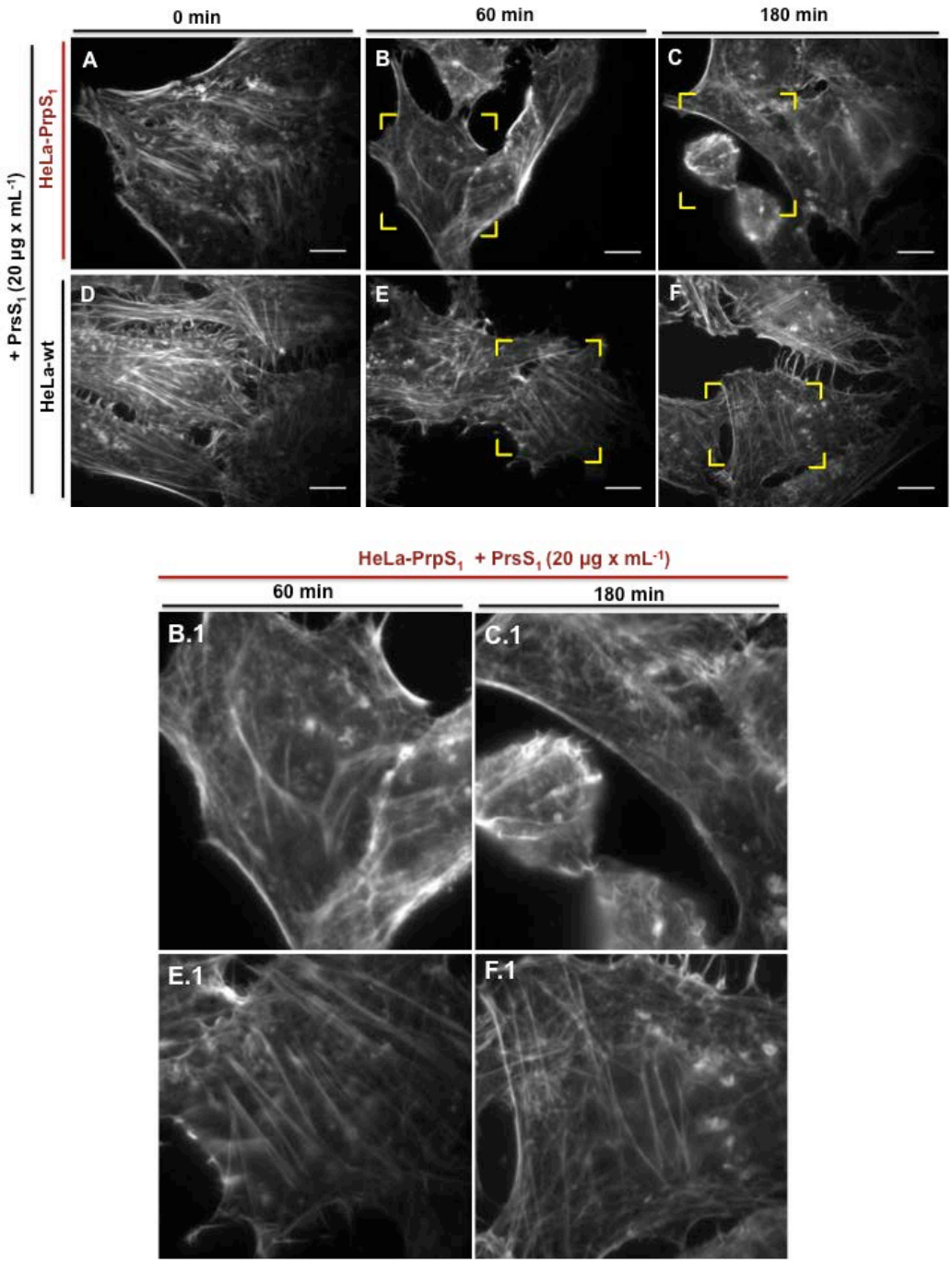

Figure 5.12. Temporal assessment of F-actin alterations of HeLa-C-PrpS$_1$ cells during treatments with PrsS. Representative images of the F-actin using 488-phalloiding. A: HeLaC-PrpS$_1$ before treatment (untreated). B: HeLa-C-PrpS$_1$ cells 60 min after exposure to PrsS$_1$. C: HeLa-C-PrpS$_1$ cells 180 min after exposure to PrsS$_1$. D: HeLa-mCh cells before treatments (untreated). E: HeLa-mCh cells 60 min after exposure to incompatible PrpS$_1$. F: HeLa-mCh cells 180 min after exposure to incompatible PrpS$_1$. Magnification of the highlighted yellow rectangle is presented in the panels below B.1, C.1, E.1 and F.1. This experiment was carried out once and at least 15 different cells were analysed for each time point. Images were taking using FITC filter: excitation 490 nm, emission 520 nm. Scale bar = 10 µm.

5.3 Discussion

In summary, this chapter investigated changes in the F-actin cytoskeleton induced by PrsS. We determined an increase in the number of “floaters” HeLa-C-PrpS_1 cells after the challenge with incompatible PrsS_1 in comparison with the control treatments (**Figure 5.3**). Part of the population of HeLa-C-PrpS_1 cells remained attached after treatments with incompatible PrsS_1. These cells exhibited a rounding up phenotype and a reduction in size (**Figure 5.1**). We interpret these results as HeLa-C-PrpS_1 cells exhibiting a response to incompatible PrsS_1, which includes a gradient in the strength of the response. The “floaters” show the strongest response, but a population of cells that remained attached to the coverslip, also responded to a lesser extent (**Figure 5.5**). Analysis of F-actin configuration in the adherent HeLa-C-PrpS_1 cell population revealed a loss in the actin stress fibres, in a dose-dependant correlation with the exposure to PrsS_1; untreated cells showed prominent and numerous actin stress fibres whereas increasing concentration of PrsS resulted in a gradual disappearing of actin stress fibres (**Figure 5.8**). Alterations were more dramatic for the incompatible combination of HeLa-C-PrpS_1 cells exposed to PrsS_1, suggesting an allele-specificity in the response, supporting the fact that the alterations are due to a real “SI-like” response (**Figure 5.10** and **Figure 5.11**). The actin analysis of “floaters” cells revealed that most of the HeLa-C-PrpS_1 cells challenged with incompatible PrsS_1 exhibited an speckled pattern, which resembled the F-actin foci formation described in during the *Papaver* SI response (**Figure 5.7** and **Table 5.1**).

Interestingly, PrpS-PrsS triggered a remarkably similar response to the SI response described in *Papaver*, suggesting that they were able to not only access, but also recruit cellular mechanisms and pathways in the host animal cell to make a "*Papaver*-like SI response". This would represent an exciting finding revealing the presence of conserved pathways through highly diverged species.

The integrity of the actin stress fibres was the most consistent alteration observed. Particularly, the disappearance of actin stress fibres in HeLa-C-PrpS_1 exposed to PrsS_1 was a clear trend. The dose-response experiments showed a close correlation between the concentration of PrsS_1 and the disappearance of actin stress fibres, suggesting that it was an authentic response.

Loss of actin stress fibres implied poor cell adherence of HeLa-C-PrpS_1 exposed to incompatible PrsS_1

Specialised cellular structures for adhesion, termed focal adhesions, are formed by actin stress fibres (Burridge et al., 1997). As mentioned in the introduction, in addition to adherence, these focal points, can translate external stimuli to the intracellular matrix (Chardin et al., 1989, Wozniak et al., 2004), mediating a variety of cellular processes (Bernstein and Bamburg, 2010). For instance, it has been reported that animal cells transformed with v-Src, a viral protein, exhibited a loss of actin filaments and a reduction in the number of focal adhesions (Frame et al., 2002). This is relevant as it provides evidence of a link between actin cytoskeleton and cell adherence. Another example is the protein family Rho GTPases, which have been profusely studied in mammalian cells (Jaffe and Hall, 2005). Rho play an essential role in the assembly of focal

adhesions and actin stress fibres (Ridley and Hall, 1992), but also has been described mediating other cellular processes such as activating transcription factors (Miralles et al., 2003) or controlling the cell cycle (Coleman et al., 2004). Rho also is involved in the regulation of the actin biding protein ADF/cofilin. ROCK is a Rho kinase that can activate by phosphorylation a family of actin-binding kinases, termed LIMK, which participate in the regulation of cofilin (Ohashi et al., 2000).

ABP have been described involved in the *Papaver* SI response (Poulter et al., 2010). Immunolocalisation experiments showed that ABP such as ADF and CAP co-localised with F-actin foci, suggesting that these protein play a role in the formation and/or maintenance of the F-actin foci during the *Papaver* SI response (Poulter et al., 2010). Similar evidence has been reported in yeast. Here, Srv2p/CAP plays a role in the actin dynamics (Chaudhry et al., 2014), and it is required for the formation of F-actin aggregates, which can lead to apoptosis (Leadsham et al., 2010). Therefore it would be interesting to investigate the possibility whether ABP are involved in the F-actin alterations we described in HeLa-C-PrpS_1 exposed to incompatible PrsS_1.

The studies showing an association between actin cytoskeleton and cell adherence in animal cells, provide robust support to the interpretation of actin stress fibres of HeLa cells involved in the response to the exposure to PrsS, and consequently linking the disappearance of actin stress fibres within the cells, with the reduction in the cell adherence leading to a detachment from the substrate in the cells with the strongest response. Thus, the increase in the number of “floaters” HeLa-C-PrpS_1 exposed to incompatible PrsS_1 represents a real cellular response. Moreover, provides valuable quantitative data to support

the allele specificity between the cognate *S*-determinant, as the significant increase was only in the incompatible treatment.

CHAPTER 6

Preliminary Attempts of Functional Transfer of *Papaver S*-determinants in *Hordeum vulgare*

6.1 Introduction

As mentioned in the introduction (Chapter 1 section 1.6) a major goal of this thesis was to assess whether it was possible to transfer functional *Papaver* SI into a highly diverged economically relevant plant species. As mentioned in Chapter 1 (section 1.4.3), manipulation and transfer functional SI has a direct application for plant breeding. Preventing self-pollination is a key point during the process of generating hybrid varieties, and therefore a long-term goal of SI research has been to transfer a SI system to other species, as converting a self-compatible (SC) species, especially staple crops such as wheat, barley or rice into a SI crop, can contribute in plant breeding providing new strategies to improve and reduce costs during the production of F1 hybrids. Existing strategies to make F1 hybrids are expensive and time consuming. This is because the emasculation of individual plants is carried out by hand, which requires a lot of manpower. An alternative method of producing F1 hybrids is the generation of male sterility lines, which do not produce fertile male flowers or pollen (Chapter 1 section 1.4.3).

From an evolutionary perspective, functional transfer of *Papaver* SI into a monocot species would represent a major breakthrough and contribution to the field of plant reproduction and plant physiology in general. As discussed in Chapters 4 and 5, this could also provide additional evidence supporting the hypothesis that PrpS-PrsS can access and recruit highly conserved signalling pathways, which eventually lead to PCD (see Chapter 1 section 1.1).

So far, functional transfer of SI has been restricted to the transfer of orthologous genes within closely related species that shared *S*-determinants (see Chapter 1 section 1.5). Self-compatible *A. thaliana*, was successfully transformed into a SI plant by transferring the corresponding *S*-determinants from *Arabidopsis lyrata* (diverged ≈ 5 MYA) and *Capsella grandiflora* (diverged ≈ 6.2 - 9.8 MYA). In *A. lyrata*, the specificity of the SI response is due to two genes codified within the *S*-locus. These genes are the female *S*-determinant SRK (*S*-locus receptor kinase) and the male *S*-determinant SCR (*S*-locus cysteine rich protein). Pollination analysis showed pollen tube growth inhibition in transgenic pollen expressing the SRC, after pollination of stigmas expressing SRK (Nasrallah et al., 2002, Boggs et al., 2009a, Boggs et al., 2009b). Interestingly, it was reported that the transformation of *S*-locus genes from *A. lyrata* resulted in different intensities of SI depending of the ecotypes of *A. thaliana* used for the transformation, indicating that the ability to exhibit Brassica-type SI also depends of other factors. Thus, in addition to the *S*-determinant, additional proteins such as PUB8, (Nasrallah et al., 2004, Boggs et al., 2009b, Liu et al., 2007) or Exo70A (Samuel et al., 2009) have been described playing a role in the SI response in Brassica.

The most obvious choice to assess whether *Papaver* SI can be functionally transferred to other angiosperms is *A. thaliana*. This model plant is a self-compatible species that has been thoroughly studied. Functional transfer to *A. thaliana* will provide new genetic, biochemical and cellular tools to study *Papaver* SI further as well as provide valuable information regarding the potential of this system in terms of its functional transference to other species. As mentioned previously in Chapter 1 (section 1.4.7), an extremely similar

response to the one described in *Papaver* including F-actin foci formation and PCD has been triggered in transgenic pollen of *A. thaliana* expressing PrpS after exposure to recombinant incompatible PrsS (de Graaf et al., 2012). Importantly, recently it has been also been demonstrated PrsS-PrpS interaction is functional *in vivo*, converting a highly diverged self-compatible *Arabidopsis* into a self-incompatible plant (Lin, 2015). Together, these data indicate that PrpS and PrsS are sufficient to trigger a *Papaver*-like SI response, which would be a unique and important characteristic of the poppy SI system in comparison with the other SI systems.

For the analysis *in vivo,* PrsS was driven by the *S-locus-related* (*SLR*) promoter. The *SLR* promoter is a stigma-specific promoter with a particularly prominent expression pattern in stigmatic papilla cells and specifically active in mature flowers. The selection and use of the *SLR* promoter was crucial for the successful functional transferral of PrsS into *Arabidopsis* stigmas as previous work attempted the functional transfer of $PrsS_1$ driven by the *STIG1* promoter from *Nicotiana tabacum* (*STIG1*::*$PrsS_1$*) did not exhibit pollen inhibition after pollinations with *At-Ntp303:PrpS-GFP* pollen (Lin, 2015). This suggested that *STIG1* promoter was not suitable for the functional expression of *A. thaliana*. One of the most likely reasons could be that *STIG1* is differentially expressed during development; it is highly expressed in young and developing flowers, and only low expression detected in mature flowers (Goldman et al., 1994, Verhoeven et al., 2005), which is when flowers are ready to be pollinated. Moreover, western blot analysis using protein extracts from stigmas transformed with *STIG1*::*$PrsS_1$* did not detect any signal that could correspond to $PrsS_1$ (Vatovec, 2012).

Before this thesis started, similar experiments were carried out in collaboration between our laboratory with Dr Wendy Harwood and her laboratory at John Innes Centre (JIC) aiming to transfer functional *Papaver* SI into *Hordeum vulgare* (barley).

Among the most relevant economic self-compatible crops, barley represents a straightforward alternative, as (even though is not a trivial), a reproducible stable transformation method has been well-established. Transformation efficiencies of 25% using an *Agrobacterium*-mediated procedure have been reported for the variety “Golden Promise” (Harwood et al., 2009). Other advantages of using barley as a monocot and cereal crop model is that its genome is diploid, whereas other cereal crops such as wheat are hexaploid, which make the genetic analysis more complex. In terms of its economic importance, barley is the second largest crop in the UK (after wheat). Additionally genetic transformation of other commercial crops such as wheat, or even different varieties of barley (other than Golden Promise) still have not been completely established (Harwood, 2012). A general difficulty for the studies using monocot species is the lack of identification of tissue-specific promoter suitable for monocot species. Even though the barley genome was sequenced whilst this project was being carried out (Mayer et al., 2012), the studies providing functional information regarding the sequences are just starting to be developed now (Munoz-Amatriain et al., 2015). Therefore, the characterisation of tissue-specific promoters (for our purposes stigma-specific promoter) still needs to be developed.

The first attempt to generate transgenic SI barley lines in our laboratory utilised the constructs details in **Table 6.1** (further detail in Chapter 2 section 2.5.1).

Table 6.1 Genetic constructs used in the first attempt to transform barley with the PrpS and PrsS. These constructs were generated by Mark Smedley at JIC.

Name	Cassette cloned into pBract202	Comments
Construct containing PrpS, the male S-determinant		
pBpS1GFP	*NTP303*::*PrpS$_1$-GFP*	*PrpS1* fused to *GFP* driven by the pollen-specific promoter *NTP303* from *Nicotiana tabacum* and cloned into pBract202, which confers resistance to hygromycin for the selection of transformants plants. Originated line named BpS1GFP
pBpS3GFP	*NTP303*::*PrpS$_3$-GFP*	*PrpS3* fused to *GFP* driven by the pollen-specific promoter *NTP303* from *Nicotiana tabacum* and cloned into pBract202, which confers resistance to hygromycin for the selection of transformants plants. Originated line named BpS3GFP
Construct containing PrsS, the female S-determinant		
pBsS3	*STIG1*::*PrsS$_3$*	*PrsS3* driven by the stigma-specific promoter *STIG1* from *Nicotiana tabacum* and cloned into pBract202, which confers resistance to hygromycin for the selection of transformants plants. Originated line named BsS3

These constructs were used for the *Agrobacterium*-mediated transformation of barley Golden Promise. More details describing this procedure are presented in section 6.2.1.2 (for further details see Chapter 2 section 2.5). After the embryogenesis and selection process, 17 plants were obtained for pBpS1GFP (BpS1GFP lines) and 25 for pBpS3GFP (BpS3GFP lines), which represents transformation efficiencies of ≈ 4% and ≈ 7% respectively considering the number of embryos transformed. For pBsS3, 17 plants were obtained (BsS3 lines), which represents a transformation efficiency of 4.3 %. These efficiencies values are higher compared to the values typically obtained for *Arabidopsis* transformation by floral dip, which are around 1% (Zhang et al., 2006)

The transformants lines were confirmed by PCR for the selectable marker *Hyg* and the presence of the transgene PrpS or PrsS. Real-time PCR were carried out to evaluate the transcription levels of PrpS. Transcripts were detected in 5 out of 7 BpS1GFP analysed lines, and 6 out of 9 BpS3GFP analysed lines. However, $PrsS_3$ transcripts were not detected in any of the 11 BsS3 lines analysed. The generation and Real-Time PCR analysis of these lines were carried out by Dr Wendy Harwood and her group at the JIC.

Based on these analyses, we selected four higher expressing BpS1GFP and four BpS3GFP lines to carry out the functional analysis in this thesis (see **Table 6.2**).

Table 6.2 Quantitative PrpS expression of BpS1 and BpS3 lines. The expression values were determined as a quotient between the transgene and the constitutive "housekeeping" gene GAPDH (PrpS/GAPDH). RNA samples were prepared from pollen.

BpS1GFP			BpS3GFP	
Line	Expression of $PrpS_1$/GAPDH		Line	Expression of $PrpS_3$/GAPDH
332-01-01	0.01695413		330-02-02	0.02160864
376-04-01	0.00167002		374-01-01	0.00451074
332-02-02	0.00124459		37401-02	0.00295281
376-03-02	0.00038519		330-01-02	0.00151253

Despite the lack of *$PrsS_3$* transcript detection, it was still possible that *$PrsS_3$* was expressed below the detection limit, and therefore $PrsS_3$ protein could potentially be present in the transgenic barley stigmas. Thus, a crossing program between BpS1GFP and BpS3GFP with pBrsS3, was carried out to determine whether the seed-set was different between compatible and incompatible crosses. The results are detailed in **Table 6.3**.

Table 6.3 Summary with crosses carried out using BsS3, BpS1GFP and BpS3GFP

Female line (stigma)	Male line (pollen)	Nº Stigmas	Seeds harvested	%
BsS3	BpS1GFP	165	91	55 (C)
BsS3	BsS3GFP	147	69	47 (I)
BsS3	Wild type	70	23	33 (C)
Wild type	BpS1GFP	66	40	61 (C)
Wild type	BpS3GFP	80	46	57 (C)

C: Compatible cross. I: Incompatible cross. On average ~10 - 15 stigmas were pollinated per spike.

Similarities in the number of seed-set and seeds harvested in the incompatible crosses in comparison with the compatible crosses and the controls using wt pollen and stigmas, suggested that these barley lines were not exhibiting SI response. As mentioned earlier, this work was carried out in collaboration with the John Innes Centre (JIC) before this thesis was started. These results are relevant because part of the experiments carried out and presented in this thesis, correspond to the continuation of this work. Additionally, this previous work provided the basis for new goals addressed during this thesis, and presented in this Chapter.

In summary, previous evidence including: 1) the absence of $PrsS_3$ transcripts in the Real-Time PCR experiments from barley stigmas transformed with *STIG1*::*PrsS*$_3$, 2) no differences in the seed-set production between incompatible and controls crosses, and 3) similar negative results in *A. thaliana* transformed with *STIG1*::*PrsS*$_{1,}$ which includes no PrsS signal in western blot analysis, and successful fertilisation and seed production in the incompatible crosses, suggested that we needed a new strategy. Considering that the *STIG1* promoter, used initially, is a developmentally-dependant promoter with expression only during immature flowers, it was reasonable to assume that *STIG1* was not a suitable promoter to drive PrsS.

Thus, one of the central goals of this thesis emerged. This was to design a new strategy to transfer functional SI to barley using an alternative promoter to drive PrsS. The Ubiquitin promoter from maize (*UBI*), has been demonstrated to be functional in wheat (Rooke et al., 2000) and barley (Bartlett et al., 2008, Hensel et al., 2011), and provides constitutive transgene expression. For “male” lines, BpS1GFP and BpS3GFP lines, as *PrpS* transcripts had been detected in transgenic barley pollen, and the cassette *NTP303*::*PrpS-GFP* had been shown to be functional in *A. thaliana*. This suggested that it was feasible to obtain functional PrpS in a highly diverged species.

This chapter describes a new attempt to obtain functional *Papaver* SI in transgenic barley plants. The first part describes the generation and analysis of the transgenic barley plants, detailing construction of the transgenic lines expressing PrsS (BsS1), and the analysis of barley lines expressing PrpS ($BpS_{1\text{-}3}$GFP), generated prior to this thesis by Dr Wendy Harwood at JIC, The second part shows different approaches aiming to confirm functional SI in the transgenic barley lines. The functional analysis included the visualisation and monitoring of the actin cytoskeleton of pollen from p$BpS_{1\text{-}3}$GFP lines exposed to SI treatments in an *in vitro* SI bioassay. and evaluation of pollen tube growth and seed-set in semi-*in vivo* and *in vivo* pollinations between pollen and stigmas from compatible and incompatible lines.

6.2 Results

6.2.1.1 Genetic constructs to transfer *PrsS* into barley

The *Papaver* $PrsS_1$ and $PrsS_3$ were cloned into the pBract211, downstream of the maize constitutive ubiquitin promoter (*UBI::*$PrsS_{1\text{-}3}$). The vector pB202 belongs to the pBract family vector and is a suitable control as it has similar characteristics with pBract211 (hygromycin resistance gene and a strong constitutive promoter CaMV 35S (in this case driving LacZ operon) but does not have the gene of interest, $PrsS_1$ (summary in **Table 6.4**). Cloning was carried out using standard molecular biology procedures (See details Chapter 2 section 2.5.2 for details).

Table 6.4 Genetic constructs to transform barley plants.

Name	Cassette	Comments
pBsS1	*UBI*::$PrsS_1$ Cloned into pBract 211	$PrsS_1$ cloned into pBract211, driven by the constitutive promoter *UBI* from maize. Resistance to kanamycin for the selection of transformants plants. Originated lined named BsS1
pB202	Empty MCS Control	Confers resistance to kanamycin for the selection of transformants plants. Originated line named B202

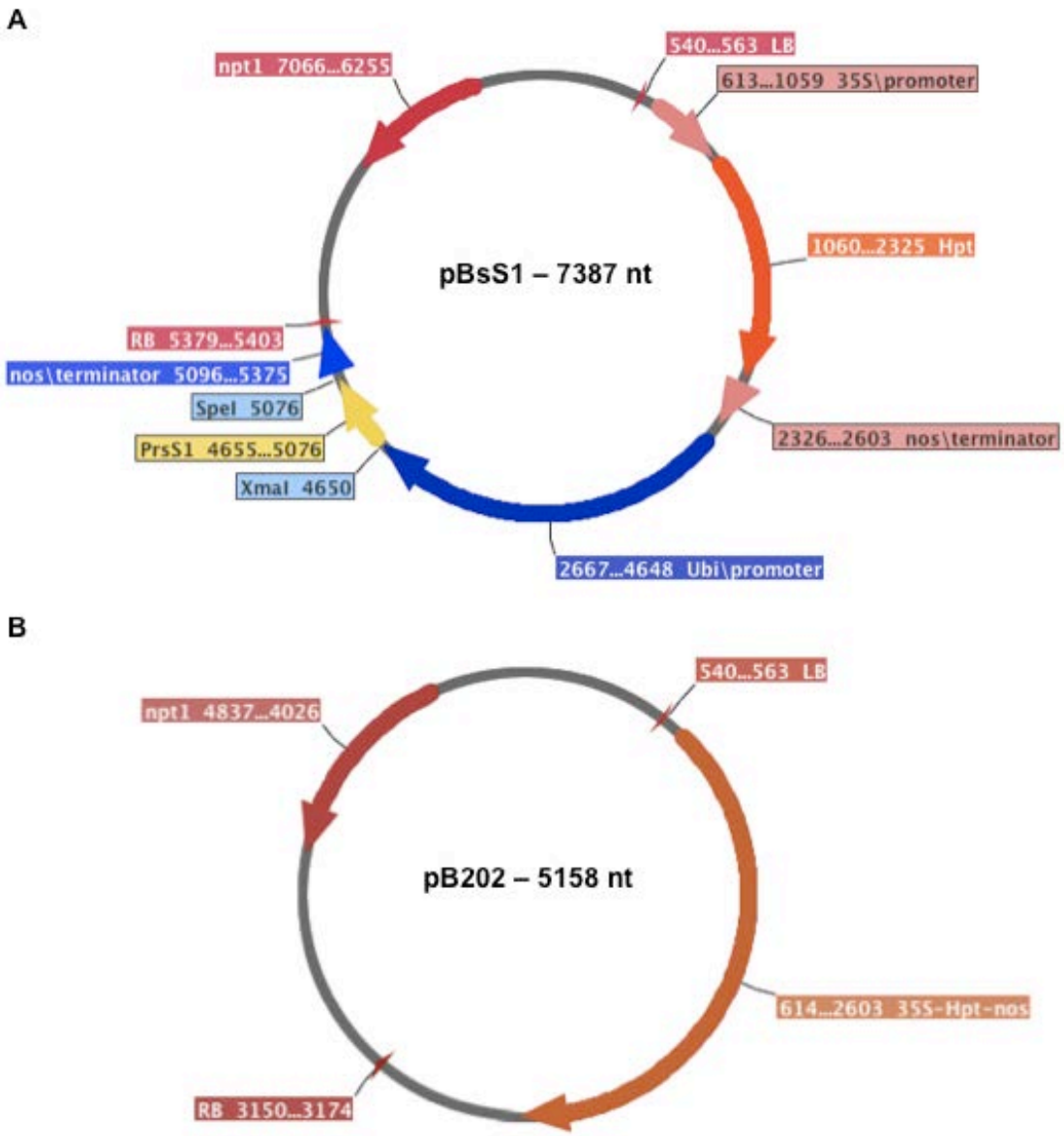

Figure 6.1 Genetic construct pBsS1 used for barley transformation. **A:** pBsS1, $PrsS_1$ gene cloned under the control of the maize *UBI* promoter in the vector pBract211. **B**: pB202, empty vector used as a control.

$PrsS_1$ was successfully cloned into pBract211 (termed pBsS1). pBsS1 and pB202 were transformed by electroporation into *A. tumefaciens* AGL1, a suitable strain for Barley transformation, and prepared for the inoculation of barley immature embryos. Chapter 2 section 2.5.3 for details).

6.2.1.2 Generation of transgenic barley lines expressing the *Papaver* female S-determinant, *PrsS*

Stable transformation of barley with pBsS1 and pB202 (control) were generated according to the protocol detailed in Harwood et al. (2009). These transformations were carried out during a visit to the Harwood lab at JIC.

Immature embryos (IE) were isolated and inoculated with *Agrobacterium* containing pBsS1 or pB202. The IE were then placed in MS agar plates containing hormones for the regeneration of the embryo into seedlings, and antibiotic for the selection of the transformant plantlets (see Chapter 2, section 2.5.3). Once the plantlets had developed roots and leaves, they were transferred to soil and glasshouse (Chapter 2 section 2.5.4). In total, 300 immature embryos (IE) were transformed with the construct pBsS1 and 150 IE were transformed with the plasmid pB202. Representative images of the regeneration process are shown in **Figure 6.2**. The arrangement of 25 of the IE ready to be transformed with *A. tumefaciens* is presented in **Figure 6.2.A**. After the transformation, these embryos were spread out and placed in a plate containing callus induction media. 4 weeks after, the callus exhibited a noticeable increase in the size of the embryos (**Figure 6.2.B)**. After 2 further weeks (6 weeks in total), callus exhibited a considerable increase in size and a noticeable "crumbly" aspect causing the breaking of some small fragments (**Figure 6.2.C**). At this stage, small green shoots were visible (**Figure 6.2.D**). Calluses and embryo-derived tissue were transferred to transition medium where the green shoots were developed to small leaves (**Figure 6.2.E**). 2 weeks after, callus and embryo-derived tissue were transferred to regeneration

media and where leaves and roots continue developing organs (**Figure 6.2.F**). Once the root system had reached a relatively vigorous stage, the plantlet was separated from the callus and transferred into a glass tube with callus induction media, which allows the elongation of roots and leaves (**Figure 6.2.G**). Finally, when the root system was established and several leaves developed, the plantlet was transferred into soil for acclimation. To retain the high humidity required, initially plastic cups were placed on top of the plantlet (**Figure 6.2.H**), and they were gradually removed until the plant was acclimatised to glasshouse conditions. All this process, from the immature embryo isolation, until the acclimatisation of a plant in the glasshouse, took between 6 and 7 months.

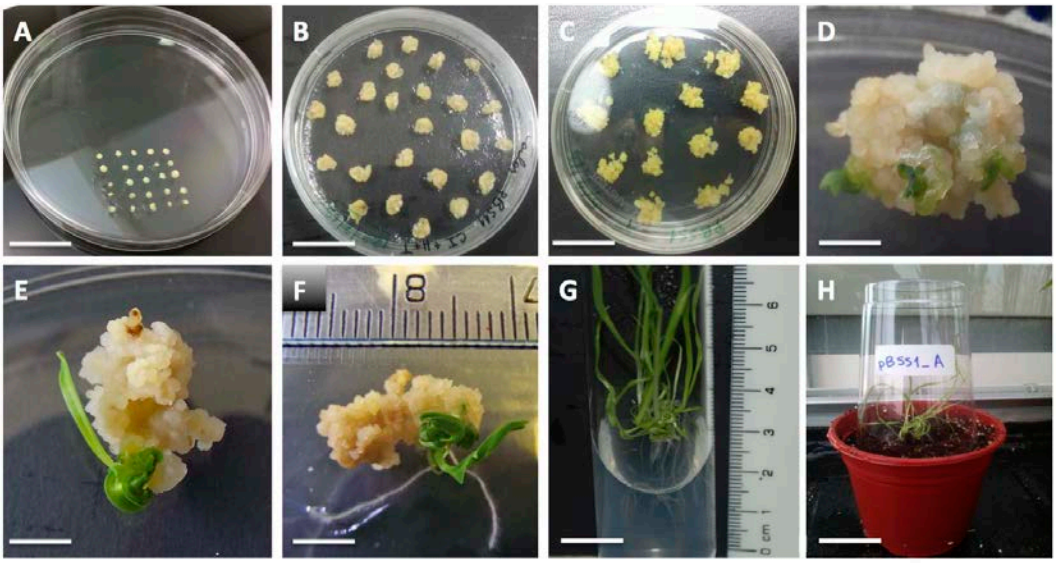

Figure 6.2 Regeneration and selection process of barley plants after transformation. **A**: immature embryos ready for transfection. **B**: 4-weeks embryos in callus induction medium. **C**: embryos in the last stage of callus induction medium. **D**: zoom to a callus exhibiting green tissue. **E**: embryo-derived tissue during the transition medium stage. **F**: callus in the regeneration medium stage. **G** small plantlet transferred to a glass culture tube containing callus induction media. **H**: barley plant in soil during the acclimation process. Scale bar in: A, B and C = 2 cm. D, E and F = 5 mm. G = 1.5 cm. H = 3.5 cm.

The efficiency of the transformation and regeneration was calculated considering embryo-derivate tissues that have developed shoots and roots at

the stage of the regeneration media, compared to the total number of embryos initially transformed. Thus, transformation efficiencies were 33% for pB202 and 50% for pBsS1, which was much more efficient than previous attempts using PrsS driven by the stigma promoter (*STIG*), which exhibited 4 and 7 % for BpS1GFP and BpS3GFP respectively, and 7 % for BsS3. 20 lines BsS1 and 12 B202 were selected to carry on with screening in order to confirm the transgenic lines.

6.2.1.3 Characterisation and analysis of *PrsS1* expression in barley transgenic lines.

6.2.1.3.1 Screening lines containing BsS1

Transformed lines were screened by amplifying *hpt* from genomic DNA. As a control, we used the *CONSTANS* gene; a family of constitutive expressed genes in barley (Griffiths et al., 2003). All the analysed lines for both BsS1 and B202, amplified a fragment from the *CONSTANS* gene (**Figure 6.3**, lower panel). Out of the 20 analysed BsS1 lines, 19 exhibited amplification product for *hyg* gene. For B202, all the 12 analysed lines showed a product for *hyg* (**Figure 6.3**, upper panel). As expected, controls PCR using wild type gDNA only revealed a band for *CONSTANS* gene, confirming that *hyg* primers were specific and suitable for the identification of the transgene. Also, no amplicon was detected for *CONSTANS* or *HTP* gene in the negative control using H_2O as a template, indicating that the amplification was not due to unspecific contamination in any of the components of the mix reaction.

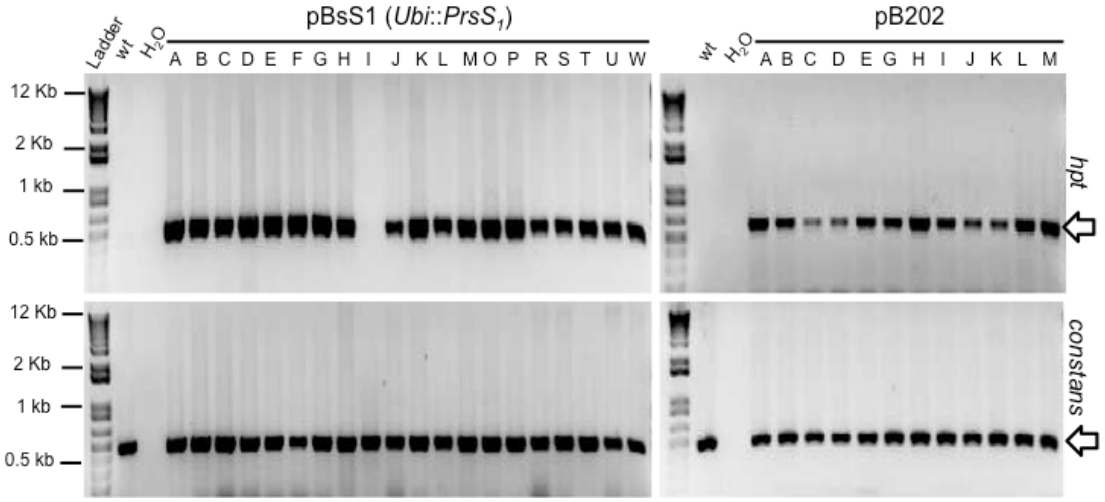

Figure 6.3. Screening of barley lines regenerated after *Agrobacterium* transformation with BsS1 and B202. Agarose gel showing the PCR from genomic DNA obtained from transformed barley lines. *CONSTANS* gene was used as a control of the quality of DNA extracted. *HPT* gene was amplified to determine the transgenic barley lines. Amplification of the gene *CONSTANS* was done as a control of the quality of DNA. Regenerated lines after transformation with BsS1: A-W. Regenerated lines after transformation with B202: A-M. wt: PCR using gDNA from wild type plants. H_2O: Negative control of the PCR using water as a template.

These results indicate that the selection procedure during the regeneration of barley lines after the transformation of embryos was a reliable method, which effectively allows the identification of the transformed lines.

6.2.1.3.2 Transcript analysis, semi quantitative RT-PCR

Transcriptional analyses to detect the mRNA of PrsS expressed in the transgenic BsS1 lines were carried out by a semiquantitative RT-PCR extracting RNA from barley leaves (Chapter 2 section 2.5.2). The actin gene from *Hordeum vulgare* was selected as a positive control because its expression is expected to remain unaltered in all the plants evaluated here. Also, because it contains two introns, specially designed primers allowed the discrimination of an

amplicon from cDNA or genomic DNA (gDNA), as they had different sizes. Thus, actin gene was used to confirm that the cDNA samples were not contaminated by gDNA, and also as control to confirm equal amount of DNA used for each reaction The fragment amplified from gDNA was 633 bp, and from cDNA 473 bp. **Figure 6.4** shows a clear size difference for *actin* amplicon from gDNA and cDNA from the transgenic lines. There was a predominant band obtained from gDNA of BsS1, which was bigger than the single band obtained from the cDNA samples (C - Y). The sample corresponding to the line “R” did not exhibit an amplicon, indicating defective cDNA preparation. The RT-PCR procedure was repeated for this line, and cDNA successfully obtained and included for the following experiments.

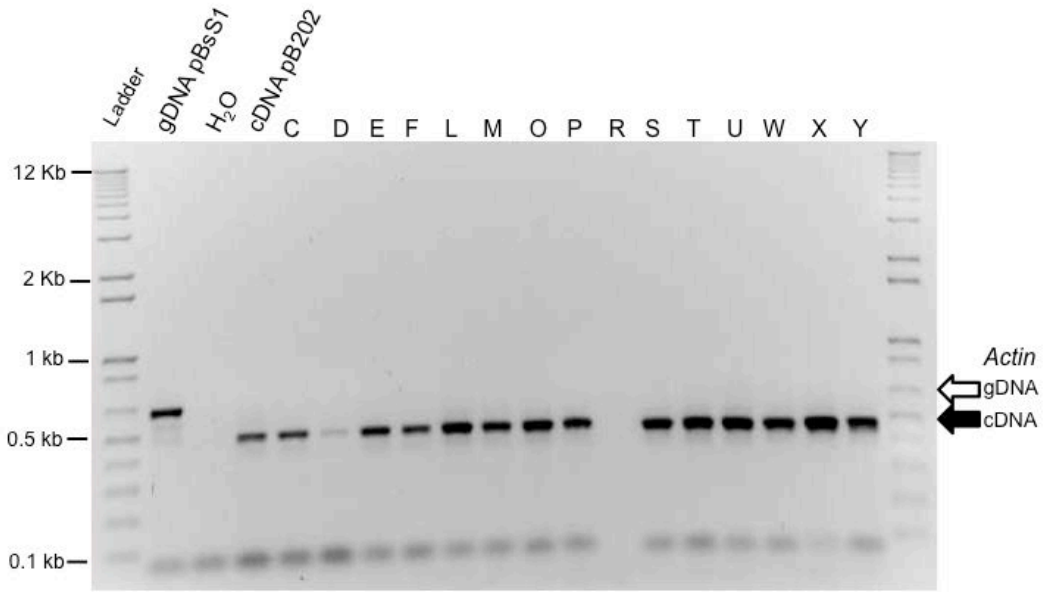

Figure 6.4 Amplification of *actin* from barley gene from gDNA and cDNA. Using genomic DNA from barley transformed with BsS1 (gDNA BsS1) as a template revealed a band corresponding to a larger size (633 bp - indicated in a white arrow), in comparison with the reaction using cDNA as a template, which produced a smaller band (473 bp - indicated in a black arrow). DNA and RNA extractions were carried out from barley leaves.

This result confirmed that the cDNA samples from the BsS1 lines did not contain gDNA, confirming that the amplification of a gene using these samples

is from cDNA and not from contamination of remaining gDNA. This is an essential control for a reliable RT-PCR.

The parameters for each PCR reaction were optimised based on the constitutive *actin* gene at 24 cycles. **Figure 6.5.A** shows the amplification of *$PrsS_1$* after a 24 cycles PCR. As it was expected, there was a noticeable and single band of the of 421 bp in 10 out of the 14 BsS1 lines evaluated, confirming that the transgene $PrsS_1$ was expressed at transcriptional level. The intensity of the *$PrsS_1$* amplicon was heterogeneous for the different lines (C - X), suggesting that there was a differential expression among the lines, with lines F, L, and X as the putative high-expressing lines. **Figure 6.5.B** shows the amplification corresponding to the constitutive housekeeping *actin*, used as a control. The uniformity in this case indicates that the differences in the *$PrsS_1$* expression are not due to differences in the amount of cDNA used as a template for the PCR, and therefore they may be due to differences in the expression of the transgene $PrsS_1$. A quantification based on the relative intensities of $PrsS_1$ respect to actin was done using the software ImageJ, and the results presented in **Figure 6.5.C.** Two lines (BsS1-F and -X) showed an expression higher that *actin*, which suggests that they are highly overexpressing lines, as the *actin* is normally a highly expressed gene. BsS1-L also showed a reasonably high expression of 0.8 respect to *actin*. This graph also shows that the expression of the $PrsS_1$ mRNA was present all the lines, despite the intensity of the band was very low in lines E, O, and S. These data provided good evidence to identify the more promising lines for further analyses.

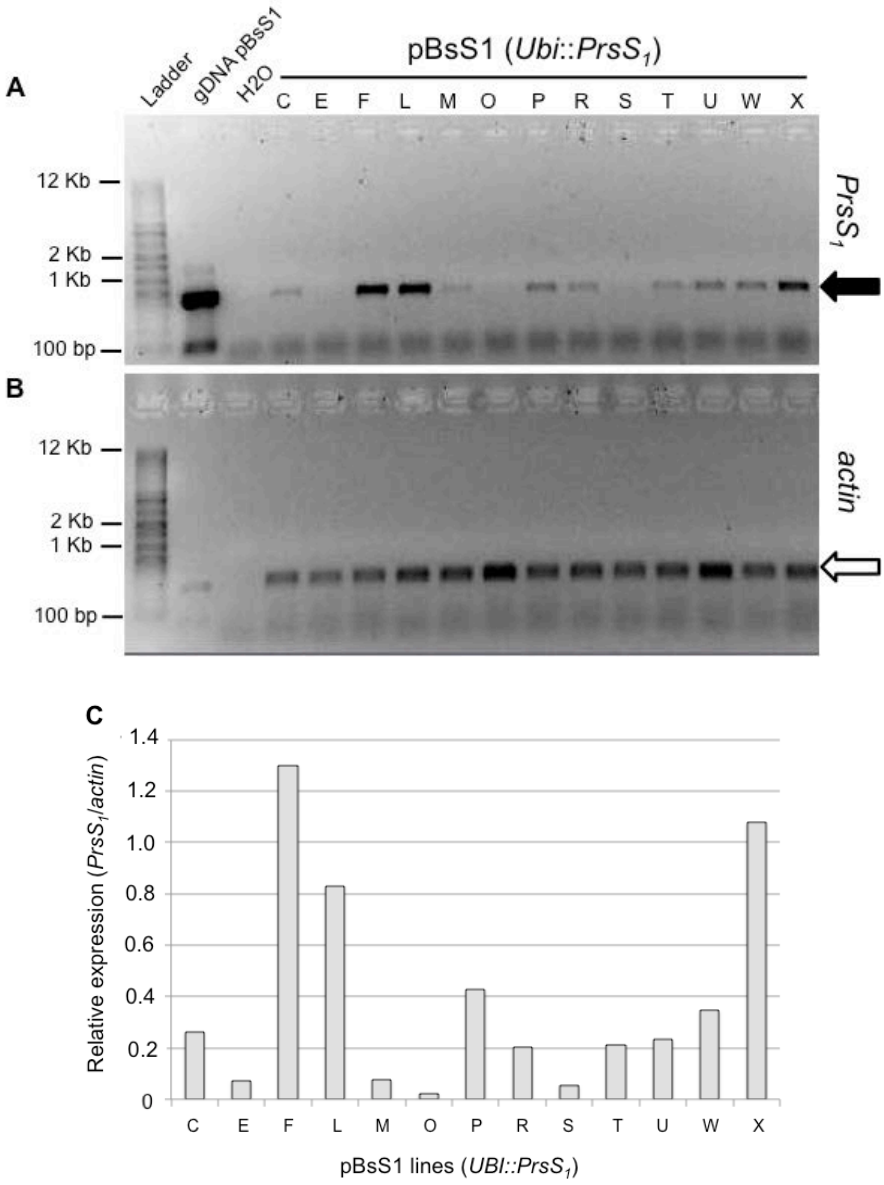

Figure 6.5 Semi quantitative RT-PCR of $PrsS_1$ in barley lines. A: agarose gel showing the RT-PCR for *$PrsS_1$* in BsS1 barley lines (C - X). Genomic DNA from BsS1 was used as a positive control. **B**: agarose gel showing the RT-PCR for *actin*, used as a loading control. **C**: semi-quantification of the expression of *$PrsS_1$* relative to the expression of *actin*, which was normalised as 100%. Barley leaves was the tissue selected for this assay.

Semiquantitative RT-PCR confirmed that *$PrsS_1$* was expressed in the BsS1 barley lines. Moreover, this experiment suggested that there was a range in the expression levels of *$PrsS_1$* in these lines. This was used as guidance to select the lines used in the following experiments, which included over-expressing

lines (F and X) but also lines a lower expression such as line P or C, aiming to cover a wide spectrum of expression levels.

To confirm the expression of $PrsS_1$ at protein level, western blot analysis was carried out in the BsS1 lines. In BsS1 lines, *$PrsS_1$* was driven by the constitutive promoter *UBI*, therefore it was expected that $PrsS_1$ protein was expressed in all the tissues. Unfortunately, using protein extraction from both stigmas and leaves, it was not possible to detect a signal of ~ 15 kDa corresponding to the size of PrsS (data not shown). Because the anti-PrsS antibody used in these experiments was the same antibody successfully used to detect PrsS in *A. thaliana* (Lin, 2015), it is more likely that the lack of signal was associated with low levels of PrsS, probably as a consequence of degradation in the cells, which has been reported when *PrsS* was driven by the strong constitutive 35S promoter in *A. thaliana* (Lin, 2015). Therefore, we did not confirm PrsS protein was expressed in these plants.

6.2.1.4 Screening and selection of transformants BsS1 and B202 lines.

Since *$PrsS_1$* in BsS1 was not tagged with any gene, and the fact that growing barley plants *in vitro* (on selective media) is not such a routine procedure as it is in *A. thaliana*, the screening for the transgenic BsS1 and B202 plants was initially limited only to PCR. This made the identification and discrimination between homozygous and heterozygous plants extremely challenging. Thus, for the functional analysis presented in the following sections, the plants were assessed for the insertion of *HYG* in their gDNA, but they were not confirmed to be homozygous or heterozygous lines. A protocol to grow barley *in vitro* was

optimised several months after. This allowed us to use MS media supplemented with hygromycin to germinate and grow barley (details in Chapter 2, section 2.5.4.3). However, at this point we did not have enough time to analyse the barley lines using this method.

Figure **6.6 shows** plantlets of transgenic barley plants growing in MS supplemented with hygromycin. **Figure 6.6.A** shows five germinated seeds with four of them developing a prominent root system with long roots of about 2 - 3 cm, suggesting they are hygromycin-resistant, whereas one of them seemed to be sensitive to hygromycin as the roots are considerably shorter (< 1 cm). **Figure 6.6.B** small plantlets growing in a 24-well plate. In this case, after the seeds germinated and began growing, the lid of the plate was removed to allow the vertical growing of the plants.

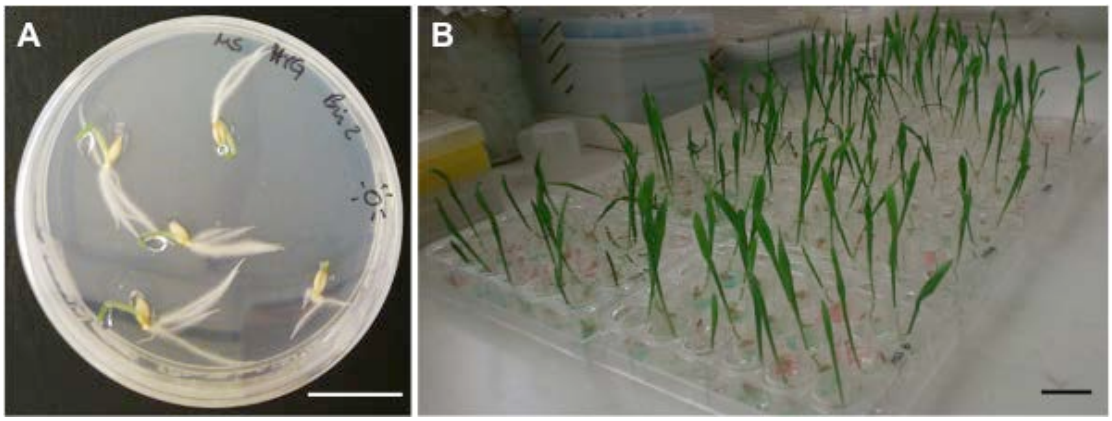

Figure 6.6. Transgenic barley seeds screening in agar-based selective MS media supplemented with hygromycin. **A**: five BsS1GFP seeds in a Petri dish; four of them have developed a noticeable root system, and one of them exhibited short roots. **B**: Scale up of the screening procedure. PrsS1GFP seeds were individually grown in a 24-well plate (one seed per well) to avoid the roots tangle among them, facilitating both the discrimination between long v/s short roots, and the transferral to soil. Scale bar = 2 cm.

This procedure was not developed in time to be used for the selection of homozygous BsS1 lines. Therefore the BsS1 and B202 lines used later on for

the functional analysis by means of semi-*in vivo* and *in vivo* pollinations (section 6.2.3.2) were not identified as heterozygous or homozygous lines.

However, this protocol of barley seed germination *in vitro* might be useful in future to identify homozygous lines.

6.2.2 Functional Analysis of Barley Lines Transformed with *Papaver rhoeas S*-determinant.

The procedures involving barley handling (pollen collection, emasculation, and pollinations), which were crucial for our approaches to assess functional SI in barley, we received advice from Dr Wendy Harwood (JIC) and Dr Katsuyuki Kakeda (Mie University, Japan). Dr Harwood has a vast expertise in the cereals such as wheat and barley, particularly in the genetic transformation of these crops. The research of Dr Kakeda specialised in self-incompatibility genes in grasses, particularly *Hordeum bulbosum* L., which is a wild species related to barley.

6.2.2.1 Analysis of pollen from barley lines BpS1GFP (*NTP303::PrpS$_1$-GFP*) and BpS3GFP (*NTP303*::*PrpS3-GFP*).

High-expressing *PrpS$_1$* (BpS1GFP) and *PrpS$_3$* (BpS3GFP) lines were selected for the functional analysis of pollen from these lines (**Table 6.2**). The analyses included the evaluation of different protocols for barley pollen germination *in vitro*. Additionally, a pollen viability assay was standardised, which provided valuable information for the interpretation of *in vitro* assays results. Finally,

pollinations semi-*in vivo* and *in vivo* were also carried out to assess whether there was any difference between compatible and incompatible pollinations, which could indicate functional SI in these barley lines.

6.2.2.1.1 Screening of transgenic pollen from BpS1GFP and BpS3GFP lines

The lines BpS1GFP and BpS3GFP had *PrpS$_1$*, and *PrpS$_3$* fused to *GFP* respectively integrated into the genome. Although of *PrpS$_1$* and *PrpS$_3$* transcripts in pollen from these lines were detected, the expression of PrpS_1-GFP and PrpS_3-GFP at protein level was not confirmed. Therefore we aimed to confirm the presence of PrpS_1-GFP and PrpS_3-GFP proteins by means of microscopic analysis assessing the fluorescence of pollen from these plants. Additionally, microscopic analysis based on the GFP fluorescence could represent a powerful tool for the discrimination between the homozygous (all the pollen exhibiting GFP emission) and the heterozygous (half of the pollen exhibiting GFP emission) lines.

Pollen grains from transgenic lines exhibited GFP emission. The emission was prominent around the edge of the pollen grain, and also forming a ring round the pollen pore (**Figure 6.7.A**). Unfortunately, fluorescence analysis of barley pollen from non-transgenic (referred to as “wild type”) plants revealed high autofluorescence in these pollen grains with a similar pattern to the one described previously for the pollen grains from transgenic lines (**Figure 6.7.B**). These are representative images of pollen collection from 8 independent plants, 4 plants BpS1GFP and 4 plants BpS3GFP (see **Table 6.4**).

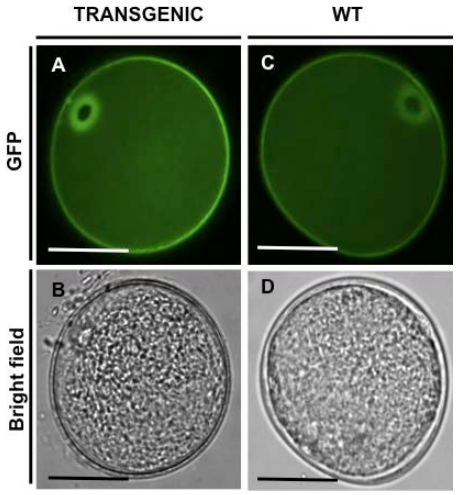

Figure 6.7. GFP emission of barley pollen. **A**: representative image of the autofluorescence of wild type (WT) pollen. **B**: bright field of A. **C**: representative image of the GFP emission from transgenic barley pollen transformed with BpS1GFP. **D**: bright field of C. Fluorescence images were taken using the FITC filter: excitation 492 nm, emission 519 nm. Scale bar = 20 µm.

Although *Arabidopsis* "wild type" pollen grains exhibit a negligible emission, *Arabidopsis* transgenic pollen expressing PrpS-GFP exhibited a noticeable GFP emission, which allowed discrimination between them (de Graaf et al., 2012). However, the barley pollen grains from transgenic lines seemed to have an obvious signal, however the comparison between pollen from transgenic $pBpS_{1-3}$GFP lines and wild type plants did not reveal a difference robust enough to obtain conclusive data from this approach. Moreover, this potential difference was only observed at 100X magnification. At lower magnification the GFP emission were indistinguishable between pollen from transgenic and wild type plants.

Western blot analyses were used as an alternative approach to confirm the expression of PrpS-GFP in pollen from BpS1GFP and BpS3GFP lines. Protein extraction of pollen from BpS1GFP (n = 8), and BpS3GFP (n = 9) were tested using an anti-GFP antibody. After five western blot experiments, it was impossible to detect a signal that could correspond to PrpS-GFP (data not

shown). Importantly, protein sample from *A. thaliana* expressing PrsS-GFP was used as a positive control to confirm the capacity of the anti-GFP antibody to detect GFP. This control revealed a band corresponding to the size of PrpS-GFP and GFP, ruling out the possibility of a defective antibody or technical issues during the western blot procedure. An additional control included re-probing the membrane with an anti-actin antibody to ensure the correct blotting of total proteins into the membrane. Together, this suggested that the levels of expression of PrpS-GFP in barley were below the detection range of anti-GFP antibody pollen.

Despite the fact that it was not possible to confirm the presence of $PrpS_{1-3}$-GFP protein in pollen from BpS1GFP and BpS3GFP lines, it was decided to carry on with the functional analyses assuming that even though the $PrpS_{1-3}$-GFP expression was low, it might still be sufficient to obtain evidence of functional SI.

6.2.2.1.2 Pollen viability and *in vitro* germination

Before commencing with the evaluation of putative functional SI, it was important to assess the viability of barley pollen after collection from the anther. This would reveal the length of time that pollen is viable, which is important for the interpretation of the results from the functional analyses. This is relevant because the life span of pollen from the grasses family is notoriously short. For example, in rice and switchgrass pollen viability decreases below 10% after 40 - 60 min released from the anther (Ge et al., 2011, Khatun and Flower, 1995).

There are several methods to stain pollen to assess its viability. Here, we evaluated the viability of barley pollen using: 1) Evans Blue, which is excluded

by living cells, and therefore stains dead cells blue (Shigaki and Bhattacharyya, 1999), and 2) Fluorescein Diacetate (FDA), which becomes fluorescent (green emission) when the dye is taken up and cleaved by a metabolically active cell (Breeuwer et al., 1995). A sample of pollen stained with Evans Blue showed virtually black cells, clearly indicating dead cells (**Figure 6.8.A**). At higher magnification, the differences became more obvious for the darker cells. However, there was a range of “grey” cells where the discrimination between dead and live cells was not obvious (**Figure 6.8.B**). Pollen grains stained with FDA exhibited a noticeable fluorescence in the live cells. Comparisons between the bright field (**Figure 6.8.C**) and fluorescence (**Figure 6.8.D**) images resulted in an evident difference between live pollen grains exhibiting fluorescence signal, and the dead pollen with no fluorescence. Despite that barley pollen had autofluorescence for GFP (**Figure 6.7**), the fluorescence emission after FDA staining was noticeably stronger.

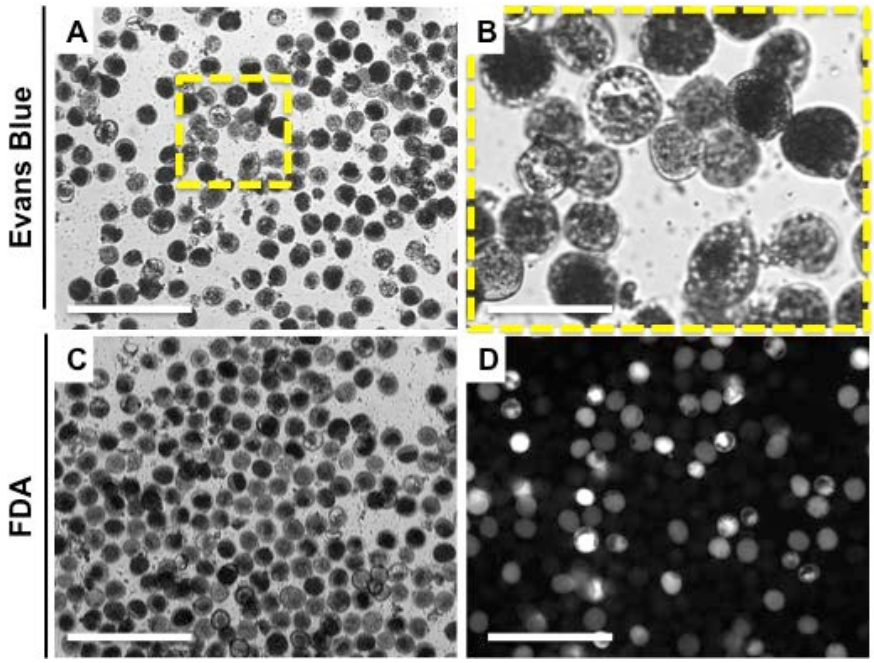

Figure 6.8. **Comparison of barley pollen viability assay using Evans Blue and Fluorescein diacetate (FDA) dyes**. **A**: Bright field of BsS1GFP pollen sample stained with Evans Blue. **B**: Magnification of the highlighted yellow square detailed in A. **C**: Bright field of BsS1GFP pollen sample stained with FDA. **D**: Fluorescence emission of BsS1 sample dyed with FDA. Fluorescence images were taken using the FITC filter: excitation 492 nm, emission 519 nm. Scale bar in A, C and D = 250 µm. In B = 100 µm.

Having established the procedure to assess the pollen viability, it was possible to quantify the viability of the pollen after collection from the anther. **Figure 6.9** shows a very rapid decrease in pollen viability within 30 min from 77% until 33% reaching levels of only 10% 1.5 h after collection. This level of 10% in the viability remained constant during measurements carried out up to 4 hours after collection (n = 3) using independent BpS1GFP lines.

.

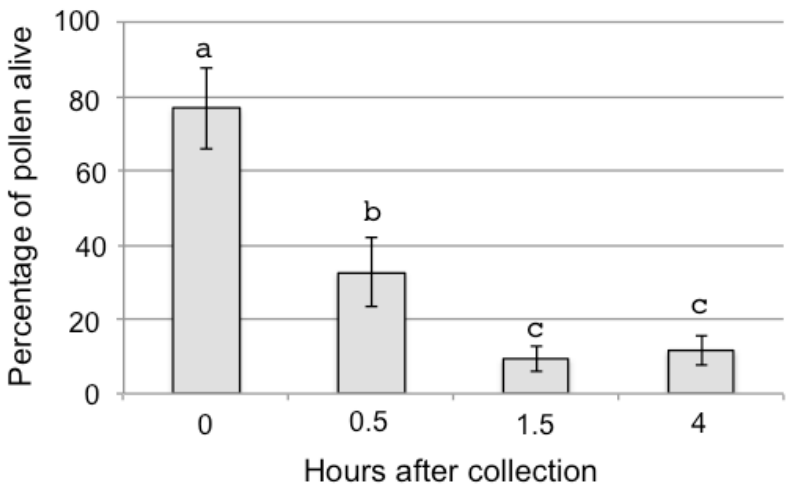

Figure 6.9 Viability of the barley pollen after collection. Viability was assesses by FDA staining Values represent the mean of the collection from three independents pBpS1 plants**.** 100 pollen grains were counted for each time point**.** Different letters above the bars indicate significant difference after one-way ANOVA ($p<0.05$).

This result indicated that the viability of barley pollen dramatically decreased once the pollen was released from the anther. This also compromised the possibility of design and carry out experiments using barley pollen *in vitro.*

In parallel with the viability assays, attempts to optimise the germination *in vitro* of barley pollen were carried out. This procedure represents a major challenge and, even though it is possible, it is a protocol that has not been optimised. As shown previously, the viability of barley pollen is very quickly reduced and also it has been reported to be cultivar-dependant, (Parzies et al., 2005), which makes likely that any recipe for germination would be restricted to a particular cultivar. We attempted to optimise a protocol for the germination *in vitro* of barley Golden Promise, following the guidance from Dr Wendy Harwood (JIC) and Dr Katsuyuki Kakeda (Mie University, Japan) both with an extensive experience in cereals reproduction. Two different germination media were tested. Moreover for each media several conditions such as temperature, time of hydration, pollen from transgenic and wild type plants, and pollen collected

from anthers at different developmental stages, were evaluated (Chapter 2, section 2.5.4.1). In total, pollen collected from 20 independent plants was evaluated. Pollen samples from the eight transgenic pBpSGFP lines (**Table 6.4**), and also from non non-transgenic barley plants were collected. Representative images are shown in **Figure 6.10**. Although pollen germination was obtained, the germination, if any, was normally exhibited for a minority of the pollen grains of the sample. Moreover the few pollen tubes that developed, exhibited a reduced length (**Figure 6.10.A)**. The ideal scenario, including germination in most of the pollen grains as well as development of long pollen tubes was obtained only in two experiments (**Figure 6.10.B** and **6.10.C**).

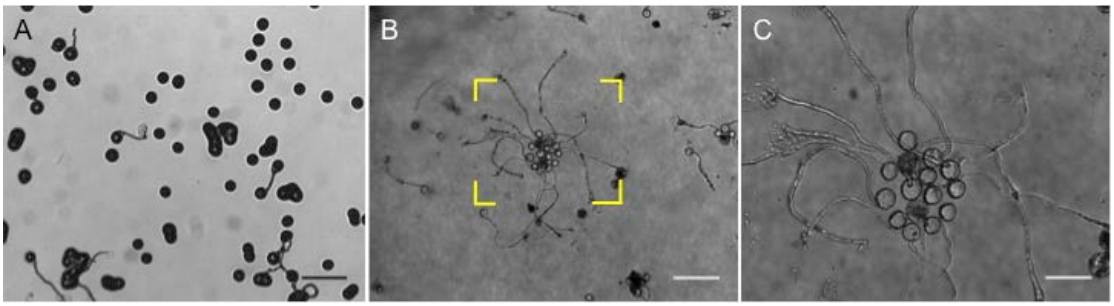

Figure 6.10 Germination on barley pollen *in vitro.* A: Representative image of a barley pollen sample exhibiting germination in a small population of pollen grains *in vitro*. **B**: Ideal situation where most of the pollen grains exhibited germination and long pollen tubes .**C**: Magnification of the yellow square indicated in B. Scale bar: A and B = 250 µm. C = 100 µm.

Barley pollen germination *in vitro* is a procedure that has not been established. Some studies have been carried out using *Hordeum bulbosum* pollen (Chakrabarti et al., 1976), Kakeda (unpublished data), but to our knowledge, there are no examples of pollen germination of *Hordeum vulgare* (Golden Promise). The media tested here were based on those developed for *Hordeum bulbosum*, which despite being related to barley is a different species. Since

pollen tubes were not essential for our experiments, the evaluation of further growth media was not carried out. Developing a new medium suitable for the barley Golden Promise represented a time consuming challenge, as major changes in the composition and concentration of components used were probably required. The other variable that was not possible to evaluate during this thesis was whether pollen from barley plants growing in the field, instead of in a glasshouse, exhibited a better response for germination and viability *in vitro*. Pollen from barley plants growing in a field is generally better quality, and therefore it may be more suitable for studies *in vitro* (Kakeda, personal communication). Unfortunately, we did not have the facilities to have a field growing transgenic barley plants.

Despite a lack of protocol for barley pollen germination *in vitro*, it was decided to continue the functional analysis assessing alterations in the actin configuration during SI. Investigation of the actin alterations during SI carried out in *A. thaliana*, were done using pollen grains so growth was not important for this investigation (de Graaf et al., 2012). Also because alterations in actin have been reported as an early event of the *Papaver* SI response, it was therefore still possible to potentially trigger actin alterations before the pollen death and observe a difference between pollen untreated and exposed to incompatible PrsS. Additionally, at this point a protocol to stain actin cytoskeleton in barley pollen had been developed, and promising data had been obtained regarding actin alterations after pH modifications in a similar fashion to the *Papaver* SI response (Chapter 1, section 1.4.6.2.6 and 1.4.6.2.8). Therefore, functional analyses monitoring the pollen actin cytoskeleton were carried out.

6.2.2.1.3 *In vitro* functional analysis of pollen from transgenic BpS1GFP and BpS3GFP barley lines.

Monitoring and imaging of the F-actin cytoskeleton changes is a key analytical tool used to assess the SI response in *Papaver* pollen. It has been described that during the *Papaver* SI response F-actin depolymerisation is stimulated, followed by the accumulation of punctate F-actin foci (Geitmann et al., 2000, Snowman et al., 2002, Poulter et al., 2010) (Chapter 1 section 1.4.6.2.6). These studies were based on the use of Rhodamine-phalloidin (Rh-ph) for staining and visualisation of the F-actin cytoskeleton in *Papaver* pollen. Thus, we aimed to use a similar experimental design to evaluate whether actin alterations were triggered in pollen from BpS1GFP and BpS3GFP exposed to incompatible PrsS. This experiment was carried out in an *in vitro* SI bioassay. Pollen was freshly collected in either liquid or solid growth media and then exposed to recombinant PrsS (Method in Chapter 2 section 2.5.5).

The first challenge was to adapt and develop a protocol to stain the F-actin in barley pollen. Our initial attempts included different permeabilisation reagents such as NP-40 and TRITONX-100 at different exposure times (1 h and 2 h) and concentrations (0.1, 0.5 and 1% v/v). In total six independent replicates for each condition and at least 30 pollen grains were examined for each time point. Even though sometimes filaments were clearly or partially observed in 20% or 30% of the grains, in most of the cases it was not possible to visualise actin filaments. However, since we were able to visualise F-actin in a few pollen grains, we concluded that the dye was suitable to stain the F-actin in barley, and the problem was probably associated with the impediment of the Rd-ph to entry into

the pollen to reach the F-actin. As the pollen coat might prevent permeabilisation of the dye to obtain F-actin staining, we attempted to dissolve or remove the pollen coat previous to carry out the actin staining protocol.

6.2.2.1.4 Development of a protocol for the staining of actin cytoskeleton in barley pollen

First, experiments were designed based on protoplasts protocols, which included treatments of pollen with a mix of macerozyme/cellulose intending to dissolve the pollen coat (n = 5). Different ratios of macerozyme and cellulose as well as time of incubation were tested but the results did not improve, and the visualisation of F-actin was still in less than 30% of the pollen grains (data not shown). We then attempted to remove the pollen coat. This included treatments with cyclohexane as described in Doughty and collaborators (1993). After this treatment pollen coat was successfully separated from the pollen grain (Doughty et al., 1993). **Figure 6.11** shows representative images of the pollen grain and the pollen coat after treatment with cyclohexane, and its comparison with untreated pollen. This experiment was carried out in duplicate and at least 30 pollen grains were assessed in each replicate. Bright field inspection using the microscope revealed that the pollen coat had been removed (**Figure 6.11.H**), whereas pollen grains exhibited a spherical shape (**Figure 6.11.G**). Comparisons between **Figures 6.11.A** - **C** demonstrated that red autofluorescence emission of the pollen after collection (**Figure 6.11.C**) was due to the pollen coat (**Figure 6.11.B**), as pollen grain without pollen coat did not exhibit fluorescence emission (**Figure 6.11.A**). Green fluorescence

emission, was present in pollen grain after pollen coat removal (**Figure 6.11.D**), and pollen coat (**Figure 6.11.E**). Pollen grains collected from the anther exhibited green autofluorescence (**Figure 6.11.F**). **Figure 6 G - I** shows the bright field of the pollen analysed.

These experiments showed that cyclohexane treatments successfully removed the pollen coat form the pollen grain. Moreover, the structural integrity of the pollen grain remained unaltered based on the fact that the pollen grains retain their spherical shape. Additionally, the pollen coat removal also helped with the imaging of the F-actin by removing the red background emission. Red autofluorescence would have interfered during the F-actin visualisation, as the F-actin stained with Rd-ph, has emission visible using the TRITC filter (red emission). Unfortunately, pollen grains still exhibited green autofluorescence after coat removal. Elimination of GFP background emission would have contributed to the screening of the homozygous BpS1GFP and BpS3GFP lines.

So, this procedure allowed us to carry on with the F-actin staining using pollen grains without pollen coat and evaluate whether the pollen coat was preventing the dye from reaching the F-actin.

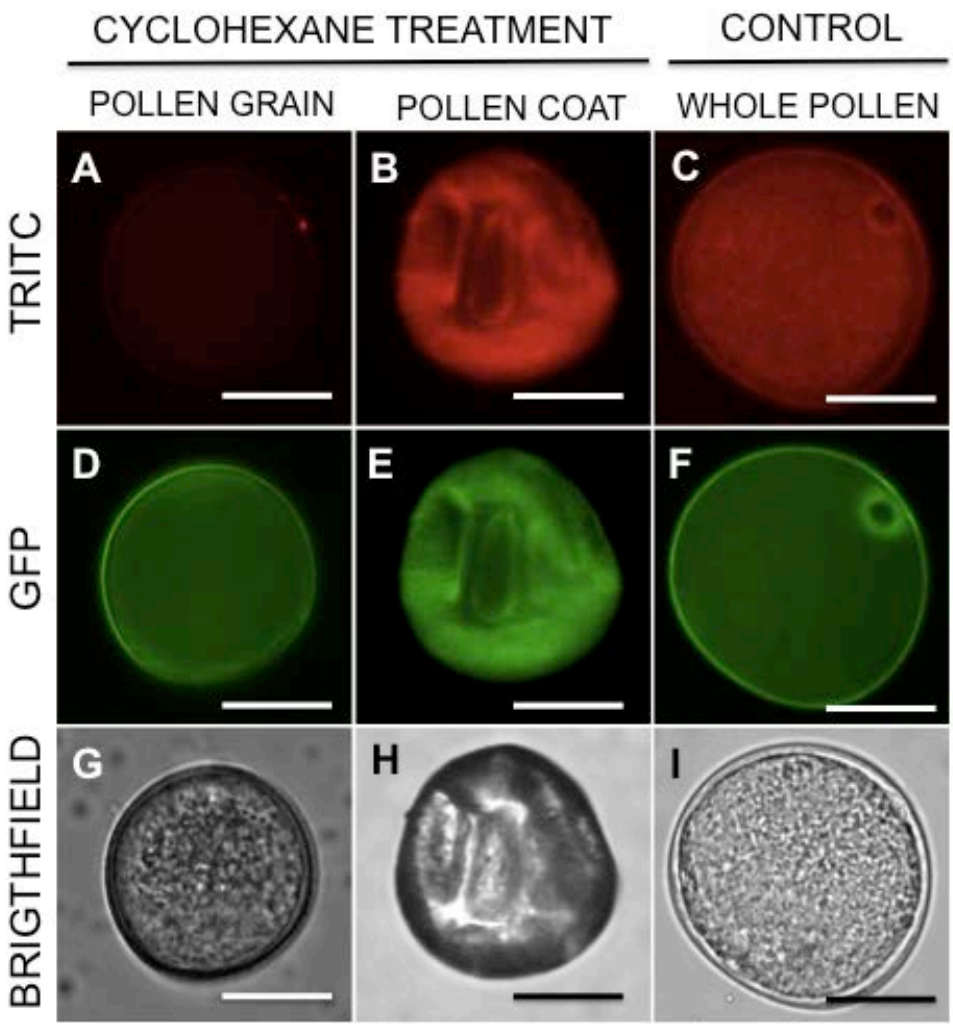

Figure 6.11. Cyclohexane treatment for barley pollen to separate the pollen coat from the pollen grain. Whole pollen (pollen grain protected by the pollen coat) has red (**C**) and green (**F**) autofluorescence. Similarly, pollen coat has red (**B**) and green (**E**) autofluorescence. Uncovered pollen grain has green autofluorescence (**D**), but not red autofluorescence (**A**). Panels **G**, **H** and **I** shows she bright field corresponding to the structures imaged in A-F. Green fluorescence images were obtained using the FITC filters: excitation 492 nm, emission 519 nm. Red fluorescence images were obtained using the TRITC filters: excitation 550 nm, emission 580 nm. Scale bar = 25 μm.

6.2.2.1.5 Effect of pH on actin configuration in barley pollen *in vitro*

As mentioned earlier (Chapter 1, section 1.4.6.2.8) artificial cytosolic acidification using propionic acid (PPA) triggers actin foci formation mimicking the natural SI response in *Papaver* (Wilkins et al., 2015). Preliminary experiments to standardise the F-actin staining protocol in barley pollen, used

PPA to mimic SI conditions, as it was simpler than performing SI experiments. This additionally helped us to explore whether similar responses to the ones described in poppy are present in barley. pH alterations were artificially generated in barley pollen treated with PPA pH 5.5 mimicking SI, and with PPA pH 7 as a control of normal physiological conditions.

Interestingly, the results showed that barley pollen exhibited actin alterations after cytosolic acidification. Moreover, these alterations were remarkably similar to the F-actin foci previously described in *Papaver* pollen and *Arabidopsis.* **Figure 6.12.A** shows representative images of the three different F-actin configurations that were used to assess the F-actin alterations: 1) NORMAL, barley pollen grains exposed to pH 7 exhibiting prominent F-actin bundles, which were organised in a mesh-like arrangement (**Figure 6.12.A.1)**, 2) FOCI, pollen grains exposed to pH 5.5 displaying predominantly a speckle pattern, generating a punctuate foci arrangement (**Figure 6.12.A.2**), and 3) INTERMEDIATE, exhibiting a mix of F-actin with less prominent bundles and also with bright speckles (**Figure 6.12.A.3**). Remarkably, the "FOCI" configuration was strikingly similar in comparison with the F-actin foci described in *Papaver* during the SI response (see Chapter 1 section 1.4.6.2.6).

Quantification revealed that under normal physiological pH 7, out of 50 pollen grains, more than 30 presented normal actin filaments (60%) whereas on average 5 pollen grains (10%) showed F-actin foci. In contrast, in pH 5.5, normal, intermediate and foci had the same frequency (n = 17). Therefore, a decrease in pH from 7 to 5.5 significantly reduced the occurrence of normal filaments by around 50% and significantly increases actin foci occurrence by around 20% ($p<0.01$) (**Figure 6.12.B**). This experiment was carried out with

pollen from three independents BsS1 lines, and 50 pollen grains were counted for each treatment.

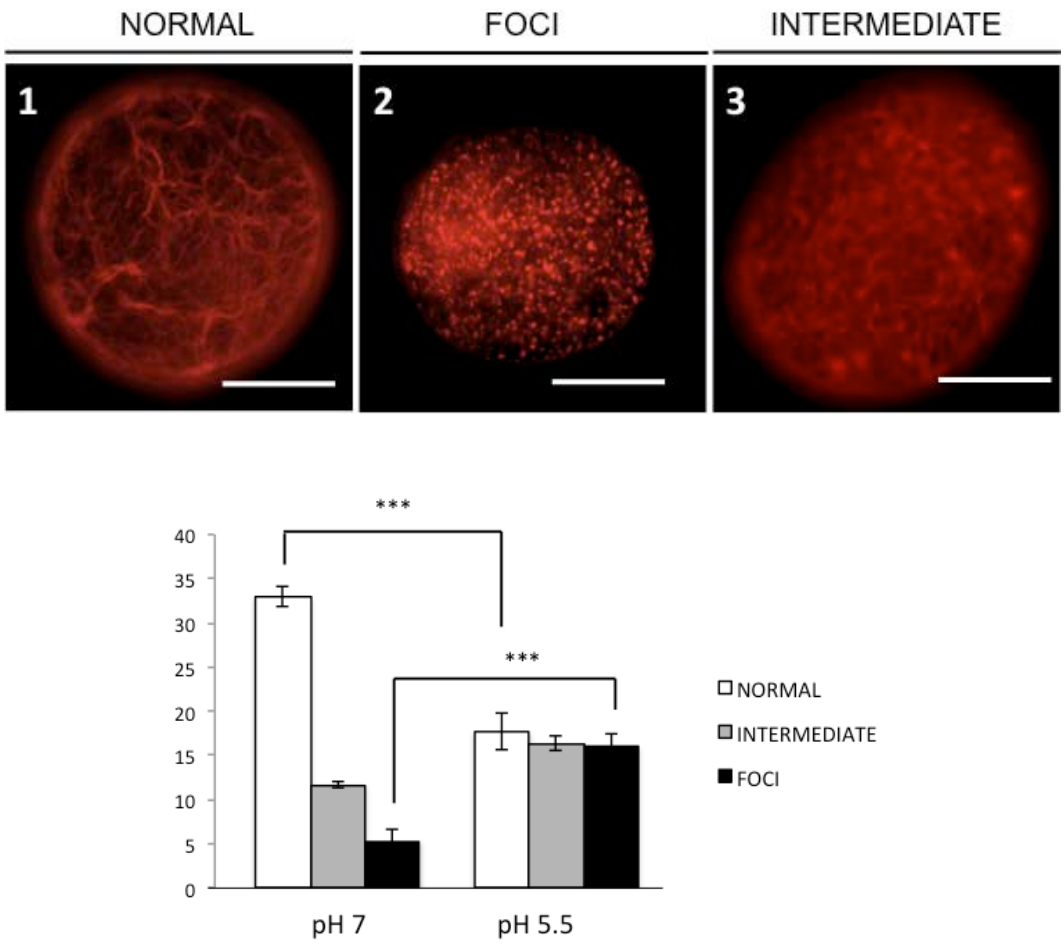

Figure 6.12. **pH effect upon actin organisation in barley pollen. A**: Three configuration of actin cytoskeleton; A.1: normal, A.2: intermediate, and A.3: foci Scale bar: 15 µm. **B**: Quantification of actin alterations at different pH values. This experiment was carried out in triplicate. Each time 50 pollen grains were counted per treatment. Error bars are SEM. One-way ANOVA, with a Tukey HSD test.

These results represented promising data because inducing actin alterations in response to pH acidification indicated that it was feasible to obtain a response similar to the *Papaver* SI response in barley. Additionally, this experiment validated the experimental design of using Rhodamine phalloidin to monitor the F-actin configuration of barley pollen using the optimised protocol developed (section 6.2.2.1.4), which used pollen coat removal.

Based on this data, it was assumed that this method was suitable to assess the actin configuration of transgenic barley pollen expressing PrpS after treatment with recombinant PrsS in an *in vitro* SI bioassay.

6.2.2.1.6 *In vitro* SI Bioassay for transgenic barley pollen expressing PrpS, BpS1GFP and BpS3GFP lines.

To evaluate whether transgenic barley pollen expressing PrpS exhibited some of the distinctive features of SI response such as actin foci, an *in vitro* bioassay was adapted based on the protocol developed for *Papaver* and *Arabidopsis* (see Chapter 2 section 2.5.5). Briefly, barley pollen from BpS1GFP and BpS3GFP lines (expressing PrpS) was collected by submerging anthers with mature pollen, into germination media in a microfuge tube. Then, pollen was transferred to a new tube and exposed to recombinant incompatible PrsS for 3 hours before carrying out the F-actin staining protocol (see Chapter 2, section 2.5.5.1)

Figure 6.13.A shows representative images of F-actin configurations in *Arabidopsis* during the *in vitro* SI bioassay (de Graaf et al., 2012). Untreated pollen grains exhibited F-actin arranged in bundles (**Figure 6.13.A.1**), whereas pollen expressing PrpS and exposed to incompatible PrsS exhibited F-actin foci (**Figure 6.13.A.2**), very similar to the F-actin foci described during the SI response in *Papaver* (Chapter 1, section 1.4.6.2.6).

Figure 6.13.B shows representative images of transgenic barley pollen during the *in vitro* SI bioassay. Based in the categories to classify the F-actin configuration of barley pollen grains described in the previous section

(6.2.2.1.5), F-actin was assessed and classified as NORMAL (**Figure 6.13.B.1**), INTERMEDIATE and FOCI (**Figure 6.13.B.2**).

Quantification of the number of pollen grains exhibiting the different acting arrangement did not reveal the expected results (**Figure 6.13.C**). Regardless of the test condition (incompatible, compatible or untreated) the majority of the pollen grains (between 44% and 66% average) showed F-actin in a normal arrangement. The intermediate category was relatively constant with an average around 30% grains for all the treatment. An average of 6 cells showed F-actin foci arrangement, after the incompatible combination of pollen from BpS1GFP was exposed to $PrsS_1$. This was very similar to the values obtained for the controls including BpS1GFP pollen exposed to compatible PrsS3, and pollen from pBpS1 and pBpS3 exposed to growth media only (untreated). The other incompatible combination BpS3GFP pollen exposed to $PrsS_3$ revealed a higher number of grains exhibiting foci (mean = 28%). This initially seemed a promising result. However similar values were also obtained for the controls of BpS3GFP pollen exposed to compatible $PrsS_1$, and pollen from wild type plants exposed to $PrsS_1$, suggesting that the increase in actin foci was probably due the experimental procedure rather than an actual SI-like response.

However, it should be remembered that these barley lines were not genotyped as homozygous or heterozygous. Therefore, if all the lines were heterozygous, a response was expected in at least half of the pollen grains. But if some the lines were homozygous, a more dramatic difference was expected between SI and the control treatments.

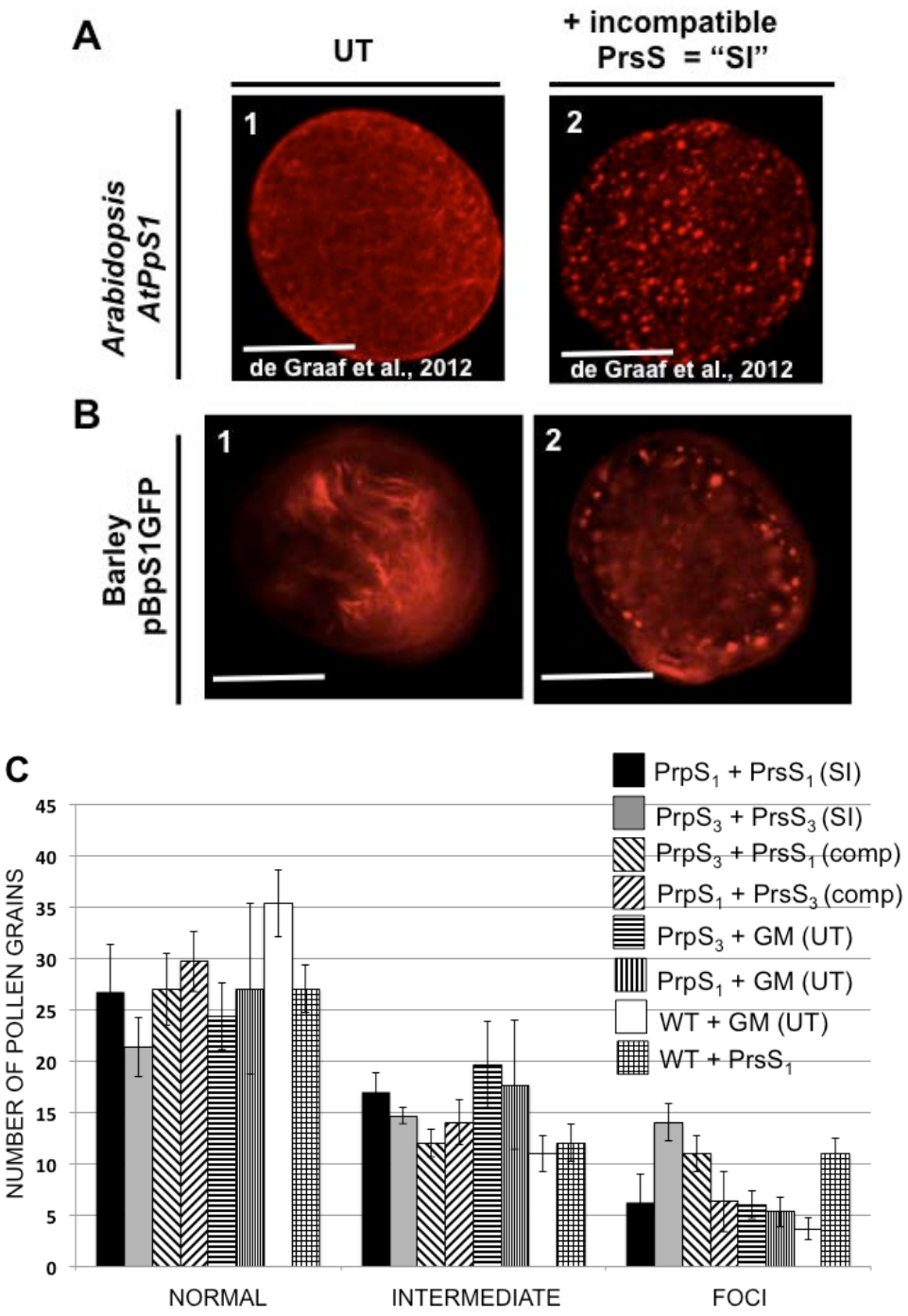

Figure 5.13. SI bioassay of transgenic barley pollen. A.1: *Arabidopsis* pollen grain untreated, normal F-actin. **A.2**: Actin foci of *Arabidopsis* pollen grain after SI treatment (de Graaf et al., 2012) Scale bar in A: 25 µm. . **B.1**: Representative image of F-actin configuration of barley pollen grain classified as "normal"**. B.2**: F- actin arrangement of barley pollen classified as "foci". Scale bar in B: 12 µm **C**: Quantification of the F-actin configuration under different treatments. Experiments were carried out in triplicates from three independent barley lines, and 50 pollen grains were counted for each condition.

Contrasting with the actin changes in the experiments obtained after pH acidification, in the SI bioassay pollen from BpS1GFP and BpS3GFP did not reveal an increase in the number of pollen grains exhibiting F-actin foci after challenge with incompatible PrsS in comparison with the controls. For all the combinations (regardless if they were compatible or incompatible), 50% of the pollen grains had normal F-actin filaments, and between 10 and 20 % displayed alterations resembling the F-actin foci described in during the *Papaver* SI response.

These data suggest that PrpS is not functional in barley. However, as also mentioned previously, the viability of barley pollen *in vitro* was extremely low. So it is possible that the lack of alterations could be due to the rapid death of the pollen *in vitro*. Therefore, it was decided to investigate using pollinations semi-*in-vivo* and *in vivo* to compare pollen tube growth in the stigma or the number of seed-set after incompatible or compatible combinations compared with pollinations using non-transfected plants.

6.2.2.2 Analysis of stigmas from barley lines transformed with *UBI*::*PrsS*$_1$, BsS1

In this section, we present the functional analysis of BsS1, using *in vitro* compatible and incompatible pollinations of transgenic barley lines. The barley lines used were those transformed with $PrsS_1$ driven by the ubiquitin promoter, termed BsS1 was previously detailed (section 6.2.1.1). It was expected that pollinations between stigmas from BsS1 plants and pollen from BpS1GFP (i.e. an incompatible combination of PrsS-PrsS) would exhibit alterations involving

inhibited pollen tube growth and a reduced number of seed-set. For compatible crosses between stigmas of BsS1 lines and pollen from BpS3GFP lines, it was expected to obtain a good pollen tube growth and a high number of seed-set, similar to the pollination using wild type plants.

Thus, compatible and incompatible pollinations represented a convenient approach to evaluate the functionality of both PrpS and PrsS in barley pollen.

A scheme with the expected compatible and incompatible crosses is shown in **Figure 6.14**. Incompatible crosses were expected when stigmas from BsS1 lines were pollinated with pollen from BpS1GFP lines, as stigmas expressing $PrsS_1$ should reject pollen expressing the cognate $PrpS_1$. Compatible crosses were expected when stigmas from BsS1 lines were pollinated with pollen from BpS3GFP, as stigmas expressing $PrsS_1$ should accept pollen expressing a different allelic combination such as $PrpS_3$. Similarly, compatible crosses were expected for stigmas from BpS3GFP lines pollinated with pollen from BpS1GFP lines. Moreover, compatible crosses were expected after self-pollinations, thus, stigmas from BsS1 lines should be successfully pollinated with pollen from BsS1 lines, as pollen from BsS1 lines are not expressing any PrpS. Moreover, crosses between non-transgenic plants were used for developing this experimental design and also to provided a reference for compatible crosses.

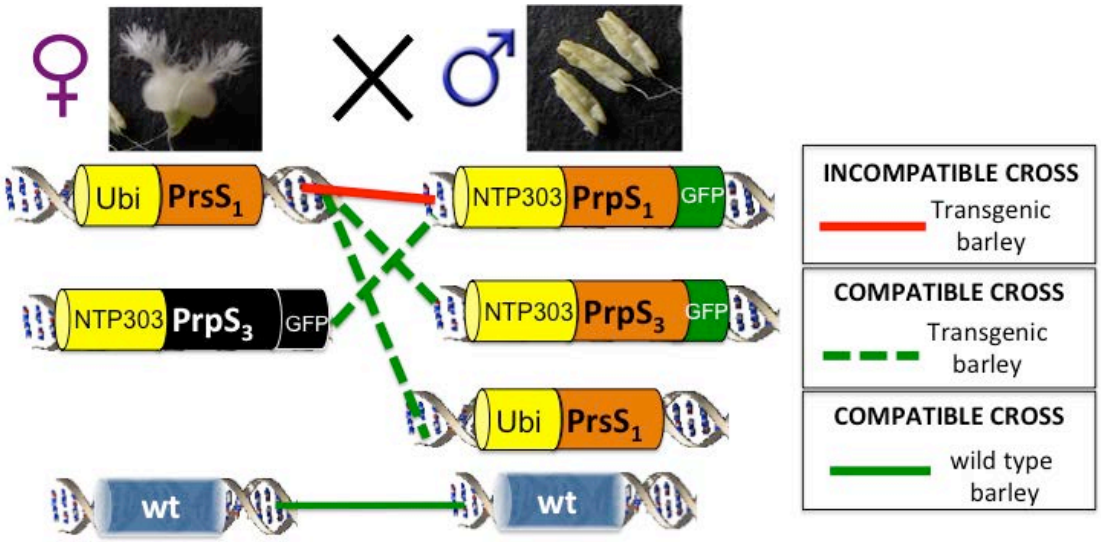

Figure 6.14 Scheme representing the expected compatible and incompatible combination between crosses of the transgenic barley. The incompatible cross was between stigmas from BsS1 lines (transformed with Ubi::$PrsS_1$) and pollen from BpS1GFP lines (transformed with NTP303::$PrpS_1$-GFP). Stigmas from BsS1 lines were compatible with pollen BpS3GFP (transformed with NTP303::$PrpS_3$-GFP) and BsS1. An additional compatible control was the cross between stigmas from BpS3GFP and pollen from BpS1GFP. PrpS or PrsS in an orange box represent that expression was expected in the organ used for the cross (stigma or pollen considering the promoter), and in a black box represent that the expression was not expected in that tissue. As a control, crosses between wild type plants were used. Incompatible crosses are outlined in a red line. Compatible crosses between transgenic plants are outlined with dashed green line. Compatible cross between wilt type (wt) plants is outlines in solid green line.

6.2.2.2.1 Development of a semi-*in-vivo* functional analysis of barley lines transformed with *Papaver S*-determinants.

We decided to perform *semi-in-vivo* pollinations, assessing the pollen tube growth on stigmas from barley lines transformed with *UBI*::*$PrsS_1$* (BsS1). For this, excised stigmas were placed on a petri dish on a layer of solid barley growth media (**Figure 6.15.C-D**), pollinated with freshly collected pollen from incompatible BpS1GFP and compatible BpS3GFP barley lines. Due to the similarities between maize and barley, we looked at studies using maize as a

grass model for pollen tube growth and guidance (Dresselhaus et al., 2011), as a reference to develop a semi-*in-vivo* pollination system in barley. Representative images of the female structures of a barley flower are presented in in **Figure 6.15.A**. A characteristic of grasses is a short style with a feathery stigma. **Figure 6.15.B** shows a detail of a pollen grains attached to stigmatic papilla cells. **Figure 6.15.C** shows the arrangement of 10 stigmas in a 35-mm petri dish ready to be pollinated. **Figure 6.15.D** shows a magnification of the barley stigma highlighted in panel C, with the bottom section immersed in a layer of solid germination media and the stigma ready to receive the pollen.

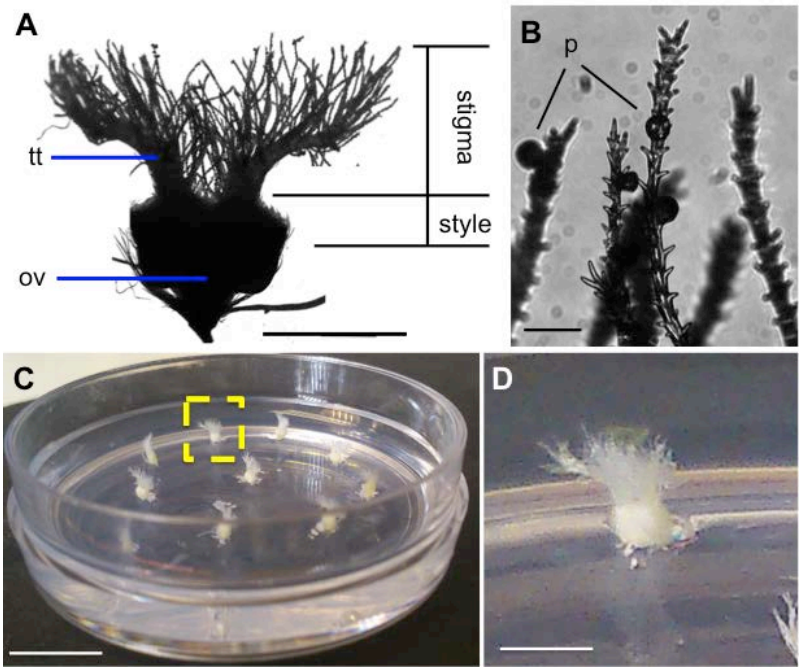

Figure 6.15. Experimental design for *semi-in-vivo* pollinations. A: representative image of the female structures of a flower in barley. Scale bar = 2 mm. **B:** Magnification of two pollen grains (p) attached to papilla cells on barley stigma. Scale bar = 0.12 mm **C:** arrangement of 10 barley stigmas placed in a 35-mm petri dish containing solid germination media Scale bar = 7 mm. **D:** magnification of the stigma highlighted in C. Scale bar = 3 mm Abbreviations: p, pollen; tt, transmitting tract; ov, ovule.

6.2.2.2.2 Semi-*in vivo* compatible and incompatible crosses

The standardisation of semi-*in vivo* pollinations and the establishment of the parameters considered as “normal” in terms of the length and shape of the pollen tube growth were established using stigmas and pollen from non-transgenic barley plants. Based on similar experiments carried out in both *Papaver* and *Arabidopsis*, it was expected that incompatible pollinations, have exhibited shorter pollen tubes and with a more irregular shape (**Figure 6.16.A**), whereas in a compatible pollination, long and straight pollen tubes were expected to be growing through the pistil (**Figure 6.16.B**).

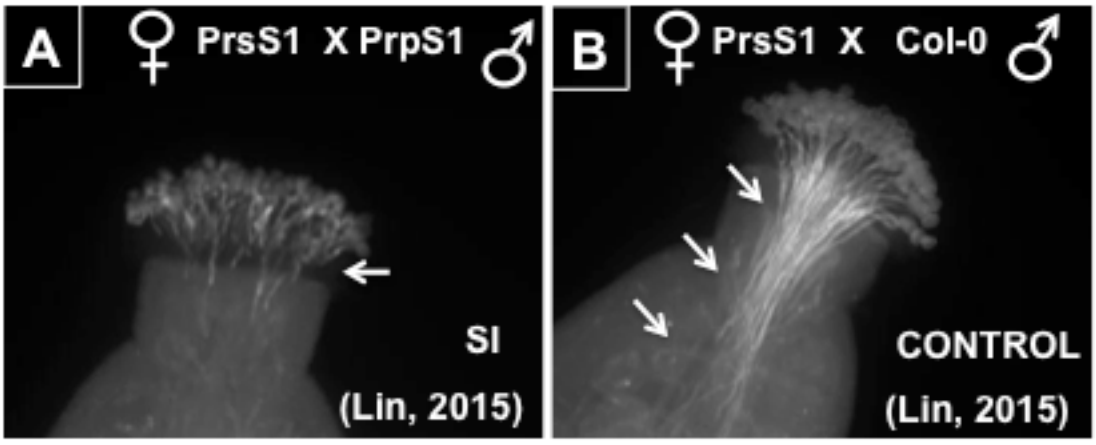

Figure 6.16. **Semi-*in-vivo* pollination using *Arabidopsis thaliana***. **A**: Incompatible pollination exhibiting short pollen tubes. Pollination carried out using stigmas from *Arabidopsis* expressing $PrsS_1$ (At-$PrsS_1$, line K9) pollinated with pollen from *Arabidopsis* expressing the cognate $PrpS_1$ (At-*PrpS1-GFP*, line BG16). **B**: Compatible pollination exhibiting long pollen tubes growing in the pistil. Pollination carried out using stigmas from *Arabidopsis* expressing $PrsS_1$ (At-$PrsS_1$, line K9) pollinated with pollen from non-transgenic *Arabidopsis* col-0. Figure adapted from (Lin, 2015)

Figure 6.17 shows a representative image of a compatible cross between non-transgenic barley lines. 10 different plants were evaluated and 8 stigmas of each plant (n = 80 stigmas in total). The upper panel of **Figure 6.17.A** shows the bright field of a barley stigma. Pollen grains were visible as grey and black

spheres. The papilla cells were tangled among them forming a mesh-like structure, which was generated as the result of the submersion in aniline blue and the subsequent squash with the coverslip for imaging. The papilla cells were mainly distributed in the upper section and towards the edges of the structure, whereas the areas corresponding the style and ovary sections were seen in the central and lower section of the structure. The bottom of this central area exhibited short and thin structures with a hair-like shape, which were tissue debris after the sample preparation. **Figure 6.17.B** shows the imaging of the same stigma using UV illumination for visualisation of the pollen tubes stained with aniline blue. **Figure 6.17.C** shows a magnification of an area corresponding to the mesh conformed by the stigmatic papilla cells and also to the transmitting track. Aniline blue staining revealed a population of long pollen tubes, but also a population of short pollen tubes growing in an irregular shape.

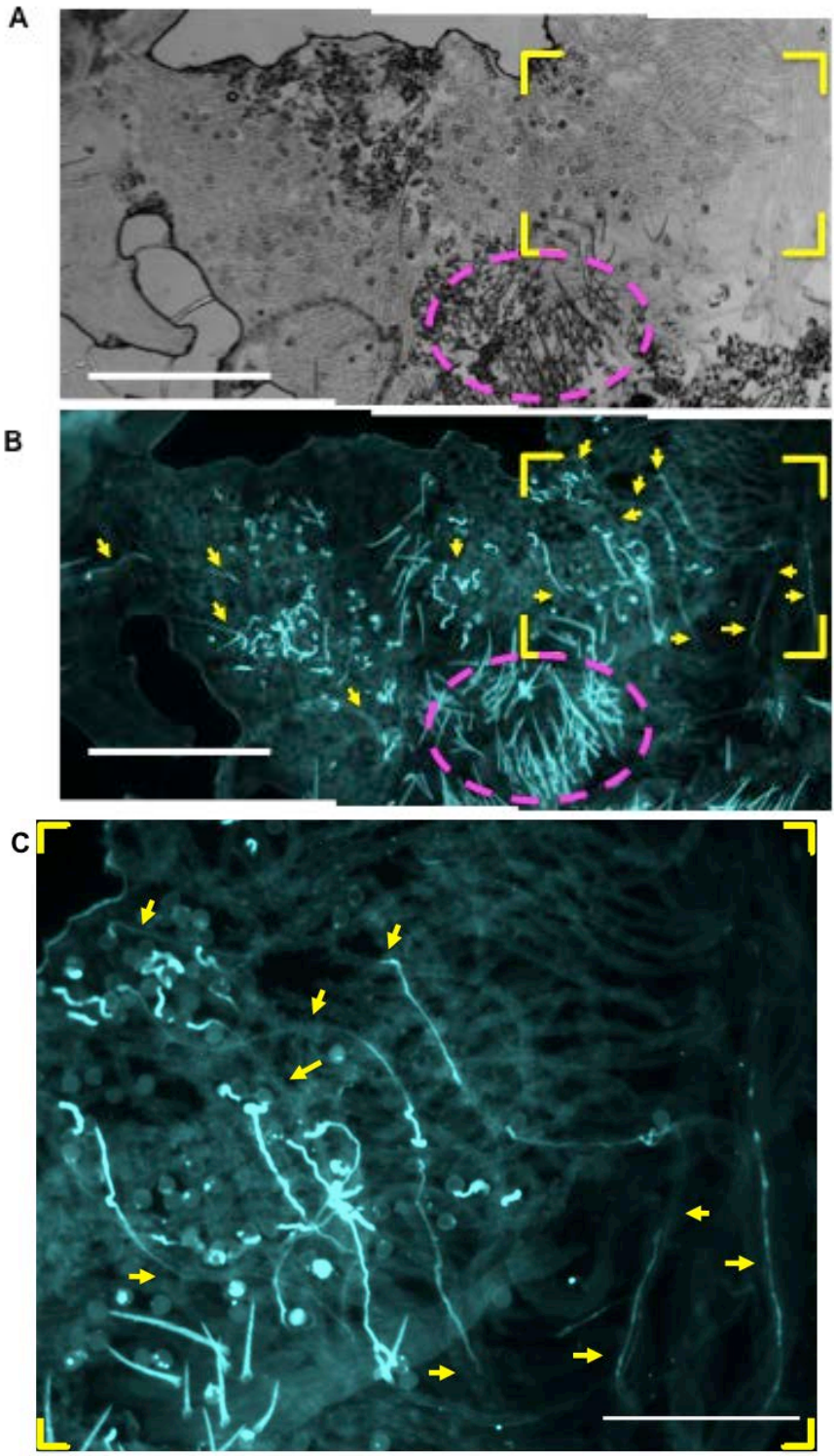

Figure 6.17. Representative images of a semi-*in vivo* pollinations corresponding to compatible crosses between wild type barley lines. A: Bright field of a structure conformed by the stigmatic papilla cells (top area), style (middle-centre area), and ovary (lower area). **B**: Correspond to the same stigma imaged using UV light, revealing pollen tubed stained with aniline blue. The purple circumference indicates part of the area corresponding to the style containing hair-like structures. Scale bar = 0.5 mm. **C:** Magnification of the area highlighted yellow square in panel B**.** Scale bar = 0.25 mm.

Due to the feathery nature of the barley stigma, the preparation of the sample for imaging, (details in Chapter 2 section 2.5.5.3), resulted in the tangled mesh-like arrangement of the stigmatic papilla cells. Additionally, it was found that the staining of the pollen tube could be disrupted along the papilla cells (**Figure 6.18**). **Figure 6.18.A** shows a bright field exhibiting main papilla cell in focus in the middle and a tangled arrangement of papilla cells around. The same field imaged using UV light, revealed the presence of one pollen tube (**Figure 6.18.B**), which in a higher magnification exhibited fading of the staining (**Figure 6.18.C**). This situation was consistently observed in all the pollinated stigmas analysed. This includes 80 stigmas from pollinations using non-transgenic plants and a total of 124 stigmas using transgenic lines.

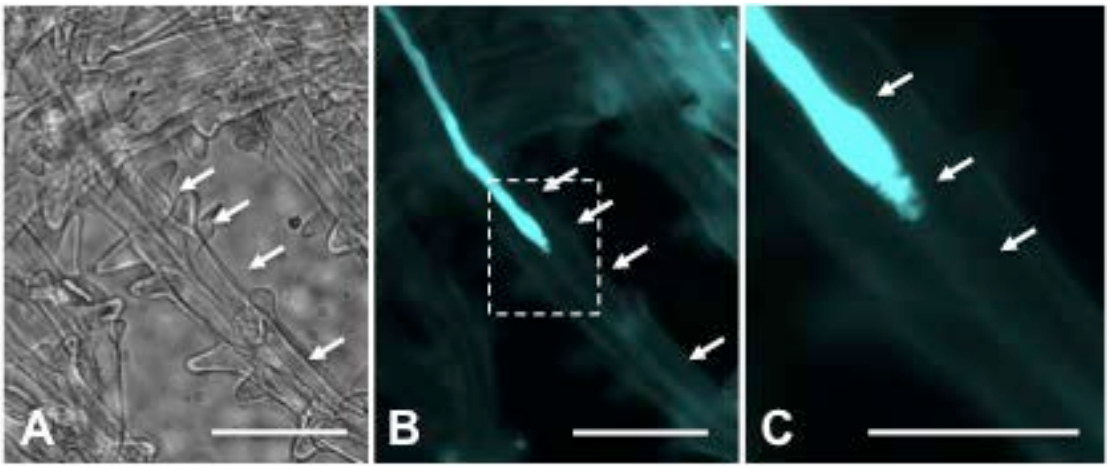

Figure 6.18 Representative images of the fading in the staining of pollen tubes. **A**: Bright field exhibiting a papilla cells in the middle. **B:** Same field described in A, revealing a pollen tube stained with aniline blue after UV illumination. Arrows indicates the section where the pollen tube staining fades. **C**: Magnification of the square section where the fading of the staining is notorious. Scale bar A-B = 100 µm and in C: 200 µm.

Because the identification of the origin and/or the tip of a pollen tube was not clear, it was impossible to trace the route of pollen tubes along the papilla cells.

Therefore, measurements of the pollen tube length were not robust enough to obtain conclusive data. Despite these results, crosses between transgenic barley lines were carried out and presented in the next section, expecting that differences between compatible and incompatible pollen tubes might be evident, despite the technical difficulties described above.

6.2.2.2.3 Evaluation of functional SI in BsS1 and BpS1GFP and BpS3GFP by means of semi-*in vivo* pollinations

Having developed the procedures for semi-*in-vivo* pollinations, compatible and incompatible crosses between lines BsS1, BpS1GFP and BpS3GFP were carried out. It was expected that the incompatible combination of stigmas from BsS1 lines pollinated with pollen from BpS1GFP (i.e. incompatible combination) would exhibit alterations in the pollen tube growth in comparison with all the other combinations, which were compatible (**Figure 6.14**).

Because these barley lines were not genotyped as homozygous or heterozygous it was still possible to obtain long tubes in the incompatible pollination, as the lines could have been heterozygous. So it could potentially look like a half compatible result (i.e. 50% pollen tubed inhibited and 50% growing). Nonetheless, it was still expected that we might observe a difference in comparison with the controls using wild type plant and compatible crosses where all the pollen tubes were expected to grow straight and long through the stigmatic papilla cells.

In order to ensure that any alteration observed was not due to a deficient stigma or pollen used for the crossing, preliminary experiments included the use of

stigmas from two different lines (one compatible and one incompatible) pollinated in parallel with pollen from the same plant. This would check the quality of the pollen used for those pollinations. The second batch of crosses included the use of stigmas from the same plant pollinated in parallel with pollen from two different plants (one compatible and one incompatible). This control would check the maturity of the stigma used for the pollination. Additionally, after the pollination was carried out, the viability of the remaining pollen in the anther was assessed in order to assess the quality of the pollen used for the pollination. It is important to stress that this viability value represents a reference value, as the pollen first released from the anther (used for the pollination) is mature and viable pollen, and the pollen remaining in the anther was not all completely mature. However, even though this was not a measure of the viability of the pollen used for the pollinations, it allowed us to confirm that the anther used for the pollination contained viable pollen.

Figure 6.19 shows a representative image of incompatible crosses using a BsS1 stigma and BpS1GFP pollen. **Figure 6.19.A** shows the bright field of a pollinated stigma. Pollen grains and tangle stigmatic papilla cells were visible in the superior area. In the inferior and central area, the section corresponding to the style exhibited short and thin structures with hair-like shape.

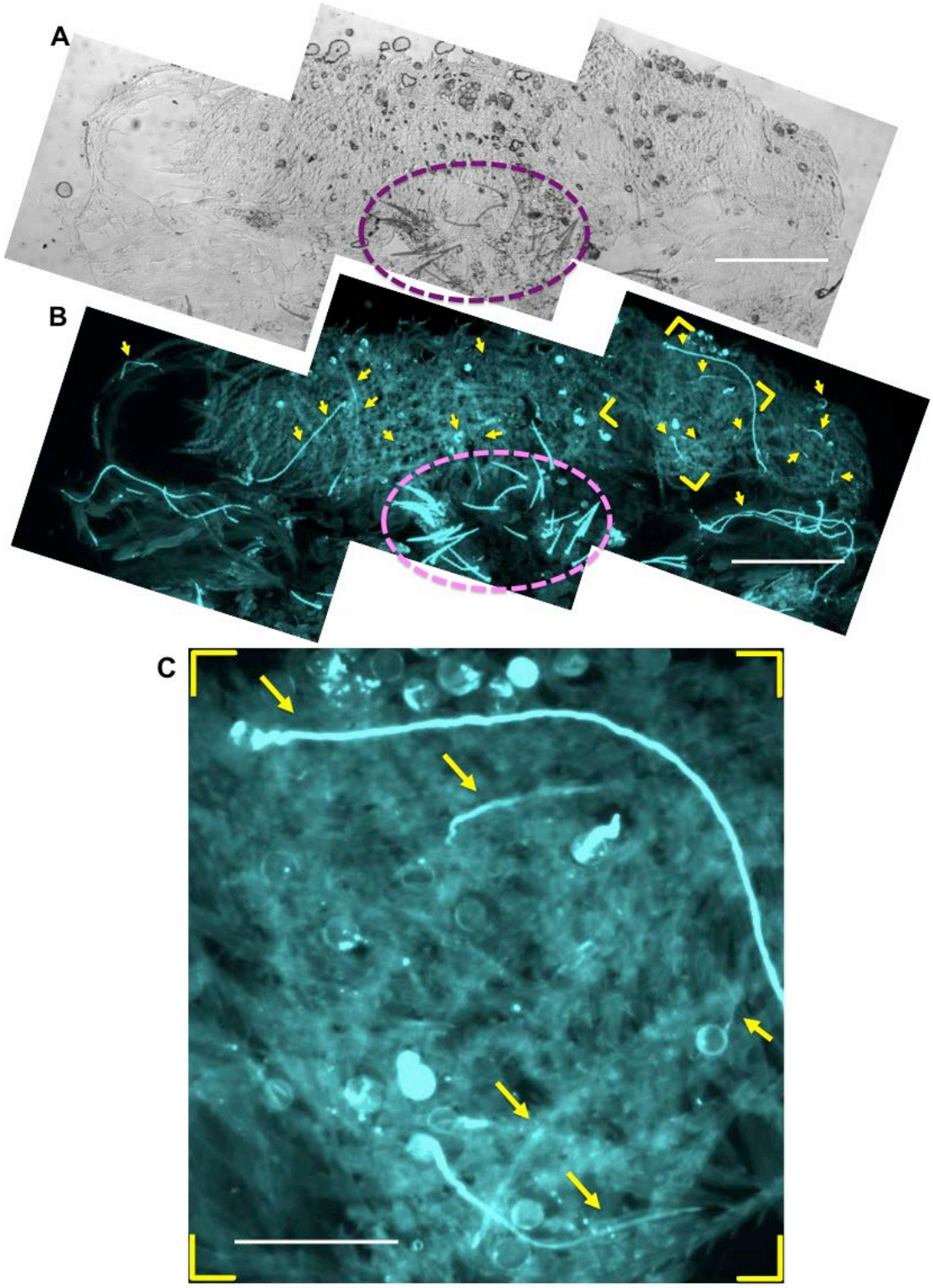

Figure 6.19. **Representative images of a semi-*in-vivo* pollinations corresponding to an incompatible cross. A:** Bright field of a structure conformed by the stigmatic papilla cells (top area), style (middle-centre area), and ovary (lower area). **B**: Correspond to the same stigma imaged using UV light showing the pollen tubes stained with aniline blue. The purple circumference indicates part of the area corresponding to the style containing hair-like structures. n = 13. Scale bar = 0.5 mm. **C:** Magnification of the area highlighted yellow square in panel B. Scale bar = 0.25 mm.

Figure 6.19.B shows the same stigma imaged using UV light. There was a population of pollen grains exhibiting bright staining, and another population of grains, which were was not stained. Also, there was a population of prominent long and bright pollen tubes, and another dim stained population of pollen tubes. **Figure 6.19.C** shows some pollen grains brighter than other pollen tubes at a higher magnification, and shows the mesh-like arrangement of the stigmatic papilla cells.

Figure 6.20 shows a representative image of a compatible pollination carried out in parallel with pollination in **Figure 6.19**, using a BpS3GFP stigma, and pollen from the same BpS1GFP plant (i.e. a compatible combination). **Figure 6.20.A** shows pollen grains and the tangle stigmatic papilla cells previously described. Imaging using florescence is shown in the **Figure 6.20.B.** Again, there was a population of bright stained pollen grains and other pollen grains un-stained. Also, long and smooth as well as uneven pollen tubes were observed. **Figure 6.20.C** shows pollen tubes that were only visible at a higher magnification.

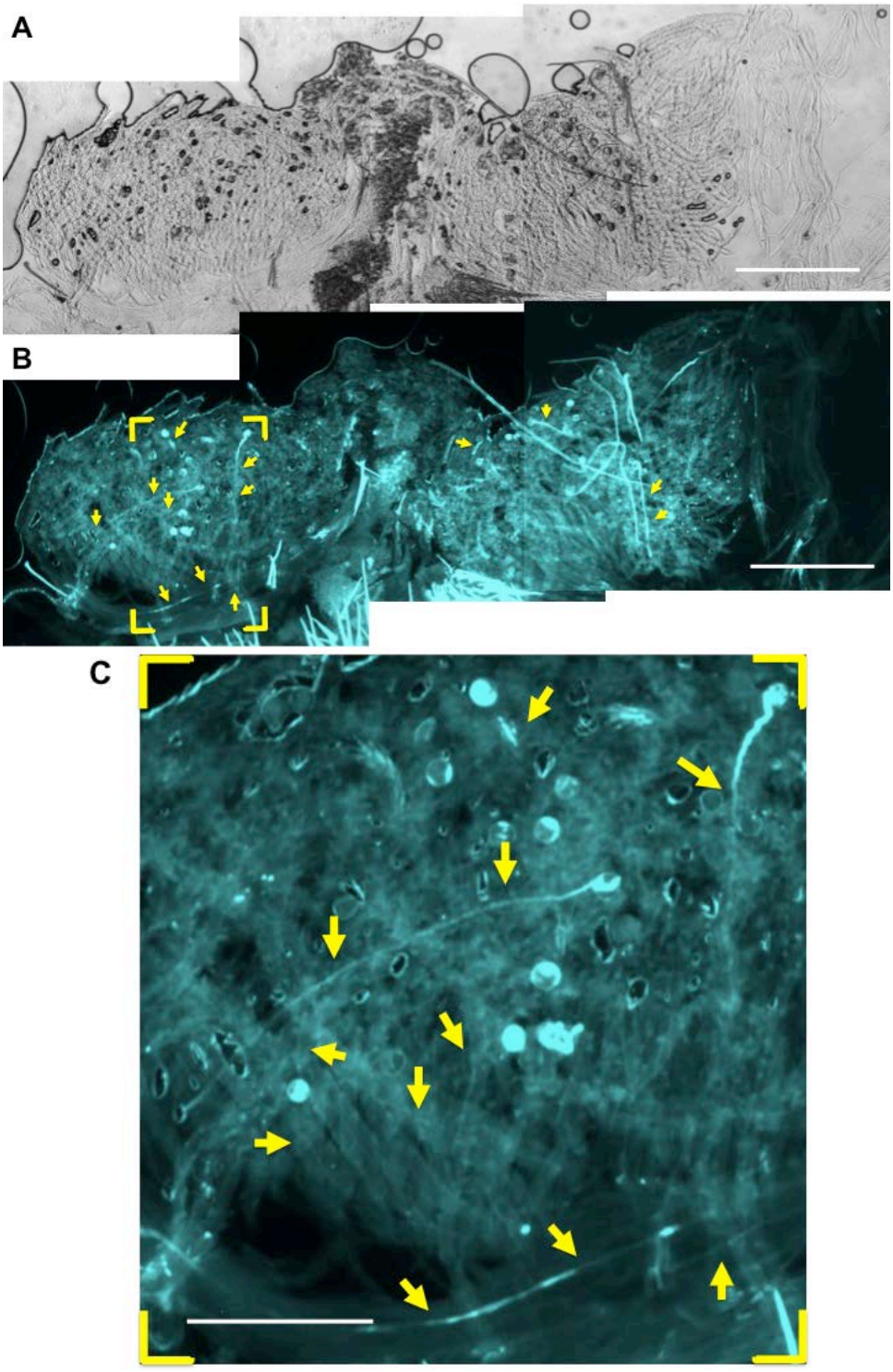

Figure 6.20. Representative images of a semi-*in vivo* pollination corresponding to a compatible cross. A: correspond to a bright field of a structure conformed by the stigmatic papilla cells (top area), style (middle-centre area), and ovary (lower area). **B**: correspond to the same stigma imaged using UV light revealing the pollen tubes stained with aniline blue. n = 10. Scale bar = 0.5 mm. **C:** Magnification of the area highlighted yellow square in panel B**.** The arrows indicate pollen tubes. Scale bar = 0.25 mm.

These experiments using pollen from the same plant to pollinate stigmas from different plants in a compatible and incompatible combination did not exhibit any consistent obvious differences between the compatible and incompatible pollinations. A population of long and short pollen tubes was present in both crosses. Moreover, the tangle arrangement of the stigmatic papilla cells prevented the reliable identification of the origin and the tip of the pollen tubes.

A representative image of the viability assay using FDA of the pollen remaining in the anther after the pollination is shown in **Figure 6.21**. **Figure 6.21.A** shows the bright field showing the pollen grains. **Figure 6.21.B** shows the live pollen emitting fluorescence in green, and **Figure 6.21.C** is the merge of panels A and B, which allows a clear discrimination between the alive and dead pollen grains. The viability estimated for this sample was 29%.

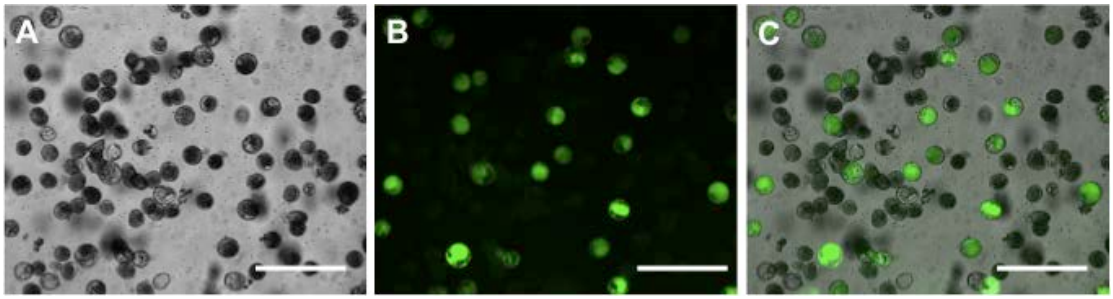

Figure 6.21. **Pollen viability estimated by staining with FDA**. Pollen $PrpS_1$ 28% alive. This assay was carried out with pollen remaining in the anther after have used it for the pollination. This provides a reference for viability; however, this is an underestimated value as the best quality pollen is the firs in fall off the anther. Fluorescence images were taken using the FITC filter: excitation 492 nm, emission 519 nm. Scale bar = 250 µm.

This experiment confirmed that the pollen used for the pollination was alive, and therefore that the anther selected contained mature pollen suitable for pollinations. However, the best quality pollen (i.e. most mature) is the first to be shed from the anther, therefore the real viability of the pollen is undetermined,

as the viability value obtained corresponds to the pollen remaining in the anther after the pollination. Consequently, it is not possible to make associations or conclusions regarding the number of pollen tubes or its length based on the pollen viability assessed, as it is probably an underestimated value compared to the pollen used for the pollinations.

Next, stigmas from the same plant were pollinated in parallel with pollen from different plants in a compatible and incompatible manner to further investigate potential differences between compatible and incompatible pollinations. **Figure 6.22** shows a representative image of an incompatible cross using a BsS1 stigma pollinated with BpS1GFP pollen. **Figure 6.22.A** shows the bright field of a pollinated stigma exhibiting the usual tangle stigmatic papilla cells. **Figure 6.22.B** shows the pollen tubes in this stigma imaged using UV light. **Figure 6.22.C** shows a magnification, which revealed several pollen tubes that were only clear after a detailed observation. Consistently with previous experiments, stigmatic papilla cells also exhibited the mesh-like arrangement.

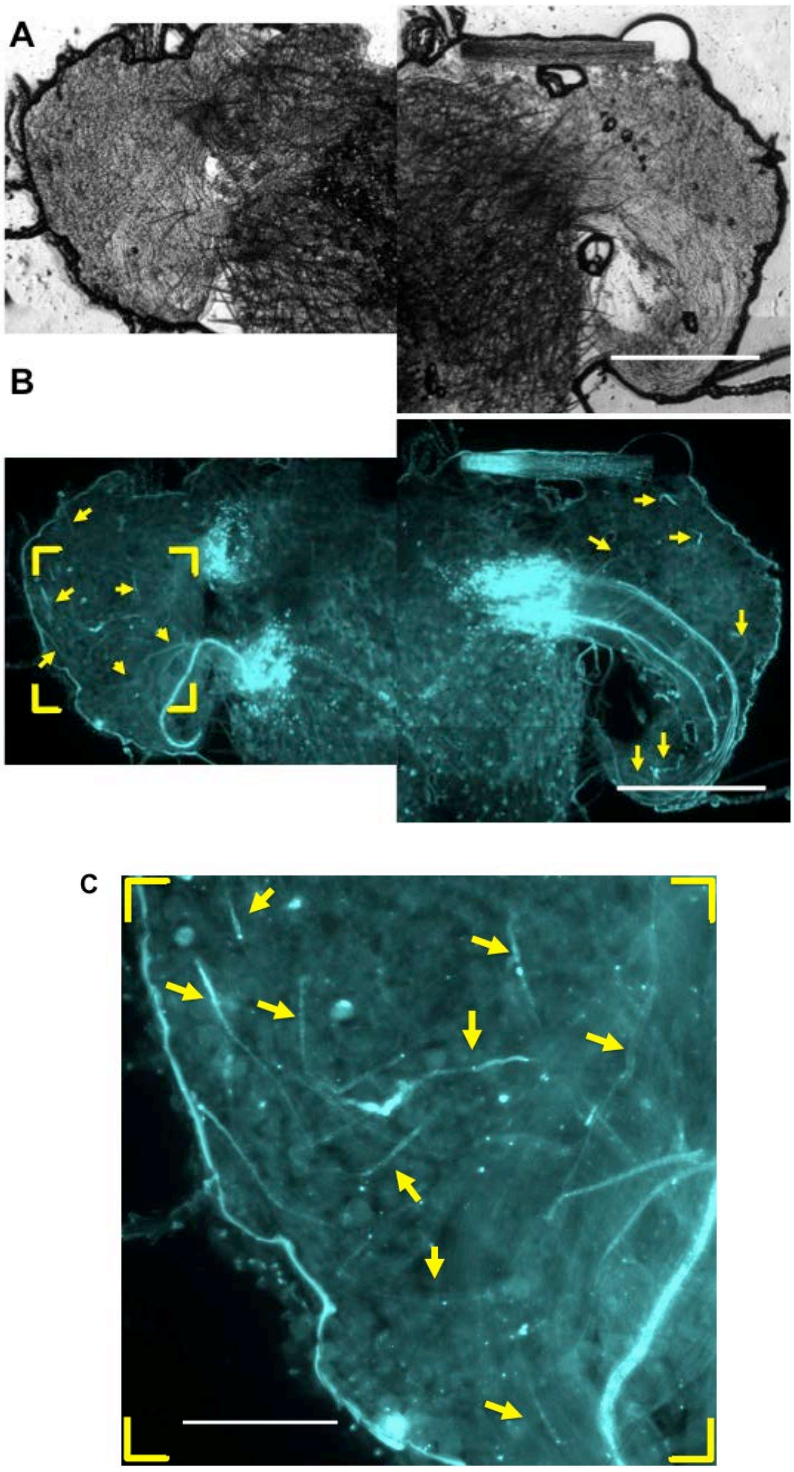

Figure 6.22. Representative images of a semi-*in vivo* pollination corresponding to incompatible crosses. A: Upper panel correspond to a bright field of a structure conformed by the stigmatic papilla cells (top area), style (middle-centre area), and ovary (lower area). **B**: Same stigma imaged using UV light revealing the pollen tubes stained with aniline blue. n = 10. Scale bar = 0.5 mm. **C:** Magnification of the area highlighted yellow square in panel B**.** The arrows indicate pollen tubes. Scale bar = 0.25 mm.

At the same time with the incompatible pollination described above, a compatible pollination was carried out using BsS1 stigmas from the same plant, but pollinated with pollen from a BsS1 plant, which should grow normally as it is a compatible combination. A representative image is shown in **Figure 6.23**. **Figure 6.23.A** shows the bright field of a pollinated stigma; pollen grains and tangle stigmatic papilla cells were visible. **Figure 6.23.B** shows the same stigma imaged using UV light. Similar to other crosses, there was a clear heterogeneity in the pollen grains and pollen tubes stained with aniline blue, exhibiting bright and dim signal. **Figure 6.23.C** shows pollen tubes that were only noticeable at a higher magnification. Additionally, this image shows the highly fluorescent hair-like shape structures, which were clearly not pollen tubes.

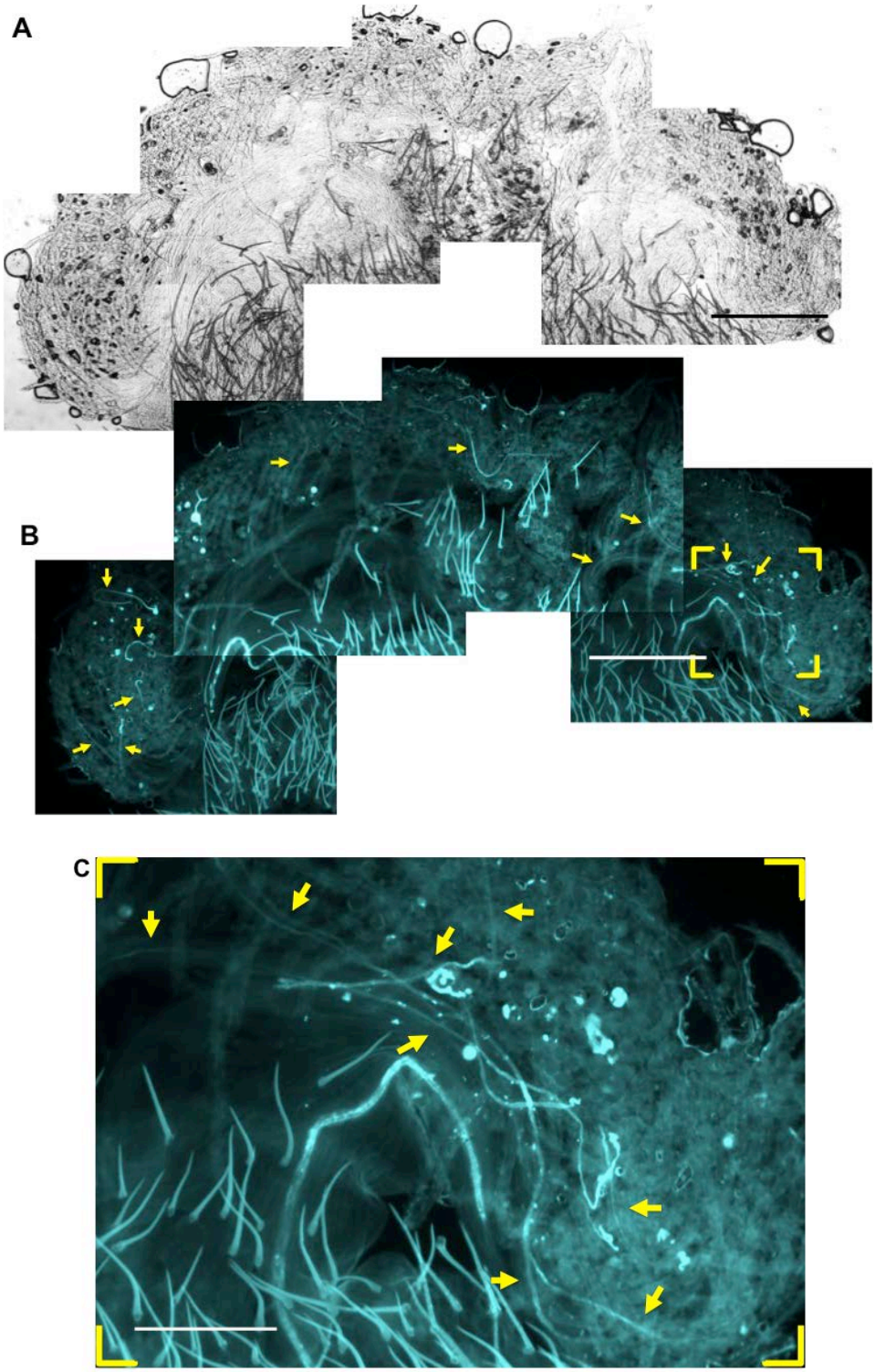

Figure 6.23. Representative images of a semi-*in vivo* pollination corresponding to a compatible cross. A: Bright field of a structure conformed by the stigmatic papilla cells (top area), style (middle-centre area), and ovary (lower area). **B**: Correspond to the same stigma imaged in A using UV light revealing the pollen tubes stained with aniline blue. Scale bar = 0.5 mm. n = 10. **C:** Magnification of the area highlighted yellow square in panel B**.** The arrows indicate pollen tubes. Scale bar = 0.25 mm.

Figure 6.24 shows the viability assay using FDA stain of the pollen remaining in the anthers after the pollinations. Pollen viability from the BpS1GFP plant (used in experiment showed in **Figure 6.22**) was 32%. Pollen viability from the BpS3GFP plant (used in experiment showed in **Figure 6.23**) was 18%. Same as the pollen viability test previously shown (**Figure 6.21**), this viability confirmed that the anther used for the pollination contained mature pollen. However, this viability does not represent the viability of the pollen used for the pollinations.

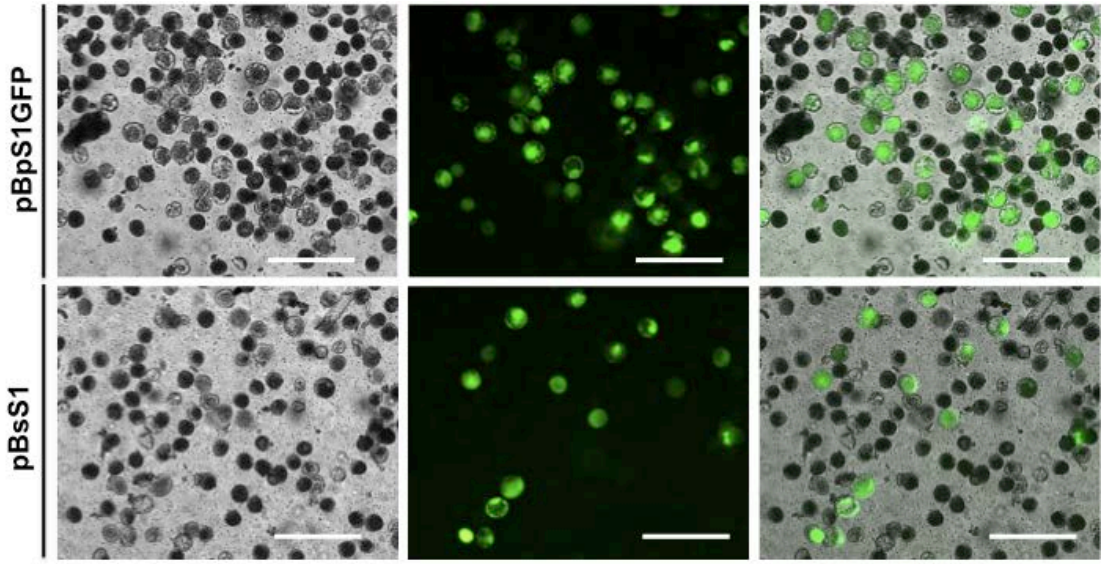

Figure 6.24. **Pollen viability estimated by staining with FDA**. Pollen from BpS1GFP and BsS1 showed 32% and 20% of viability respectively. This assay was carried out with pollen remaining in the anther after have used it for the pollination. This provides a reference for viability; however, this is an underestimated value as the best quality pollen is the first in fall off the anther and it was used for the pollinations. Fluorescence images were taken using the FITC filter: excitation 492 nm, emission 519 nm Scale bar 250 µm.

Unfortunately, the results obtained from the pollinations using transgenic barley lines were similar to the results obtained from the crosses using “wild type” plants. Thus, obvious differences based in the comparison between the pollen

tube growth in compatible and incompatible crosses were not observed. The main difficulty was the tangle arrangement of the stigmatic papilla cells, which made impossible to obtain reliable measurements of the pollen tube length and consequently conclusive data from the comparisons of these experiments.

Additional pollinations revealed similar results (data not shown). These included 21 stigmas pollinated with incompatible pollen, 11 stigmas pollinated with compatible pollen and 4 stigmas from the control lines transformed with the empty vector, B202.

Considering all the data, *semi-in-vivo* pollinations were not suitable to evaluate functional SI in transgenic barley lines. Therefore we decided to try *in vivo* pollinations, comparing the number of seeds produced after compatible and incompatible combination of pollinations *in vivo*.

6.2.2.2.4 *In vivo* functional analysis of barley lines transformed with Papaver *S*-determinants.

The difference between the number of seeds produced by compatible and incompatible pollination represents a robust test to evaluate functional SI as the ultimate goal of this mechanism is to prevent the production of seeds after incompatible pollinations. So, despite the fact that this approach cannot provide information regarding the underlying mechanism, it can potentially provide definitive data as to whether these transgenic barley lines have SI response after incompatible pollinations.

It was expected that incompatible crosses using stigmas from BsS1 and pollen from BpS1GFP lines produced a reduced number of seeds in comparison with

compatible crosses between compatible transgenic plants and wild type plants. As with the previous functional analysis semi-*in-vivo* and *in vitro*, it was possible that the difference between incompatible and compatible lines might be less obvious, as some of these lines were potentially heterozygous lines. If this was the case, an SI response would be triggered in only half of the pollen grains.

After discussion with Dr Kakeda, based on his experience with the self-incompatible grass *Hordeum bulbosum*, the pollen obtained from plants grown at 18°C, and especially pollen from plants grown in the field, exhibited a remarkably better response for studies involving pollen (i.e. *in vitro* germinations, or pollinations), compared with pollen from barley plants grown in a glasshouse at 22 - 23°C (personal communication).

A batch of crosses were carried out with barley plants grown indoors at 18°C. Additionally, another batch of plants grown at 23°C was used to carry out a parallel set of crosses.

Table 6.5 shows a summary with the results for the crossing programmes carried out using the transgenic barley lines. At 18°C, 80 BsS1 stigmas from two independent lines were pollinated with incompatible pollen from three independent BpS1GFP lines in six different crosses. In total, 64 seeds were collected from these crosses. As a control, six compatible crosses were carried out, which included 81 BsS1 stigmas from three independent lines, pollinated with pollen from three independent BpS3GFP lines in six different crosses. In total 61 seeds were collected from these crosses. These results revealed a seed-set of 80 % and 75 % for incompatible and compatible crosses respectively (percentage obtained using the number of stigmas pollinated as a 100%). For the crosses with plants at 23 C, five different incompatible crosses

were carried out. In total 32 seeds were collected after 60 BsS1 stigmas from three independent lines were pollinated with BpS1GFP pollen from three independent lines. This represents a seed-set of 53%. Five different control crosses of BsS1 stigmas from three independent lines pollinated with compatible BpS3GFP pollen from three independent lines were carried out. Of these 58 pollinated stigmas, 30 seeds were harvested, which represents a 52 % of seed-set. Additional controls using BpS1GFP and BpS3GFP (not expressing PrsS) as a female parent were carried out twice using two independent lines as a female parent and two independent lines as a male parent. 14 seeds were harvested from 21 BpS1GFP stigmas pollinated with BpS1GFP pollen (38% seed-set). 15 seeds were harvested after 22 BpS1GFP stigmas were pollinated with BpS3GFP pollen (68% seed-set). Also 15 seeds were collected after 22 BpS3GFP stigmas were pollinated with BpS1GFP pollen (68% seed-set). Finally, 22 BpS3GFP stigmas pollinated with BpS3GFP pollen produced 12 seeds (55% seed-set).

Table 6.5 Crossing programme with the transgenic barley lines transformed with PrpS and PrsS.

Number indep. crosses	Female parent ♀	Male parent ♂	Number stigmas pollinated	Number seeds harvested	Condition (% seed set)
Plants grown at 18ºC					
6	BsS1	BpS1GFP	80	56	SI (70%)
6	BsS1	BpS3GFP	81	59	Comp (72%)
Plants grown at 23ºC					
5	BsS1	BpS1GFP	60	32	SI (53%)
5	BsS1	BpS3GFP	58	30	Comp (52%)
2	BpS1GFP	BpS1GFP	21	8	Comp (38)
2	BpS1GFP	BpS3GFP	22	15	Comp (68%)
2	BpS3GFP	BpS1GFP	22	15	Comp (68%)
2	BpS3GFP	BpS3GFP	22	12	Comp (55%)

Two batches of plants were grown at different temperatures and evaluated. A set of plants at 18ºC, and another at 23ºC.

A student's t-test analysis revealed that there were no significant differences in the number of seeds produced between compatible and incompatible pollinations between these barley lines. This suggests that an SI response was not triggered in these barley lines.

The batch of plants grown at 18°C showed an average seed-set of 71% (including 12 crosses and 161 stigmas in total). This was higher than the batch of plants grown at 23°C, which exhibited an average seed-set of 55% (including 18 crosses and 112 stigmas in total). This result confirmed that seed-set of plants grown at 18°C was higher in comparison with plants grown at 23ºC, which agrees with observations made by Dr Kakeda in *H. bulbosum* (personal communication). This is useful information for future studies.

6.3 Discussion

Transformation efficiency of barley embryos transformed with Papaver female *S*-determinant $PrsS_1$

Methods using *Agrobacterium*-mediated techniques offer a number of advantages over biolistic-mediated techniques (Travella et al., 2005). Higher transformation efficiencies, more stability of the expression and inheritance of the transgene are some examples (Harwood et al., 2009). Transformations efficiencies around 25 - 30% have been described in the literature for the Golden Promise variety (Bartlett et al., 2008). During this project, similar values were obtained for transformations with pB202 (30%), and a higher efficiency for transformation with pBsS1 (50%). This confirmed that the transformation procedure is reliable protocol, especially considering that the transformations

were carried out at JIC and the regeneration process at the University of Birmingham.

Assessment of transgenic material from barley lines transformed with the female *S*-determinant, $PrsS_1$, and with male S-determinant, $PrpS_1$ and $PrpS_3$

The expression of *PrsS* was assessed by means of semiquantitative PCR. This experiment confirmed the presence of *PrsS* transcripts and also allowed to select the lines exhibiting higher levels of expression aiming to use the best lines for the functional analysis. On the other hand, Real-Time PCR were used to assess the expression of *PrpS*. These results confirmed the expression of *PrpS* and were used to select the over-expressing lines to carry on the functional analysis.

Together, these results revealed the expression of *PrpS* and *PrsS* at transcript level confirming the successful transformation of the barley plants. Additionally, detection of *PrsS* transcripts confirmed that transgenic barley lines were expressing *PrsS*.

Nonetheless, it was not possible to detect PrsS or PrpS proteins in the barley transgenic plants. Lines transformed with *PrsS* were analysed by means *of* western blot using an antibody against PrsS. The same antibody was previously successfully used to detect PrsS in mature stigmas of transgenic *Arabidopsis* lines (Lin, 2015), indicating that the antibody was suitable to detect PrsS. This suggested that either the expression levels were below the sensitivity of the antibody, or there was a failure during the synthesis, processing and/or targeting of PrsS to the plasma membrane. Previous studies attempting the

functional transfer of *Papaver* SI into *A. thaliana* were only successful after the evaluation of different promoters driving the expression of the female *S*-determinant, PrsS (Vatovec, 2012, de Graaf et al., 2012, Lin, 2015). The cassette used to obtain functional PrsS in *Arabidopsis in vivo* included the SLR1 promoter, a promoter from *Arabidopsis* expressed specifically in mature stigmas (Lin, 2015). The barley lines generated and evaluated during this thesis included the maize ubiquitin promoter (ubi) to drive the expression of PrsS. Despite the ubiquitin promoter already having functionally tested in barley (Bartlett et al., 2008), our data suggested that the expression of PrsS, if any, in the barley stigmas was low. Therefore a more suitable promoter, which provides higher levels of PrsS expression in mature barley stigmas, could be a key aspect to obtain functional SI in barley. However, a major limiting factor inhibiting advances in cereal crops transgene technology is that many of the best-characterised plant promoters have been developed in dicotyledonous species (Hensel et al., 2011). Currently the barley genome is available (Mayer et al., 2012), and functional studies have started to be carried out in the last few years (Munoz-Amatriain et al., 2015). Therefore it is expected that tissue-specific promoters (particularly pollen and stigma specific promoters) from barley will be available soon. These promoters could potentially be essential to design a new strategy aiming to generate new barley lines exhibiting a high expression of PrsS and PrpS for functional SI.

The analysis to confirm the expression of PrpS-GFP at protein level included: 1) GFP fluorescence using microscopic analysis, and 2) western blot using antibodies against GFP. Unfortunately, barley pollen exhibited a considerably high level of autofluorescence (in both pollen coat and pollen grain); therefore

the examination of barley pollen expressing PrpS-GFP proved technically unreliable to identify the homozygous lines or to confirm the expression of PrpS-GFP. Moreover western blot analysis using antibodies against GFP did not prove the expression PrpS-GFP fusion. Therefore it was not possible to confirm if PrpS was expressed in pollen.

The genetic cassette (*NTP303::PrpS-GFP*) used here to transform barley was the same as that used to obtain PrpS functional in *Arabidopsis* pollen *in vitro* (de Graaf et al., 2012) and *in vivo* (Lin, 2015).

Barley pollen showed a rapid decrease of its viability in vitro

One of the main problems we faced for the *in vitro* studies was that the pollen longevity in the *Poaceae* (grasses) family is short compared with other species. This means that the viability of the pollen sharply decreases over time, making its study very difficult. In rice, studies described that 1 h after anthesis the pollen viability decreased from over 80% to less than 10% (Khatun and Flower, 1995). In *Shorgum bicolor*, a grass cultivated for the grain production, the pollen viability decreased to 20% 4 hours after pollen shedding (Tunistra and Wedel, 2000). In switchgrass, even after 20 min (at 24ºC), the pollen germination percentage of some cultivars was reduced from 80 to 40% and below 10% after 40 min (Ge et al., 2011).

Despite all the different alternatives assessed, it was not possible to obtain germination rates around 50% or more as is described in the literature for a barley relative *Hordeum bulbosum* (Chakrabarti et al., 1976). Pollen viability and germination varies depending on the genotype and even cultivar (Parzies et al., 2005). This could explain difficulties for developing a germination system

in this thesis. Kakeda (Kakeda et al., 2008) and Chakrabarti (Chakrabarti et al., 1976) used *H. bulbosum*, instead of *H. vulgare* for their studies.

As a consequence of the reduced viability of the pollen *in vitro*, the development and use of an SI bioassay is restricted. However the development of a protocol to stain and visualise F-actin filaments represents a major contribution of this work to further studies involving barley pollen.

Screening and genotyping of homozygous barley lines transformed with *PrsS* and *PrpS*

As it was mentioned before, GFP fluorescence was very high in non-transgenic barley pollen and therefore it was not possible to use this method for the screening of the homozygous lines. The genetic construct for the transformation with *PrsS* did not contain any fluorescent tag and therefore the selection of the homozygous lines needed to be based in the use of the antibiotic resistant.

Unfortunately the development of a protocol for the germination of barley seeds *in vitro* was not established in time to be used as a tool for the screening of the homozygous transgenic barley plants in this thesis. Additionally, considering that the sterilisation procedure is more aggressive in this protocol in comparison with the standard protocols (*e.g.* to sterilise *Arabidopsis* seeds), it is possible that some seeds are killed as a result of the long exposure of bleach and not due to the antibiotic. This is something that has to be evaluated and considered in the future if this strategy is used.

In vitro functional analysis of barley pollen from barley lines transformed with *PrpS*

As mentioned before, the feasibility of the *in vitro* studies was limited due to a rapid decrease in the viability of the barley pollen outside the anther. Nonetheless the studies evaluating the effect of an artificial decrease in the cytosolic pH in barley pollen, indicated that a decrease in the pH was enough to trigger actin alterations resembling the F-actin foci described previously during the *Papaver* SI response (Wilkins et al., 2015). The fact that similar responses were visible in barley pollen represents positive evidence to support the strategy of using barley as a feasible model for transferring *Papaver* SI and detection of SI events downstream of the initial PrsS-PrpS interaction. This suggests common subcellular mechanism and pathways between barley and *Papaver*.

Semi-*in-vivo* functional analysis of barley stigmas from barley lines transformed with *PrsS,* and barley pollen from lines transformed with *PrpS*

The semi-*in-vivo* analysis revealed technical difficulties in assessing the pollen tube growth. Unlike *Arabidopsis* and *Papaver,* the feathery shape of the stigmatic papilla cells in barley obscured any clear visualisation of the pollen tube growth through the stigma and style. This is a general problem when studying pollen tube growth in grasses. Studies in *Lolium perenne* using a similar experimental design (Klaas et al., 2011), have shown comparable images to the ones we presented here.

Data obtained from the *Arabidopsis* analysis showed that semi-*in-vivo* pollinations exhibited a range of strength in the SI response even in plants originated within the same line (Lin, 2015). So it is possible that the three independent BsS1 barley lines analysed here, exhibited a weak SI response and more lines needed to be tested. In this context, it has been described that the genetic background can have an effect in the functionality of SI (Nasrallah et al., 2004). Therefore, an alternative strategy to consider in further studies is to evaluate a different variety of barley. Although as mentioned before, the variety used here, Golden Promise, has the highest transformation efficiencies (Harwood et al., 2009).

In vivo* functional analysis of barley lines transformed with *PrsS* and *PrpS

Results from the *in vivo* pollinations clearly demonstrated that the seed-set values for compatible and incompatible crosses were very similar. This allows ruling out the possibility of functional SI in these transgenic barley lines. These results also confirmed that crosses using plants grown at 18ºC showed higher seed-set production in comparison with crosses of plants grown at 23ºC.

Conclusions

The functional analysis carried out during this thesis suggests that the barley lines evaluated here (BsS1, BpS1GFP and BpS3GFP) did not exhibit functional SI. However, since PrsS or PrpS were not detected at protein level, the lack of differences between the compatible and incompatible pollination does not rule out barley as a candidate to transfer *Papaver* SI.

Barley still represents the most feasible model to attempt functional transfer of *Papaver* SI into a monocot crop. A new strategy using new promoters that optimise expression of both *PrpS* and *PrsS* in relevant cells represent a promising objective to be carried out in future work.

CHAPTER 7

General Discussion

7.1 Introduction

As mentioned in Chapter 1 (section 1.5), PrpS and PrsS are functional in *Arabidopsis in vivo*, transforming a normally self- compatible plant into a self-incompatible one (Lin, 2015). Moreover experiments *in vitro* using transgenic *Arabidopsis* pollen expressing PrpS and challenged with incompatible PrsS revealed that the pollen exhibited a remarkably similar response to the one described in *Papaver* including F-actin foci formation and caspase-like activity activation (de Graaf et al., 2012). Together, these provided robust evidence suggesting that PrpS-PrsS had the potential to work as a "plug and play" system in a host cell, triggering a conserved set of cellular responses. This thesis aimed to explore the versatility of the Papaver SI system further, by attempting to functionally transfer Papaver SI into highly diverged heterologous model systems, including: yeast, *Arabidopsis* mesophyll protoplast (Chapter 3), mammalian HeLa cells (Chapter 4 and Chapter 5), and a monocot cereal, namely barley (Chapter 6).

Our data show that PrsS-PrpS interaction is functional in non-reproductive/vegetative cells. Moreover data obtained from mammalian epithelial HeLa cells revealed promising evidence suggesting that PrpS-PrsS can be functional in highly diverged species, accessing and recruiting highly conserved ancient cellular signalling components including: 1) transient Ca^{2+} increases, suggesting Ca^{2+}-signalling, 2) cationic channel activity, and 3) actin cytoskeleton alterations.

7.2 Exploring the functionality of PrpS in mammalian HeLa cells

As mentioned in Chapter 1 (section 1.1), many signalling pathways have been conserved during evolution. Some of these signalling pathways (i.e. $[Ca^{2+}]_i$ and F-actin alterations) have been described playing a role during the *Papaver* SI response. Our data suggested that PrpS-PrsS interaction accesses and recruits "universal" signalling components from the HeLa cells triggering alterations that resemble the ones described during the *Papaver* SI response.

7.2.1 HeLa-C-PrpS$_1$ cells exhibited dramatic alterations after exposure to incompatible PrsS$_1$

Chapter 5 assessed F-actin configuration in HeLa cells expressing PrpS exposed to PrsS in a compatible and incompatible combination. We established that specifically the incompatible combination (HeLa-C-PrpS$_1$ exposed to PrsS$_1$) had a detrimental effect on the cell adherence, as it was the only combination tested that exhibited a significant increase in the number of cells floating off the culture. Remarkably, some of the actin alterations exhibited in these "floaters" resembled the *Papaver* F-actin foci seen during SI. Importantly, the reduction in adherence had a correlation with the disappearance of actin stress fibres, which have been described as responsible for the cell adherence properties in other epithelial cells (Pellegrin and Mellor, 2007).

As mentioned in Chapter 5 (section 5.1), in animal cells, actin stress fibres form part of a structure termed focal adhesions, which in addition to its role in cell adherence, plays a role mediating signalling between the extracellular media

and the intracellular physiology (Burridge et al., 1997). This provides a concrete link between an external stimuli (in this case $PrsS_1$ as a ligand) and intracellular signalling involving actin cytoskeleton alterations.

This also opens the possibility to study whether actin-binding proteins (ABP) may also be involved in the response. As they have been described participating in the *Papaver* SI response (Poulter et al., 2010) and animal cells, regulating the dynamics of the stress fibers and focal adhesion (Kim and McCulloch, 2011, Lee and Dominguez, 2010).

In Chapter 4 we monitored $[Ca^{2+}]_i$ in HeLa-C-$PrpS_1$ cells exposed to compatible and incompatible PrsS. Live cell Ca^{2+} imaging experiments revealed increases in $[Ca^{2+}]_i$ of up to 3.5-fold specifically after challenge with incompatible $PrsS_1$. In contrast, exposure to compatible $PrsS_8$ exhibited negligible alterations to $[Ca^{2+}]_i$, suggesting a specific response for the cognate PrsS. This evidence supports the idea that the increases in $[Ca^{2+}]_i$ are an authentic response, as allele-specificity is a characteristic of the *Papaver* SI response. Moreover, these increases in $[Ca^{2+}]_i$ were rapid (with in the range of seconds) and transient (only when HeLa-C-$PrpS_1$ cells were exposed to $PrsS_1$), also characteristics of the *Papaver* SI response (Franklin-Tong et al., 1997, Franklin-Tong et al., 1993b).

7.2.2 Investigating the role of PrpS mediating the channel activity

As mentioned in Chapter 1 (section 1.4.6.2), the current model of the *Papaver* SI response includes that PrpS might act as the Ca^{2+} channel allowing the Ca^{2+} influx responsible for the increase in the $[Ca^{2+}]_i$ in *Papaver* pollen.

In Chapter 4, we measured the currents generated through the plasma membrane of HeLa-C-PrpS_1 cells during the exposure to PrsS. The results showed that large current influxes (> 2-fold) were generated after incompatible combination (e.g. HeLa-PrpS_1 challenged with PrsS_1) whilst the compatible combination (e.g. HeLa-PrpS_1 challenged with PrsS_8) or controls (e.g. HeLa-mCh challenged with PrsS_1) showed the generation of much smaller inward currents. This demonstrates that PrpS-PrsS interaction is sufficient to trigger ion flux through the plasma membrane, in a *S*-allele specific manner, providing further evidence showing that the *Papaver* SI response is mediated by an ion channel. Further experiments are needed in order to obtain conclusive data regarding the nature of the current generated after PrpS-PrsS interaction, the data suggests a non-specific cation channel. This agrees with electrophysiological experiments carried out in *Papaver* pollen protoplasts (Wu et al., 2011). However, because we obtained channel activity in HeLa-mCh exposed to PrsS, our data does not conclude that PrpS is a channel. For further experiments using a similar approach, it is important to use a cell line that does not exhibit background currents.

In summary, the observations during the SI bioassay experiments of HeLa-C-PrpS_1 exposed to PrsS including: 1) number of cells floating off, 2) actin stress fibres disappearance, 3) currents generated in the plasma membrane, and 4) increases in $[Ca^{2+}]_i$, revealed that the more severe/extreme alterations were consistently exhibited for the incompatible combination of HeLa-PrpS_1 challenged with incompatible PrsS_1. This provides support to consider the alterations as a real cellular response, suggesting that HeLa-C-PrpS_1 is sensing and responding specifically to PrsS_1.

All together, the results observed in HeLa cells represent strong evidence suggesting that PrpS is functional in mammalian HeLa cells. Moreover, PrpS-PrsS interaction is able to access and recruit components from conserved signalling pathways in highly diverged cells.

7.2.3 HeLa-C-PrpS$_1$ cells exhibited a heterogeneity in the level of alterations after exposure to incompatible PrsS$_1$

In the experiments carried out to evaluate the functionally of PrpS in HeLa cells, we detected a heterogeneity in the alterations exhibited after the challenged with incompatible PrsS (e.g. HeLa-PrpS$_1$ exposed to PrsS$_1$). This heterogeneity included cells exhibiting very dramatic alterations, but also cells exhibiting lesser alterations. This heterogeneity is commonly seen in numerous cell types, including the increases in the $[Ca^{2+}]_i$ in pollen during the *Papaver* SI response.

The F-actin stain microscopy analysis carried out in Chapter 5 showed that: 1) the disappearance of actin stress fibres was correlated with the increasing concentration of incompatible PrsS$_1$ used for the challenge, 2) the increase in floating cells was obtained only at the higher concentration of treatments with incompatible PrsS$_1$, and 3) that structures resembling the F-actin foci described in *Papaver* were more abundant in floating cells. This led us to consider a gradient in the strength of the alterations between the HeLa cells.

The live-cell calcium imaging experiments shown in Chapter 4 revealed increases in the $[Ca^{2+}]_i$ of up to 3.5-fold greater than the levels before the exposure to incompatible PrsS, however most of the cells showed smaller increases between 0.2 - 0.3-fold, denoting a difference in the response.

The patch-clamp experiments in HeLa-C-$PrpS_1$ also detected differences in the alterations of the current generated through the membrane. HeLa-C-$PrpS_1$ exposed to incompatible $PrsS_1$ showed differences of up to 5-fold in the amplitudes of the inwards current generated. Similarly currents generated in HeLa-mCh exposed to $PrsS_1$ also exhibited differences of up to 3-fold in the intensity.

This heterogeneity could be due to normal differences inherent to a biological system or alternatively to a consequence of malfunctioning during the synthesis and/or processing of PrpS in the secretory pathway, probably as a consequence of over-expression. As we showed in the microscopic analyses, the fluorescence from PrpS-mCherry fusion was not homogeneously distributed in the cells. The fluorescence was not distributed neatly along the edge of the cell as expected.

7.2.4 HeLa-mCh exposed to PrsS exhibited small channel activity

We also detected small alterations in the actin configuration and generation of currents during patch-clamp experiments of HeLa-mCh (HeLa without PrpS expressed) combinations challenged with PrsS. Since these alterations were much smaller in comparison to the incompatible combination, we interpreted these alterations as a background response, which suggests that HeLa could naturally sense PrsS as a ligand. This is an interesting result as it might represent additional evidence indicating a conserved signalling pathway, as it would denote that there are innate components in HeLa cells that can identify

and respond to PrsS, producing alterations in the physiology of the cells. However, this result does not allow to confirm if PrpS is a ion channel.

7.3 Future work to determine the nature of PrpS as a ion channel

A promising experimental approach to characterise PrpS as a putative channel, is by cell-free protein synthesis. This technique is particularly useful in the expression of membrane proteins as it directly couples the protein synthesis with an artificial hydrophobic environment, reducing the formation of non-functional aggregates such as inclusion bodies (Schwarz et al., 2008). Complementing this technique with electrophysiological experiments, represent a neat system without any background effects or interference from the host cell.

In collaboration with Mark Shneider and Renate Scheibe at University of Osnabrueck, we generated the genetic constructs in order to carry out these experiments. **Figure 7.1** shows the diagrams with the genetic constructs generated.

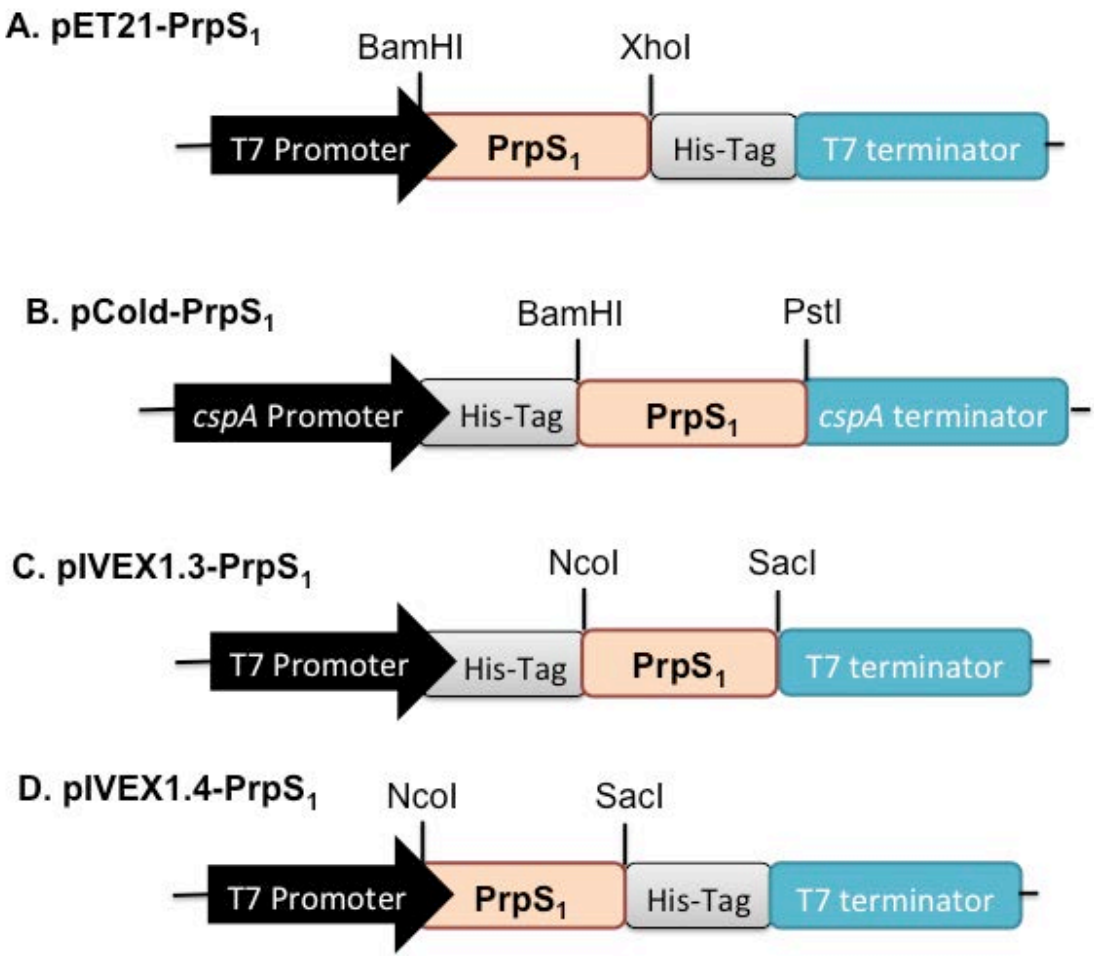

Figure 7.1 Genetic constructs for the expression of PrpS in a cell-free system. A: $PrpS_1$ cloned in pET21a(+) (pET21a-$PrpS_1$) is a vector designed for the production of large quantity of protein. C-terminal His-tag. **B**: $PrpS_1$ cloned in pColdI DNA (pCold-$PrpS_1$) is a vector designed for a cold-shock induction of protein expression. N-terminal His-tag. **C:** $PrpS_1$ cloned in pIVEX1.3 (pIVEX1.3-$PrpS_1$) is a vector designed for expression *in vitro* in the cell-free system. N-terminal His-tag. **D**: $PrpS_1$ cloned in pIVEX1.4 (pIVEX1.4-$PrpS_1$) is a vector designed for expression *in vitro* in the cell-free system C-terminal His-tag.

Once these genetic constructs were checked by sequencing, they were sent to the University of Osnabrueck were preliminary experiments successfully expressed $PrpS_1$. Follow up experiments, including the functional analysis are pending.

7.4 Exploring the functionality of PrpS in unicellular model systems

Chapter 3 explored the functionality of PrpS in yeast and *Arabidopsis* mesophyll protoplasts. PrpS was successfully expressed in both cellular systems, however the patterns expression was not homogeneously distributed, suggesting issues related with the synthesis of PrpS. Functional analysis, revealed decreases in the viability of protoplasts expressing PrpS exposed to incompatible PrsS. This decrease in viability showed allelic-specificity, and to some extent could be prevented by treatments with caspase inhibitors, suggesting that a “SI-like” response was triggered. Nonetheless, these data were not conclusive as the differences in the viability and death prevention between the different treatments (i.e. incompatible, compatible and untreated) were not as clear as they were in similar experiments using *Arabidopsis* pollen expressing PrpS challenged with incompatible PrsS (de Graaf et al., 2012). We interpreted these lesser differences as a consequence of main three factors: 1) relatively high proportion of dead protoplasts, inherent to the protoplasts preparation and transfection protocols, 2) the low transfection efficiencies, which could have prevented to observe a more notorious difference in the results, and 3) heterogeneity in the expression of PrpS associated with potential issues during the synthesis of PrpS and/or its targeting to the plasma membrane.

In yeast expressing PrpS, the viability after exposure to PrsS, did not reveal differences between the treatments (i.e. incompatible, compatible, and untreated combinations), suggesting that PrpS was not functional in yeast. However, this could be a consequence of the abnormal $PrpS_1$-GFP accumulation in some intracellular organelles part of the secretory pathway

(e.g. ER or GA), suggested by the heterogeneous GFP pattern expression. Therefore, using a different heterologous model could improve the expression of PrpS, increasing the possibilities of obtain functional PrpS in a model system. Additionally, future work may also include the evaluation of a different cellular target of *Papaver* SI such as F-actin, as actin cytoskeleton has been thoroughly studied in yeast (Gourlay and Ayscough, 2005, Leadsham et al., 2010, Goode et al., 2015).

Future experiments, evaluating different promoters aiming to improve the expression of PrpS could contribute to obtain conclusive data from these experiments.

7.5 Evolutionary implications of functional *Papaver* SI in highly diverged cellular model.

The Cladogram in **Figure 7.2** shows the evolutionary relationships based on the amino acid sequences of a highly conserved protein, actin. This cladogram grouped the organism as expected: plants (monocot and dicot), animals and fungi. *Arabidopsis* and *P. rhoeas* diverged ~144MYA, and monocot from dicot ~160 (Bell et al., 2010). The clade corresponding to animals and fungi grouped with a closer ancestor in comparison with plants.

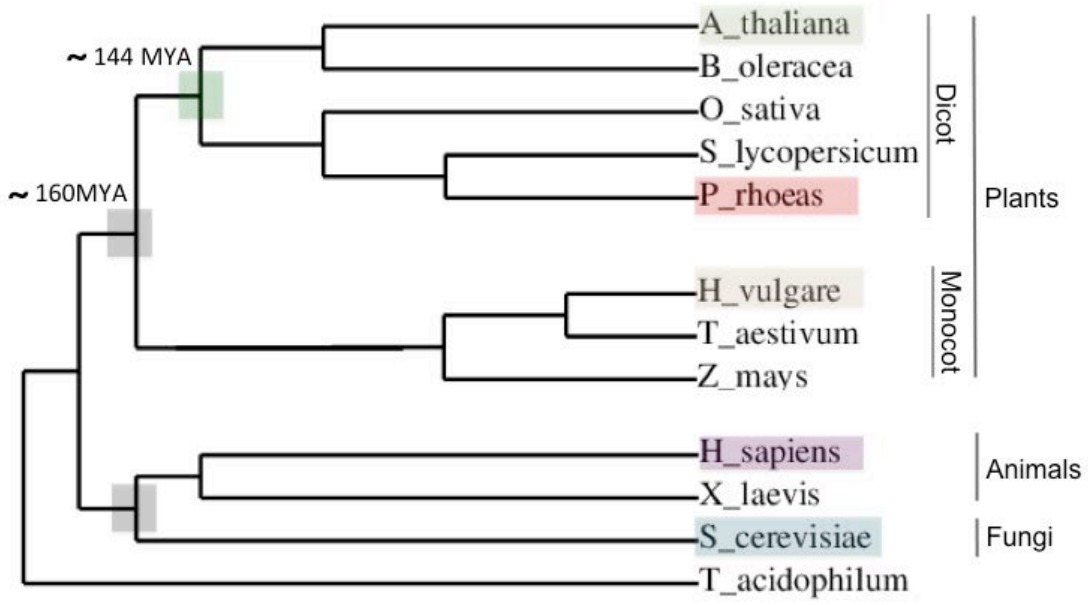

Figure 7.2. Cladogram showing the evolutionary relationships based on the amino acidic sequences of the actin protein. The phylogenetic analysis included: MUSCLE software for the sequence alignment and Gblocks for refinement. PhyML3.1/3.0 aLTR and TreeDyn softwares were used for the phylogeny and tree rendering respectively. Boostrapt values are shown in red on top of the corresponding branch. The archaea *Thermophilus acidophilum* was used as an outside group to root the cladogram. This work was carried out the platform available in by (Dereeper et al., 2008). Estimation of the diversion between *A. thaliana* and *Papaver* ~144 MYA; estimation between monocots and dicots ~160 MYA (Bell et al., 2010). The species studied in this thesis, and the nodes representing the last common ancestor are highlighted in colour boxes. A_thaliana: *Arabidopsis thaliana*. B_olaracea: O_sativa*: Oryza sativa.* *S*_lycopersicum: *Solanum lycopersicum*. P_roheas: *Papaver rhoeas.* H_vulgare: *Hordeum vulgare*. T_aestivum: *Triticum aestivum*. Z_mays: *Zea mays.* H_sapiens: *Homo sapiens*. X_laevis: *Xenopus laevis.* S_cerevisiae: *Saccharomyces cerevisiae.*

The fact that our data suggest that PrsS-PrpS interaction triggers cellular responses in mammalian HeLa cells, suggest that the poppy S-determinants may be triggering a highly conserved set of responses in eukaryotic cells. This provides support to attempt functional transfer of PrsS and PrpS into monocots, which is a closer group to poppy, in comparison with animal cells. Functional SI in highly diverged cellular model would contribute to the studies elucidating the evolution of different SI systems in plants. Moreover, in a more general

prospect, it could be useful to study mechanism such as the self/non-self recognition systems in eukaryotes.

Self/non-self mechanisms have a huge importance, as it is the fundamental base for the most of the immune system. It has been described that plants an animals shared several mechanism as part of the immune response (Taylor, 1998).

7.6 Biotechnological impact of functional *Papaver* SI in highly diverged cellular model.

As mentioned in the Chapter 1 (section 1.4.3) SI can be used as a tool to generate F1 hybrids. Therefore if PrpS-PrsS can be functionally transferred into an economically relevant self-compatible crop to make it self-incompatible, this system could provide a new strategy to generate F1-hybrids seeds. In this context, a process to patent PrpS and PrsS has started (Franklin-Tong et al., 2010)

Probably the main problem in our attempt to transfer PrpS and PrsS into barley, was the inability to detect PrpS and PrsS at the protein level. We decided to carry on with the functional analysis assuming that if some PrpS and PrsS was expressed, some differences would have been noticeable between compatible and incompatible crosses. However, because we did not see differences between these combinations, we cannot make categorical conclusions.

7.7 Concluding remarks

Our data suggests that PrpS-PrsS interaction can access and recruit conserved cellular components from highly diverged species and cell types including, Ca^{2+}-signalling and actin cytoskeleton. Moreover, our date confirmed that PrpS-PrsS interaction triggers currents through the plasma membrane.

At the same time, our results open new questions, is PCD involved?, can the expression of PrpS be improved? And if so, does it have an effect in the functionality?

The evidence we have presented here is a concrete example of how universal signalling pathways have probably evolved from an ancient common ancestor.

CHAPTER 8

List of References

ALBERTS, B., JOHNSON, A., LEWIS, J., RAFF, M., ROBERTS, K. & PETER, W. 2008. *Molecular biology of the cell,* New York, Garland Science.

ALLEN, G. J., MUIR, S. R. & SANDERS, D. 1995. Release of Ca2+ from individual plant vacuoles by both InsP3 and cyclic ADP-ribose. *Science,* 268**,** 735-7.

ASAI, T., TENA, G., PLOTNIKOVA, J., WILLMANN, M. R., CHIU, W. L., GOMEZ-GOMEZ, L., BOLLER, T., AUSUBEL, F. M. & SHEEN, J. 2002. MAP kinase signalling cascade in Arabidopsis innate immunity. *Nature,* 415**,** 977-83.

AYSCOUGH, K. R., STRYKER, J., POKALA, N., SANDERS, M., CREWS, P. & DRUBIN, D. G. 1997. High rates of actin filament turnover in budding yeast and roles for actin in establishment and maintenance of cell polarity revealed using the actin inhibitor latrunculin-A. *J Cell Biol,* 137**,** 399-416.

BALK, J., LEAVER, C. J. & MCCABE, P. F. 1999. Translocation of cytochrome c from the mitochondria to the cytosol occurs during heat-induced programmed cell death in cucumber plants. *FEBS Lett,* 463**,** 151-4.

BARTLETT, J. G., ALVES, S. C., SMEDLEY, M., SNAPE, J. W. & HARWOOD, W. A. 2008. High-throughput Agrobacterium-mediated barley transformation. *Plant Methods,* 4**,** 22.

BEERMANN, S., VAUTH, M., HEIN, R., SEIFERT, R. & NEUMANN, D. 2014. Distinct signalling pathways of murine histamine H1- and H4-receptors expressed at comparable levels in HEK293 cells. *PLoS One,* 9**,** e107481.

BEI, Q. & LUAN, S. 1998. Functional expression and characterization of a plant K+ channel gene in a plant cell model. *Plant J,* 13**,** 857-65.

BELL, C. D., SOLTIS, D. E. & SOLTIS, P. S. 2010. The age and diversification of the angiosperms re-revisited. *Am J Bot,* 97**,** 1296-303.

BERGER, F., HAMAMURA, Y., INGOUFF, M. & HIGASHIYAMA, T. 2008. Double fertilization - caught in the act. *Trends Plant Sci,* 13**,** 437-43.

BERNSTEIN, B. W. & BAMBURG, J. R. 2010. ADF/cofilin: a functional node in cell biology. *Trends Cell Biol,* 20**,** 187-95.

BERRIDGE, M. J. 1993. Inositol trisphosphate and calcium signalling. *Nature,* 361**,** 315-25.

BERRIDGE, M. J., BOOTMAN, M. D. & LIPP, P. 1998. Calcium--a life and death signal. *Nature,* 395**,** 645-8.

BERRIDGE, M. J. & TAYLOR, C. W. 1988. Inositol trisphosphate and calcium signaling. *Cold Spring Harb Symp Quant Biol,* 53 Pt 2**,** 927-33.

BERTL, A., ANDERSON, J. A., SLAYMAN, C. L. & GABER, R. F. 1995. Use of Saccharomyces cerevisiae for patch-clamp analysis of heterologous membrane proteins: characterization of Kat1, an inward-rectifying K+ channel from Arabidopsis thaliana, and comparison with endogeneous yeast channels and carriers. *Proc Natl Acad Sci U S A,* 92**,** 2701-5.

BOGGS, N. A., DWYER, K. G., NASRALLAH, M. E. & NASRALLAH, J. B. 2009a. In vivo detection of residues required for ligand-selective activation of the S-locus receptor in Arabidopsis. *Curr Biol,* 19**,** 786-91.

BOGGS, N. A., NASRALLAH, J. B. & NASRALLAH, M. E. 2009b. Independent S-locus mutations caused self-fertility in *Arabidopsis thaliana*. *PLoS Genet,* 5**,** e1000426.

BOSCH, M. & FRANKLIN-TONG, V. E. 2007. Temporal and spatial activation of caspase-like enzymes induced by self-incompatibility in *Papaver* pollen. *Proc Natl Acad Sci U S A,* 104**,** 18327-32.

BRADFORD, M. M. 1976. A rapid and sensitive method for the quantitation of microgram quantities of protein utilizing the principle of protein-dye binding. *Anal Biochem,* 72**,** 248-54.

BREEUWER, P., DROCOURT, J. L., BUNSCHOTEN, N., ZWIETERING, M. H., ROMBOUTS, F. M. & ABEE, T. 1995. Characterization of uptake and hydrolysis of fluorescein diacetate and carboxyfluorescein diacetate by intracellular esterases in Saccharomyces cerevisiae, which result in accumulation of fluorescent product. *Appl Environ Microbiol,* 61**,** 1614-9.

BURRIDGE, K., CHRZANOWSKA-WODNICKA, M. & ZHONG, C. 1997. Focal adhesion assembly. *Trends Cell Biol,* 7**,** 342-7.

CANNELL, M. B., BERLIN, J. R. & LEDERER, W. J. 1987. Intracellular calcium in cardiac myocytes: calcium transients measured using fluorescence imaging. *Soc Gen Physiol Ser,* 42**,** 201-14.

CARDENAS, L., LOVY-WHEELER, A., KUNKEL, J. G. & HEPLER, P. K. 2008. Pollen tube growth oscillations and intracellular calcium levels are reversibly modulated by actin polymerization. *Plant Physiol,* 146**,** 1611-21.

CARDENAS, L., LOVY-WHEELER, A., WILSEN, K. L. & HEPLER, P. K. 2005. Actin polymerization promotes the reversal of streaming in the apex of pollen tubes. *Cell Motil Cytoskeleton,* 61**,** 112-27.

CHAKRABARTI, T., SUBRAHMANYAM, N. C. & DOY, C. H. 1976. *In vitro* germinationof barley pollen *Barley Genetics Newsletter,* 6**,** 90.

CHANG, L. & KARIN, M. 2001. Mammalian MAP kinase signalling cascades. *Nature,* 410**,** 37-40.

CHARDIN, P., BOQUET, P., MADAULE, P., POPOFF, M. R., RUBIN, E. J. & GILL, D. M. 1989. The mammalian G protein rhoC is ADP-ribosylated by Clostridium botulinum exoenzyme C3 and affects actin microfilaments in Vero cells. *EMBO J,* 8**,** 1087-92.

CHARLESWORTH, D. & CHARLESWORTH, B. 1987. Inbreeding depression and its evolutionary consequences. *Annu Rev Ecol Syst,* 18**,** 15.

CHARLESWORTH, D. & WILLIS, J. H. 2009. The genetics of inbreeding depression. *Nat Rev Genet,* 10**,** 783-96.

CHAUDHRY, F., JANSEN, S., LITTLE, K., SUAREZ, C., BOUJEMAA-PATERSKI, R., BLANCHOIN, L. & GOODE, B. L. 2014. Autonomous and in trans functions for the two halves of Srv2/CAP in promoting actin turnover. *Cytoskeleton (Hoboken),* 71**,** 351-60.

CHEN, W. T. 1981. Mechanism of retraction of the trailing edge during fibroblast movement. *J Cell Biol,* 90**,** 187-200.

CHENG, S. H., ZHUANG, J. Y., FAN, Y. Y., DU, J. H. & CAO, L. Y. 2007. Progress in research and development on hybrid rice: a super-domesticate in China. *Ann Bot,* 100**,** 959-66.

CHEUNG, A. Y. & WU, H. M. 2008. Structural and signaling networks for the polar cell growth machinery in pollen tubes. *Annu Rev Plant Biol,* 59**,** 547-72.

CHUA, B. T., VOLBRACHT, C., TAN, K. O., LI, R., YU, V. C. & LI, P. 2003. Mitochondrial translocation of cofilin is an early step in apoptosis induction. *Nat Cell Biol,* 5**,** 1083-9.

COLEMAN, M. L., MARSHALL, C. J. & OLSON, M. F. 2004. RAS and RHO GTPases in G1-phase cell-cycle regulation. *Nat Rev Mol Cell Biol,* 5**,** 355-66.

COLOSIMO, A., GONCZ, K. K., HOLMES, A. R., KUNZELMANN, K., NOVELLI, G., MALONE, R. W., BENNETT, M. J. & GRUENERT, D. C. 2000. Transfer and

expression of foreign genes in mammalian cells. *Biotechniques,* 29**,** 314-8, 320-2, 324 passim.
CRAMER, L. P., SIEBERT, M. & MITCHISON, T. J. 1997. Identification of novel graded polarity actin filament bundles in locomoting heart fibroblasts: implications for the generation of motile force. *J Cell Biol,* 136**,** 1287-305.
CRAWFORD, J. R. & JACOBSON, B. S. 1998. Extracellular calcium regulates HeLa cell morphology during adhesion to gelatin: role of translocation and phosphorylation of cytosolic phospholipase A2. *Mol Biol Cell,* 9**,** 3429-43.
CROW, J. F. 1998. 90 years ago: the beginning of hybrid maize. *Genetics,* 148**,** 923-8.
DALLE-DONNE, I., ROSSI, R., MILZANI, A., DI SIMPLICIO, P. & COLOMBO, R. 2001. The actin cytoskeleton response to oxidants: from small heat shock protein phosphorylation to changes in the redox state of actin itself. *Free Radic Biol Med,* 31**,** 1624-32.
DARWIN, C. 1876. The Effects of Cross and Self-Fertilisation in the Vegetable Kingdom. *In:* MURRAY, J. (ed.). London.
DE GRAAF, B. H., RUDD, J. J., WHEELER, M. J., PERRY, R. M., BELL, E. M., OSMAN, K., FRANKLIN, F. C. & FRANKLIN-TONG, V. E. 2006. Self-incompatibility in *Papaver* targets soluble inorganic pyrophosphatases in pollen. *Nature,* 444**,** 490-3.
DE GRAAF, B. H., VATOVEC, S., JUAREZ-DIAZ, J. A., CHAI, L., KOOBLALL, K., WILKINS, K. A., ZOU, H., FORBES, T., FRANKLIN, F. C. & FRANKLIN-TONG, V. E. 2012. The Papaver Self-Incompatibility Pollen S-Determinant, PrpS, Functions in Arabidopsis thaliana. *Curr Biol,* 22**,** 154-9.
DEREEPER, A., GUIGNON, V., BLANC, G., AUDIC, S., BUFFET, S., CHEVENET, F., DUFAYARD, J. F., GUINDON, S., LEFORT, V., LESCOT, M., CLAVERIE, J. M. & GASCUEL, O. 2008. Phylogeny.fr: robust phylogenetic analysis for the non-specialist. *Nucleic Acids Res,* 36**,** W465-9.
DIETER, P. & MARME, D. 1980. Ca(2+) transport in mitochondrial and microsomal fractions from higher plants. *Planta,* 150**,** 1-8.
DIONNE, M. S. 2013. Comparative immunology: allorecognition and variable surface receptors outside the jawed vertebrates. *Curr Opin Immunol,* 25**,** 608-12.
DODD, A. N., KUDLA, J. & SANDERS, D. 2010. The language of calcium signaling. *Annu Rev Plant Biol,* 61**,** 593-620.
DOUGHTY, J., HEDDERSON, F., MCCUBBIN, A. & DICKINSON, H. 1993. Interaction between a coating-borne peptide of the Brassica pollen grain and stigmatic S (self-incompatibility)-locus-specific glycoproteins. *Proc Natl Acad Sci U S A,* 90**,** 467-71.
DRESSELHAUS, T. & FRANKLIN-TONG, N. 2013. Male-Female Cross-Talk during Pollen Germination, Tube Growth and Guidance, and Double Fertilization. *Mol Plant*.
DRESSELHAUS, T., LAUSSER, A. & MARTON, M. L. 2011. Using maize as a model to study pollen tube growth and guidance, cross-incompatibility and sperm delivery in grasses. *Ann Bot,* 108**,** 727-37.
EAVES, D. J., FLORES-ORTIZ, C., HAQUE, T., LIN, Z., TENG, N. & FRANKLIN-TONG, V. E. 2014. Self-incompatibility in Papaver: advances in integrating the signalling network. *Biochem Soc Trans,* 42**,** 370-6.
ECKARDT, N. A. 2006. Cytoplasmic Male Sterility and Fertility Restoration. *Plant Cell,* 18**,** 515-517.

ENGQVIST-GOLDSTEIN, A. E. & DRUBIN, D. G. 2003. Actin assembly and endocytosis: from yeast to mammals. *Annu Rev Cell Dev Biol,* 19**,** 287-332.

FARAH, M. E. & AMBERG, D. C. 2007. Conserved actin cysteine residues are oxidative stress sensors that can regulate cell death in yeast. *Mol Biol Cell,* 18**,** 1359-65.

FERNANDEZ GOMEZ, J. & WILSON, Z. A. 2014. A barley PHD finger transcription factor that confers male sterility by affecting tapetal development. *Plant Biotechnol J,* 12**,** 765-77.

FOOTE, H. C., RIDE, J. P., FRANKLIN-TONG, V. E., WALKER, E. A., LAWRENCE, M. J. & FRANKLIN, F. C. 1994. Cloning and expression of a distinctive class of self-incompatibility (S) gene from *Papaver rhoeas* L. *Proc Natl Acad Sci U S A,* 91**,** 2265-9.

FOSSATI, A. & INGOLD, M. 1970. A male-sterile mutant in *Triticum aestivum*. *Wheat Information Service (Kyoto),* 30**,** 2.

FRAME, M. C., FINCHAM, V. J., CARRAGHER, N. O. & WYKE, J. A. 2002. v-Src's hold over actin and cell adhesions. *Nat Rev Mol Cell Biol,* 3**,** 233-45.

FRANKLIN-TONG, N. & FRANKLIN, C. 1993. Gametophytic self-incompatibility: contrasting mechanisms for Nicotiana and *Papaver*. *Trends Cell Biol,* 3**,** 340-5.

FRANKLIN-TONG, N., RIDE, J., READ, N. D., TREWAVAS, A. J. & FRANKLIN, C. 1993a. The self-incompatibility response in *Papaver rhoeas* is mediated by cytosolic free calcium. *The Plant Journal,* 4**,** 14.

FRANKLIN-TONG, V., FRANKLIN, F. & DE, G. B. 2010. Engineering of plants to exhibit self-incompatibility. Google Patents.

FRANKLIN-TONG, V. E. 1999. Signaling and the modulation of pollen tube growth. *Plant Cell,* 11**,** 727-38.

FRANKLIN-TONG, V. E., DROBAK, B. K., ALLAN, A. C., WATKINS, P. & TREWAVAS, A. J. 1996. Growth of Pollen Tubes of *Papaver rhoeas* Is Regulated by a Slow-Moving Calcium Wave Propagated by Inositol 1,4,5-Trisphosphate. *Plant Cell,* 8**,** 1305-1321.

FRANKLIN-TONG, V. E., HACKETT, G. R. & HEPLER, P. K. 1997. Ratio-imaging of Ca2+i in the self-incompatibility response in pollen tubes of *Papaver rhoeas*. *Plant J,* 12**,** 1375-1386.

FRANKLIN-TONG, V. E., HOLDAWAY-CLARKE, T. L., STRAATMAN, K. R., KUNKEL, J. G. & HEPLER, P. K. 2002. Involvement of extracellular calcium influx in the self-incompatibility response of *Papaver rhoeas*. *Plant J,* 29**,** 333-45.

FRANKLIN-TONG, V. E., LAWRENCE, M. J. & F.C.H, F. 1988. An *in vitro* biassay for the stigmatic product of the self-incompatibility gene in *Papaver rhoeas* L. *New Phytol,* 110**,** 9.

FRANKLIN-TONG, V. E., RIDE, J. & F.C.H, F. 1995. Recombinant stigmatic self-incompatibility (S-) protein elicits a Ca2+ transient in pollen of *Papaver rhoeas*. *The Plant Journal,* 8**,** 8.

FRANKLIN-TONG, V. E., RIDE, J. P., READ, N. D., TREWAVAS, A. J. & F.C.H., F. 1993b. The self-incompatibility response in *Papaver rhoeas* is mediated by cytosolic free calcium. *Plant J,* 4**,** 14.

FRANKLIN-TONG, V. E., RUUTH, E., MARMEY, P., LAWRENCE, M. J. & FRANKLIN, F. C. H. 1989. Characterization of a stigmatic component from *Papaver rhoeas* L. which exhibits the specific activity of a self-incompatible (S-) gene product. *New Phytol,* 112**,** 8.

FRASER, J. A. & HEITMAN, J. 2004. Evolution of fungal sex chromosomes. *Mol Microbiol,* 51**,** 299-306.

GARCIA-MATA, R., BEBOK, Z., SORSCHER, E. J. & SZTUL, E. S. 1999. Characterization and dynamics of aggresome formation by a cytosolic GFP-chimera. *J Cell Biol,* 146**,** 1239-54.

GE, Y., FU, C., BHANDARI, H., BOUTON, J., BRUMMER, C. & WANG, Z. 2011. Pollen Viability and Longevity of Swithgrass (*Panicum vigatum* L.). *CROP SCIENCE,* 51.

GEE, K. R., BROWN, K. A., CHEN, W. N., BISHOP-STEWART, J., GRAY, D. & JOHNSON, I. 2000. Chemical and physiological characterization of fluo-4 Ca(2+)-indicator dyes. *Cell Calcium,* 27**,** 97-106.

GEITMANN, A., SNOWMAN, B. N., EMONS, A. M. & FRANKLIN-TONG, V. E. 2000. Alterations in the actin cytoskeleton of pollen tubes are induced by the self-incompatibility reaction in *Papaver rhoeas*. *Plant Cell,* 12**,** 1239-51.

GIAEVER, G., CHU, A. M., NI, L., CONNELLY, C., RILES, L., VERONNEAU, S., DOW, S., LUCAU-DANILA, A., ANDERSON, K., ANDRE, B., ARKIN, A. P., ASTROMOFF, A., EL-BAKKOURY, M., BANGHAM, R., BENITO, R., BRACHAT, S., CAMPANARO, S., CURTISS, M., DAVIS, K., DEUTSCHBAUER, A., ENTIAN, K. D., FLAHERTY, P., FOURY, F., GARFINKEL, D. J., GERSTEIN, M., GOTTE, D., GULDENER, U., HEGEMANN, J. H., HEMPEL, S., HERMAN, Z., JARAMILLO, D. F., KELLY, D. E., KELLY, S. L., KOTTER, P., LABONTE, D., LAMB, D. C., LAN, N., LIANG, H., LIAO, H., LIU, L., LUO, C., LUSSIER, M., MAO, R., MENARD, P., OOI, S. L., REVUELTA, J. L., ROBERTS, C. J., ROSE, M., ROSS-MACDONALD, P., SCHERENS, B., SCHIMMACK, G., SHAFER, B., SHOEMAKER, D. D., SOOKHAI-MAHADEO, S., STORMS, R. K., STRATHERN, J. N., VALLE, G., VOET, M., VOLCKAERT, G., WANG, C. Y., WARD, T. R., WILHELMY, J., WINZELER, E. A., YANG, Y., YEN, G., YOUNGMAN, E., YU, K., BUSSEY, H., BOEKE, J. D., SNYDER, M., PHILIPPSEN, P., DAVIS, R. W. & JOHNSTON, M. 2002. Functional profiling of the Saccharomyces cerevisiae genome. *Nature,* 418**,** 387-91.

GIBBON, B. C., KOVAR, D. R. & STAIGER, C. J. 1999. Latrunculin B has different effects on pollen germination and tube growth. *Plant Cell,* 11**,** 2349-63.

GILL, D. J., CHIA, J., SENEWIRATNE, J. & BARD, F. 2010. Regulation of O-glycosylation through Golgi-to-ER relocation of initiation enzymes. *J Cell Biol,* 189**,** 843-58.

GILROY, S., FRICKER, M. D., READ, N. D. & TREWAVAS, A. J. 1991. Role of Calcium in Signal Transduction of Commelina Guard Cells. *Plant Cell,* 3**,** 333-344.

GODFRAY, H. C., BEDDINGTON, J. R., CRUTE, I. R., HADDAD, L., LAWRENCE, D., MUIR, J. F., PRETTY, J., ROBINSON, S., THOMAS, S. M. & TOULMIN, C. 2010. Food security: the challenge of feeding 9 billion people. *Science,* 327**,** 812-8.

GOLDMAN, M. H., GOLDBERG, R. B. & MARIANI, C. 1994. Female sterile tobacco plants are produced by stigma-specific cell ablation. *EMBO J,* 13**,** 2976-84.

GOLDMAN, R. D., LAZARIDES, E., POLLACK, R. & WEBER, K. 1975. The distribution of actin in non-muscle cells. The use of actin antibody in the localization of actin within the microfilament bundles of mouse 3T3 cells. *Exp Cell Res,* 90**,** 333-44.

GOLDRAIJ, A., KONDO, K., LEE, C. B., HANCOCK, C. N., SIVAGURU, M., VAZQUEZ-SANTANA, S., KIM, S., PHILLIPS, T. E., CRUZ-GARCIA, F. & MCCLURE, B. 2006. Compartmentalization of S-RNase and HT-B degradation in self-incompatible Nicotiana. *Nature,* 439**,** 805-10.

GOODE, B. L., ESKIN, J. A. & WENDLAND, B. 2015. Actin and endocytosis in budding yeast. *Genetics,* 199**,** 315-58.

GORING, D. R., BANKS, P., FALLIS, L., BASZCZYNSKI, C. L., BEVERSDORF, W. D. & ROTHSTEIN, S. J. 1992. Identification of an S-locus glycoprotein allele introgressed from B. napus ssp. rapifera to B. napus ssp. oleifera. *Plant J,* 2**,** 983-9.

GOTTLIEB, R. A., GIESING, H. A., ZHU, J. Y., ENGLER, R. L. & BABIOR, B. M. 1995. Cell acidification in apoptosis: granulocyte colony-stimulating factor delays programmed cell death in neutrophils by up-regulating the vacuolar H(+)-ATPase. *Proc Natl Acad Sci U S A,* 92**,** 5965-8.

GOURLAY, C. W. & AYSCOUGH, K. R. 2005. Identification of an upstream regulatory pathway controlling actin-mediated apoptosis in yeast. *J Cell Sci,* 118**,** 2119-32.

GOURLAY, C. W., CARPP, L. N., TIMPSON, P., WINDER, S. J. & AYSCOUGH, K. R. 2004. A role for the actin cytoskeleton in cell death and aging in yeast. *J Cell Biol,* 164**,** 803-9.

GRIFFITHS, S., DUNFORD, R. P., COUPLAND, G. & LAURIE, D. A. 2003. The evolution of CONSTANS-like gene families in barley, rice, and Arabidopsis. *Plant Physiol,* 131**,** 1855-67.

GUAN, Y., GUO, J., LI, H. & YANG, Z. 2013. Signaling in pollen tube growth: crosstalk, feedback, and missing links. *Mol Plant,* 6**,** 1053-64.

HAGIWARA, S. 1973. Ca spike. *Adv Biophys,* 4**,** 71-102.

HAGIWARA, S. & NAKAJIMA, S. 1966. Differences in Na and Ca spikes as examined by application of tetrodotoxin, procaine, and manganese ions. *J Gen Physiol,* 49**,** 793-806.

HALL, A. 1998. Rho GTPases and the actin cytoskeleton. *Science,* 279**,** 509-14.

HAMILL, O. P., MARTY, A., NEHER, E., SAKMANN, B. & SIGWORTH, F. J. 1981. Improved patch-clamp techniques for high-resolution current recording from cells and cell-free membrane patches. *Pflugers Arch,* 391**,** 85-100.

HANCOCK, C. N., KENT, L. & MCCLURE, B. A. 2005. The stylar 120 kDa glycoprotein is required for S-specific pollen rejection in Nicotiana. *Plant J,* 43**,** 716-23.

HAQUE, T. 2015. *Investigating the Targets and Mechanism Regulating Self-Incompatibility in Papaver rhoeas Pollen.* PhD, University of Birmingham.

HARADA, Y., TAKAGAKI, Y., SUNAGAWA, M., SAITO, T., YAMADA, L., TANIGUCHI, H., SHOGUCHI, E. & SAWADA, H. 2008. Mechanism of self-sterility in a hermaphroditic chordate. *Science,* 320**,** 548-50.

HARWOOD, W. A. 2012. Advances and remaining challenges in the transformation of barley and wheat. *J Exp Bot,* 63**,** 1791-8.

HARWOOD, W. A., BARTLETT, J. G., ALVES, S. C., PERRY, M., SMEDLEY, M. A., LEYLAND, N. & SNAPE, J. W. 2009. Barley transformation using Agrobacterium-mediated techniques. *Methods Mol Biol,* 478**,** 137-47.

HAUGLAND, R. P., GREGORY, J., SPENCE, M. T. Z. & JOHNSON, I. D. 2002. *Handbook of fluorescent probes and research products*, Molecular Probes.

HEATH, J. P. 1983. Behaviour and structure of the leading lamella in moving fibroblasts. I. Occurrence and centripetal movement of arc-shaped microfilament bundles beneath the dorsal cell surface. *J Cell Sci,* 60**,** 331-54.

HEATH, J. P. & DUNN, G. A. 1978. Cell to substratum contacts of chick fibroblasts and their relation to the microfilament system. A correlated interference-

reflexion and high-voltage electron-microscope study. *J Cell Sci,* 29**,** 197-212.
HELLENS, R. P., EDWARDS, E. A., LEYLAND, N. R., BEAN, S. & MULLINEAUX, P. M. 2000. pGreen: a versatile and flexible binary Ti vector for Agrobacterium-mediated plant transformation. *Plant Mol Biol,* 42**,** 819-32.
HENRIKSEN, G. H. & ASSMANN, S. M. 1997. Laser-assisted patch clamping: a methodology. *Pflugers Arch,* 433**,** 832-41.
HENSEL, G., HIMMELBACH, A., CHEN, W., DOUCHKOV, D. K. & KUMLEHN, J. 2011. Transgene expression systems in the Triticeae cereals. *J Plant Physiol,* 168**,** 30-44.
HEPLER, P. K., KUNKEL, J. G., ROUNDS, C. M. & WINSHIP, L. J. 2012. Calcium entry into pollen tubes. *Trends Plant Sci,* 17**,** 32-8.
HERSKOWITZ, I. 1992. Fungal physiology. Yeast branches out. *Nature,* 357**,** 190-1.
HESLOP-HARRISON, J. 1982. Pollen-stigma interaction and cross-incompatibility in the grasses. *Science,* 215**,** 1358-64.
HESS, P., LANSMAN, J. B. & TSIEN, R. W. 1986. Calcium channel selectivity for divalent and monovalent cations. Voltage and concentration dependence of single channel current in ventricular heart cells. *J Gen Physiol,* 88**,** 293-319.
HIGASHIYAMA, T. & TAKEUCHI, H. 2015. The mechanism and key molecules involved in pollen tube guidance. *Annu Rev Plant Biol,* 66**,** 393-413.
HO, J. & BRETSCHER, A. 2001. Ras regulates the polarity of the yeast actin cytoskeleton through the stress response pathway. *Mol Biol Cell,* 12**,** 1541-55.
HOLDAWAY-CLARKE, T. L., FEIJO, J. A., HACKETT, G. R., KUNKEL, J. G. & HEPLER, P. K. 1997. Pollen Tube Growth and the Intracellular Cytosolic Calcium Gradient Oscillate in Phase while Extracellular Calcium Influx Is Delayed. *Plant Cell,* 9**,** 1999-2010.
HOMA, S. T. & SWANN, K. 1994. A cytosolic sperm factor triggers calcium oscillations and membrane hyperpolarizations in human oocytes. *Hum Reprod,* 9**,** 2356-61.
HOODBHOY, T. & DEAN, J. 2004. Insights into the molecular basis of sperm-egg recognition in mammals. *Reproduction,* 127**,** 417-22.
HORWITZ, A., DUGGAN, K., BUCK, C., BECKERLE, M. C. & BURRIDGE, K. 1986. Interaction of plasma membrane fibronectin receptor with talin--a transmembrane linkage. *Nature,* 320**,** 531-3.
HUA, Z. H., FIELDS, A. & KAO, T. H. 2008. Biochemical models for S-RNase-based self-incompatibility. *Mol Plant,* 1**,** 575-85.
HUSSEY, P. J., KETELAAR, T. & DEEKS, M. J. 2006. Control of the actin cytoskeleton in plant cell growth. *Annu Rev Plant Biol,* 57**,** 109-25.
HWANG, I., CHEN, H. C. & SHEEN, J. 2002. Two-component signal transduction pathways in Arabidopsis. *Plant Physiol,* 129**,** 500-15.
ILIC, D., FURUTA, Y., KANAZAWA, S., TAKEDA, N., SOBUE, K., NAKATSUJI, N., NOMURA, S., FUJIMOTO, J., OKADA, M. & YAMAMOTO, T. 1995. Reduced cell motility and enhanced focal adhesion contact formation in cells from FAK-deficient mice. *Nature,* 377**,** 539-44.
INATOMI, K. & SLAUGHTER, J. C. 1971. The Role of Glutamate Decarboxylase and γ -Aminobutiric Acid in Germinating Barley. *J Exp Bot,* 22**,** 10.

IWANO, M., SHIBA, H., MIWA, T., CHE, F. S., TAKAYAMA, S., NAGAI, T., MIYAWAKI, A. & ISOGAI, A. 2004. Ca2+ dynamics in a pollen grain and papilla cell during pollination of Arabidopsis. *Plant Physiol,* 136**,** 3562-71.

IWANO, M. & TAKAYAMA, S. 2012. Self/non-self discrimination in angiosperm self-incompatibility. *Curr Opin Plant Biol,* 15**,** 78-83.

JAFFE, A. B. & HALL, A. 2005. Rho GTPases: biochemistry and biology. *Annu Rev Cell Dev Biol,* 21**,** 247-69.

JORDAN, N. D., FRANKLIN, F. C. & FRANKLIN-TONG, V. E. 2000. Evidence for DNA fragmentation triggered in the self-incompatibility response in pollen of *Papaver rhoeas*. *Plant J,* 23**,** 471-9.

KAKEDA, K. 2009. S locus-linked F-box genes expressed in anthers of Hordeum bulbosum. *Plant Cell Rep,* 28**,** 1453-60.

KAKEDA, K., IBUKI, T., SUZUKI, J., TADANO, H., KURITA, Y., HANAI, Y. & KOWYAMA, Y. 2008. Molecular and genetic characterization of the S locus in Hordeum bulbosum L., a wild self-incompatible species related to cultivated barley. *Mol Genet Genomics,* 280**,** 509-19.

KAKEDA, K., JORDAN, N. D., CONNER, A., RIDE, J. P., FRANKLIN-TONG, V. E. & FRANKLIN, F. C. 1998. Identification of residues in a hydrophilic loop of the *Papaver rhoeas* S protein that play a crucial role in recognition of incompatible pollen. *Plant Cell,* 10**,** 1723-32.

KANDASAMY, M. K., PAOLILLO, D. J., FARADAY, C. D., NASRALLAH, J. B. & NASRALLAH, M. E. 1989. The S-locus specific glycoproteins of Brassica accumulate in the cell wall of developing stigma papillae. *Dev Biol,* 134**,** 462-72.

KARMAZINOVA, M. & LACINOVA, L. 2010. Measurement of cellular excitability by whole cell patch clamp technique. *Physiol Res,* 59 Suppl 1**,** S1-7.

KENNELLY, P. J. & POTTS, M. 1996. Fancy meeting you here! A fresh look at "prokaryotic" protein phosphorylation. *J Bacteriol,* 178**,** 4759-64.

KHATUN, S. & FLOWER, T. J. 1995. The estimation of pollen viability in rice. *Journal of Experimental Botany,* 46.

KIM, H. & MCCULLOCH, C. A. 2011. Filamin A mediates interactions between cytoskeletal proteins that control cell adhesion. *FEBS Lett,* 585**,** 18-22.

KIM, T. K. & EBERWINE, J. H. 2010. Mammalian cell transfection: the present and the future. *Anal Bioanal Chem,* 397**,** 3173-8.

KITASHIBA, H., LIU, P., NISHIO, T., NASRALLAH, J. B. & NASRALLAH, M. E. 2011. Functional test of Brassica self-incompatibility modifiers in Arabidopsis thaliana. *Proc Natl Acad Sci U S A,* 108**,** 18173-8.

KLAAS, M., YANG, B., BOSCH, M., THOROGOOD, D., MANZANARES, C., ARMSTEAD, I. P., FRANKLIN, F. C. & BARTH, S. 2011. Progress towards elucidating the mechanisms of self-incompatibility in the grasses: further insights from studies in Lolium. *Ann Bot,* 108**,** 677-85.

KO, K. S., ARORA, P. D., BHIDE, V., CHEN, A. & MCCULLOCH, C. A. 2001. Cell-cell adhesion in human fibroblasts requires calcium signaling. *J Cell Sci,* 114**,** 1155-67.

KREIS, T. E. & BIRCHMEIER, W. 1980. Stress fiber sarcomeres of fibroblasts are contractile. *Cell,* 22**,** 555-61.

KUBO, K., ENTANI, T., TAKARA, A., WANG, N., FIELDS, A. M., HUA, Z., TOYODA, M., KAWASHIMA, S., ANDO, T., ISOGAI, A., KAO, T. H. & TAKAYAMA, S. 2010.

Collaborative non-self recognition system in S-RNase-based self-incompatibility. *Science,* 330**,** 796-9.
LAEMMLI 1970. Cleavage of structural proteins during the assembly of the head of bacteriophage T4. *Nature,* 227**,** 5.
LAWRENCE, M. J., AFZAL, M. & KENRICK, J. 1978. The Genetical Control of Self-incompatibility in *Papaver roheas*. *Heredity* 40**,** 14.
LEADSHAM, J. E., KOTIADIS, V. N., TARRANT, D. J. & GOURLAY, C. W. 2010. Apoptosis and the yeast actin cytoskeleton. *Cell Death Differ,* 17**,** 754-62.
LEE, S. H. & DOMINGUEZ, R. 2010. Regulation of actin cytoskeleton dynamics in cells. *Mol Cells,* 29**,** 311-25.
LEONARD, C. J., ARAVIND, L. & KOONIN, E. V. 1998. Novel families of putative protein kinases in bacteria and archaea: evolution of the "eukaryotic" protein kinase superfamily. *Genome Res,* 8**,** 1038-47.
LEVINGS, C. S., 3RD 1993. Thoughts on Cytoplasmic Male Sterility in cms-T Maize. *Plant Cell,* 5**,** 1285-1290.
LI, G., LIANG, W., ZHANG, X., REN, H., HU, J., BENNETT, M. J. & ZHANG, D. 2014. Rice actin-binding protein RMD is a key link in the auxin-actin regulatory loop that controls cell growth. *Proc Natl Acad Sci U S A,* 111**,** 10377-82.
LI, S., SAMAJ, J. & FRANKLIN-TONG, V. E. 2007. A mitogen-activated protein kinase signals to programmed cell death induced by self-incompatibility in *Papaver* pollen. *Plant Physiol,* 145**,** 236-45.
LIN, Z. 2015. *Functional Transfer of the Papaver SI system into Self-Compatible A. thaliana and Investigating the Role of the Proteasome in the Papaver SI Response.* PhD, University of Birmingham.
LIPPMAN, Z. B. & ZAMIR, D. 2007. Heterosis: revisiting the magic. *Trends Genet,* 23**,** 60-6.
LIPSCOMBE, D., MADISON, D. V., POENIE, M., REUTER, H., TSIEN, R. Y. & TSIEN, R. W. 1988. Spatial distribution of calcium channels and cytosolic calcium transients in growth cones and cell bodies of sympathetic neurons. *Proc Natl Acad Sci U S A,* 85**,** 2398-402.
LIU, P., SHERMAN-BROYLES, S., NASRALLAH, M. E. & NASRALLAH, J. B. 2007. A cryptic modifier causing transient self-incompatibility in Arabidopsis thaliana. *Curr Biol,* 17**,** 734-40.
LIU, Y., YAN, Z., CHEN, N., DI, X., HUANG, J. & GUO, G. 2010. Development and function of central cell in angiosperm female gametophyte. *Genesis,* 48**,** 466-78.
LONGIN, C. F., MUHLEISEN, J., MAURER, H. P., ZHANG, H., GOWDA, M. & REIF, J. C. 2012. Hybrid breeding in autogamous cereals. *Theor Appl Genet,* 125**,** 1087-96.
LUNDQVIST, A. 1954. Studies on Self-Sterility in Rye, Secale Cereale L. *Hereditas,* 40**,** 16.
MAATHUIS, J. M., TAYLOR, A. R., ASSMANN, S. M. & SANDERS, D. 1997. Seal-promoting solutions and pipette perfusion for patch clamping plant cells. *Plant J,* 11**,** 891-6.
MADEO, F., FROHLICH, E. & FROHLICH, K. U. 1997. A yeast mutant showing diagnostic markers of early and late apoptosis. *J Cell Biol,* 139**,** 729-34.
MATSUYAMA, S., LLOPIS, J., DEVERAUX, Q. L., TSIEN, R. Y. & REED, J. C. 2000. Changes in intramitochondrial and cytosolic pH: early events that modulate caspase activation during apoptosis. *Nat Cell Biol,* 2**,** 318-25.

MAYER, K. F., WAUGH, R., BROWN, J. W., SCHULMAN, A., LANGRIDGE, P., PLATZER, M., FINCHER, G. B., MUEHLBAUER, G. J., SATO, K., CLOSE, T. J., WISE, R. P. & STEIN, N. 2012. A physical, genetic and functional sequence assembly of the barley genome. *Nature,* 491**,** 711-6.

MAZZURCO, M., SULAMAN, W., ELINA, H., COCK, J. M. & GORING, D. R. 2001. Further analysis of the interactions between the Brassica S receptor kinase and three interacting proteins (ARC1, THL1 and THL2) in the yeast two-hybrid system. *Plant Mol Biol,* 45**,** 365-76.

MCCLURE, B., CRUZ-GARCIA, F. & ROMERO, C. 2011. Compatibility and incompatibility in S-RNase-based systems. *Ann Bot,* 108**,** 647-58.

MCCLURE, B. A. & FRANKLIN-TONG, V. 2006. Gametophytic self-incompatibility: understanding the cellular mechanisms involved in "self" pollen tube inhibition. *Planta,* 224**,** 233-45.

MESSERLI, M. & ROBINSON, K. R. 1997. Tip localized Ca2+ pulses are coincident with peak pulsatile growth rates in pollen tubes of Lilium longiflorum. *J Cell Sci,* 110 (Pt 11)**,** 1269-78.

MILLER, D. D., SCORDILIS, S. P. & HEPLER, P. K. 1995. Identification and localization of three classes of myosins in pollen tubes of Lilium longiflorum and Nicotiana alata. *J Cell Sci,* 108 (Pt 7)**,** 2549-63.

MINET, M., DUFOUR, M. E. & LACROUTE, F. 1992. Complementation of Saccharomyces cerevisiae auxotrophic mutants by Arabidopsis thaliana cDNAs. *Plant J,* 2**,** 417-22.

MIRALLES, F., POSERN, G., ZAROMYTIDOU, A. I. & TREISMAN, R. 2003. Actin dynamics control SRF activity by regulation of its coactivator MAL. *Cell,* 113**,** 329-42.

MOSHELION, M. & ALTMAN, A. 2015. Current challenges and future perspectives of plant and agricultural biotechnology. *Trends Biotechnol,* 33**,** 337-42.

MOWLA, S. B., CUYPERS, A., DRISCOLL, S. P., KIDDLE, G., THOMSON, J., FOYER, C. H. & THEODOULOU, F. L. 2006. Yeast complementation reveals a role for an Arabidopsis thaliana late embryogenesis abundant (LEA)-like protein in oxidative stress tolerance. *Plant J,* 48**,** 743-56.

MUNOZ-AMATRIAIN, M., LONARDI, S., LUO, M., MADISHETTY, K., SVENSSON, J. T., MOSCOU, M. J., WANAMAKER, S., JIANG, T., KLEINHOFS, A., MUEHLBAUER, G. J., WISE, R. P., STEIN, N., MA, Y., RODRIGUEZ, E., KUDRNA, D., BHAT, P. R., CHAO, S., CONDAMINE, P., HEINEN, S., RESNIK, J., WING, R., WITT, H. N., ALPERT, M., BECCUTI, M., BOZDAG, S., CORDERO, F., MIREBRAHIM, H., OUNIT, R., WU, Y., YOU, F., ZHENG, J., SIMKOVA, H., DOLEZEL, J., GRIMWOOD, J., SCHMUTZ, J., DUMA, D., ALTSCHMIED, L., BLAKE, T., BREGITZER, P., COOPER, L., DILBIRLIGI, M., FALK, A., FEIZ, L., GRANER, A., GUSTAFSON, P., HAYES, P. M., LEMAUX, P., MAMMADOV, J. & CLOSE, T. J. 2015. Sequencing of 15,622 gene-bearing BACs clarifies the gene-dense regions of the barley genome. *Plant J*.

MURASE, K., SHIBA, H., IWANO, M., CHE, F. S., WATANABE, M., ISOGAI, A. & TAKAYAMA, S. 2004. A membrane-anchored protein kinase involved in Brassica self-incompatibility signaling. *Science,* 303**,** 1516-9.

NAGASE, H., FUKUYAMA, H., TANAKA, M., KAWANE, K. & NAGATA, S. 2003. Mutually regulated expression of caspase-activated DNase and its inhibitor for apoptotic DNA fragmentation. *Cell Death Differ,* 10**,** 142-3.

NAGATA, T., IIZUMI, S., SATOH, K., OOKA, H., KAWAI, J., CARNINCI, P., HAYASHIZAKI, Y., OTOMO, Y., MURAKAMI, K., MATSUBARA, K. & KIKUCHI, S. 2004. Comparative analysis of plant and animal calcium signal transduction element using plant full-length cDNA data. *Mol Biol Evol,* 21**,** 1855-70.

NARUMIYA, S., ISHIZAKI, T. & WATANABE, N. 1997. Rho effectors and reorganization of actin cytoskeleton. *FEBS Lett,* 410**,** 68-72.

NASRALLAH, M. E., LIU, P. & NASRALLAH, J. B. 2002. Generation of self-incompatible Arabidopsis thaliana by transfer of two S locus genes from A. lyrata. *Science,* 297**,** 247-9.

NASRALLAH, M. E., LIU, P., SHERMAN-BROYLES, S., BOGGS, N. A. & NASRALLAH, J. B. 2004. Natural variation in expression of self-incompatibility in Arabidopsis thaliana: implications for the evolution of selfing. *Proc Natl Acad Sci U S A,* 101**,** 16070-4.

NELSON, D. E., REPETTI, P. P., ADAMS, T. R., CREELMAN, R. A., WU, J., WARNER, D. C., ANSTROM, D. C., BENSEN, R. J., CASTIGLIONI, P. P., DONNARUMMO, M. G., HINCHEY, B. S., KUMIMOTO, R. W., MASZLE, D. R., CANALES, R. D., KROLIKOWSKI, K. A., DOTSON, S. B., GUTTERSON, N., RATCLIFFE, O. J. & HEARD, J. E. 2007. Plant nuclear factor Y (NF-Y) B subunits confer drought tolerance and lead to improved corn yields on water-limited acres. *Proc Natl Acad Sci U S A,* 104**,** 16450-5.

NELSON, D. L., NELSON, D. L., LEHNINGER, A. L. & COX, M. M. 2008. *Lehninger principles of biochemistry,* New York, W.H. Freeman.

NICOLIA, A., MANZO, A., VERONESI, F. & ROSELLINI, D. 2014. An overview of the last 10 years of genetically engineered crop safety research. *Crit Rev Biotechnol,* 34**,** 77-88.

NOBES, C. D., LAURITZEN, I., MATTEI, M. G., PARIS, S., HALL, A. & CHARDIN, P. 1998. A new member of the Rho family, Rnd1, promotes disassembly of actin filament structures and loss of cell adhesion. *J Cell Biol,* 141**,** 187-97.

O'BRIEN, M., MAJOR, G., CHANTA, S.-C. & MATTON, D. P. 2004. Isolation of S-RNase binding proteins from *Solanum chacoense*: identification of an SBP1 (RING finger prtoein) orthologue. *Sexual Plant Reproduction,* 17**,** 6.

ODAKA, C., SANDERS, M. L. & CREWS, P. 2000. Jasplakinolide induces apoptosis in various transformed cell lines by a caspase-3-like protease-dependent pathway. *Clin Diagn Lab Immunol,* 7**,** 947-52.

OHASHI, K., NAGATA, K., MAEKAWA, M., ISHIZAKI, T., NARUMIYA, S. & MIZUNO, K. 2000. Rho-associated kinase ROCK activates LIM-kinase 1 by phosphorylation at threonine 508 within the activation loop. *J Biol Chem,* 275**,** 3577-82.

OOSAWA, Y. 1989. Ionic currents of channels that are permeable to monovalent and divalent cations. *Biophys J,* 56**,** 1217-23.

PANCHUK-VOLOSHINA, N., HAUGLAND, R. P., BISHOP-STEWART, J., BHALGAT, M. K., MILLARD, P. J., MAO, F., LEUNG, W. Y. & HAUGLAND, R. P. 1999. Alexa dyes, a series of new fluorescent dyes that yield exceptionally bright, photostable conjugates. *J Histochem Cytochem,* 47**,** 1179-88.

PAPIN, J. A., HUNTER, T., PALSSON, B. O. & SUBRAMANIAM, S. 2005. Reconstruction of cellular signalling networks and analysis of their properties. *Nat Rev Mol Cell Biol,* 6**,** 99-111.

PARZIES, H. K., SCHNAITHMANN, F. & GEIGER, H. H. 2005. Pollen viability of *Hordeum ssp* genopypes with different flowering characteristics. *Euphytica,* 145**,** 6.

PELLEGRIN, S. & MELLOR, H. 2007. Actin stress fibres. *J Cell Sci,* 120**,** 3491-9.

PHUMICHAI, C. & HOSAKA, K. 2006. Cryptic improvement for fertility by continuous selfing of diploid popatoes using *Sli* gene. *Euphytica,* 149**,** 7.

POULTER, N. S. 2009. *INVESTIGATING THE ROLE OF THE CYTOSKELETON AND SIGNALLING IN THE SELF-INCOMPATIBILITY RESPONSE OF PAPAVER RHOEAS.* DOCTOR OF PTHYLOSOPHY, University of Brimingham.

POULTER, N. S., BOSCH, M. & FRANKLIN-TONG, V. E. 2011. Proteins implicated in mediating self-incompatibility-induced alterations to the actin cytoskeleton of *Papaver* pollen. *Ann Bot,* 108**,** 659-75.

POULTER, N. S., STAIGER, C. J., RAPPOPORT, J. Z. & FRANKLIN-TONG, V. E. 2010. Actin-binding proteins implicated in the formation of the punctate actin foci stimulated by the self-incompatibility response in *Papaver*. *Plant Physiol,* 152**,** 1274-83.

POULTER, N. S., VATOVEC, S. & FRANKLIN-TONG, V. E. 2008. Microtubules are a target for self-incompatibility signaling in *Papaver* pollen. *Plant Physiol,* 146**,** 1358-67.

RANTY, B., ALDON, D. & GALAUD, J. P. 2006. Plant calmodulins and calmodulin-related proteins: multifaceted relays to decode calcium signals. *Plant Signal Behav,* 1**,** 96-104.

RAPPOPORT, J. Z. & SIMON, S. M. 2008. A functional GFP fusion for imaging clathrin-mediated endocytosis. *Traffic,* 9**,** 1250-5.

REA, A. C. & NASRALLAH, J. B. 2008. Self-incompatibility systems: barriers to self-fertilization in flowering plants. *Int J Dev Biol,* 52**,** 627-36.

RHINER, C., LOPEZ-GAY, J. M., SOLDINI, D., CASAS-TINTO, S., MARTIN, F. A., LOMBARDIA, L. & MORENO, E. 2010. Flower forms an extracellular code that reveals the fitness of a cell to its neighbors in Drosophila. *Dev Cell,* 18**,** 985-98.

RIDLEY, A. J. & HALL, A. 1992. The small GTP-binding protein rho regulates the assembly of focal adhesions and actin stress fibers in response to growth factors. *Cell,* 70**,** 389-99.

ROOKE, L., BYRNE, D. & SALGUEIRO, S. 2000. Marker gene expression driven by the maize ubiquitin promoter in transgenic wheat. *Annals of Applied Biology,* 136**,** 167-172.

RUDD, J. J., FRANKLIN, F., LORD, J. M. & FRANKLIN-TONG, V. E. 1996. Increased Phosphorylation of a 26-kD Pollen Protein Is Induced by the Self-Incompatibility Response in *Papaver rhoeas*. *Plant Cell,* 8**,** 713-724.

RUDD, J. J. & FRANKLIN-TONG, V. E. 2003. Signals and targets of the self-incompatibility response in pollen of *Papaver rhoeas. J Exp Bot,* 54**,** 141-8.

RUDD, J. J., OSMAN, K., FRANKLIN, F. C. & FRANKLIN-TONG, V. E. 2003. Activation of a putative MAP kinase in pollen is stimulated by the self-incompatibility (SI) response. *FEBS Lett,* 547**,** 223-7.

SAITO, T., SHIBA, K., INABA, K., YAMADA, L. & SAWADA, H. 2012. Self-incompatibility response induced by calcium increase in sperm of the ascidian Ciona intestinalis. *Proc Natl Acad Sci U S A,* 109**,** 4158-62.

SAKMANN, B. & NEHER, E. 1984. Patch clamp techniques for studying ionic channels in excitable membranes. *Annu Rev Physiol,* 46**,** 455-72.

SAMBROOK, J., MANIATIS, T. & FRITSCH, E. F. 1989. *Molecular cloning : a laboratory manual,* Cold Spring Harbor, N.Y., Cold Spring Harbor Laboratory Press.

SAMUEL, M. A., CHONG, Y. T., HAASEN, K. E., ALDEA-BRYDGES, M. G., STONE, S. L. & GORING, D. R. 2009. Cellular pathways regulating responses to compatible and self-incompatible pollen in Brassica and Arabidopsis stigmas intersect at Exo70A1, a putative component of the exocyst complex. *Plant Cell,* 21**,** 2655-71.

SAWADA, H., INOUE, N. & IWANO, M. 2014. *Sexual Reproduction in Animal and Plants*, Springer Open.

SCHLUTER, K., JOCKUSCH, B. M. & ROTHKEGEL, M. 1997. Profilins as regulators of actin dynamics. *Biochim Biophys Acta,* 1359**,** 97-109.

SCHNEIDER, C. A., RASBAND, W. S. & ELICEIRI, K. W. 2012. NIH Image to ImageJ: 25 years of image analysis. *Nat Methods,* 9**,** 671-5.

SCHOPFER, C. R., NASRALLAH, M. E. & NASRALLAH, J. B. 1999. The male determinant of self-incompatibility in Brassica. *Science,* 286**,** 1697-700.

SCHWARZ, D., DOTSCH, V. & BERNHARD, F. 2008. Production of membrane proteins using cell-free expression systems. *Proteomics,* 8**,** 3933-46.

SHIGAKI, T. & BHATTACHARYYA, M. K. 1999. Color coding the cell death status of plant suspension cells. *Biotechniques,* 26**,** 1060-2.

SHULL, G. H. 1908. The Composition of a Field of Maize. *Journal of Heredity,* os-4**,** 296-301.

SILVA, N. F., STONE, S. L., CHRISTIE, L. N., SULAMAN, W., NAZARIAN, K. A., BURNETT, L. A., ARNOLDO, M. A., ROTHSTEIN, S. J. & GORING, D. R. 2001. Expression of the S receptor kinase in self-compatible Brassica napus cv. Westar leads to the allele-specific rejection of self-incompatible Brassica napus pollen. *Mol Genet Genomics,* 265**,** 552-9.

SMALL, J. V., ROTTNER, K., KAVERINA, I. & ANDERSON, K. I. 1998. Assembling an actin cytoskeleton for cell attachment and movement. *Biochim Biophys Acta,* 1404**,** 271-81.

SMERTENKO, A. P., DEEKS, M. J. & HUSSEY, P. J. 2010. Strategies of actin reorganisation in plant cells. *J Cell Sci,* 123**,** 3019-28.

SNOWMAN, B. N., KOVAR, D. R., SHEVCHENKO, G., FRANKLIN-TONG, V. E. & STAIGER, C. J. 2002. Signal-mediated depolymerization of actin in pollen during the self-incompatibility response. *Plant Cell,* 14**,** 2613-26.

SONG, X., MA, Q., HAO, X. & LI, H. 2012. Roles of the actin cytoskeleton and an actin-binding protein in wheat resistance against Puccinia striiformis f. sp. tritici. *Protoplasma,* 249**,** 99-106.

STAIGER, C. J. 2000. Signaling to the Actin Cytoskeleton in Plants. *Annu Rev Plant Physiol Plant Mol Biol,* 51**,** 257-288.

STAIGER, C. J., GOODBODY, K. C., HUSSEY, P. J., VALENTA, R., DROBAK, B. K. & LLOYD, C. W. 1993. The profilin multigene family of maize: differential expression of three isoforms. *Plant J,* 4**,** 631-41.

STAIGER, C. J., POULTER, N. S., HENTY, J. L., FRANKLIN-TONG, V. E. & BLANCHOIN, L. 2010. Regulation of actin dynamics by actin-binding proteins in pollen. *J Exp Bot,* 61**,** 1969-86.

STERN, B., OLSEN, L. C., TRÖBE, C., RAVNEBERG, H. & PRYME, I. F. 1997. Improving mammalian cell factories: The selection of signal peptide has a major

impact in recombinant protein synthesis and secretion in mammalian cells. *Trends in Cell & Molecular Biology,* 2**,** 17.

STONE, S. L., ANDERSON, E. M., MULLEN, R. T. & GORING, D. R. 2003. ARC1 is an E3 ubiquitin ligase and promotes the ubiquitination of proteins during the rejection of self-incompatible Brassica pollen. *Plant Cell,* 15**,** 885-98.

SUDO, K., PARK, J. I., SAKAZONO, S., MASUKO-SUZUKI, H., OSAKA, M., KAWAGISHI, M., FUJITA, K., MARUOKA, M., NANJO, H., SUZUKI, G., SUWABE, K. & WATANABE, M. 2013. Demonstration in vivo of the role of Arabidopsis PLIM2 actin-binding proteins during pollination. *Genes Genet Syst,* 88**,** 279-87.

SWARBRECK, S. M., COLACO, R. & DAVIES, J. M. 2013. Plant calcium-permeable channels. *Plant Physiol,* 163**,** 514-22.

SYNGENTA. 2013. *HyvidoTM Cash Back Yield Guarantee [online]* [Online]. http://www3.syngenta.com/country/uk/en/Crops/Cereals/Hyvido/Pages/HybridBarley.aspx. 2015].

SZABO, I., NEGRO, A., DOWNEY, P. M., ZORATTI, M., LO SCHIAVO, F. & GIACOMETTI, G. M. 2000. Temperature-dependent functional expression of a plant K(+) channel in mammalian cells. *Biochem Biophys Res Commun,* 274**,** 130-5.

TAKASAKI, T., HATAKEYAMA, K., SUZUKI, G., WATANABE, M., ISOGAI, A. & HINATA, K. 2000. The S receptor kinase determines self-incompatibility in Brassica stigma. *Nature,* 403**,** 913-6.

TAKAYAMA, S. & ISOGAI, A. 2005. Self-incompatibility in plants. *Annu Rev Plant Biol,* 56**,** 467-89.

TAKAYAMA, S., SHIMOSATO, H., SHIBA, H., FUNATO, M., CHE, F. S., WATANABE, M., IWANO, M. & ISOGAI, A. 2001. Direct ligand-receptor complex interaction controls Brassica self-incompatibility. *Nature,* 413**,** 534-8.

TANSENGCO, M. L., IMAIZUMI-ANRAKU, H., YOSHIKAWA, M., TAKAGI, S., KAWAGUCHI, M., HAYASHI, M. & MUROOKA, Y. 2004. Pollen development and tube growth are affected in the symbiotic mutant of Lotus japonicus, crinkle. *Plant Cell Physiol,* 45**,** 511-20.

TAYLOR, C. B. 1998. Defense responses in plants and animals--more of the same. *Plant Cell,* 10**,** 873-6.

TAYLOR, L. P. & HEPLER, P. K. 1997. Pollen Germination and Tube Growth. *Annu Rev Plant Physiol Plant Mol Biol,* 48**,** 461-491.

TESTER, M. & LANGRIDGE, P. 2010. Breeding technologies to increase crop production in a changing world. *Science,* 327**,** 818-22.

THOMAS, C., THOLL, S., MOES, D., DIETERLE, M., PAPUGA, J., MOREAU, F. & STEINMETZ, A. 2009. Actin bundling in plants. *Cell Motil Cytoskeleton,* 66**,** 940-57.

THOMAS, D., TOVEY, S. C., COLLINS, T. J., BOOTMAN, M. D., BERRIDGE, M. J. & LIPP, P. 2000. A comparison of fluorescent Ca2+ indicator properties and their use in measuring elementary and global Ca2+ signals. *Cell Calcium,* 28**,** 213-23.

THOMAS, S. G. & FRANKLIN-TONG, V. E. 2004. Self-incompatibility triggers programmed cell death in *Papaver* pollen. *Nature,* 429**,** 305-9.

THOMAS, S. G., HUANG, S., LI, S., STAIGER, C. J. & FRANKLIN-TONG, V. E. 2006. Actin depolymerization is sufficient to induce programmed cell death in self-incompatible pollen. *J Cell Biol,* 174**,** 221-9.

TOJKANDER, S., GATEVA, G. & LAPPALAINEN, P. 2012. Actin stress fibers--assembly, dynamics and biological roles. *J Cell Sci,* 125**,** 1855-64.
TOJKANDER, S., GATEVA, G., SCHEVZOV, G., HOTULAINEN, P., NAUMANEN, P., MARTIN, C., GUNNING, P. W. & LAPPALAINEN, P. 2011. A molecular pathway for myosin II recruitment to stress fibers. *Curr Biol,* 21**,** 539-50.
TOWBIN, H., STAEHELIN, T. & GORDON, J. 1979. Electrophoretic transfer of proteins from polyacrylamide gels to nitrocellulose sheets: procedure and some applications. *Proc Natl Acad Sci U S A,* 76**,** 4350-4.
TRAVELLA, S., ROSS, S. M., HARDEN, J., EVERETT, C., SNAPE, J. W. & HARWOOD, W. A. 2005. A comparison of transgenic barley lines produced by particle bombardment and Agrobacterium-mediated techniques. *Plant Cell Rep,* 23**,** 780-9.
TREWAVAS, A. J. & MALHO, R. 1998. Ca2+ signalling in plant cells: the big network! *Curr Opin Plant Biol,* 1**,** 428-33.
TROMBETTA, E. S. & PARODI, A. J. 2003. Quality control and protein folding in the secretory pathway. *Annu Rev Cell Dev Biol,* 19**,** 649-76.
TSIEN, R. Y. 1988. Fluorescence measurement and photochemical manipulation of cytosolic free calcium. *Trends Neurosci,* 11**,** 419-24.
TUDOR, R. 2009. *Identification od a Mitogen-Activated Protein Kinase p56, which Mediated the Self-Incompatibility Response in Papaver rhoeas.* PhD, University of Birmingham.
TUNISTRA, M. R. & WEDEL, J. 2000. Estimation of pollen viability in grain sorghum. *CROP SCIENCE,* 40**,** 3.
UOZUMI, N., NAKAMURA, T., SCHROEDER, J. I. & MUTO, S. 1998. Determination of transmembrane topology of an inward-rectifying potassium channel from Arabidopsis thaliana based on functional expression in Escherichia coli. *Proc Natl Acad Sci U S A,* 95**,** 9773-8.
VATOVEC, S. 2012. *Investigating the Mechanism of Self-Incompatibility in Papaver roheas and Functional Transfer of Papaver S-Determinants to Arabidopsis thaliana.* PhD, University of Birmingham.
VERHOEVEN, T., FERON, R., WOLTERS-ARTS, M., EDQVIST, J., GERATS, T., DERKSEN, J. & MARIANI, C. 2005. STIG1 controls exudate secretion in the pistil of petunia and tobacco. *Plant Physiol,* 138**,** 153-60.
VERY, A. A. & DAVIES, J. M. 2000. Hyperpolarization-activated calcium channels at the tip of Arabidopsis root hairs. *Proc Natl Acad Sci U S A,* 97**,** 9801-6.
VITALE, A. & RAIKHEL, N. V. 1999. What do proteins need to reach different vacuoles? *Trends Plant Sci,* 4**,** 149-155.
WANG, H. J., WAN, A. R. & JAUH, G. Y. 2008. An actin-binding protein, LlLIM1, mediates calcium and hydrogen regulation of actin dynamics in pollen tubes. *Plant Physiol,* 147**,** 1619-36.
WANG, P., HAWKINS, T. J., RICHARDSON, C., CUMMINS, I., DEEKS, M. J., SPARKES, I., HAWES, C. & HUSSEY, P. J. 2014. The plant cytoskeleton, NET3C, and VAP27 mediate the link between the plasma membrane and endoplasmic reticulum. *Curr Biol,* 24**,** 1397-405.
WELSCH, R., WUST, F., BAR, C., AL-BABILI, S. & BEYER, P. 2008. A third phytoene synthase is devoted to abiotic stress-induced abscisic acid formation in rice and defines functional diversification of phytoene synthase genes. *Plant Physiol,* 147**,** 367-80.

WHEELER, M. J., DE GRAAF, B. H., HADJIOSIF, N., PERRY, R. M., POULTER, N. S., OSMAN, K., VATOVEC, S., HARPER, A., FRANKLIN, F. C. & FRANKLIN-TONG, V. E. 2009. Identification of the pollen self-incompatibility determinant in *Papaver rhoeas*. *Nature,* 459**,** 992-5.

WHEELER, M. J., VATOVEC, S. & FRANKLIN-TONG, V. E. 2010. The pollen S-determinant in *Papaver*: comparisons with known plant receptors and protein ligand partners. *J Exp Bot,* 61**,** 2015-25.

WILKINS, K. A., BANCROFT, J., BOSCH, M., INGS, J., SMIRNOFF, N. & FRANKLIN-TONG, V. E. 2011. Reactive oxygen species and nitric oxide mediate actin reorganization and programmed cell death in the self-incompatibility response of *Papaver*. *Plant Physiol,* 156**,** 404-16.

WILKINS, K. A., BOSCH, M., HAQUE, T., TENG, N., POULTER, N. S. & FRANKLIN-TONG, V. E. 2015. Self-incompatibility-induced programmed cell death in field poppy pollen involves dramatic acidification of the incompatible pollen tube cytosol. *Plant Physiol,* 167**,** 766-79.

WOO, H. J., QIN, Y., PARK, S. Y., PARK, S. K., CHO, Y. G., SHIN, K. S., LIM, M. H. & CHO, H. S. 2015. Development of Selectable Marker-Free Transgenic Rice Plants with Enhanced Seed Tocopherol Content through FLP/FRT-Mediated Spontaneous Auto-Excision. *PLoS One,* 10**,** e0132667.

WOZNIAK, M. A., MODZELEWSKA, K., KWONG, L. & KEELY, P. J. 2004. Focal adhesion regulation of cell behavior. *Biochim Biophys Acta,* 1692**,** 103-19.

WU, J., WANG, S., GU, Y., ZHANG, S., PUBLICOVER, S. J. & FRANKLIN-TONG, V. E. 2011. Self-incompatibility in *Papaver rhoeas* activates nonspecific cation conductance permeable to Ca2+ and K+. *Plant Physiol,* 155**,** 963-73.

WYRSCH, P., BLENN, C., PESCH, T., BENEKE, S. & ALTHAUS, F. R. 2013. Cytosolic Ca2+ shifts as early markers of cytotoxicity. *Cell Commun Signal,* 11**,** 11.

YAKUNIN, A. F. & HALLENBECK, P. C. 1998. A luminol/iodophenol chemiluminescent detection system for western immunoblots. *Anal Biochem,* 258**,** 146-9.

YANG, B., THOROGOOD, D., ARMSTEAD, I. & BARTH, S. 2008. How far are we from unravelling self-incompatibility in grasses? *New Phytol,* 178**,** 740-53.

YAO, C. K., LIN, Y. Q., LY, C. V., OHYAMA, T., HAUETER, C. M., MOISEENKOVA-BELL, V. Y., WENSEL, T. G. & BELLEN, H. J. 2009. A synaptic vesicle-associated Ca2+ channel promotes endocytosis and couples exocytosis to endocytosis. *Cell,* 138**,** 947-60.

YOO, S. D., CHO, Y. H. & SHEEN, J. 2007. Arabidopsis mesophyll protoplasts: a versatile cell system for transient gene expression analysis. *Nat Protoc,* 2**,** 1565-72.

ZHANG, X., HENRIQUES, R., LIN, S. S., NIU, Q. W. & CHUA, N. H. 2006. Agrobacterium-mediated transformation of Arabidopsis thaliana using the floral dip method. *Nat Protoc,* 1**,** 641-6.

ZHAO, J. H., REISKE, H. & GUAN, J. L. 1998. Regulation of the cell cycle by focal adhesion kinase. *J Cell Biol,* 143**,** 1997-2008.